Tracking Volcanic Sulphate

Modelling tropospheric volcanic sulphate formation and its oxygen isotopic signatures

Tommaso Galeazzo

Thèse de doctorat:
Sorbonne Université

Spécialité:
Chimie de l'Atmosphère
Géochimie

SCIENCES SORBONNE UNIVERSITÉ

Front cover: Fuego Volcano, Guatemala; November, 2017.
Copyright: Angel Borrayo ©.

Tracking Volcanic Sulphate

Modelling tropospheric volcanic sulphate formation and its oxygen isotopic signatures

Tommaso Galeazzo

Thèse de doctorat de la Sorbonne Université

École Doctorale:

ED398 - Géosciences, Ressources Naturelles et Environnement

Spécialitée:

Chimie de l'Atmosphère, Géochimie

Thèse dirigée par Slimane Bekki[1] et Erwan Martin[2]

[1]LATMOS/IPSL, Sorbonne Université, UVSQ, Université Paris-Saclay, CNRS, Paris, France
[2]ISTeP, Sorbonne Université, CNRS, Paris, France

Composition du jury:

Rapporteur:	M. Pierre Cartigny,	IPGP, Paris
Rapporteur:	M. Wahid Mellouki,	ICARE, Paris
Président du jury:	Mme. Chrystèle Sanloup,	Sorbonne Université - ISTeP, Paris
Examinateur:	Mme. Tjarda Roberts,	LPC2E, Orléans
Examinateur:	Mme. Sophie Szopa,	LSCE, Paris
Co-directeur de thèse:	M. Erwan Martin,	Sorbonne Université - ISTeP, Paris
Directeur de thèse:	M. Slimane Bekki,	LATMOS, Paris

Resumé

Les émissions volcaniques sont une source importante de polluants atmosphériques, notamment le soufre. Le soufre volcanique est oxydé et forme des aérosols sulfatés secondaires qui diffusent le rayonnement solaire incident, influençant significativement le climat, comme l'illustre le refroidissement global de la surface observé après de très grandes éruptions volcaniques. Les émissions de soufre volcanique dans la troposphère ne peuvent influencer le climat qu' à une échelle limitée, principalement à l'échelle locale et régionale. Néanmoins, les sulfates volcaniques troposphériques sont importants pour les dépôts acides et ont des effets néfastes sur la santé humaine. De grandes incertitudes subsistent en ce qui concerne le cycle troposphérique du soufre volcanique, en particulier son oxydation et sa conversion en aérosols sulfatés dans les panaches volcaniques. De plus, des observations récentes montrent que les panaches volcaniques peuvent aussi contenir de grandes quantités d'halogènes réactifs qui détruisent l'ozone et affectent le budget des oxydants atmosphériques. Jusqu'à présent, le rôle des halogènes volcaniques dans la chimie du panache volcanique (y compris l'oxydation du soufre) a tendance à être ignoré.

Le but de ce travail est d'étudier l'oxydation du soufre dans une large gamme de panaches volcaniques et l'influence des halogènes volcaniques sur la chimie du panache. Parallèlement, il explore également la manière dont la composition isotopique en oxygène du sulfate volcanique, à savoir l'excès de ^{17}O ($\Delta^{17}O$), peut servir de traceurs des processus d'oxydation et les contraintes qu'elle peut fournir sur les voies d'oxydation du soufre. Contrairement à la plupart des sulfates troposphériques, les sulfates recueillis sur les cendres volcaniques d'origine troposphériques ont tendance à être caractérisés par un manque ou absence danomalie isotopique ($\Delta^{17}O$). Cette caractéristique inhabituelle indique que le soufre volcanique peut être sujet à une dynamique d'oxydation particulière. Dans ce travail, le traitement du soufre volcanique est étudié à l'aide d'un modèle de boîte photochimique (CiTTyCAT), qui contient des descriptions de la chimie hétérogène du soufre et des halogènes sur des phases riches en eau liquide et des aérosols sulfatés. Le schéma chimique est couplé à un schéma de transfert d'isotopes de l'oxygène, permettant de suivre l'évolution du $\Delta^{17}O$ du sulfate volcanique

Les résultats de modélisation suggèrent qu'en présence de gouttelettes d'eau et de cendres, l'oxydation du soufre dans les panaches volcaniques est principalement due à l'oxydation en phase aqueuse par O_2 catalysée par les ions de métaux de transition (TMI). Les émissions d'halogènes favorisent davantage la dominance de O_2/TMI en induisant des événements d'appauvrissement d'ozone (ODE) et en rendant l'oxydation aqueuse par H_2O_2 et celle gazeuse par OH encore moins significatives. Il en résulte un sulfate volcanique avec de faibles valeurs de $\Delta^{17}O$. En l'absence de gouttelettes d'eau, la chimie du panache est en grande partie déterminée par la chimie hétérogène sur les aérosols primaires sulfatés. Les oxydants dominants du soufre dans ces panaches volcaniques sont le OH et le H_2O_2; leurs contributions respectives à l'oxydation dépendent de la charge en halogènes volcaniques. Le taux d'oxydation du soufre est fortement réduit par rapport aux panaches volcaniques contenant des gouttelettes d'eau. Les valeurs de $\Delta^{17}O$ des sulfates produits en l'absence des gouttelettes deau sont élevées, contrairement aux mesures isotopiques des sulfates recueillis sur les cendres volcaniques tropoériques. Les résultats démontrent que les isotopes de l'oxygène dans les sulfates fournissent de fortes contraintes sur le bilan chimique du soufre dans les panaches volcaniques et sur le rôle des halogènes volcaniques.

Abstract

Volcanic emissions are an important source of atmospheric pollutants, notably sulphur. Volcanic sulphur is oxidised and forms secondary sulphate aerosols which backscatter incoming solar radiation towards space, thus influencing significantly the climate, as observed during global surface cooling occurring after very large volcanic eruptions. Volcanic sulphur emissions in the troposphere can only influence the climate on a limited scale, mostly on local and regional extents. Nonetheless, tropospheric volcanic sulphates are important for acid deposition, for sulphur pollution events, vog formation, and hazardous effects on human health. Large uncertainties are still pertaining to the tropospheric cycle of volcanic sulphur, in particular its oxidation and conversion into sulphate aerosols within volcanic plumes. In addition, recent observations show that volcanic plumes can also contain large amounts of reactive halogens that destroy ozone and affect the budget of atmospheric oxidants. So far, the role of volcanic halogens in volcanic plume chemistry tends to be ignored.

The purpose of the present work is to investigate sulphur oxidation taking place within a wide range of volcanic plumes and the influence of volcanic halogens on plume chemistry. In parallel, it also explores the way the oxygen isotopic composition of volcanic sulphate, namely the ^{17}O-excess (Δ^{17}O), can serve as tracers of oxidation processes, hence providing constraints on sulphur oxidation pathways. In contrast to most sulphates of tropospheric origins, tropospheric volcanic sulphates collected from volcanic ash-deposits are mostly characterised by a lack of ^{17}O-excess (Δ^{17}O). This unusual feature indicates that volcanic sulphur may be subject to peculiar oxidation dynamics. In this work, volcanic sulphur processing is investigated with the aid of a photochemical box-model (CiTTyCAT), which contains descriptions of sulphur and halogens heterogeneous chemistry on liquid water-rich phases and sulphuric acid aerosols. The chemical scheme is coupled to an oxygen isotope transfer scheme, monitoring the evolution of volcanic sulphate Δ^{17}O.

Main results from modelling suggest that, in presence of water droplets and halogens, sulphur oxidation is driven by the aqueous phase oxidation by O_2 catalysed by transition metal ions (TMI). In particular, halogens emissions can induce ozone depletion events (ODEs), making the aqueous oxidation by H_2O_2 and the gas phase oxidation by OH negligible. Resulting produced sulphate have low Δ^{17}O values, in consistence with isotopic measurements on sulphate extracted from tropospheric volcanic ash. In absence of water droplets, sulphur oxidation is largely driven by heterogeneous chemistry on primary sulphate aerosols. Notably, ozone depletion events occur fast, and the rate of sulphur oxidation is severely reduced. In this case, sulphur oxidation is due to heterogeneous oxidation by OH and H_2O_2. It is also inversely correlated to halogens loading, suggesting prolonged sulphur atmospheric lifetime in occurrence of halogens activation. In volcanic plumes made of sulphate aerosols, Δ^{17}O of produced sulphate are high, in contrast with isotopic measurements conducted on tropospheric volcanic ash. These results demonstrate that sulphates oxygen isotopes provide strong constraints on the chemical budget of sulphur within volcanic plumes, and on the role of volcanic halogens on plume chemistry.

Contents

List of Figures

xi

List of Tables

Klyuchevskaya Sopka, Kamchatka, Russia. Credits: NASA ©, via spaceflight1.nasa.gov

---

Introduction

---

1 Background

Volcanoes have been an integral part of the Earth's geological evolution throughout different eras. Since the formation of the planet, a significant fraction of atmospheric gases has originated from volcanic degassing, whereas submarine volcanic activity has been responsible for mineral dissolution within seawater (Oppenheimer et al., 2013). Volcanism contributes significantly, indeed, to the essential exchange of elements from the mantle to the atmosphere and the hydrosphere of the Earth (Robock, 2000; Gaillard et al., 2011; Kasting et al., 2012).

In the mantle, chemical elements are stored in vast amounts below crustal level in the form of melts and minerals. The most mobile elements are easily removed from mantle crystals during partial melting, generating magmas. These silicate liquids (magmas) can further transfer chemical compounds to the Earth's surface via volcanism. Notably, during degassing magmas and lavas can release chemical species as volatile gases. At the same time, a large part of volcanic activity is submarine in nature (mid-oceanic ridges, representing 60-80 thousands of km of volcanic chains at the ocean floors) and therefore quite poorly constrained (Oppenheimer et al., 2013). Via deep sea vents volcanic activity exchanges chemicals with seawater, where biological activity started to flourish thanks to the chemical activity of simple carbon compounds and to warmer temperatures (possibly in proximity of hydrothermal vents) (Kelley et al., 2002). Since volcanism is also linked to the evolution of primordial oceans, the impacts of volcanic activity on the history of the Earth, or its ongoing influence on the atmosphere and climate, should not be downplayed (Mather, 2008; Duggen et al., 2009; Ayris and Delmelle, 2012a).

Nowadays it is rather challenging to quantify the actual impacts of volcanic emissions. Because of the complex mix of volcanic gases, the chemistry occurring in volcanic plumes is expected to be very complicated and different from the chemistry of the the background atmosphere (Mather, 2008). In addition, the mix of hazardous events and hostile conditions generally found in proximity of volcanic vents makes it difficult to experimentally probe the atmospheric chemistry associated with the release of volcanic gases. As a consequence, the degree of knowledge pertaining to the physico-chemical transformations in the atmosphere, and ultimately the fate of volcanic emissions, is still fairly limited.

A deeper understanding of the climatic impacts of volcanic activity has been maturing during the last decades, especially through the multiple investigations conducted after the eruption of Mount Pinatubo in 1991 (McCormick et al., 1995; Robock, 2013). At the same time, there are still large uncertainties on the extensive impacts on the atmosphere of present day emissions, or of eruptions from the past. The Intergovernmental Panel on Climate Change (IPCC) recognises that explosive volcanic events provide significant amounts of chemically active gases and particles to the atmosphere (Stocker et al., 2013). It is, therefore, recognised that violent explosive eruptions have had transient effects on global climate, and that certainly massive eruptions have acted as drivers for precedent climatic shifts. Nowadays, however, many trace gases emitted in the atmosphere are of anthropogenic origin. Consequently, in an atmosphere so highly perturbed by human activities it is rather difficult to discern the present imprint of volcanic emissions.

In the past, most of the scientific investigations on the impacts of volcanic activity on the atmosphere and climate have focused on the fate of volcanic emissions in the stratosphere, whereas their fate in the troposphere has been slightly overlooked. Nowadays there is growing evidence showing that passive volcanic degassing and small eruptions can influence on a large scale the budgets of tropospheric sulphate aerosol (Textor et al., 2004; Mather, 2008). At the same time, tropospheric volcanic emissions can also impact the life of human beings, since they can be a significant source of sulphur pollutants (Mather et al., 2003). Volcanic gases, indeed, can induce hazardous health effects that can influence lives of populations living in proximity of volcanic systems (Durand and Grattan, 2001; Longo, 2013). Finally, injection of ashes and tephra in the atmosphere as a result of explosive events can have larger economic impacts by significantly altering air traffic (Oxford Economics, 2010; Mazzocchi et al., 2010), crops yield and vegetation (Ayris and Delmelle, 2012b).

In order to assess the tropospheric impacts of volcanism it is necessary to understand the physico-chemical processes driving the atmospheric fate of volcanic emissions. Notably, further investigations are needed to constrain the fate of sulphur and halogen compounds, which are released in high concentrations during both explosive eruptions and degassing activity. In particular, sulphur emissions are of crucial interest to the regulation of the Earth's system, since they can induce several effects on the atmosphere, having also an influence

on climate. It is becoming clearer that volcanic activity and injection of large amounts of sulphur in the atmosphere have multiple effects on climate, both on global and regional scales. There are several sources of information on the chemistry of volcanic plumes, typically measurements and models (Mather et al., 2003; von Glasow, 2010). Modelling, especially, can provide an useful tool for the study of atmospheric reactions undergoing in volcanic plumes (Roberts et al., 2009; Bobrowski and Platt, 2007; von Glasow and Crutzen, 2013). Computational models, indeed, enable to trace the expected of atmospheric physico-chemical processing which are difficult to probe experimentally. Meanwhile, fractionation of stable isotopes can provide significant clues to the determination of the atmospheric pathways of species oxidation (Harris et al., 2012b,c). Consequently, a chemical model providing isotopic compositions of its atmospheric species has the potential to be better validated.

2 Volcanic emissions

Within the extent of global natural emissions, volcanic activity is responsible for the injection of considerable amounts of sulphur in the atmosphere (Robock, 2000; Stevenson et al., 2003a). Before industrial times, volcanoes could accounted for 20 to 47 % of the natural sulphur annual flux to the atmosphere (Andres and Kasgnoc, 1998; Stocker et al., 2013). Nowadays, however, most atmospheric sulphur emissions are dominated by anthropogenic activity. Since the advent of the industrial revolution volcanic contribution to the annual sulphur flux of the atmosphere corresponds to roughly 10% of total atmospheric sulphur emissions (Stevenson et al., 2003a), with anthropogenic emissions being the bulk of the atmospheric sulphur flux and accounting for 70% of total sulphur emissions (Smith et al., 2011). On the other hand, because of the relatively remote locations and altitudes of most volcanoes, volcanic sulphur remains still the biggest source of sulphates in the middle and high troposphere (Chin and Jacob, 1996; Stevenson et al., 2003a).

Volcanoes cycle between different stages of activity, mostly divided among effusive and erupting stages. Generally, erupting phases or events alternate with passive degassing periods, although time intervals between different stages might be rather long. To make an example for different styles of degassing, nowadays it is possible to observe:

- explosive and effusive eruptions for Mayon in the Philippines and Acatenango in Guatemala;

- persistent degassing for Mt. Erebus in Antarctica and Masaya in Nicaragua.

The main gases injected in the atmosphere via volcanic activity are H_2O and CO_2, followed by lower but significant concentrations of SO_2, H_2S, various halogen species (Br, Cl and F compounds), and mercury (Hg) (Textor et al.,

Specie	vol, %	Mt·year^{-1}
H_2O	50-90	-
CO_2	1-40	75
SO_2	1-25	1.5-50
H_2S	1-10	1-2.8
COS	10^{-4}-10^{-2}	0.006-0.1
CS_2	10^{-4}-10^{-2}	0.007-0.096
HCl	1-10	0.4-11
HBr	-	0.0078-0.1
HF	$< 10^{-3}$	0.06-6

Table 1.1: The table shows budget estimations for gas species released by volcanic activity. The relaticve fluxes have been computated using a general circulation model (AGCM). Credits: (Textor et al., 2004).

2004). The mean composition of volcanic emissions and the respective atmospheric annual mass fluxes are summarised in Table:1.1. Chemical speciation of volcanic gases emissions is not the same for different volcanic systems (Textor et al., 2004). The geodynamics leading to magma production determine the composition of volatiles and minerals entrapped in magmas, and volcanic gases speciation depends highly on the geological processes responsible for magma production. Notably, melts chemical composition depends largely on volcanoes location among the tectonic plates of the planet, in particular regarding halogen versus sulphur contents of magmas and emissions. As example, the geology of subducting plates can be significantly influenced by oceanic fluids. For instance, during oceanic crust generation and evolution, hydrated halogens-rich minerals form because hydrothermal activity induces hydration of the oceanic lithosphere. As fluids are gradually released from the subducting lithospere (subduction fluids), they are transferred to the overlying mantle wedge which gets hydrated (formation of hydrated and halogen rich minerals). The interaction between fluids and the mantle (metasomatism) leads to a decrease in melting temperature for the mantle wedge, hence generating magmas as a result of the partial melting of the mantle. At this stage, all mobile elements, such as halogens, are transferred to magmas, which might finally rise up to the planet surface. As a result, magma composition of volcanoes along volcanic arcs (chain of volcanoes typical of subduction zones) is highly enriched in halogens, notably because of the entrapment of sea-water during subduction (Straub and Layne, 2003; Aiuppa et al., 2009).

From an atmospheric perspective, sulphur species are the volcanic gases responsible for most of the climatic impacts linked to volcanic emissions (Robock, 2000). In particular, sulphur atmospheric emissions lead to formation of considerable amounts of sulphate aerosols which can absorb and scatter solar radiation, hence affecting radiative properties of the atmosphere (Haywood and

4

Boucher, 2000; Carslaw et al., 2009). The two main mechanisms leading to sulphate aerosols formation are gas to particle conversion of precursor compounds (mainly SO_2, H_2S and OCS), and condensation of sulphate and solids directly emitted from volcanic vents (Allen et al., 2002).

Sulphur is oxidised in the atmosphere via multiple reaction channels via both aqueous phase and gas phase reactions. The atmospheric oxidation of SO_2 is responsible for the production of secondary sulphates, which can easily condense to form new sulphate aerosols thanks to their large hygroscopicity (Seinfeld and Pandis, 2016). As a consequence, there is much interest in understanding and in assessing the fate and magnitude of volcanic sulphur emissions, with the purpose to size volcanic sulphate production for different volcanic systems.

In addition to sulphur, volcanic emissions contain other reactive gases which can undergo multi-phase chemistry in the troposphere, notably halogens (e.g. chlorine, bromine, iodine). Halogens can be converted into radicals in the gas phase, leading for instance to ozone depletion events (Roberts et al., 2009; von Glasow, 2010; Vance et al., 2010; Boichu et al., 2011), which might influence sulphur oxidation in volcanic plumes (Cadoux et al., 2015). Therefore, because of their atmospheric reactivity the potential impact of halogens on the chemistry of volcanic plumes should not be underestimated.

2.1 Volcanic sulphur degassing

Persistent degassing is the largest source if volcanic gases into the atmosphere, notably volcanic sulphur. Time averaged results from modelling simulations somewhat estimate a large flux of volcanic sulphur to the atmosphere, of about $14 \, \mathrm{Tg \cdot year^{-1}}$ (Graf et al., 1997). On the other hand spectrometer data (COSPEC) measurements suggest an annual volcanic sulphur flux to the atmosphere of of roughly $10.5 \, \mathrm{Tg \cdot year^{-1}}$. The contribution of sporadically explosive eruptions to the total volcanic sulphur budget is significantly low compared to persistent degassing, accounting for only 1% of annual volcanic emissions (Andres and Kasgnoc, 1998).

It is worth noticing, however, the disproportion between volcanic sulphur emissions to the atmosphere (i.e. $\approx$10% of total sulphur emissions), and the contribution of volcanic sulphate to the total atmospheric sulphate burden. Global models, indeed, suggest that volcanic sulphate aerosols contribute for as high as 18% to the total column of sulphate in the atmosphere (Chin et al., 1996). It is estimated that volcanic sulphate aerosols could be more easily produced in the atmosphere (Graf et al., 1997), and that since most volcanic emissions are released in the free troposphere where deposition processes are inhibited compared to the boundary layer, volcanic sulphate has a longer atmospheric residence time (Stevenson et al., 2003a). Therefore, persistent degassing constitutes an important source of sulphur in the free atmosphere (Mather, 2008).

The main sulphur compounds among volcanic emissions are respectively SO_2 and H_2S (Textor et al., 2004). The ratio of H_2S/SO_2 is defined as the *redox ratio*, a parameter proportional to multiple thermodynamical variables, such as: temperature, oxygen fugacity, pressure and water mole fraction of melts. Generally, the redox ratio increases with pressure, lower temperatures and lower oxygen fugacity (Wallace, 2001; Oppenheimer et al., 2013). As a consequence, depending on the stage of eruption and of magma release, the SO_2/H_2S ratio can also change over single eruptive events.

In silica melts the prevailing sulphur species are S^{2-} and SO_4^{2-}, which differentiate in the gas phase through a complex mix of redox reactions. As a result, the ratio of sulphide and sulphate minerals in volcanic melts can be used to estimate the ratio of sulphur gases that might be released in the gas phase (Oppenheimer et al., 2013). Experimental measurements indicate that large amounts of SO_2 are frequently emitted in relation to high temperature volcanic emissions, while large H_2S concentrations are an indicator of hydrothermal contribution to volcanic gases generation, being also related to low temperature vents degassing (Oppenheimer et al., 2013).

Primary and secondary sulphate emissions

Most of volcanic sulphates are formed in the gas phase as a consequence of SO_2 processing in the atmosphere. However, multiple gas phase reactions can occur within the time gases are released from the crater rim and the time they reach the volcanic vent.

At such elevated temperatures ($\approx$ 600-1000°C) a portion of sulphur trace gases can be oxidised to form H_2SO_4 (Gerlach, 2004; Roberts et al., 2009; von Glasow, 2010), producing sulphate particles that can be emitted directly from volcanic vents. These highly acidic sulphate aerosols can constitute the bulk of volcanic aerosol emissions in proximity of volcanic vents (Allen et al., 2002), and they are defined as "primary sulphates" (Mather et al., 2004a,b). From the moment the plume is released in the atmosphere, in-plume heterogeneous chemistry can be activated, inducing sustained SO_2 oxidation in the plume. Sulphate produced by in-plume chemical processing is defined as "secondary sulphate", and it constitutes the bulk of volcanic sulphates aerosols measured far from volcanic sites. In proximity of volcanic vents, indeed, H_2SO_4/SO_2 ratios are rather low and within the order of 1% (Allen et al., 2002; Mather et al., 2004a,b). The small amount of sulphate emitted at the vent confirms that most of in-plume sulphates should be formed away from volcanic vents by SO_2 processing in the atmosphere. In plumes from passive degassing sulphate concentrations follow diurnal variations, which are most likely caused via SO_2 oxidation by OH and H_2O_2 during daytime (Kroll et al., 2015). Notably, if primary sulphates were the major source of volcanic sulphates, the concentration of sulphates in the plume would otherwise remain constant. Since most of volcanic sulphates are produced once the plume is released by the vent, it is rather crucial to
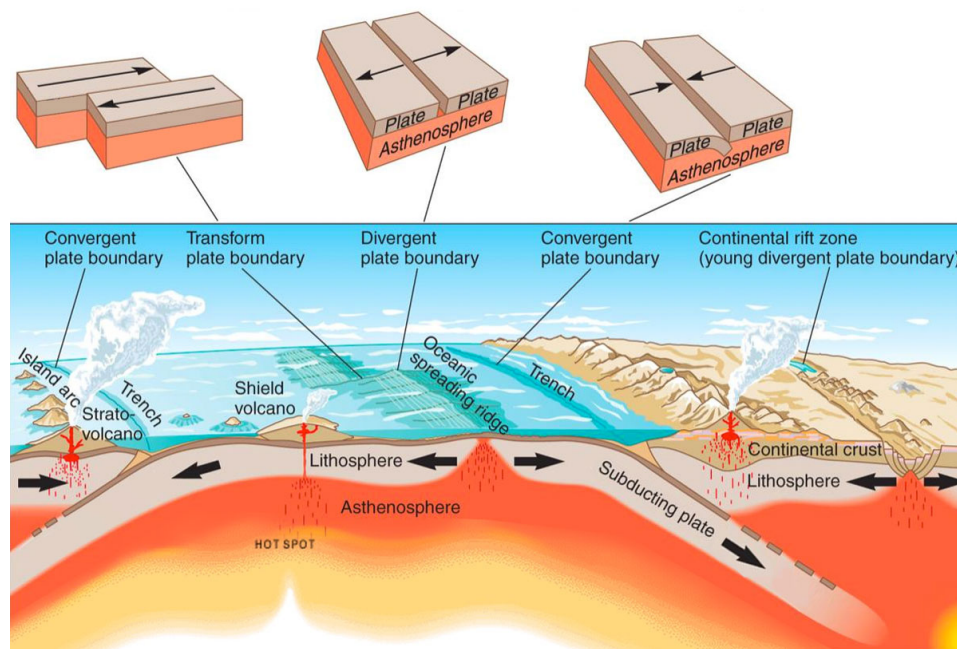
Figure 1.1: Volcanic systems develop at different locations among the tectonic plates. Common examples are: Kuril Islands for island arc volcanoes, Kilauea for hotspot shield volcanoes, Cerro Negro for continental arc volcanoes, and Erta' Ale for continental rift volcanoes. Credits: USGS ©.

understand how environmental conditions promotes the production of sulphates at different plume conditions. SO_2 processing is therefore, fundamental for volcanic sulphate formation.

2.2 Halogen degassing and solid particles emissions

Halogens emissions

The most abundant halogen species among volcanic emissions are respectively: HCl, HF and HBr (Martin et al., 2006; Aiuppa, 2009; Aiuppa et al., 2009). Bromine and chlorine compounds constitute the bulk of volcanic halogen emissions, and they both have significant impacts on the chemistry of the atmosphere (Parrella et al., 2012; Saiz-Lopez and von Glasow, 2012; von Glasow and Crutzen, 2013). Recently, multiple studies have been suggesting that the tropospheric impacts of volcanic halogen emissions could have been overlooked (Aiuppa et al., 2005a; Grellier et al., 2014; Simpson et al., 2015). In recent years, indeed, detection of bromine oxide (BrO) in aged volcanic plumes (e.g. 30 minutes after plume ejection) has confirmed that reactive Br compounds are commonly emitted within volcanic plumes (Bobrowski and Platt, 2007; Bobrowski et al., 2007), and that quick destruction of ozone can occur during the first stages

of plume diffusion in the troposphere (Vance et al., 2010; Boichu et al., 2011). Observed ozone depletion events (ODEs) confirm that volcanic bromine species react quickly in the gas-phase (Bobrowski et al., 2003; Oppenheimer et al., 2006) through heterogeneous phase reactions and a combination of halogen and nitrogen catalytic cycles (von Glasow, 2010).

It has been suggested that in some extent volcanic halogen emissions could account as a major source of BrO in the free troposphere, hence impacting significantly the chemical composition of the atmosphere above the boundary layer (Oppenheimer et al., 2013). Injection of chemically active species in the free troposphere (or close to the tropopause) is particularly significant at polar latitudes, where halogen species can accumulate in winter to finally promote massive ozone destruction in spring (Vance et al., 2010; Saiz-Lopez and von Glasow, 2012). Radical reactions promoted by halogens species photolysis can also induce ozone holes in the upper troposphere as observed in occurrence of the Kasatochi eruption of 2008 (Theys et al., 2009).

The halogen content of volcanic gases, however, varies considerably on the composition of melts, and on the location of volcanic systems along the plates of the crust. As release of halogen species from magma controls the input of ozone depleting species into the atmosphere (Gerlach, 2004; Pyle and Mather, 2009), different volcanic settings can potentially have different impact on the atmosphere because of the halogen content of their emissions. The different kind of volcanic settings of the planet are shown in **Fig.:1.1** in function to location on the tectonic plates of the Earth. Halogen rich magmas are usually found in volcanic arcs (Pyle and Mather, 2009; Aiuppa et al., 2009), while continental rift and hotspot volcanoes are usually characterised by low contents of halogens and by high percentages of sulphur emissions. On the other hand, plumes degassing from rift and hotspot volcanoes tend to have rather low halogen loadings (Aiuppa et al., 2009; Pyle and Mather, 2009).

Solid particles emissions

The composition of magma is also crucial to the style of eruption, since its volatile content promotes the production of more or less viscous melts. Magma viscosity is a function of the silica content, responsible for more or less polymerized "structures" of melts. Multiple parameters can affect magma viscosity and polymerization, notably volatile content, the amount of crystals and temperature. Generally, magma generated by partial melting of the mantle is basaltic in composition (50wt.% SiO_2). This magma tends to evolve chemically through different processes (fractional crystallisation, crustal contamination/assimilation, magma mixing, etc.), and during its differentiation (chemical evolution), it tends to become more and more SiO_2-rich, with contents up to 75wt.% (rhyolitic composition) for highly differentiated magmas. During most virulent eruptions, less fragmented magma gas release is combined to injection of solid particles and other solids in the form of ash, lapilli and bombs.

These solid substrates are potentially important for in-plume chemistry, since they provide reactive surfaces for heterogeneous reactions. Notably, during explosive events large quantities of water and coarse particles are emitted. Solid particles, notably ash, can be scavenged by hydrometeors, providing a reactive substrate for aqueous phase chemistry (Tabazadeh and Turco, 1993). During explosive eruptions characterised by high quantities of ash, the heterogeneous uptake can become a significant pathway of SO_2 oxidation in erupting plumes (Mather et al., 2003). On the other hand, in volcanic plumes without condensing water, also suspended particles and sulphate aerosols can provide reactive surfaces for the oxidation of volcanic SO_2 (Eatough et al., 1994; Langmann, 2014). It has been observed, indeed, that during effusive eruptions and passive degassing some fine silicate particles can also be released from the surface of magma from bubble breaking, and that some primary sulphate aerosols are released directly at the vent. Besides, compared to explosive eruptions very few solid particles are detected in plumes emitted during passive degassing (Martin et al., 2006), which are mostly ash-free. A schematic representation of the main processes linked to volcanic activity is reported in **Fig.:1.2**.

Volcanic ash and rocks contains iron rich minerals, composed in different compositions by Fe(II) and Fe(III) among their crystal structures (Rose et al., 2006). The total amount of Fe released in solid particles accounts between 1-12 wt% of the total mass of the solid phase. Notably, in magmatic rocks between 1-10 wt% of total solid mass is composed by FeO, while Fe_2O_3 can reach values as high as 0.5-3 wt% (Rose and Durant, 2009). The most common solid material ejected during explosive eruptions is glass, which is followed by a mixture of various minerals (e.g. hematite, magnetite). In volcanic ashes heavy metals are commonly found as rock particles of different sizes (Rose et al., 2006; Mather et al., 2012), as well as metallic and mineral dust. In particular, these small solid particles may provide reactive surfaces for heterogeneous reactions to occur (Davidovits et al., 2006; Cwiertny et al., 2008; Langmann, 2014). As a result, during explosive eruptions multiphase chemistry occurring within volcanic liquid phases could be rather significant, potentially promoting conversion of halogens into halogen radicals (von Glasow and Crutzen, 2013), and enhancing SO_2 processing.

3   Climatic and environmental impacts of volcanism

Volcanic emissions provide a significant amount of natural atmospheric pollutants climate forcers (Robock, 2000; LeGrande et al., 2010), inducing different atmospheric responses, as summarised in **Fig.:1.3**. The chemistry and the composition of the atmosphere is affected by the release of concentrated volcanic plume, in particular because of the release of large amounts of SO_2.

The oxidation of volcanic sulphur bearing gases leads to the formation of sulphate aerosols, which can perturb the radiative forcing of the planet (Stocker
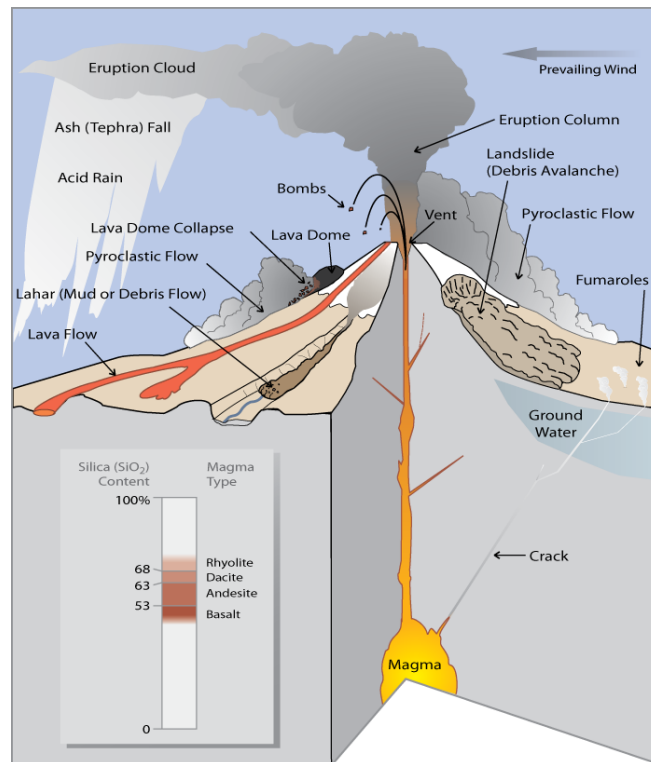
Figure 1.2: A simplified representation of an ash-rich explosive eruption, of degassing activity and the most common volcanic hazards. The figure illustrates different stages of explosive eruptions, including ash release from erupting clouds and degassing from fumaroles. In the panel in the lower left corner, volcanic melts are schematically classified by their silica content. Credits: USGS.

et al., 2013) via interaction with incoming solar radiation. The climatic impacts of subaerial volcanism on the atmosphere, however, highly depends on the extent of degassed material, on the nature of the eruption, and on the altitude or release of the plume. An useful scale of comparison for eruptive activity is the Volcanic Explosive Index (VEI), which classifies eruption events accounting for: the height of eruption columns, the mass of material ejected during the eruption, and the duration of the event (Newhall and Self, 1982).

The altitude reached by volcanic plumes within the atmosphere is a particularly sensitive parameter, inducing very different climatic and environmental feedbacks on planetary atmospheric chemistry and physics. It is possible to distinguish two main classes of climatic responses, respectively summoned by: stratospheric and tropospheric climatic impacts (Robock, 2000). In addition to altitude, also latitude plays a role for climatic aftermaths of volcanic eruptions. Volcanic plumes reaching the atmosphere at high latitudes induce climatic impacts at hemispherical scales, while volcanic eruptions occurring at tropical
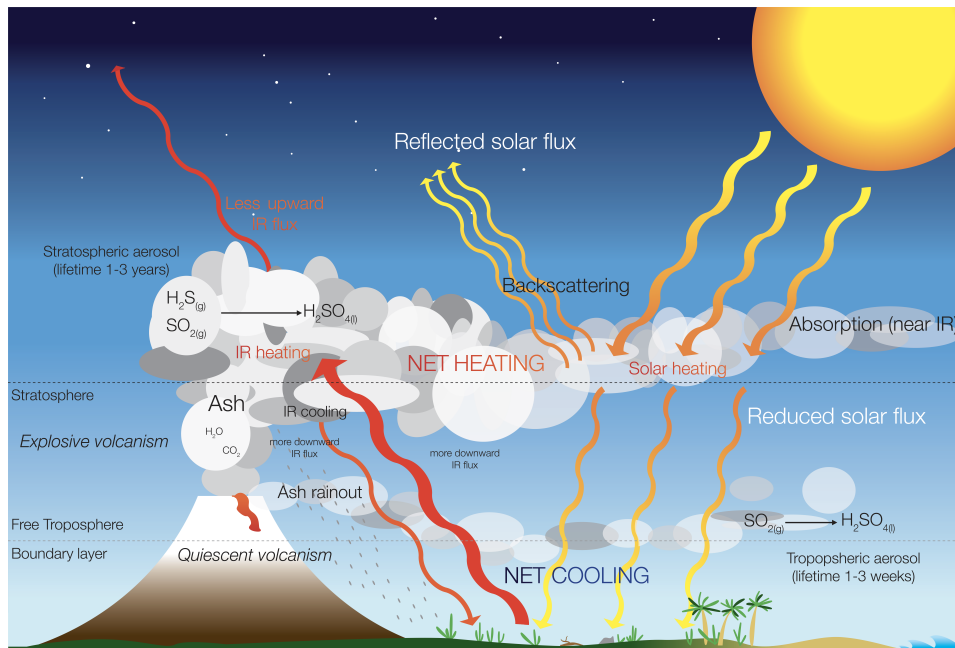
Figure 1.3: Schematic representation of the main climatic feedbacks due to volcanic degassing, adaptation from Robock et al., 2000. Atmospheric impacts are represented for both tropospheric and stratospheric emissions.

latitudes can induce effects on global extents. The different climatic impacts are mostly related to atmospheric circulation, and to volcanic emissions diffusion around the globe.

3.1 Stratospheric impacts

Explosive eruptions resulting in the release of a plume within the stratosphere are defined as stratospheric eruptions. These events lead to atmospheric responses that have global impacts on the climate of the planet, since they can release large amounts of tephra and reactive gases above the tropopause where aerosols residence lifetime is long. These eruptive events occur rather sporadically and they are defined as *Plinian eruptions*. The main aftermath of plinian eruptions is the perturbation of the aerosol load of the stratosphere, leading to stratospheric ozone depletion and climatic effects due to optical properties of aerosols, therefore the interaction with incoming solar radiation (Robock, 2013). Aerosols, indeed, absorb and scatter incoming sunlight and therefore they prevent solar radiation to reach the lower layers of the atmosphere. The most pervasive atmospheric responses due to plinian eruptions are due to changes in the radiative properties of the atmosphere, resulting in a net warming effect for the stratosphere and in a net cooling effect for the troposphere.

In 1991 the eruption of Mt. Pinatubo resulted in an opportunity to study

SAGE II 1020 nm Optical Depth

91-April-10 to 91-May-13

91-June-15 to 91-July-25

91-August-23 to 91-September-30

93-December-5 to 94-January-16

$<10^{-3}$　10^{-2}　$>10^{-1}$
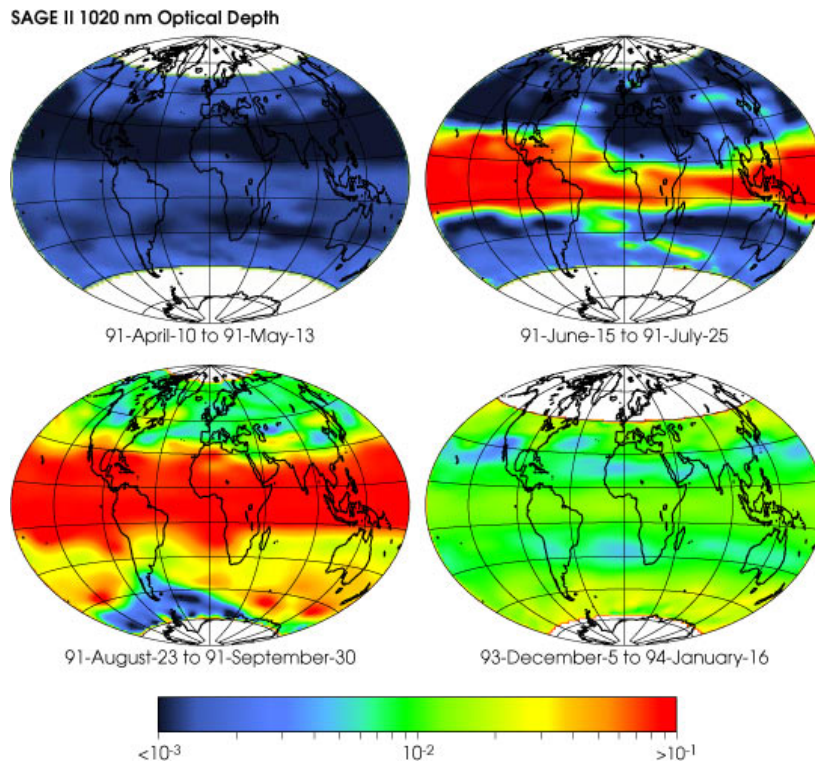
Figure 1.4: The figure shows the evolution of the optical thickness of the strato-sphere as a function of time and aerosol load before and after the eruption of June 15th, 1991. The optical thickness is measured in units of nm. The images have been recorded through the SAGE satellite. Credits: (McCormick et al., 1995).

atmospheric responses to large volcanic eruptions, and to the release of volcanic gases in the upper atmosphere. Mt. Pinatubo plume reached an altitude of about 40 km within the stratosphere, releasing 17-20 Tg of SO_2 into the stratosphere, while producing via multiple-phase chemistry almost 30 Tg of sulphate aerosols. The SO_2 rich volcanic cloud circumnavigated the planet within 22 days from the eruption (McCormick et al., 1995), and after 38 days most of SO_2 had already been converted to stratospheric sulphate aerosols. Within three months from the eruption a thin layer of sulphate aerosols had covered the entire planet, lasting for as long as three years within the stratosphere.

Thanks to satellite measurements, for the first time in the modern era it was possible to observe the development of a stratospheric volcanic plume in the atmosphere, together with sulphate aerosols formation and diffusion at high altitudes. Notably, Mt. Pinatubo eruption enabled to directly observe the impact of volcanic aerosols on the radiative forcing of the planet, in relation to the changes in optical properties of the upper atmosphere. For instance, in **Fig.:1.4** the temporal evolution of the optical thickness of the stratosphere as
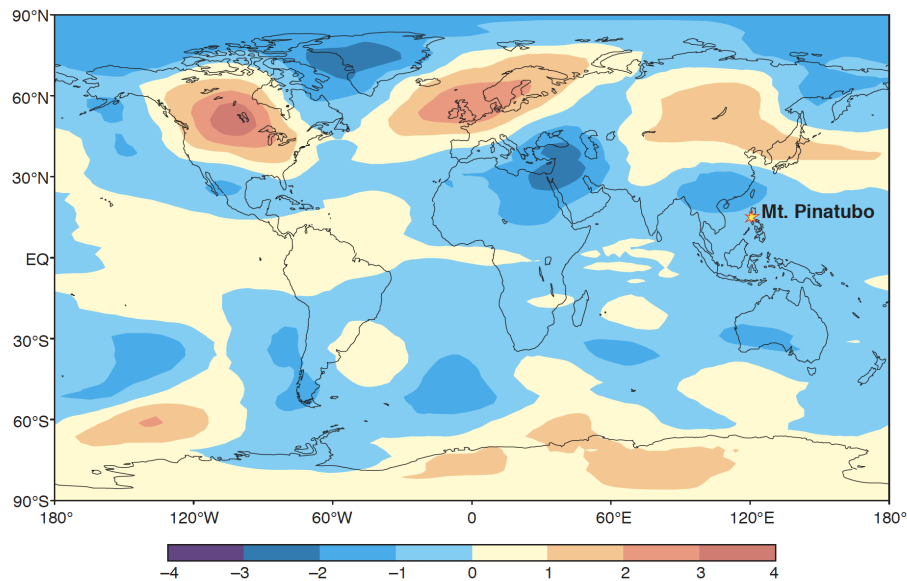
Figure 1.5: Average temperature anomalies (K) recorded during the first months of 1993. Credits: (Robock, 2002).

observed by the Stratospheric Aerosol and Gas Experiment (SAGE) satellite is reported for both pre- and after-eruption months. High concentrations of sulphate aerosols enhanced the albedo of the planet by about 5% (Minnis et al., 1993a), and atmospheric perturbations were felt on a global scale for about 2 years after the eruption. At the peak of stratospheric volcanic aerosols concentration, the radiative forcing of the planet was estimated at about -3 $W \cdot m^{-2}$ as a consequence of the higher albedo of the stratosphere (Stenchikov et al., 1998). The injection of high quantities of SO_2 during eruption induced also a depletion in stratospheric O_3, which was about 6% lower than the mean atmospheric concentrations measured before the eruption. Destruction of ozone occurred in conjunction to production of high levels of $HONO_2$ (Koike et al., 1994), indicating that heterogeneous chemistry involving halogen radicals, NOx, and ozone might had effectively been taking place.

After the eruption different climatic feedbacks were observed throughout the planet, and mean temperatures dropped of about $0.5°C$ between the summer of 1991 and the end of 1993 (Robock, 2002). At the same time, global precipitations were lowered in intensity, and anomalous temperature patterns were recorded in the Northern Hemisphere (NH) during the couple of winters and summers that followed the eruption (Robock, 2013). The map in **Fig.:1.5** shows the average temperature records observed during the early months of 1993. Between 1991 and 1993, the average winter temperatures of the NH were enhanced of roughly 2-3 degrees over Northern Europe and Northern America. While

on the other hand, summer temperatures were below seasonal averages over the same regions for a couple of years following the event. These temperature patterns have also been reported in historical records that followed the eruption of Mt. Tambora in 1815 (Veale and Endfield, 2016), suggesting that these climate feedbacks can commonly occur after the occurrence of massive plinian eruptions at tropical latitudes. The same patterns have been observed also in the case of the massive Samalas eruption in 1257 (Gao et al., 2008; Stoffel et al., 2015; Luterbacher and Pfister, 2015).

3.2 Tropospheric impacts

Compared to stratospheric eruptions, tropospheric volcanic eruptions induce climatic responses that have less evident repercussions on the atmosphere and regional climate. For instance, tropospheric emissions have climatic impacts limited to regional scales, besides having multiple environmental effects on surrounding volcanic regions, affecting notably vegetation and air quality.

The main volcanic compounds that can appreciably impact the chemistry of the troposphere are halogens, nitrogen and sulphur compounds. In their radical forms, halogens can deplete atmospheric ozone entrained in volcanic plumes, and their emissions are of particular interest for in-plume chemical reactions. Since in order to promote the destruction of ozone halogens need to be in radical form, halogens emissions have to be processed via multiphase chemistry (i.e. heterogeneous chemistry) in order to become chemically reactive. The detection of high concentrations of BrO in multiple volcanic plumes suggest that in-plume chemistry might follow similar chemical mechanisms to the ones observed during bromine explosion events occurring at polar latitudes in spring (Bobrowski et al., 2003; Oppenheimer et al., 2006). High levels of BrO within a plume, indeed, suggest heterogeneous chemistry on sulphate aerosols, and possibly ash, should be taking place (von Glasow, 2010).

Recent modelling studies suggest that some nitrogen chemistry can undergo in plumes, notably to promote the mobilization and photochemistry of reactive halogens in the young plume (Roberts et al., 2009, 2012). This hypothesis is confirmed by observations, which report the unexpected presence of $HONO_2$ and HO_2NO_2 within some volcanic plumes (Oppenheimer et al., 2010). Generally, these compounds are generated by anthropogenic activity, but, in proximity of volcanic vents and in remote areas, local sources of NO_2 and NO must to be accounted. In volcanic vents the only available nitrogen compound is atmospheric N_2, indicating that the only source in-situ for reactive nitrogen is its chemical fixation. Initially, from the moment of degassing at crater rim to gas ejection from the vent, the temperature is high and atmospheric nitrogen could be converted into more reactive forms in the gas phase. Eventually, reactive nitrogen (NO_x) produced in the hot-phase could drive halogens mobilization in the young plume. The production of biologically active nitrogen via chemical fixation is of particular interest. Notably, NO_x can form nitrate, which has enhanced fertilizing activity

14

for plants. Overall, nitrogen fixation within the hot phase could have positive effects on vegetation which might benefit from high rates of nitrate production in proximity of volcanic areas (Huebert et al., 1999; Oppenheimer et al., 2013).

Sulphur compounds constitute a high percentage of volcanic gas emissions, and in plumes without condensing water, lower rates of SO_2 oxidation results in its longer lifetime (Kroll et al., 2015). As SO_2 has longer lifetimes, volcanic emissions can affect the life of communities living in proximity of volcanic areas when plumes are advected in the atmosphere. Volcanic regions are mostly located at the tropics and they are rather fertile lands. Therefore, a significant portion of the global population lives in proximity of active volcanoes. It is estimated that, indeed, around 455 millions people (9% of the world population) live close to historically active volcanic systems (Peterson, 1988; Small and Naumann, 2001). High concentrations of aerosols as a result of volcanic sulphur conversion can further promote heterogeneous chemistry and particles condensation. Therefore, an increase in chemical processing of anthropogenic gases associated with volcanic aerosols can lead to major pollution events. Generally, sulphate aerosols and overexposure to high concentrations of SO_2 can induce cardiovascular diseases (Longo et al., 2008; Longo, 2013), while high concentrations of sulphates can also induce the formation of "vog" (volcanic smog) and pollution events in urban areas. For instance, Southern Italy is frequently exposed to high percentages of SO_2 and sulphate aerosols, due to frequent degassing of Mt. Etna (Graf et al., 1998), and the air quality of Mexico City is also frequently influenced by emissions from the Popocatpétl volcano (Raga et al., 1999; de Foy et al., 2009). In Hawai'i, Kilauea'a contributes significantly to the formation of pollution events in Hawai'i due to vog (Longo, 2013), as illustrated in **Fig.:1.6**. Therefore, volcanic sulphur processing in urban areas can account as a severe health issue.

Other environmental impacts of volcanic tropospheric activity are related to volcanic gases deposition. As volcanic emissions deposit on the ground through dry and wet deposition, acidic species such as H_2SO_4, $HONO_2$, or HF, are carried to soils and on the surface of plants and buildings. The adsorption of acids into the ground can modify mineralogy and the pH of soils, while chemical burning can occur in presence of significant depositions of acids on plants leaves (Delmelle et al., 2001; Delmelle, 2003). Besides, deposition of ash and minerals can also have positive effects on land plantations, since ash brings new minerals into the soil. In addition volcanic ash deposition on the surface of oceans can enhance the concentrations of biologically active Fe(II) concentrations. Resulting silica dissolution releases high concentrations of Fe, which further stimulates phytoplankton growing and blooms (Langmann, 2014).

Since tropospheric volcanic activity have multiple effects on the environment, it is difficult to understand the real aftermaths of tropospheric emissions. A first step would be to constrain the chemical budgets of volcanic sulphate, and to better understand how different plume conditions affect volcanic sulphate production. While it is challenging to measure the evolution of volcanic gases in
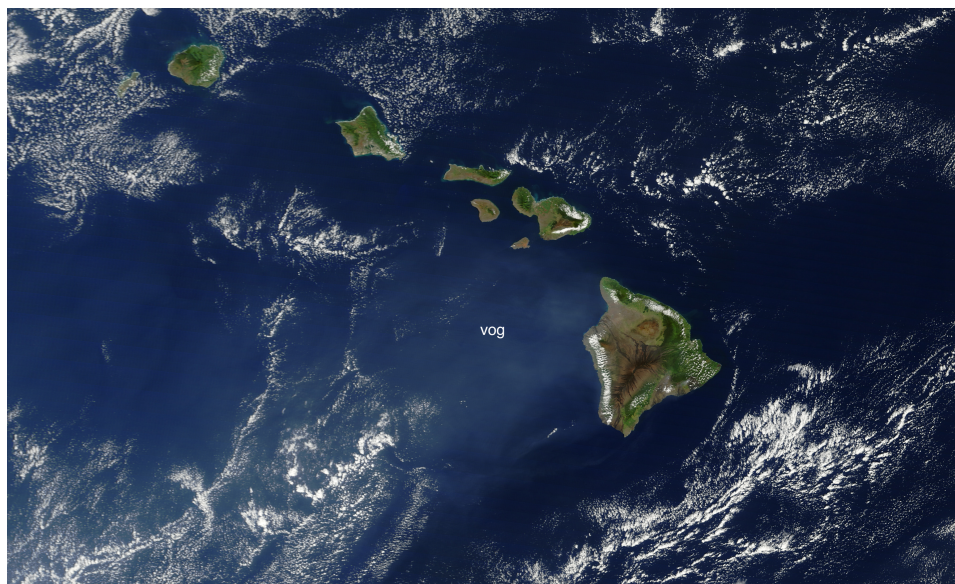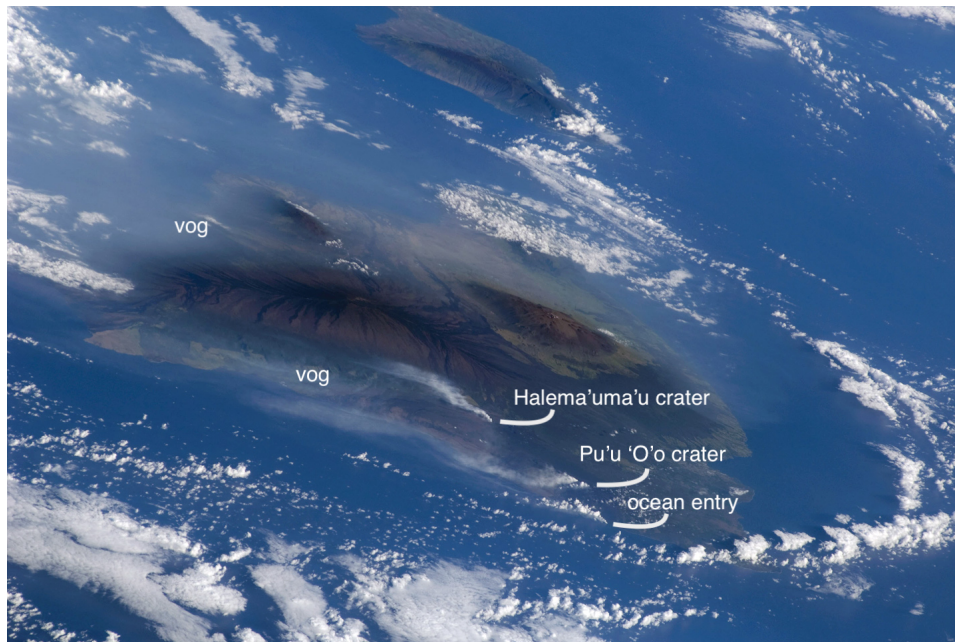
Figure 1.6: Top image: a view from space of the island of Hawai'i, May 13th, 2009; a dense layer of vog is covering the island, impacting the air quality in Honolulu and major urban sites. The emissions from the Halema'uma'u crater, the Pu'u 'O'o crater and the lava entering the ocean are the major sources of reactive volcanic volatiles. Bottom image: a view from space of the Hawaiian Archipelago, December 9th, 2009; volcanic emissions induce extensive vog production that extends for miles along the island arc. Credits: NASA, 2009.

plumes, modelling simulations can help to probe the fate of volcanic gases as they are released into the troposphere. Notably, sulphate aerosols are produced in gas and liquid phase by a limited number of reactions, producing characteristic isotopic signatures in secondary sulphates. Since, isotopic fractionations provide significant constraints on the relative importance of each SO_2 oxidation pathway, observable isotopic fractionations for O isotopes can untangle in-plume reaction dynamics for volcanic SO_2 oxidation.

4   Isotopic fractionations and volcanic activity

4.1   Isotopic fractionations

Stable isotopes are powerful tools to the interpretation of budgets and processing of chemical compounds in the atmosphere. Notably the isotopic composition of atmospheric species can be used as a tracer to detect chemical transformation in the atmosphere. Chemical reactions can generate, indeed, peculiar isotopic distributions, depending on the physical and chemical environment of chemical compounds.

Molecules having the same elemental composition and structure but different isotopic compositions are defined as *isotopologues*. Variations in the relative abundances of stable isotopes can be produced via a combination of chemical and physical processes defined as *isotopic fractionations*. Notably, stable isotopes partitioning between substances and physical phases depends in large part on the different masses of isotopically substituted molecules. The different mass of isotopologues, indeed, has an impact on molecular stabilization via quantum mechanical effects. As a result, isotopologues are characterised by different chemical reaction rates for the same chemical process. Besides, since chemical reactivity of molecules is mostly governed by their electronic structure, isotopologues tend to undergo the same chemical reactions, consequently inducing isotopic fractionations.

In nature, oxygen can be found with three stable isotopes, repartitioned as: ^{16}O (99.86%), ^{17}O (0.0375%) and ^{18}O (0.1995%). Sulphur on the other hand has four natural isotopes, repartitioned as: ^{32}S (95.02%), ^{33}S (0.75%), ^{34}S (4.21%) and ^{36}S (0.02%). The isotopic ratio of a sample is described through the delta notation (δ^x), and it is expressed in units permil ($‰$). Isotopic compositions are defined through the comparison of samples isotopic ratios to those of international standards (R_{std}), such as the Vienna Standard Mean Ocean Water (VSMOW) (Coplen, 1994) for oxygen, and the Vienna Canyon Diablo Troilite (VCDT) for sulphur (Ding et al., 2001). The $\delta^n X$ of a compound is defined as: Where $^n R$ represents the ratio of isotopic abundances of one

$$\delta^n X(‰) = \left(\frac{^n R_x}{^n R_{std}} - 1 \right) \tag{1.1}$$

specific element, as illustrated in the following example for oxygen isotopes:

$$^{17}R = \frac{^{17}O}{^{16}O} \tag{1.2}$$

It is possible to define a fractionation rate for a reaction by comparing the isotopic ratios of products and reactants. Fractionation rates are defined by the kinetic fractionation factor (α_x):

$$\alpha_n = \frac{^{n}R_{products}}{^{n}R_{reactants}} \tag{1.3}$$

Oxygen isotopic fractionations by physical or chemical processes, mostly, induce a change of the $^{17}O/^{16}O$ ratio which is commonly half the magnitude of the respective change in the $^{18}O/^{16}O$ ratio. Isotopic fractionations respecting this relationship are defined as Mass Dependent Fractionations (MDF), and they are typically divided in: *equilibrium fractionations* and *kinetic isotope effects* (KIE). The first class of isotopic fractionations originates from exchange of isotopes between different species, different phases, or between molecules of the same species. These isotopic fractionations do not arise from net chemical reactions, and they are mostly temperature dependent (Young et al., 2002). Typical examples of equilibrium fractionations are the ^{18}O exchange between H_2O and $CaCO_3$, and the enrichment of ^{18}O observed for liquid water during the evaporation of water vapour. The second class of isotopic fractionations results primarily from chemical reactions. Kinetic isotope effects are formed, indeed, because of specific differences in chemical reactions rates for isotopologues of a given species. On a general level, lighter isotopologues have greater kinetic energy and they move faster than heavier isotopologues. At the same time, heavier molecules are energetically more stable and they need more energy to undergo the same reaction. Atomic bonds formed by heavier isotopes require, indeed, more energy to be broken, hence lighter isotopologues participate to chemical reactions at a slightly faster pace. KIE are particularly useful, since resulting isotopic fractionations can be used as tracers for atmospheric reactions. A typical example of a KIE is the atmospheric reaction of $^{13}CH_4$ and $^{12}CH_4$ with OH.

There is a third less common class of isotopic fractionations, which does not depend directly on kinetic or mass dependent effects of isotopologues. These isotopic fractionations are defined as Mass-Independent Fractionations (MIF), and they are generated either by photochemistry, or by transfer of anomalous isotopes from other chemical species (Thiemens, 2006). Notably, photochemistry contributes significantly to the generation of atmospheric MIF, such in the case of oxygen isotopes in ozone, and of sulphur isotopes in sulphate produced in the stratosphere. MIFs are quantitatively defined by $\Delta^{n}X$ (Coplen, 2011), which represents the deviations from the terrestrial fractionation line (TFL) describing

mass-dependent isotopic distributions. Oxygen MIF are defined by the $\Delta^{17}O$ notation as illustrated in Eq.: 1.4, while sulphur MIFs are defined by two different variables $\Delta^{33}S$ and $\Delta^{36}S$, as shown in Eq.: 1.4-1.6.

$$\Delta^{17}O(‰) = \delta^{17}O - \left[\left(1 + \delta^{18}O\right)^{0.52} - 1\right] \tag{1.4}$$

$$\Delta^{33}S(‰) = \delta^{33}S - \left[\left(1 + \delta^{34}S\right)^{0.515} - 1\right] \tag{1.5}$$

$$\Delta^{36}S(‰) = \delta^{36}S - \left[\left(1 + \delta^{34}S\right)^{1.90} - 1\right] \tag{1.6}$$

Ozone is a key reactant in the atmosphere, and it has one of the largest known O-MIF (also referred as oxygen isotopic anomaly). It is characterised by equal enrichments in ^{17}O and ^{18}O. Ozone is also one of the only atmospheric trace gases generated with an intrinsic O-MIF, not inherited from other molecules via atmospheric reactions (Johnston and Thiemens, 1997; Thiemens, 2006). The large isotopic anomaly of ozone originates from differences in stabilization energies during recombination reaction of O_2 and O. Heavier ozone isotopologues are energetically favourable, inducing the isotopic enrichment commonly observed in the molecule (Marcus, 2013).

The mean isotopic signature of tropospheric ozone is around 25.0 ‰ (Heidenreich III et al., 1986; Johnston and Thiemens, 1997; Vicars and Savarino, 2014). However, the isotopic distribution within the molecular structure is not stochastic, and heavier isotopologues are concentrated at terminal sites (Janssen and Tuzson, 2006; Bhattacharya et al., 2008; Marcus, 2013). Experimental measurements suggest that oxygen atoms at the edges of the molecule are characterised by $\Delta^{17}O \approx 40‰$ (Vicars and Savarino, 2014). In addition, they suggest that ozone terminal atoms are most likely involved in 90% of its chemical reactions (Savarino et al., 2007). Consequently, it is possible to define a reactive isotopic signature for ozone ($\Delta^{17}O\,(O_3{}^*)$), encompassing isotopic distributions within the molecular structure, and preferential terminal sites reactivity. Considering the mean isotopic composition of the bulk molecule, the isotopic anomaly of reactive ozone can be estimated (Savarino et al., 2008). For the mean isotopic value of 25.0 ‰ of the bulk molecule, $\Delta^{17}O\,(O_3{}^*)$ equals 36.0 ‰.

As shown in **Fig.:1.7**, isotopic fractionations are observed in each major oxygen bearing specie. The larger the isotopic anomaly carried by atmospheric molecules, the bigger is the deviation from isotopic compositions of terrestrial samples (i.e. TFL). O-MIF of atmospheric oxidants are inherited directly or indirectly from ozone and its photochemical reactions (Lyons, 2001). Since during chemical reactions the isotopic anomaly of atmospheric oxidants can be transferred to their reaction products, oxygen MIF (O-MIF) can be used as an efficient tracker for oxidation of atmospheric chemical compound (Lyons, 2001).

Contrary to O-MIF, there are large uncertainties on the origins of S-MIF in atmospheric sulphates, since multiple mechanisms have been proposed for
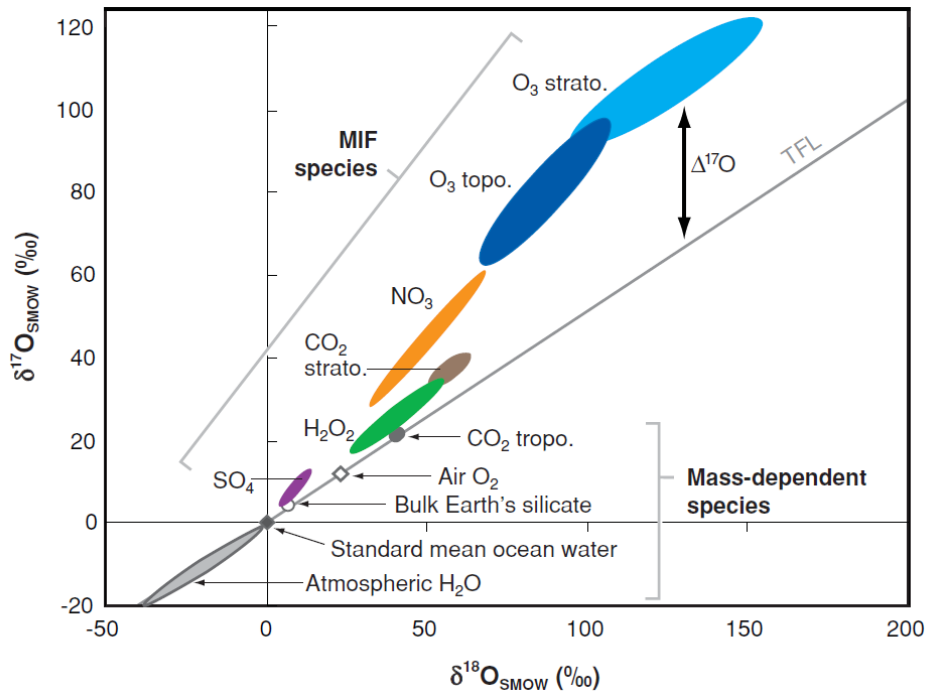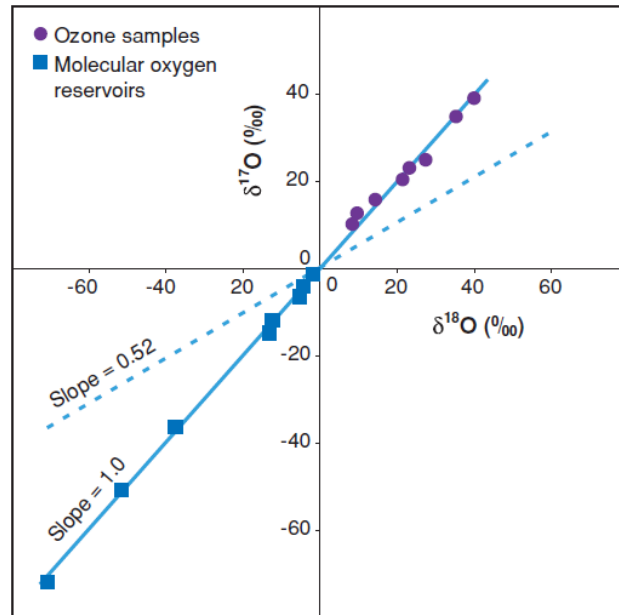
Figure 1.7: The upper figure shows the relation between $\delta^{17}O$ and $\delta^{18}O$ in atmospheric ozone. The lower figure depicts O-MIF of oxygen bearing atmospheric species; deviations from the terrestrial fractionation line (TFL) represent the magnitude of $\Delta^{17}O$. Credits: (Thiemens, 2006).

its production. Laboratory studies have been able to reproduce S-MIF from both reduced and oxidized sulphur compounds via high energy UV radiation (Farquhar, 2000). These results suggest that anomalous fractionations are generated by different photochemical processes, notably depending on the wavelength of the radiation interacting with sulphur compounds. The main photochemical reactions involved in the production of S-MIF are: photooxidation of SO_2 ($220 < \lambda < 320$ nm), photoexcitation of SO_2 ($240 < \lambda < 350$ nm) and SO_2 photolysis ($\lambda < 220$ nm) (Pavlov et al., 2005; Lyons, 2007; Ono et al., 2013; Whitehill et al., 2013, 2015; Ono, 2017).

Mass independent fractionations can be conserved in reaction products, especially in chemically stable compounds such as sulphates and nitrates. Notably, these species can be found in solid rocks and geological sediments from ancient eras, providing a geological record for the atmospheric processing of sulphur and nitrogen in the past. For instance isotopic fractionations from ancient sediments can give informations on the evolution of the oxidative properties of the atmosphere within different geological eras (Bao, 2015).Therefore, S-MIF and O-MIF store useful informations also for paleoclimate reconstructions. Sulphur deposits older than 2.45 Gyr have significant S-MIF which disappears with the advent of the Proterozoic era (Farquhar, 2000), as shown in **Fig.:1.8**. Model simulations suggest that low concentrations of atmospheric ozone should be responsible for the generation of S-MIF (Claire et al., 2014). As high values of S-MIF are observed in sulphate deposits from the Archean and the early Proterozoic, it has been suggested that throughout these eras sulphate might have been produced in absence of ozone, possibly in a reducing atmosphere. As most of atmospheric ozone is formed from O_2, S-MIF values similar to the ones found in Archean geological records should have been formed in oxygen poor atmosphere (e.g. $<10^{-5}$ of present day concentrations) (Pavlov and Kasting, 2002). The formation of S-MIF depends, indeed, on the exposure of sulphur compounds to highly energetic UV radiation, which is prevented by high concentrations of atmospheric ozone, hence O_2.

Nowadays, Δ^{33}S of atmospheric sulphate tends towards zero for sulphates produced at low altitudes below the ozone layer, hence for tropospheric produced sulphate (Ono, 2017). However, in the stratosphere S-MIF remains a good tracker for probing processing of sulphur trace gases for altitudes above the ozone layer (Thiemens, 2006; Whitehill and Ono, 2012; Whitehill et al., 2013, 2015).

4.2 Isotopic composition of atmospheric sulphates

Oxygen MIF provides crucial insight on the contribution of single SO_2 oxidation pathways during sulphate production. Notably, because sulphate O-MIF is inherited from atmospheric oxidants during SO_2 oxidation. In the troposphere sulphate can be generated, indeed, by the reactions of SO_2 with OH in the gas phase, and by H_2O_2, O_3, O_2/TMI, HOX (X = Br, Cl) and NO_2 in the liquid
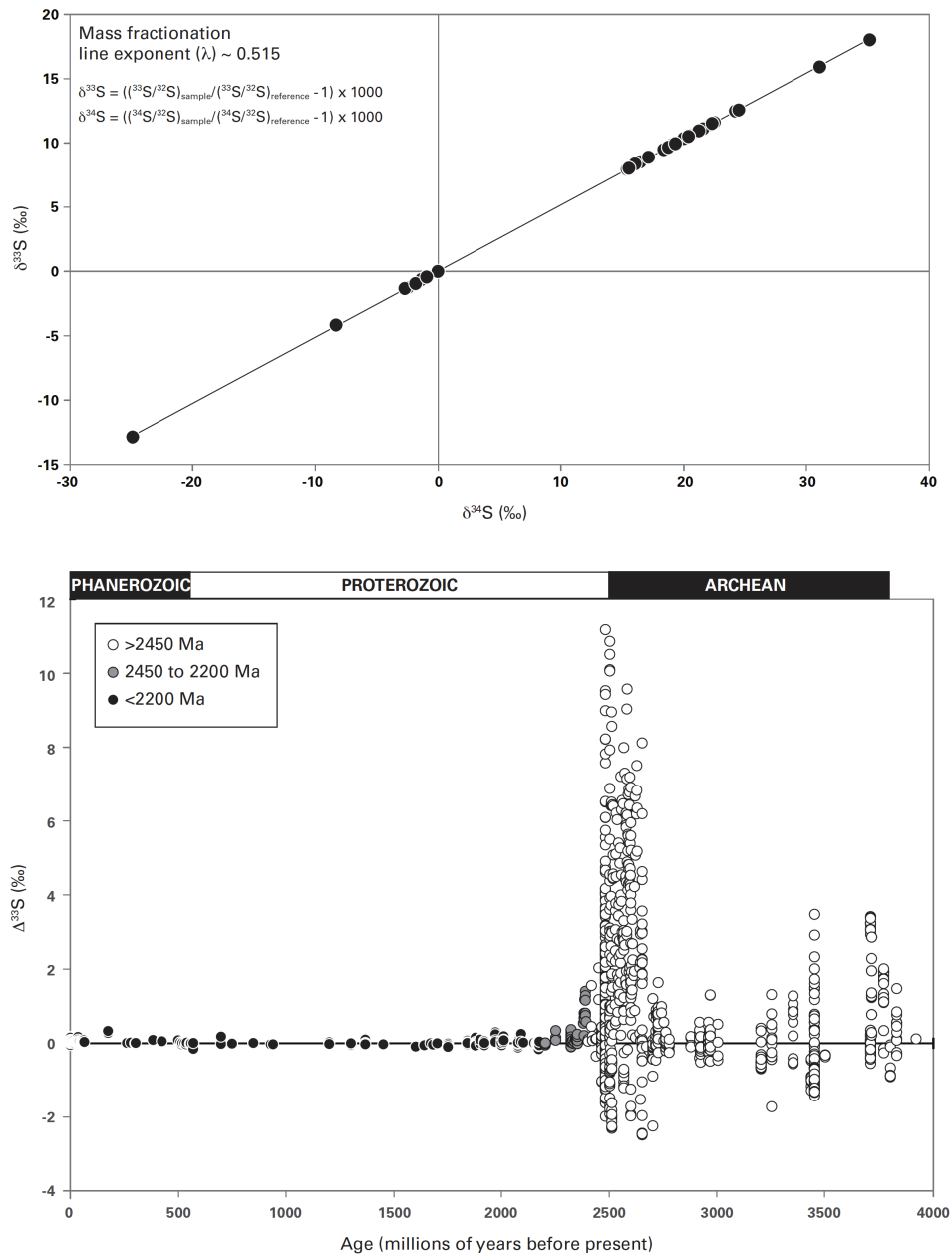
Figure 1.8: The upper figure shows the relation between δ^{34}S and δ^{33}S in terrestrial sulphur. Deviations from the TFL represent the magnitude of S-MIF. The lower plot shows the change in Δ^{33}S reported in sulphides and sulphates collected from sediment rocks formed before and after the Archean era. Deviations from the terrestrial fractionation line (TFL) disappear at the advent of the Proterozoic era. Credits: (Farquhar and Wing, 2003).

phase (Savarino et al., 2000; Harris et al., 2012b,c, 2013; He et al., 2014; Chen et al., 2017). The isotopic composition of the oxidants of atmospheric SO_2 are relatively well known, and, therefore, the contribution of different SO_2 oxidation channels from the final O-MIF of sulphate can be possibly inferred.

Atmospheric OH is produced by the reaction of $O^1(D)$ with water vapour. For mean tropospheric conditions the hydroxil radical does not carry O-MIF, and as a result tropospheric sulphates produced in the gas phase are characterised by $\Delta^{17}O$ of about 0 ‰ (Savarino et al., 2000). Atmospheric H_2O_2 has a $\Delta^{17}O$ of about 1.50-2.00 ‰ (Savarino and Thiemens, 1999a,b), generating sulphates with O-MIF of 0.87 ‰. Tropospheric O_2 molecules have a small negative $\Delta^{17}O$ of about -0.34 ‰ (Young et al., 2002, 2014; Martin et al., 2014), and they generate sulphates with O-MIF equal to -0.09 ‰ (considered MD since within the error limit of experimental measurements). Atmospheric HOX is supposed to have a high $\Delta^{17}O$, since its oxygen atom is directly inherited by ozone. However, because of the oxidation mechanism involved during sulphur oxidation it is suggested that produced sulphates carry $\Delta^{17}O \approx 0$‰ (see chapter 3 and 5). Atmospheric O_3 has $\Delta^{17}O(O_3^\star)$ of about 36‰, producing sulphate with O-MIF of about 9‰. Finally, the oxygen isotopic composition of NO_2 depends on its formation pathways, and it is highly dependent on environmental conditions. However, since most NOx is produced in presence of ozone, NO_2 shoukd carry positive O-MIF, producing sulphates with positive O-MIF.

Overall, tropospheric sulphates have $\Delta^{17}O$ around 1-2 ‰ (Lee and Thiemens, 2001; Patris et al., 2007). However, since sulphate can be generated at different chemical conditions within the troposphere, they carry different O-MIF depending on the peculiar environment where they have been produced. Sulphates from sea salt aerosols (SSA) are characterised by high positive $\Delta^{17}O$ between 1.0 and 7.3 ‰ (Alexander et al., 2005, 2012). The high alkaline environment, indeed, promotes the SO_2 heterogeneous oxidation via O_3, which is the dominant pathway of sulphate formation in the marine environment. Besides recent investigations suggest also significant contribution of HOX in the marine boundary layer (MBL), contributing to production of up to 30% of total sulphate produced above oceans (Chen et al., 2016, 2017).

Recent measurements and model simulations suggest the SO_2 oxidation catalysed by TMI could be the main pathway of sulphate production in clouds and in tropospheric aerosols (Alexander et al., 2009; Harris, 2013; Harris et al., 2014). Notably, it has been suggested that this sulphur oxidation channel might be particularly dominant in polluted environments, where the presence of dust and Fe(III) is enhanced by human activity (Han et al., 2016). Besides, anthropogenic sulphates are commonly characterised by O-MIF in the range of 1-2 ‰, which is in contrast to MDF fractionations formed during SO_2 oxidation by O_2/TMI. Recently, it has been observed that in large urban areas the SO_2 oxidation led by NO_2 could also contribute significantly to sulphate production (He et al., 2014), potentially justifying high O-MIF values observed on anthropogenic sulphates.

Different kind of informations can be gained by $\delta^{34}S$ of sulphate aerosols,

mostly regarding SO_2 emission sources. Sulphate $\delta^{34}S$ is mostly representative of kinetic or equilibrium isotopic effects involved during SO_2 production and atmospheric release. For instance, marine biogenic SO_2 has a $\delta^{34}S$ in the range of 14-22 ‰ (Rees and Holt, 1991), while anthropogenic SO_2 is characterised by $\delta^{34}S$ fractionations within of -5 and 7 ‰ (Krouse and Grinenko, 1991; Nielsen et al., 1991). Since $\delta^{34}S$ variations observed during SO_2 oxidation (Harris et al., 2012a,b,c) have to be specified for very constrained sources, it is rather difficult to use this variable for assessing tropospheric processing of SO_2.

4.3   Isotopic fractionations in volcanic sulphates

It is possible to distinguish sulphates generated during stratospheric eruptions, from those produced during tropospheric volcanic activity. Different MIFs are generated, indeed, by the processing of volcanic SO_2 in the troposphere and in the stratosphere, because of radically different environmental and chemical conditions. Notably, large differences in S-MIF and O-MIF are observed between volcanic sulphates generated in the troposphere or in the stratosphere.

Sulphur isotopes fractionations

Nowadays, S-MIF production is limited to the stratosphere, since high UV radiation is needed for the activation of sulphur photochemical reactions (Ono, 2017). Consequently, only sulphates from Plinian eruptions can display significant S-MIF, because of direct injection of the plume into the stratosphere (Savarino et al., 2003b; Baroni et al., 2008). During the last 15 years, useful informations have been gained from volcanic sulphates generated during Plinian eruptions and collected from ice cores in Antarctica. In particular, S-MIF presence has brought some informations on how SO_2 can be chemically processed in the stratosphere. $\Delta^{33}S$ for stratospheric volcanic sulphates of a same ice sample follow a temporal evolution along the depth of the sampled fragment, varying from an initial positive value of about +1 ‰ (deep-ice sulphates), to a final fractionation of -1 ‰ (shallow-ice sulphates) (Savarino et al., 2003a; Baroni et al., 2007, 2008). The activation of different photochemical reactions, SO_2 self-shielding, and fractional isotopic distillation (i.e. Rayleigh's distillation) are all responsible for the observed temporal trends. Remarkably, $\Delta^{33}S$ can provide informations on the activation of different SO_2 photochemical oxidation channels in the stratosphere at different stages after plume release, hence providing also some informations on chemical lifetime of volcanic SO_2 and photochemical reaction rates.

   S-MIFs are not the only sulphur isotopic fractionations that have been measured in volcanic gases. Notably, $\delta^{34}S$ fractionations are formed during SO_2 degassing. This sulphur MDF has potential application to the assessment of magmatic SO_2 degassing fluxes to the atmosphere; it is, indeed, peculiar to melts chemical speciation and degassing processes (Oppenheimer et al., 2013).
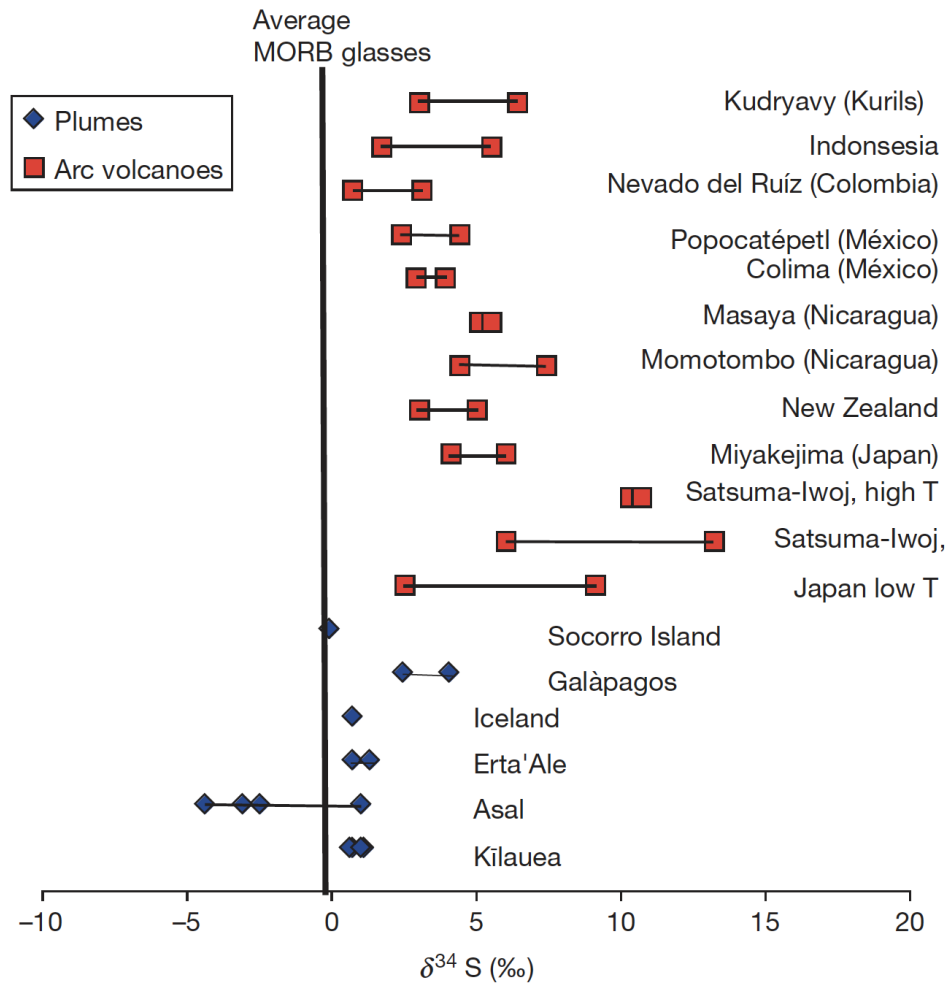
Figure 1.9: Fractionations in sulphur volcanic gases (SO_2 + H_2S) for different volcanic systems. The measurements were made combining fumarole and plume samples. Fractionations are compared to $\delta^{34}S$ of mid-ocean ridge basalt (MORB). Credits: (Oppenheimer et al., 2013).

The variables influencing the extent of $\delta^{34}S$ in volcanic gases are: the rate of sulphur degassing from melts, the compositional ratio SO_4^{2-}/S^{2-} of the magma, the ratio of SO_2/H_2S in the gas phase (proportional to the oxygen fugacity of gases and on the water content of melts) and the temperature of magma (Mandeville et al., 2009; De Moor et al., 2010; Oppenheimer et al., 2013).

Different $\delta^{34}S$ fractionations are observed for arc and plume volcanoes, and they are mostly linked to different speciation of sulphur trace gases, silica content and mineralization in melts of different systems. The table in **Fig.:1.9** summarises the experimental fractionation observed in volcanic sulphur gases for different volcanic systems. Plume and rift volcanic gases are characterised

25

by low δ^{34}S, and the average fractionation is between -2.8 and 3.5 ‰. On the contrary, volcanic sulphur volatiles from arc-volcanoes tend to be enriched in heavy sulphur isotopes; the average δ^{34}S is within 2.2 and 13.5 ‰. An important contribution to δ^{34}S is the geological origin of the sulphur of volcanic systems. Melts from arc-volcanoes are more enriched by sea water subducted directly into the mantle, which contributes significantly to the sulphur budget of melts (Oppenheimer et al., 2013). Since the isotopic fractionation of sea sulphate has δ^{34}S equal to 21 ‰, island arc volcanoes tend to be enriched in heavy sulphur isotopes (Alt et al., 1993). However, at the current state of knowledge it is difficult to apply volcanic δ^{34}S to the study of sulphur cycling within the mantle, and SO_2 degassing. Further investigations are, indeed, needed before being able to asses volcanic sulphur fluxes from degassing via MDF observed in volcanic sulphur volatiles. As a result, together with S-MIF, this parameter will be not further investigated during this study, also because the main purpose of this work is the investigation of volcanic SO_2 oxidation in the troposphere.

Oxygen isotopes fractionations

The stratosphere is characterised by low temperatures and dry conditions. Notably, liquid water cannot form because of immediate sublimation of ice crystals due to low pressure and temperatures (Seinfeld and Pandis, 2016). Volcanic SO_2 reaching the stratosphere cannot be oxidised in the aqueous phase, since water is mostly present as water vapour. Accordingly, in the stratosphere SO_2 is mostly oxidised by the gas phase reaction with OH (Bekki, 1995; Savarino et al., 2003a), and by a combination of photochemical reactions (Ono, 2017). Notably, OH is formed in the stratosphere with a very large Δ^{17}O(OH), since the rate of isotopic exchange with water vapour is very low due to the extremely dry conditions. Modelling experiments suggest that OH formed in the stratosphere should carry a Δ^{17}O(OH) with value between 2-45 ‰ (Lyons, 2001; Alexander et al., 2002), which is inherited by produced sulphate. Consequently, stratospheric volcanic sulphates are characterised by a large positive O-MIF, inherited from OH (Savarino et al., 2003a).

In the troposphere SO_2 can be oxidised via multiple reactions, notably in the aqueous phase. It is suggested, indeed, that most tropospheric SO_2 is oxidised via heterogeneous reactions in the liquid phase of atmospheric hydrometeros (Stevenson et al., 2003a; Berglen et al., 2004; Park et al., 2004; Alexander et al., 2009). Notably, during SO_2 oxidation sulphate with positive O-MIF are generated if SO_2 oxidation by O_3 and H_2O_2 are dominant, while sulphate with mass-dependent O-MIF are formed if SO_2 oxidation by O_2/TMI, HOX or OH prevail (Savarino et al., 2000; Alexander et al., 2009). In contrast to stratospheric volcanic sulphates, those produced in the troposphere do not carry significant positive O-MIF. On the contrary, tropospheric volcanic sulphates collected from volcanic ash-deposits are characterised by a Δ^{17}O $\approx$ 0.0$\pm$0.1‰ (Bao et al., 2003; Martin et al., 2014; Martin, 2018), independently to location in the globe.

26

This is also observed for volcanic sulphate collected very far from volcanic vents, in regions where secondary sulphate is expected to vastly dominate.

The lack of O-MIF in tropospheric volcanic sulphate is rather fascinating, since it suggests that SO_2 oxidation within tropospheric volcanic plumes follow peculiar reaction pathways, as for SO_2 oxidation on sea-salt aerosols, or on mineral dust and clouds (Alexander et al., 2005; Harris et al., 2012a,b,c). Within a volcanic plume there are, indeed, radically different chemical conditions if compared to the mean tropospheric composition. Notably, the combination of large SO_2 and halogens concentrations generate an extremely intricate chemical environment. Moreover, halogens chemistry should radically alter in-plume oxidants concentrations, since halogen radicals can destroy ozone via auto-catalytic reactions (Bobrowski and Platt, 2007; Roberts et al., 2009; von Glasow and Crutzen, 2013). For instance, halogens radicals might drastically reduce O_3 and OH concentrations within a plume, altering its oxidative conditions over the long run. At the same time, halogens are commonly thought to be washed out by in-plume particles and water droplets, and therefore halogens activation might not occur within water rich volcanic plumes. Mass dependent isotopic fractionations suggest a dominant contribution by SO_2 oxidation pathways producing mass-dependent sulphates, notably OH, O_2/TMI, or possibly HOX.

5   Objectives and study outline

Nowadays, it is still highly uncertain how tropospheric sulphate is generated within tropospheric plumes, since in-plume chemistry is very intrigued and complex. There is very little insight on volcanic sulphur oxidation in the troposphere because few investigations have focused on chemical processing of volcanic SO_2, in function of different volcanic emission scenarios.

The purpose of the present box-modelling study is to explore in detail the oxidation and fate of volcanic sulphur in tropospheric volcanic plumes. The final goal is to understand to what extent the chemical environment of a dense volcanic plume may affect sulphur dynamics and pathways of oxidation. Another purpose is to unveil the impact of halogens on in-plume chemistry, depending to different plume conditions. Notably, halogens reactivity influences tropospheric oxidants concentrations, and potentially volcanic sulphur oxidation and its tropospheric lifetime. In addition, also particles liquid phase, and water content might vary enormously within different plumes. The study is performed using a photochemical box-model, monitoring sulphate oxygen isotopic composition. Modelled sulphate O-MIF are used to validate model results from this work, and they are compared to oxygen isotopic compositions of tropospheric volcanic sulphates from volcanic ash-deposits from present and historical tropospheric eruptions (Bao et al., 2003; Martin et al., 2014; Martin, 2018).

Outline

To pursue this investigation CiTTyCAT has been enriched by a detailed sulphur heterogeneous chemistry scheme, describing SO_2 oxidation within cloud water droplets and within the liquid phase of volcanic sulphate aerosols (primary sulphates). The chemical scheme has been implemented also by an halogens heterogeneous chemical module, describing halogens heterogeneous reactions in plumes water droplets or sulphate aerosols. Finally, the chemical scheme is coupled to an oxygen isotopes transfer scheme, describing the evolution of O-MIF in produced and deposited sulphates. This work is structured as follows:

- The **second chapter** describes the modelling framework of CiTTyCAT, and the main physical and chemical processes added to the model to describe heterogeneous chemistry within water droplets or sulphate aerosols. In more details, the chapter focuses on heterogeneous chemistry, which is implemented differently depending on the composition of the liquid phase of volcanic plumes particles. Finally, the second chapter also describes the new oxygen isotopes transfer scheme added to the main framework of the model to describe O-MIF formation in tropospheric sulphates.

- The **third chapter** describes how the new version of CiTTyCAT has been applied to treat sulphur and halogens heterogeneous chemistry. In particular, there is a thorough description of: mass-transfer fluxes between gas phase and in-plume particles, volcanic gases partitioning between liquid and gas phases, pH evolution within cloud droplets, sulphur aqueous equilibria and dissociation, sulphur oxidation (within water droplets and concentrated sulphuric acid), and halogens heterogeneous chemistry.

- The **fourth chapter** includes a first application of the model. This study focuses on volcanic sulphur oxidation dynamics within a volcanic cloud in presence of high concentrations of SO_2, water and ash. Notably, the O_2/TMI, OH and H_2O_2 pathways relative importances are explored for different plume scenarios, within a range of plausible conditions for volcanic plumes. The modelled O-MIF are finally compared to the oxygen isotopic signatures measured on volcanic sulphates from tropospheric volcanic ash-deposits.

- The **fifth chapter** describes a second application of the model. The second investigation focuses on volcanic SO_2 oxidation in presence of halogens. In addition, this time the model investigates also SO_2 oxidation and relative sulphate isotopic signatures formed within sulphate aerosols, in absence of cloud water droplets. The aim of this second investigation is to determine the influence of volcanic halogens on in-plume oxidants concentrations, hence on sulphur oxidation dynamics. Notably, this time also the SO_2 oxidation reaction by HOX (HOX = HOCl + HOBr) is added

to the possible pathways of volcanic sulphate production. Halogens role on SO$_2$ oxidation is explored for different plume scenarios, notably with regards to halogens and sulphur loadings. Finally, the modelled isotopic signatures are compared to the oxygen isotopic signatures measured experimentally on sulphates from tropospheric volcanic ash-deposits.

- The **sixth chapter** collects the main outcomes of this work, and it suggest further perspective of investigation, or eventually model application.

CHAPTER 2

Modelling

"Everything should be made as simple as possible, but not simpler"

A. Einstein

1 Introduction

There are several approaches that can be used to study phenomena and their impacts. Typically, investigations can be conducted through laboratory experiments, observations and/or numerical modelling. The object of this study is the sulphur oxidation in volcanic plumes. Volcanic plumes are rather constrained unusual settings where the concentrations of emitted species and aerosols are high, creating a chemical environment very different from the surrounding (background) atmospheric conditions. Note that term "plume" here refers not only to dense plumes coming out of the volcanic emission source (e.g. crater) but also to volcanic clouds, i.e. air masses perturbed by volcanic emissions, advected by the winds and appearing totally detached from the emission sources.

The chosen approach to conduct this research is numerical modelling. A numerical model is a virtual simulator of reality. The design of a model and model experiments is highly dependent on the aspect of the question that is tackled and on the computing resources available. The main focus here is on the chemical environments of volcanic plumes, and on the physical-chemical processing and fate of chemically active sulphur and halogen species. For this reason, the dynamics of the plume are more or less ignored, or more precisely they are treated in a highly simplified. Without the high computing costs associated with model representations of dynamics, the chemistry scheme can be very detailed in the photochemical model. As it will be illustrated in the

31

later, a detailed description of chemistry including isotopes was needed to gain an accurate representation of the evolution of volcanic emissions.

Photochemical box-models are used to describe the evolution of chemical species concentrations in an air mass under the action of physical and chemical processes. These numerical tools simulate efficiently the effect of atmospheric chemical processes using chemical kinetics data. Because of their low computational costs, it is possible to describe the overall chemistry in a very detailed way, notably heterogeneous chemical processes resulting from the presence of liquid phases (sulphate aerosols, cloud droplets). Another advantage of box-models is that they allow to study the chemistry in atmospheric environments which are difficult to probe through direct measurements. For instance, it is difficult to carry out in-situ measurements in dangerous environments, or to make remote (often optical) measurements in optically dense plumes. In addition, key reactive short-lived species such as radicals are still very difficult to observe. Models simulate what is difficult or not possible to measure. Overall, photochemical box models appear to be efficient, cheap and simple tools for exploring the chemistry of volcanic plumes, without the risks and hazards linked to atmospheric measurements.

There are also downsides to the use of box models. The box-model is used here to simulate the average chemical composition of volcanic plumes. It is not adapted to resolve the specific chemical evolution of air masses composing the volcanic plume, i.e. the 3-D distribution of the plume chemical composition. In summary, the chemical heterogeneity of a volcanic plume is ignored. In addition, compared to more complex atmospheric models, a box-model is not adapted to investigate atmospheric processes whose effects extend on large spatio-temporal scales. In order to follow the evolution of chemicals at regional scales it is, indeed, necessary to couple photochemical schemes to transport schemes. One modelling framework to couple chemistry and dynamics is the Eulerian framework whose model grid is more or less regular and fixed. The resulting models are called Eulerian chemistry-transport models. Another possible approach is to advect chemical box models along multiple trajectories, as it is done in Lagrangian models. In principle the most accurate comparison of model simulations to specific experimental measurements is done by coupling the simulation of physico-chemical and transport processes. However, the first step is to explore the chemistry involved during the processing of volcanic emissions of chemically active species. The photochemical box-model used for this study is called CiTTyCAT. It is used to investigate volcanic sulphur chemistry and relative isotopic transfer during production of sulphates in the troposphere. CiTTyCAT is a well-established model which can accurately describe tropospheric photochemistry and atmospheric mixing (Evans et al., 2000; Real et al., 2007). Obviously, model results will need to be evaluated against experimental data.

In general, assessing the processing and ultimate fate of atmospheric species requires closing its budget which involves the quantification of both the burden and the fluxes (that is, source/sink rates) associated with the different

32

processes acting on the chemical species, such as emissions, chemical reactions, transport and deposition. Conventional methods rely mostly on models that are evaluated and constrained with atmospheric concentration measurements, because there is no direct means of measuring chemical fluxes associated with individual reactions (Morin et al., 2008). This represents a necessary but incomplete validation of models. In contrast, the measurement of isotopic composition of atmospheric species provides direct insights into the nature and importance of individual chemical fluxes (Brenninkmeijer et al., 2003). Therefore, physico-chemical models containing also a description of isotopes can be better evaluated and constrained using not only atmospheric concentration measurements but also isotopic measurements

The current chapter describes the development of the model and descriptions of physico-chemical processes. The processes implemented in CiTTyCAT are: mass transfer, aqueous chemistry of sulphur and halogens in cloud droplets, heterogeneous chemistry (i.e. reactive uptake) on sulphate aerosols, and an isotopic transfer scheme for sulphate production. The following section describes the heterogeneous chemistry framework used in the case of either water droplets, or sulphate aerosols. The third section deals with the overall sulphur chemistry scheme in the gas and aqueous phases. The final section illustrates how isotopic mass balance equations are implemented in the model to simulate the transfer of O-MIF from atmospheric oxidants to the sulphur oxidation end-product, sulphate. This new version of the model is then applied to investigate the fate of volcanic sulphur and the results are presented in the next chapters.

2   Mass-balance equations and kinetics of reaction

The evolution of atmospheric concentrations is described by mass balance equations and reaction kinetics. Mass conservation is expressed through the so-called continuity equation. Atmospheric processes treated in the model are: emissions, photochemical and chemical reactions (in the gas and liquid phases), mixing with background air, and mass loss due to deposition to the Earth's surface.

The continuity equation describes the production and destruction of species, as defined in Eq.:2.1.

$$\frac{d[C]_i}{dt} = \sum_j P_j - \sum_m L_m - D_i - M_i \qquad (2.1)$$

where: $[C]_i$,   concentration of i

         P_j,   production rate via channel j

         L_m,   loss rate via channel m

         D_i,   deposition rate of specie i

         M_i,   mixing rate of i with background air

Chemical reactions

Production and loss terms are defined by reaction rates, which are the product of reaction constants (k) and reactants concentration. In the chemical scheme, the temporal evolution of compounds is treated via differential equations (Eq.:2.2). Continuity equations are numerically integrated by CiTTyCAT equation solver.

$$\frac{d[C]_i}{dt} = \sum_j k_{(p,j)} \cdot [A] \cdot [B] - \sum_m k_{(l,m)} \cdot [C]_i \cdot [D] \qquad (2.2)$$

where: $k_{(p,j)}$,   reaction constant for the production via channel j

         $[A], [B], [D]$,   concentration of species A, B, D involved during production or loss of C_i

         $k_{(l,m)}$,   reaction constant for loss process of C_i via channel m

Reaction rates are estimated depending on the value of reaction rate constants. Arrhenius equations introduce reaction rates variability with temperature, hence reaction constants temperature dependence:

$$k_b(T) = A \cdot \left(\frac{T}{300} \right)^{-n} \cdot exp \left(\frac{-E_a}{RT} \right) \qquad (2.3)$$

where: A,   pre-exponential factor of the Arrhenius equation, proportional to specific collisional properties of the molecule

         n exponential term describing temperature dependence of the pre-exponential factor ($-1 < n < +1$, but mostly $n = 0$)

         T,   temperature of the system

         E_a,   activation energy for the reaction

         R,   universal gas constant

Termolecular reactions depend on the collision of three molecules to undergo gas-phase reactions. In CiTTyCAT, termolecular rate constants are reduced to effective second-rate constants, following Troe's formulation, as shown:

$$k_t(T, [M]) = \left(\frac{k_0(T) \cdot [M]}{1 + k_0(T) \cdot [M]/k_\infty(T)} \right) \cdot F^{\left(1+[log_{10}(k_0(T) \cdot [M]/k_\infty(T))]^2\right)^{-1}}$$

(2.4)

where:
$k_0(T)$, low-pressure limit rate constant
$k_\infty(T)$ high-pressure limit rate constant
$[M]$, atmospheric density
F, constant with 0.6 value

Photolysis rates are evaluated using the Fast-J code (Wild et al., 2000). Tropospheric photolysis reactions are calculated considering the presence of clouds and mean tropospheric aerosol loading. The Fast-J algorithm optimizes computational time by selecting seven specific wavelengths at which it evaluates photolytic intensity ($\bar{I}(\lambda_k)$). Wavelengths are selected within the range of 289-850 nm; these values represent the center of radiation bins for which weighted solar fluxes are calculated. Weighted solar fluxes are then used to evaluate photolysis constant (j_i), as illustrated:

Bin (nm)	1	2	3	4	5	6	7
BEGIN $\lambda_{k,7}$	289.00	298.25	307.45	312.45	320.30	345.00	412.45
END $\lambda_{k,7}$	298.25	307.45	312.45	320.30	345.00	412.45	850.00
AVERAGE $< \lambda >$	294.00	303.00	310.00	316.00	333.00	380.00	574.00

$$j_i = \sum_k \bar{\sigma}_i(\lambda_k, T) \cdot \bar{\phi}_i(\lambda_k, T) \cdot \bar{I}(\lambda_k) \cdot \Delta\lambda_k$$

(2.5)

where:
$\bar{\sigma}_i$, average cross-section of specie i in wavelength bin k
$\bar{\phi}_i$, average quantum yield of specie i for wavelength bin k
$\bar{I}(\lambda_k)$, actinic flux per wavelength bin
$\Delta\lambda_k$, wavelength bin

Deposition

Deposition is treated as a first-order process and it is applied only to species dissolved in cloud water droplets or contained in aerosols. Deposition rate coefficients (k_d) are assumed to be proportional to the mean lifetime of cloud

droplets or sulphate aerosols either in the free troposphere or in the boundary layer. Deposition rates are defined as:

$$D_i = -k_{(d,i)} \cdot [C]_i \qquad (2.6)$$

where: D_i,   flux of deposition
$k_{(d,i)}$ deposition constant of i, dependent on species average lifetime
$[C]_i$,   atmospheric concentration of i

Mixing

Mixing with background atmosphere is expressed by a sample first-order process. It is parametrised by a simple linear relaxation scheme, resulting in an exponential decay of plume concentrations towards background concentrations. Box dilution due to mixing is expressed as:

$$M_i = K_{mix} \cdot ([C]_i - [C]_{i,bck}) \qquad (2.7)$$

where: $M_{(i)}$,   mixing flux
K_{mix},   mixing rate
$[C]_i$,   concentration of specie i in the box
$[C]_{i,bck}$,   concentration of specie i in background atmosphere

Mixing rates reflect the magnitude of turbulence of the system. The higher the value of K_{mix} the higher is mass exchange with outside atmosphere.

3   Heterogeneous phase chemistry

Interactions between gas-phase molecules and liquids play an important role in the atmosphere, where liquid phase interactions are involved into a wide range of processes, such as: acid deposition, haze events, ozone depletion events, aerosols formation and regional climate.

In the atmosphere, the condensed phase can constitute a small volume compared to the gas phase. However, collisions between particles and atmospheric gases are rapid and they can occur on a large scale. For example in tropospheric clouds, where water droplets have an average radius of about 5 μm, the collision time is around 1 second. Considering an average 10^{-7} cloud

droplet-to-gas volume ratio, potential liquid phase interaction can significantly alter chemical processing of atmospheric gases if gas uptake is promoted (Davidovits et al., 2006). The initial uptake into atmospheric condensed phases is just one in a series of multiple steps involved in heterogeneous processing of chemical species. Following gas-particle collisions, liquid phase reactions can lead, indeed, to production of new chemical species, that can be released or further react in the condensed phase. Therefore, heterogeneous processes constitute a crucial step for atmospheric processing of chemical species.

The kinetics of gas-liquid interactions are difficult to asses both theoretically and experimentally. Analytical parametrization of all the steps involved in heterogeneous phase reactions is, indeed, rather complex. A theoretical framework that is widely used in atmospheric studies is the formulation of gas uptake. This model allows to decouple and incorporate most of the factors affecting gas-liquid interactions. The overall net gas-uptake is described by the uptake coefficient (γ_i). The net maximum flux of species i to the condensed phase is parametrised by $J_{i(tot)}$ (molecules $\cdot$ cm^{-2}s^{-1}), expressed as:

$$J_{i(tot)} = \frac{\gamma_i \cdot \overline{\nu}_i}{4} \cdot [C_i]$$
(2.8)

where: $[C_i]$,   is the concentration in the gas phase of i
           $\overline{\nu}_i$,   average molecular speed of i

In this mass-transport formulation γ_i expresses the general probability that a molecule enters into the condensed phase. In this scenario the γ_i is only limited by the accommodation of i into the liquid phase. However, for most atmospheric gases, the uptake coefficient into the condensed phase is not a constant parameter. It varies with time and especially with the change in the chemical composition of the condensed phase and the air. γ, indeed, encompasses multiple processes that influence the uptake of trace gases into the liquid phase, respectively: molecular diffusion in the gas phase, transfer through the gas-liquid interface, diffusion in the liquid bulk phase, liquid chemical reactions and all the saturation effects (Davidovits et al., 2006; Ammann et al., 2013). A schematic representation of the major processes affecting gas-particle interactions is shown in **Fig.:2.1**. All these interactions are highly influenced by the physico-chemical composition of gas and liquid phases.

In this new version of CiTTyCAT heterogeneous chemistry has been implemented differently for water droplets and atmospheric particles. Less informations are available for liquid phase reactions and equilibria in the condensed phase of atmospheric aerosols. Therefore, it is difficult to separately describe the single contributions involved during the uptake of chemical species on aerosols. However, the reactive uptake resistance model incorporates effects that cannot be easily included into the analytical formulation of aerosols liquid phase chemical equilibria.
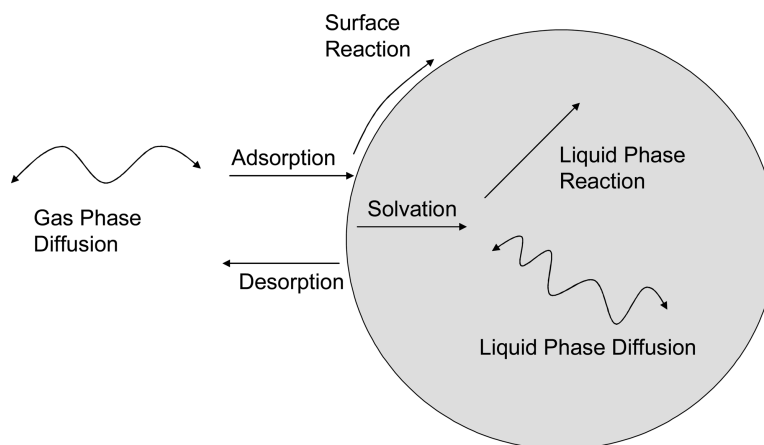
Figure 2.1: Visualization of main physical and chemical processes involved during the interactions of atmospheric gases and particles. Credits: (Davidovits et al., 2006).

Based on these premises, in this new version of CiTTyCAT aqueous phase chemistry is explicitly included (i.e. mass-transfers, aqueous chemical equilibria, aqueous chemical rates), while heterogeneous phase chemistry on the surface or within other atmospheric particles is treated implicitly via reactive uptake coefficients (γ_r). The latter includes all major contributions to uptake into a single variable.

3.1 Water droplets

The processes involved in the heterogeneous chemistry of cloud droplets are treated explicitly considering respectively the net mass flux to the liquid phase, and chemical reactions and equilibria within the aqueous phase.

Mass-transfer

When the species is dissolving in the droplets, one can assume thermodynamical equilibrium between the aqueous concentration of i in the sublayer and the gas phase concentration just above the liquid surface. This equilibrium is determined by the Henry's law coefficient of the species, included in the model via $[C_i]_s$ evaluation. In absence of significant liquid and gas phase limitations to uptake, the maximum gas-to-droplets flux ($J_{i(tot)}$) is limited by the rate at which molecules cross the interface between gas and liquid phase. This parameter described by the accommodation coefficient (α_i):

$$\alpha_i = \frac{N_{abs}}{N_{cls}} \qquad (2.9)$$

where: N_{abs}, number of gas molecules absorbed by the condensed phase
N_{cls}, number of gas molecule collisions with condensed phase

If the flux is limited by the accommodation at the surface, the kinetic regime flux to a single droplet of radius R_p is given by:

$$J_{K(i)} = \pi R_p^2 \overline{\nu}_i \alpha_i \cdot ([C_i] - [C_i]_s) \tag{2.10}$$

Considering:

$$[C_i]_s = p_i \cdot H_i \tag{2.11}$$

where: α_i, accommodation coefficient of species i onto liquid substrate
R_p, particle radius
$[C_i]_s$, concentration of specie i just above above the liquid surface
p_i, partial pressure of i
H_i, Henry's law coefficient of i

This flux approximation is valid only under kinetic regime, where the freepath of gas molecules is above the size of atmospheric particles. At these conditions, the rate of molecular dissolution is limited by the rate of kinetic collision. In most cases the rate of dissolution is governed by boundary conditions (e.g. competition between continuum and kinetic regimes), which are converged into the *transition regime* formulation.

The transition regime approach evaluates mass-transfer fluxes ($J_{(i)}$) through a more complex formulation, which matches the shift from kinetic to continuum regimes of dissolution depending on the size of atmospheric particles and on the thermodynamic properties of the system. Assuming r as the boundary reactive radius, Δ as the boundary distance from the surface of atmospheric particles, and R_p as the effective radius of particles, it is possible to define spatial regions and particle sizes at which continuum or kinetic regimes better constrain the rates of molecular dissolution. This approach is also defined as *flux matching*, and it assumes that: continuum theory applies to the region where the radius of atmospheric particles match $r \geq \Delta + R_p$, while kinetic regime applies to the region where $R_p \leq r \leq \Delta + R_p$. Therefore, assuming a Δ in the order of the freepath of trace gases, it is possible to switch from continuum to kinetic regimes depending on the conditions of gas-particle interactions. A schematic representation of the three different regimes of gas-particle interactions is represented in **Fig.:2.2**.

In order to parametrize the influence of temperature and pressure, mass fluxes are expressed in function of the Knudesen's number (K_n), a dimensionless parameter. The former variable represents the probability of encounter between molecules and suspended aqueous particles. Depending on the size of atmospheric particles with respect the mean molecular free path of i (λ_i), a correction factor is introduced to cover from the kinetic to the continuum regime
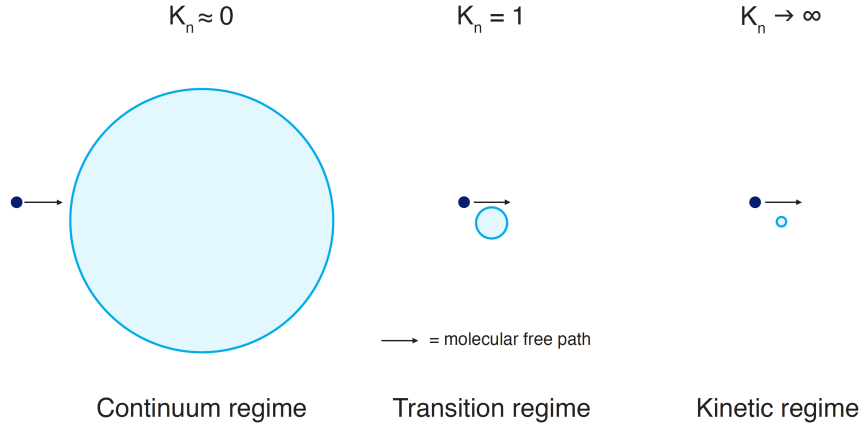
Figure 2.2: A schematic representation of the three main mass-transfer regimes for gas to liquid dissolution of atmospheric compounds into atmosphric particles.

(Seinfeld and Pandis, 2016). In our case, the expression for the transition regime correction factor is taken from Dahneke (Dahneke, 1983). Assuming that $\Delta = \lambda_i$, D_{air} as the diffusion coefficient of gas species in air, and the theoretical ratio between $J_{K(i)}$ and $J_{C(i)}$ (Seinfeld and Pandis, 2016), the final flux to a single droplet can be derived:

$$\frac{J_{K(i)}}{J_{C(i)}} = \frac{\alpha_i \cdot \overline{\nu_i}}{4 \cdot D_{air}} \cdot R_p \tag{2.12}$$

$$\frac{J_{(i)}}{J_{C(i)}} = \frac{1 + K_n}{1 + 2K_n(1 + K_n)/\alpha_i} \tag{2.13}$$

$$\frac{J_{(i)}}{J_{K(i)}} = \frac{J_{C(i)}}{J_{K(i)}} \cdot \frac{J_{(i)}}{J_{C(i)}} = \frac{4D_{air}}{\alpha_i \overline{\nu}_i R_p} \cdot \frac{1 + K_n}{1 + 2K_n(1 + K_n)/\alpha_i} \tag{2.14}$$

$$J_{(i)} = \pi R_p^2 \overline{\nu}_i \alpha_i \cdot \frac{4D_{air}}{R_p \overline{\nu}_i \alpha_i} \cdot \frac{1 + K_n}{1 + 2K_n(1 + K_n)/\alpha_i} \cdot ([C_i] - [C_i]_s) \tag{2.15}$$

$$J_{(i)} = 4\pi R_p D_{air} \cdot \frac{1 + K_n}{1 + 2K_n(1 + K_n)/\alpha_i} \cdot ([C_i] - [C_i]_s) \tag{2.16}$$

where:

$$K_n = \frac{\lambda_i}{R_p} = \frac{2 \cdot D_{air}}{\overline{\nu}_i \cdot R_p} \tag{2.17}$$

$$\lambda_i = \frac{2 \cdot D_{air}}{\overline{\nu}_i} \tag{2.18}$$

Note here that for $K_n \to \infty$:

$$\frac{J_{(i)}}{J_{C(i)}} \to \frac{\alpha_i}{2K_n} \tag{2.19}$$

While for $K_n \to 0$:

$$\frac{J_{(i)}}{J_{C(i)}} \to 1 \tag{2.20}$$

Aqueous phase reactions

Since the model CiTTyCAT resolves continuity equations for species with gas-phase concentration units, liquid phase concentrations in cloud water droplets (e.g. M) and rate constants have to be expressed into gas-phase units in the code in order to be treated by chemistry solver (Seinfeld and Pandis, 2016). Liquid phase reaction rates are converted to equivalent gas phase reaction rates considering the liquid water content (LWC) of the box. The LWC has different values depending on different cloud typologies, typically: mean saturated clouds (0.1 g m^{-3}), water-rich cumulus clouds (0.5-1 g m^{-3}), and cumulonimbus clouds (1-2 g m^{-3}) (Laj et al., 1997; Rosenfeld and Lensky, 1998; Pruppacher et al., 1998; Korolev et al., 2007; Carey et al., 2008).

Units have been converted to treat liquid phase rates in a gas-like fashion, via the following expression:

$$R_i(Ms^{-1}) = k_{i,l} \cdot [\mathrm{C}_i]_{(l)}[\mathrm{A}]_{(l)} \tag{2.21}$$

$$K_j^{l-g} = \frac{k_{(i,l)} \cdot 10^3}{N_A \cdot w_l} \tag{2.22}$$

$$R_i' = K_j^{l-g} \cdot [\mathrm{C}_j]^{l-g}[A]^{l-g} \tag{2.23}$$

where: N_a,   Avogadro's number
          w_l,   liquid water mixing ratio ($w_l = 10^{-6} \cdot LWC$)
          LWC,   liquid water content (liquid water suspended in 1 m^{-3} of air, g m^{-3})
          $[\mathrm{C}_i]_{l-g}$,   gas phase equivalent concentration of liquid species

Therefore, the LWC can play a crucial role in aqueous oxidation of chemical species, since it controls the extent of aqueous phase chemical rates. In this version of CiTTyCAT droplet radius is fixed, therefore, LWC controls also droplets concentration.

3.2 Sulphate aerosols

Reactive uptake

The uptake of atmospheric gases into sulphate aerosols is parametrised via a resistance model. This representation is based on an electrical circuit analog, where each process influencing the uptake is described as a resistance term. The overall uptake into liquid phase is decoupled into different resistances that can be combined in series or parallel to define the total rate of uptake. This new definition of the uptake coefficient includes all the heterogeneous processes into a single variable, defined by the reactive uptake coefficient (γ_r). The reactive uptake replaces γ_i in Eq.:2.8 to describe the overall net uptake of i in the liquid phase.

In the uptake resistor model gas-particle heterogeneous processes described in **Fig.:2.1** are typically split in gas, surface and resistances to uptake. The γ_r takes the following form:

$$\frac{1}{\gamma_r} = \frac{1}{\Gamma_{d,i}} + \frac{1}{\alpha_i} + \frac{1}{\Gamma_{b,i} + \Gamma_{sol,i}} \tag{2.24}$$

where: $\Gamma_{d,i}$,   gas-phase resistance to uptake
         α_i,   surface resistance to uptake (accommodation coefficient)
         $\Gamma_{b,i}$,   resistance to uptake due to liquid phase reactions
         $\Gamma_{sol,i}$,   resistance to uptake due to liquid solubility

The first term in the right side of the equation represents the resistance to the uptake due to gas-phase diffusion ($\Gamma_{d,i}$), and it is expressed as:

$$\frac{1}{\Gamma_{d,i}} = \frac{0.75 + 0.238 K_n}{K_n(1 + K_n)} \tag{2.25}$$

The value of α_i is usually given, and it is typically obtained by laboratory experiments. It is a molecular parameter that changes within different condensed phases (e.g. water droplet or sulphate aerosols).

When surface reactions are absent, the resistance due to solubility and liquid reactions are represented by two parallel resistances. The uptake coefficient evolves with time depending on solvation and liquid diffusion limits. Liquid saturation depends on the time of exposure of the liquid to gas species. Longer exposures induce saturation of the liquid phase and an enhancement of the resistance to uptake. The resistance due to saturation/solubility ($\Gamma_{sol,i}$) is expressed as:

$$\frac{1}{\Gamma_{sol,i}} = \frac{4H_i RT}{\overline{\nu}_i} \sqrt{\frac{\tau\pi}{D_{l,i}}} \qquad (2.26)$$

where: H_i,   Henry's law coefficient of of i
        R,   ideal gas constant
        τ,   particle exposure time to trace gases
        $D_{l,i}$,   liquid phase diffusion of species i

If chemical reactions are occurring in the liquid phase the resistance to uptake is lowered. The final resistance to uptake due to liquid phase reactions ($\Gamma_{b,i}$) is expressed as:

$$\frac{1}{\Gamma_{b,i}} = \frac{4H_i RT}{\overline{\nu}_i} \sqrt{D_{l,i} \cdot k'} \qquad (2.27)$$

where: k',   first order constant of liquid phase reaction

When liquid phase reactions are second order, they are converted to the equivalent pseudo-first order reactions. The reaction constant is expressed as $k' = k" \cdot [Y]$, where $[Y]$ is the concentration of the chemical species in excess in the liquid phase. However, if liquid phase reactions are faster than liquid diffusion in the gas phase, $\Gamma_{b,i}$ is expressed as a function of the reacto-diffusive length (l, cm):

$$l = \sqrt{\frac{D_{l,i}}{k'}} \qquad (2.28)$$

$$\frac{1}{\Gamma_{b,i}} = \frac{4H_i RT}{\overline{\nu}_i} \cdot \sqrt{D_{l,i} \cdot k_b'} \cdot [coth(R_p/l) - (l/R_p)] \qquad (2.29)$$

For atmospheric particles (e.g. aerosols small droplets), indeed, l can be in the order or even larger than the size of suspended particles, and the reacto-diffusive length introduces a dimensional constraint for which the volume of the particle limits the rate of uptake of gases. If $l > R_p$ the reactant can fill, indeed, the entire liquid phase and the uptake becomes limited by the volume of particles (Davidovits et al., 2006). A schematic representation of gas-particle interactions implemented in CiTTyCAT for water droplets and sulphate aerosols during this work is illustrated in **Fig.:2.3**.
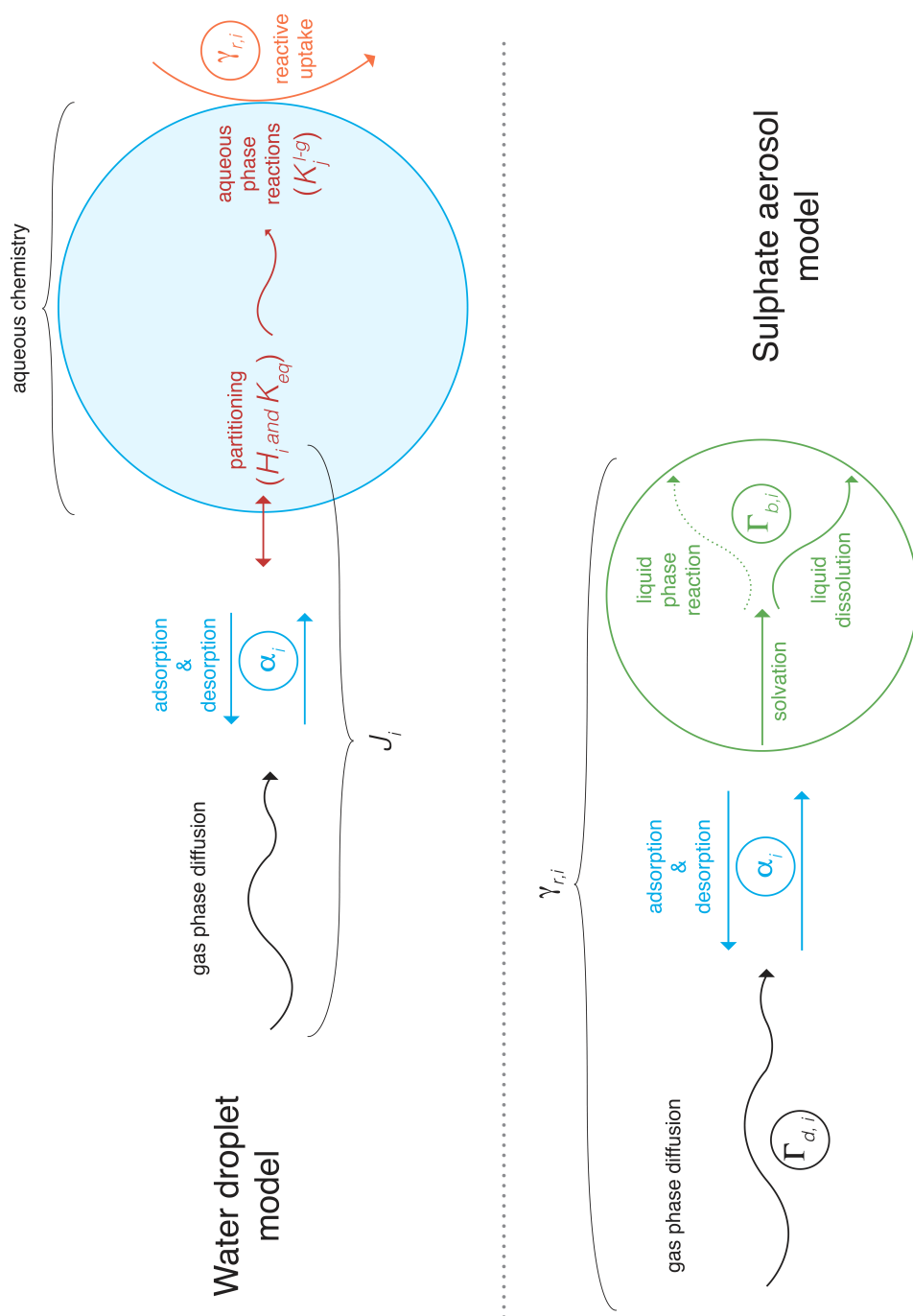
Figure 2.3: A schematic representation of gas-particle interactions implemented in CiTTyCAT.

4 Modelling O-MIF transfer

Ozone is a key chemical reactive species of the troposphere. Its isotopic anomaly is intrinsically generated (through photolysis and recombination reactions) instead of being inherited by isotopes transfer like for most atmospheric species (Marcus, 2013). Other oxygen-bearing species in the atmosphere can gain excess-^{17}O by transfer of this ozone anomaly via reactions with ozone itself, reactions with species that have already inherited the ozone anomaly, or via anomalous kinetic isotopic effect (Roeckmann, 1998; Lyons, 2001; Michalski et al., 2003).

Transfer of O-MIF among atmospheric species is process-specific and can be used as a signature to trace the chemistry of species as they react with specific oxidants. Once the isotopic anomalies of the oxidants are characterised, the resulting Δ^{17}O of an end-oxidation product is simply a linear combination of the isotopic signatures of all the oxidation channels weighted by their respective contributions, to the total production of the end-oxidation products. A fraction of the initial anomaly can be transferred from reactants to products during chemical reactions, resulting in process specific isotopic signatures. Therefore, once the number of oxygen atoms which are transferred from initial reactants during the oxidation is assessed, final isotopic compositions provide direct insights into the nature and importance of individual oxidation fluxes (Savarino et al., 2007; Morin et al., 2008; Martin et al., 2014).

In order to follow Δ^{17}O evolution of reaction products, isotopic transfer schemes are embedded into continuity equations. A new variable, the **Anomaly Product**, is defined by the product of mass equations and O-MIF transfers. Following mass-balance production and loss terms, the new isotopic mass-balance equation becomes:

$$\frac{d}{dt}\left([C] \cdot \Delta^{17}O(C)\right) = \sum_i \left(P_i \cdot \Delta^{17}O_i(C)\right) - \left(\sum_j L_j\right) \cdot \Delta^{17}O(C) \quad (2.30)$$

Considering that no other isotopic anomaly is introduced in the system, and that short term variations of Δ^{17}O are negligible, the O-MIF of a given species is equal to the Δ^{17}O induced by the combination of its different chemical sources, weighted on relative strength of single reaction transfer rates. The system, indeed, is assumed to be in a steady state. Therefore, if the system is in steady state, the final isotopic anomaly obeys Eq.:2.31:

$$\Delta^{17}O(C) = \frac{\sum_i \left(P_i \cdot \Delta^{17}O_i(C)\right)}{\sum_i P_i(C)} \quad (2.31)$$

In this new version of CiTTyCAT, the anomaly product is directly evaluated

by an external integration module implemented in the model. This approach does not affect significantly the results.

Solving the continuity equation

CiTTyCAT builds continuity equations through a chemical scheme compiler, DELOAD. The differential equations describing the evolution of chemical concentrations are resolved via a numerical integrator of differential stiff equation, SVODE (Evans et al., 2000). The structure of DELOAD does not allow to define an anomaly product hat could be integrated by the numerical integrator while being separated from the chemical scheme. Therefore, the temporal evolution of the anomaly product, hence O-MIF, is integrated via an external module that does not interfere with mass-balance continuity equations processed by SVODE. By doing so the chemical and the isotopic transfer schemes are totally separated and independent.

An accurate method to estimate precise solutions of ordinary differential equations is the 4th Runge-Kutta method (4th-RKM). This numerical method estimates the evolution of numerical variables, by using the projections of its derivatives at mid-points of integration. Considering the differential equation:

$$\frac{dy(t)}{dt} = y'(t) = f(y(t), t) \tag{2.32}$$

If initial conditions $y(t_0) = y_0$ are known, the following assumptions are true:

$$k_1 = f(y(t_0), t_0) \tag{2.33}$$

$$k_2 = f\left(y(t_0) + k_1\frac{h}{2}, t_0 + \frac{h}{2}\right) \tag{2.34}$$

$$k_3 = f\left(y(t_0) + k_2\frac{h}{2}, t_0 + \frac{h}{2}\right) \tag{2.35}$$

$$k_4 = f\left(y(t_0) + k_3 h, t_0 + h\right) \tag{2.36}$$

$$y(t_0 + h) = y(t_0) + \left(\frac{1}{6}k_1 + \frac{1}{3}k_2 + \frac{1}{3}k_3 + \frac{1}{6}k_4\right) \cdot h \tag{2.37}$$

where: $y(t_0)$, initial y value
h, time step
k_1, slope of the function at t_0
k_2, slope of the function half way through time step (evaluated

46

using slope k_1)

k_3,   slope of the function half way through time step (evaluated
using slope k_2)

k_4,   slope of the function as computed at full temporal step
(evaluated using slope k_3)

Final isotopic compositions are calculated considering that integration accuracies of the 4th-RKM do not deviate significantly from the ones of SVODE. As a result, CiTTyCAT integrates chemical concentrations, and the 4th-RKM estimates the temporal evolution of the anomaly product. The isotopic composition $\Delta^{17}\mathrm{O(C)}$ found on reaction products is therefore obtained by the ratio of the 4th-RKM AP with the concentration calculated by CiTTyCAT:

$$\Delta^{17}\mathrm{O(C)}_f(t) = \frac{[\mathrm{C}]_{RKM}(t)}{[\mathrm{C}]_{CTC}(t)} \cdot \Delta^{17}\mathrm{O(C)}_{RKM}(t) \qquad (2.38)$$

$$[\mathrm{C}]_{CTC}(t) = [\mathrm{C}]_{RKM}(t) \qquad (2.39)$$

$$\Delta^{17}\mathrm{O(C)}_f(t) \approx \Delta^{17}\mathrm{O(C)}_{RKM}(t) \qquad (2.40)$$

where: $[\mathrm{C}]_{RKM}(t)$,   [C] evaluated via 4th-RKM at time t

$[\mathrm{C}]_{CTC}(t)$,   [C] calculated by CiTTyCAT at time t

$\Delta^{17}\mathrm{O(C)}_{RKM}$ (t),   O-MIF evaluated via 4th-RKM at time t

Once isotopic signatures of single channels of reaction are known, the fraction of isotopic anomaly transferred by each pathway could be assessed.

The isotopic-chemical module implemented in this new version of CiTTy-CAT can be used to assess the isotopic composition of those chemical species whose oxygen isotopic signatures are constrained. Such is the case for example of tropospheric nitrates or sulphates. Throughout this study this new isotopes-chemical scheme is applied to sulphur heterogeneous chemistry of the troposphere. The aim is to reproduce observed isotopic signatures of volcanic sulphate, in order to assess the dominant sulphur oxidation pathways in tropospheric volcanic plumes.

CHAPTER 3

Application to volcanic plumes

CiTTyCAT is a well-established photochemical box model, which can accurately portray tropospheric photochemistry and atmospheric mixing. Previous versions of CiTTyCAT had included a very detailed description of the gas-phase tropospheric chemistry of key atmospheric chemical species. The model has been successfully used, indeed, to investigate the origin of polluted layer over the North Atlantic, and to infer information concerning the photochemical and physical processing of non methane hydrocarbons in the troposphere (Methven et al., 2006; Real et al., 2007; Arnold et al., 2007). CiTTyCAT has been also previously adapted to study atmospheric chemistry and nitrogen heterogeneous reactions in polar regions. Notably, implementation of the model chemical scheme with an isotopic transfer scheme accounting for $\Delta^{17}O$ production in nitrates has also proven successful in depicting seasonal isotopic composition of reactive nitrogen in polar regions (Morin et al., 2008).

CiTTyCAT older versions, however, miss a detailed chemical scheme covering multi-phase sulphur and halogen chemistry in the troposphere. Heterogeneous reactions occurring within water droplets and on sulphate aerosols are fundamental to evaluate chemical processing of volcanic emissions. Volcanic plumes are, indeed, rather constrained unusual settings where the concentrations of emitted species and aerosols are high. Notably, sulphur and halogens emissions create a chemical environment very different from the surrounding background atmosphere. In order to be able to use CiTTyCAT to probe volcanic plumes chemistry, the model had to be extended to include sulphur and halogens liquid and gas chemistry. As a matter of fact, the chemical scheme incorporated in previous version of the model had resulted too simplified for the purpose of this work. Based on theoretical framework displayed in the previous chapter, a new version of CiTTyCAT has been developed to include a detailed description

of sulphur and halogens chemistry. Notably, mass-transfer of chemical species, sulphur liquid chemistry (i.e. both within water droplets and sulphate aerosols), and halogens multi-phase reactions and radical cycles have been extensively implemented.

Atmospheric sulphur is oxidised to produce sulphate in both liquid and gas phases. Modelling simulations suggest that most tropospheric sulphur is oxidised in the liquid phase of aerosols and clouds(Chin and Jacob, 1996; Chin et al., 2000; Berglen et al., 2004). Experimental observations provide also extensive evidence that aqueous phase chemistry and heterogeneous reactions on reactive surfaces, such as iron dust, are among the main tropospheric sulphate sources (Harris, 2013; Harris et al., 2014; He et al., 2014; Han et al., 2016). As a result, there is significant interest related to the determination of aqueous and heterogeneous sulphate production channels.

Within volcanic emissions H_2O compose the bulk of gas emissions, constituting up to 90% of gaseous emissions in certain plumes (Textor et al., 2004; Oppenheimer et al., 2013). During explosive eruptions, presence of silicate mineral ash provides a reactive surface for heterogeneous reactions and for water to condense in volcanic plumes (Langmann, 2014). In condensing volcanic plumes, volcanic SO_2 might then be processed in both gas and liquid phases, because of high concentration of water and solid particles. Besides, during passive degassing volcanic water vapour might not reach saturation concentration, and just a fraction can be absorbed on primary particles within the plume. Among in-plume particles emitted at the vent primary sulphate are enough hygroscopic to attract water and form aqueous sulphate aerosols. In this scenario volcanic SO_2 can still be oxidised within non-condensing volcanic plumes either via heterogeneous reactions on sulphate aerosols, or by OH in the gas phase.

It is worth noticing that SO_2 oxidation within condensing and non-condensing volcanic plumes can be quiet different. Therefore, one could question if the nature of the condensed phase could control SO_2 lifetime and transport, while simultaneously governing in-plume sulphate production pathways, hence different volcanic SO2 processing in the troposphere over the long term. Isotopic composition of sulphate can provide informations on the origins and processing of SO_2 within volcanic plumes, becoming a constraint for budget and composition of volcanic sulphur emissions. Single channels of SO_2 oxidation are therefore explored within different plume scenarios. The corresponding isotopic signatures are then modelled via isotopic-transfer scheme to pinpoint SO_2 in-plume chemical processing within different scenarios.

This chapter focuses on reactions and physico-chemical processes that have been added to account for sulphur and halogens gas and liquid phase chemistry. The new extended chemical scheme have also been coupled to a new oxygen isotope scheme, that has enabled to monitor the transfer of oxygen isotopes during sulphur oxidation. The aim of this chapter is to describe in more details the heterogeneous reactions and the isotope transfer schemes that have been

applied to investigate volcanic sulphate production and isotopic composition. In more details, two different versions of CiTTyCAT have been developed to simulate either condensing volcanic plumes or non-condensing volcanic plumes. Notably, the condensed phase within the two models are different, and so are the physico-chemical schemes that have to be implemented. The first version of the model involves heterogeneous chemistry in water droplets (condensing volcanic plume), while the second version treats heterogeneous chemistry in sulphate aerosols (non-condensing volcanic plume). The first section of the chapter elucidates sulphur chemistry and sulphate production respectively in gas phase, water droplets, and in the bulk phase of sulphate aerosols. The second section describes halogen multiphase chemistry in water droplets and in the bulk phase of sulphate aerosols. The third and last section illustrates how sulphur oxidation reactions have been merged to the isotopic transfer scheme to track the isotopic composition of volcanic sulphates.

1 Sulphur chemistry

1.1 Gas phase oxidation of SO_2

The main SO_2 oxidation channel in the gas phase is the reaction with the hydroxil radical (Calvert et al., 1978). Almost 20% of tropospheric sulphate is generated by the reaction between SO_2 and OH (Tanaka et al., 1994; Berglen et al., 2004). Consequently, this pathway of sulphate production is still a major contributor to the budget of atmospheric sulphate.

OH production depends mostly on photodissociation of atmospheric ozone in presence of water. O_3 photolysis produces a singlet excited oxygen atom ($O^1(D)$), a highly reactive species which can relax only by colliding with other atmospheric molecules (quenching). Within the time $O^1(D)$ reaches its relaxed state the encounter with a water molecule results in OH radicals production (Seinfeld and Pandis, 2016).

$$a \cdot O_3 + h\nu \longrightarrow O + O_2$$
$$b \cdot O_3 + h\nu \longrightarrow O^1(D) + O_2$$

$$O^1(D) + M \longrightarrow O + M$$
$$O^1(D) + H_2O \longrightarrow 2\,OH$$
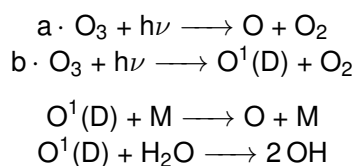
Atmospheric OH is produced in higher quantities during daytime hours while there are no significant channels of production during night-time hours, because of the lack of UV radiation.

In the atmosphere, sulphate production in the gas phase is initiated by the termolecular reaction between OH radicals and SO_2, followed by a series of multiple gas phase reactions:

$$SO_2 + OH + M \xrightarrow{k_1} HOSO_2 + M \quad k_1 = 3.2 \cdot 10^{-12} \text{cm}^3\text{mol}^{-1}\text{s}^{-1}$$
$$HOSO_2 + O_2 \xrightarrow{k_2} SO_3 + HO_2 \quad k_2 = 4.3 \cdot 10^{-13} \text{cm}^3\text{mol}^{-1}\text{s}^{-1}$$
$$SO_3 + H_2O \xrightarrow{k_3} H_2SO_4 \quad k_3 = 1.2 \cdot 10^{-15} \text{cm}^3\text{mol}^{-1}\text{s}^{-1}$$
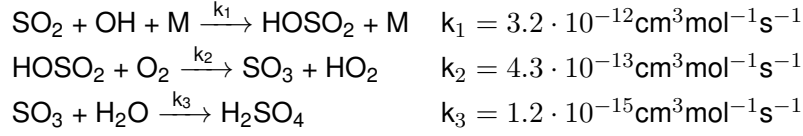
The first reaction is the limiting step to sulphate production, since it involves the contribution of three molecules to let the chemical reaction to take place. Eventually gaseous sulphate is produced by the reaction between SO_3 and H_2O.

1.2 Aqueous phase oxidation of SO_2

Gas SO_2 is mildly soluble in water, and it undergoes multiple dissociations to produce $SO_{2(aq.)}$, HSO_3^- and SO_3^{2-}. Dissociation of sulphur compounds is driven by liquid phase pH, so does sulphate production. In the model SO_2 compounds are grouped as follows in the S(IV) family:

$$[\text{S(IV)}] = [SO_2]_{(g)} + [SO_2]_{(aq.)} + [HSO_3^-] + [SO_3^{2-}] \tag{3.1}$$

Aqueous S(IV) species are partitioned in the liquid phase at different ratios depending on the following pH dependent equilibria:

$$SO_{2(g)} + H_2O \rightleftharpoons SO_{2(aq.)}$$
$$SO_{2(aq.)} \xrightleftharpoons{Ka_1} HSO_3^- + H_3O^+$$
$$HSO_3^- \xrightleftharpoons{Ka_2} SO_3^{2-} + H_3O^+$$
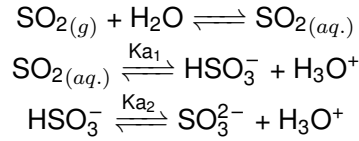
Where:

$$Ka_1 = \frac{[H^+][HSO_3^-]}{[SO_2]_{aq.}} \tag{3.2}$$

$$Ka_2 = \frac{[H^+][SO_3^{2-}]}{[HSO_3^-]} \tag{3.3}$$

SO_2 solubility depends on the pH of solution, and on the rate of S(IV) oxidation in the liquid phase. Gas-liquid partitioning is controlled by an effective Henry's law coefficient ($H_{SO_2}^*$), which links effective SO_2 dissolution to aqueous phase equilibria:

$$H_{SO_2} = \frac{C_{SO_2}}{p_{SO_2}} \tag{3.4}$$

$$H_{SO_2}^* = H_{SO_2} \cdot \left(1 + \frac{K_{a1}}{[H^+]} + \frac{K_{a1} \cdot K_{a2}}{[H^+]^2} \right) \tag{3.5}$$

where: K_{a1}, first dissociation equilibrium constant for S(IV)

K_{a2}, second dissociation equilibrium constant for S(IV)

$[H^+]$, concentration of hydrogen ions in water phase

Considering pH, $H^*_{SO_2}$, and water phase equilibria, S(IV) aqueous phase concentrations are evaluated iteratively as:

$$[SO_2]_{(aq.)} = H^*_{SO_2} \cdot p_{SO_2} \tag{3.6}$$

$$[HSO_3^-] = \frac{Ka_1 \cdot [SO_2]_{(aq.)}}{[H^+]} = \frac{Ka_1 H^*_{SO_2} p_{SO_2}}{[H^+]} \tag{3.7}$$

$$[SO_3^{2-}] = \frac{Ka_2 \cdot [HSO_3^-]}{[H^+]} = \frac{Ka_1 Ka_2 H^*_{SO_2} p_{SO_2}}{[H^+]} \tag{3.8}$$

Relative abundances of S(IV) aqueous compounds depending on pH are illustrated in **Fig.:3.1**.

Not only SO_2, but also sulphate can dissociate in aqueous solution to generate HSO_4^- and SO_4^{2-}. The first dissociation is virtually immediate and complete, and it is generally assumed that sulphate dissociates completely to HSO_4^- in the aqueous phase (Seinfeld and Pandis, 2016):
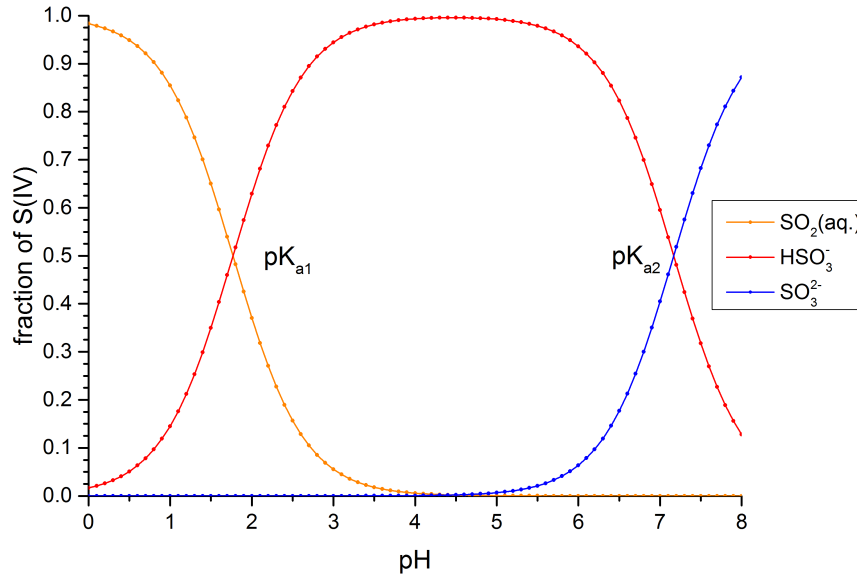
Figure 3.1: Partitioning of aqueous SO_2 depending on pH of liquid solution. Relative abundances are implemented depending on aqueous phase dissociation equilibria.

$$\text{H}_2\text{SO}_4 \xrightarrow{\text{K}_{s1}} \text{HSO}_4^- + \text{H}_3\text{O}^+$$

$$\text{HSO}_4^- \xrightleftharpoons{\text{K}_{s2}} \text{SO}_4^{2-} + \text{H}_3\text{O}^+$$
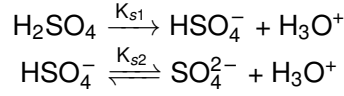
Where:

$$K_{s2} = \frac{[\text{H}^+][\text{SO}_4^{2-}]}{[\text{HSO}_4^-]} \tag{3.9}$$

In the model gaseous sulphate and sulphate aqueous species are grouped in the S(VI) family:

$$[\text{S(VI)}] = [\text{H}_2\text{O}_4]_{(g)} + [\text{HSO}_4^-] + [\text{SO}_4^{2-}] \tag{3.10}$$

In aqueous solution oxidation mechanisms are not the same for all aqueous S(IV) compounds, therefore sulphate production can also be controlled by pH. Certain oxidation reactions can only occur within specific pH ranges, because dissolved atmospheric oxidants react at different rates with different aqueous compounds from the S(IV) family (Seinfeld and Pandis, 2016).

Sulphate, halogens and nitric acid are the main acidic compounds which can be found in in the aqueous phases of volcanic plumes (Textor et al., 2004; Gerlach, 2004; Oppenheimer et al., 2013). Therefore, in this new version of CiTTyCAT, the pH of water droplets is evaluated iteratively at each timestep considering liquid phase concentrations of: HSO_3^-, SO_3^{2-}, HSO_4^-, SO_4^-, Br^-, Cl^- and NO_3^-. The balance equation describing pH evolution becomes:

$$[\text{H}^+] = [\text{HSO}_3^-] + 2 \cdot [\text{SO}_3^{2-}] + [\text{HSO}_4^-] + 2 \cdot [\text{SO}_4^-] + [\text{Br}^-] + [\text{Cl}^-] + [\text{NO}_3^-] \tag{3.11}$$

Henry's law coefficients

In the liquid phase of particles suspended in volcanic plumes, multiple gas species can dissolve in the liquid phase. Notably, dissolved O_3, H_2O_2, and HOX (HOX = HOBr + HOCl) can react with S(IV) to produce S(VI).

Dissolution rates are governed by Henry's law coefficients, or by effective Henry's law coefficients. Species gas-liquid partitioning depends on temperature, as Henry's law coefficient are not constant parameters. The temperature dependence of Henry's law coefficients is given by the Van't Hoff equation:

$$H_i(T_1) = H_i^0 \cdot exp\left[\frac{-\Delta H_i}{R} \cdot \left(\frac{1}{T_1} - \frac{1}{T_0}\right)\right] \tag{3.12}$$

And:

$$C_i^{diss}(T) = H_i(T) \cdot p_i \tag{3.13}$$

where:
    H_i^0,   Henry's law coefficient for i at standard conditions
    ΔH_i,   enthalpy for solution
    R,   ideal gas constant
    C_i^{diss},   concentration of i dissolved in the liquid phase
    p_i,   partial pressure of i in the gas phase

Table 3.1: Henry's law coefficients and physical parameters used during water droplets (WD) simulations.

Specie	H^0 (M)	$\Delta H_i/R$ (K)	α_i
sulphur dioxide			
SO_2	1.24	3100.	$1.1 \cdot 10^{-1}$
ozone			
O_3	$9.40 \cdot 10^{-3}$	2300.	$1.0 \cdot 10^{-2}$
hydrogen peroxide			
H_2O_2	$7.45 \cdot 10^4$	7000.	$1.8 \cdot 10^{-1}$
hydrochloric acid			
HCl	19.0	600.	$6.4 \cdot 10^{-2}$
chlorine			
Cl_2	$9.30 \cdot 10^{-2}$	2300.	$5.1 \cdot 10^{-5}$
hypochlorous acid			
HOCl	$6.60 \cdot 10^2$	5900.	$6.0 \cdot 10^{-2}$
hydrobromic acid			
HBr	25.0	370.	$6.8 \cdot 10^{-2}$
bromine			
Br_2	$7.60 \cdot 10^{-1}$	3720.	$3.0 \cdot 10^{-2}$
hypobromous acid			
HOBr	$1.32 \cdot 10^3$	5900.	$6.0 \cdot 10^{-1}$
bromine monochloride			
BrCl	$9.40 \cdot 10^{-1}$	5600.	$3.3 \cdot 10^{-1}$
nitric acid			
$HONO_2$	$2.10 \cdot 10^5$	8700.	$5.4 \cdot 10^{-2}$
sulphuric acid			
H_2SO_4	∞		$6.5 \cdot 10^{-1}$

Henry's law coefficient's used for WD are from R. Sander's tabulations for water as a solvent (Sander, 2015). Accommodation coefficients are implemented for water particles and from JPL's evaluations (Sander et al., 2006).

Henry's law coefficients for the main atmospheric soluble species integrated in the new chemical scheme are summarised in Table:3.1. Reported values are typical for water as a condensed phase and they have been taken from JPL's datasheet (Sander, 2015).

It is important to stress out that in this new version of CiTTyCAT liquid phase

diffusion is considered instantaneous within the liquid phase. It is assumed, indeed, that S(IV) and other species concentrations are uniform within the liquid phase. As a consequence, aqueous reaction rates are considered uniform throughout water droplets.

1.3   Sulphate production in water droplets

Following the aqueous phase chemistry scheme recently implemented in CiTTy-CAT, each S(IV) aqueous oxidation rate is expressed as:

$$-\left(\frac{d[\text{S(IV)}]}{dt}\right)_j = K_j^{l-g} \cdot [\text{S(IV)}]^{l-g}[\text{C}_j]^{l-g} \qquad (3.14)$$

where: K_j^{l-g}, j aqueous rate constant of reaction in gas-
                                phase equivalent (conversion into gas-phase units)
        $[\text{S(IV)}]^{l-g}$,   S(IV) gas-phase equivalent aqueous concentration
        $[\text{C}_j]^{l-g}$,   oxidant gas-phase equivalent aqueous concentration

This new version of CiTTyCAT describes explicitly not only the exchanges of soluble species of interest between gas phase and cloud droplets (e.g. S(IV), O_3, H_2O_2, SO_2, HOX and H_2SO_4), but also aqueous chemistry. Notably, sulphate production reactions are implemented for each S(IV) aqueous species.

Aqueous S(IV) oxidation by dissolved O_3

$$SO_{2(aq.)} + O_3 \xrightarrow{k_0} S(VI) + O_2$$
$$HSO_3^- + O_3 \xrightarrow{k_1} S(VI) + O_2$$
$$SO_3^{2-} + O_3 \xrightarrow{k_2} S(VI) + O_2$$
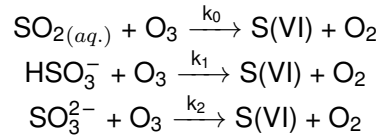
$$-\frac{d[\text{S(IV)}]}{dt} = \left(k_0[SO_{2(aq.)}] + k_1[HSO_3^-] + k_1[SO_3^{2-}]\right) \cdot [O_3] \qquad (3.15)$$

where: $k_0 = 2.4 \cdot 10^4 \cdot \text{M}^{-1}\text{s}^{-1}; k_1 = 3.7 \cdot 10^5 \cdot \text{M}^{-1}\text{s}^{-1}; k_2 = 1.5 \cdot 10^9 \cdot \text{M}^{-1}\text{s}^{-1}$

Ozone can dissolve in water solutions and it reacts with each compound from the S(IV) family (Seinfeld and Pandis, 2016). S(VI) oxidation via O_3 reaction is crucial at pH above 5, such for cloud droplets and sea-salt aerosols (SSA) in the marine boundary layer (MBL) (Alexander et al., 2005, 2012). At alkaline pH the oxidation rate can grow up to four orders of magnitude, hence the reaction can account as a major sulphate production channel. This reaction, however, is self-limiting, since S(VI) production enhances acidity in aqueous solutions, thus slowing down the overall oxidation rate.

At average atmospheric conditions atmospheric hydrometeors pH is around 3 - 6 (Faloona, 2009), and S(IV) is mostly found as HSO_3^-. In volcanic clouds,

however, dissolution of halogens halides and sulphate in plume water droplets can induce a rather acidic pH (e.g. below 4) (Langmann, 2014). It is therefore expected that S(IV) by O_3 would not compete significantly with other sulphur aqueous oxidation pathways in volcanic plumes.

Aqueous S(IV) oxidation by dissolved H_2O_2

$$HSO_3^- + H_2O_2 \overset{K}{\rightleftharpoons} SO_2OOH^- + H_2O$$
$$SO_2OOH^- + H^+ \xrightarrow{k_{H_2O_2}} + S(VI)$$

$$-\frac{d[S(IV)]}{dt} = \frac{k_{H_2O_2}[H^+][H_2O_2][HSO_3^-]}{1 + K[H^+]} \tag{3.16}$$
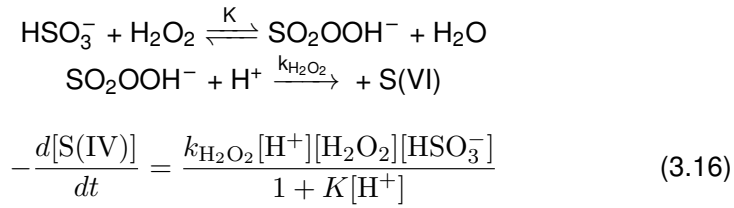
where: $k_{H_2O_2} = 7.5 \cdot 10^7 \cdot M^{-2} s^{-1}$; $K = 13 \cdot M^{-1}$

At atmospheric pH, the most competitive sulphate production channel is the reaction of HSO_3^- with dissolved H_2O_2. The reaction is very fast and S(IV) rarely coexist with H_2O_2 in the aqueous phase, thus being commonly depleted from the core of tropospheric clouds (Zuo and Hoigne, 1993; Laj et al., 1997). Atmospheric H_2O_2 is generally formed as a byproduct of the HO_x cycle, or by anthropogenic activity, and it in remote areas H_2O_2 is found at 0.5 ppbv concentrations (Herrmann et al., 2000).

Because of relatively low pH values in in volcanic cloud droplets, it is expected that H_2O_2 would contribute significantly to S(VI) production. Besides, S(IV) partitioning shifts towards $SO_{2(aq.)}$ as acidity increases in the aqueous phase. Therefore, enhanced S(VI) production might inhibit S(IV) reaction with H_2O_2 over the long run.

Aqueous S(IV) oxidation by dissolved O_2 catalysed by Iron and Manganese

$$S(IV) + \frac{1}{2}O_2 \xrightarrow{TMI} S(VI) \quad TMI = Fe(III) + Mn(II)$$

$$-\frac{d[S(IV)]}{dt} = 750 \cdot [Mn(II)] \cdot [S(IV)] + 2600 \cdot [Fe(III)] \cdot [S(IV)] +$$
$$+ 1.0 \cdot 10^{10} \cdot [Mn(II)] \cdot [Fe(III)] \cdot [S(IV)] \tag{3.17}$$
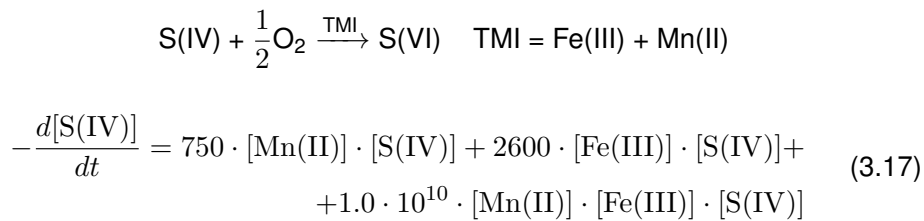
In the aqueous phase, transition metal ions (TMI) can catalyse the oxidation of S(IV) by dissolved O_2. Iron acts as an efficient oxidation catalyst when in the ferric state (Fe(III)), while manganese has catalytic effects in the Mn(II) oxidation state. In atmospheric droplets Fe(III) is present at concentrations around 0.3-2.0

μM (Seinfeld and Pandis, 2016), while Mn(II) is generally found at concentrations around 0.1·[Fe(III)]. In water solutions, interaction within metals generate a synergistic effect that enhances the S(IV) oxidation by O_2 (Brandt et al., 1994; Brandt and van Eldik, 1995). The pseudo first-order constant of reaction is proportional to concentrations of both iron and manganese, as illustrated above in Eq.:3.17

Growing evidence suggests that this SO_2 oxidation channel contributes largely to the budget of atmospheric sulphate, especially when high concentrations of TMI can be reached in solution (Harris et al., 2012c; Harris, 2013; He et al., 2014; Han et al., 2016). During explosive eruptions coarse material can be emitted in the form of ash. Because of enhanced acidity and of magmatic mineral composition, significant amounts of Fe(III) can be released from the solid phase (Langmann, 2014). It is therefore expected that this oxidation channel might contribute significantly to S(VI) in-plume production.

Aqueous S(IV) oxidation by dissolved HOX

$$SO_3^{2-} + HOX \xrightarrow{k_{(SO_3^{2-},X)}} XSO_3^- + OH^-$$
$$XSO_3^- + OH^- \longrightarrow SO_4^{2-} + X^- + 2H^+$$

$$HSO_3^- + HOX \xrightarrow{k_{(HSO_3^-,X)}} XSO_3^- + H_2O$$
$$XSO_3^- + H_2O \longrightarrow SO_4^{2-} + X^- + 2H^+$$
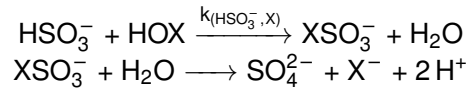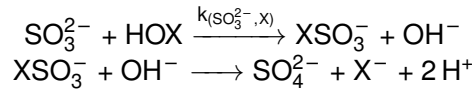
$$-\frac{d[\text{S(IV)}]}{dt} = k_{(HSO_3^-,X)}[HSO_3^-][HOX] + k_{(SO_3^{2-},X)}[SO_3^{2-}][HOX] \quad (3.18)$$

where: $k_{(HSO_3^-,Cl)}$, 7.6· $10^8 M^{-1} s^{-1}$ (Fogelman et al., 1989)
$\quad\quad\quad\quad k_{(HSO_3^-,Br)}$, 3.2· $10^8 M^{-1} s^{-1}$ (Liu and Margerum, 2001)
$\quad\quad\quad\quad k_{(SO_3^{2-},Cl)}$, 7.6· $10^8 M^{-1} s^{-1}$ (Fogelman et al., 1989)
$\quad\quad\quad\quad k_{(SO_3^{2-},Br)}$, 5.0· $10^9 M^{-1} s^{-1}$ (Troy and Margerum, 1991)

There is growing evidence that in the marine boundary layer (MBL) and on sea salt aerosols (SSA), the reaction between S(IV) and HOX can promote S(VI) production (Vogt et al., 1996; Von Glasow et al., 2002b; Chen et al., 2016). At alkaline pH typical of aerosols and clouds of the MBL (Faloona, 2009), the HOX (HOX = HOBr + HOCl) oxidation pathway might account for as much as 33-50% of total sulphate produced (Chen et al., 2016). On a global scale the oxidation of S(IV) operated by hypohalous acids (HOX) contributes at lower extents, and model simulations and isotopic constraints suggest, indeed, that these reactions might account for 8% of global sulphate production (Chen et al., 2017). The reaction is initialised by the nucleophilic attack of S(IV) on HOX. It follows a

quick hydrolysis of the reaction product, hence S(VI) formation. There are some uncertainties regarding reaction rate constants, and single contribution of HOX species to S(IV) oxidation. Notably, there is a lack of informations concerning HSO_3^- oxidation by HOCl. As a consequence, in the new version of CiTTyCAT it is assumed that $k_{(HSO_3^-, Cl)}$ has the same value as $k_{(SO_3^{2-}, Cl)}$ (Schmidt et al., 2016; Chen et al., 2016). This assumption does not to significantly affect the overall S(IV) oxidation rate.

Halogens are commonly emitted in volcanic plumes together with sulphur (Textor et al., 2004; Mather et al., 2006). HOX can be produced in volcanic plumes as a result of halogens heterogeneous chemistry (see Chapter 5 for detailed halogens chemistry). No studies on SO_2 oxidation in volcanic clouds and plumes have been conducted so far, and there are little informations on the impact of halogen chemistry during the oxidation of volcanic SO_2 in the troposphere. However, it is expected that S(IV) oxidation by HOX might contribute significantly to S(VI) production because of the high halogens concentrations within volcanic plumes.

1.4 Heterogeneous oxidation of SO$_2$: reactive uptake

Concentrated sulphuric acid solutions (sulphate aerosols) constitute the condensed phase of non-condensing volcanic plumes from passive degassing (Mather et al., 2003). When relative humidity is above 40%, sulphate particles are composed by a mixture of liquid water and sulphate (Ammann et al., 2013). However, liquid phase pH can be incredibly low reaching values around 0 (Allen et al., 2002). In liquid phase, at pH values below 3 SO_2 oxidation can still occur via the reactions with O_2/TMI and H_2O_2. Besides, chemical reactions within sulphate aerosols are difficult to parametrise because of lack of informations regarding the reaction mechanisms occurring in sulphur acid. Consequently, chemical reactions occurring in sulphate aerosols are implemented via the reactive uptake formulation. It is the case for both halogens and sulphur species. In particular, SO_2 oxidation is also modelled via reactive uptake of SO_2.

In sulphate aerosols, high acidity influences the chemical environment of the solution. The overall chemical activity of sulphate aerosols solutions does not dependent only on the chemical activity of liquid water (α_{H_2O}). Notably, S(IV) reaction rate constants need to be corrected to account for the chemical activity of hydrogen ions (a_H^+). This parameter is extrapolated from sulphate aerosols mass composition (wt, %) (DeMore et al., 1997; Sander et al., 2006), as following illustrated:

$$a_H^+ = e^h \tag{3.19}$$

Where:

$$h = 60.51 - 0.095 \cdot wt + 0.0077 \cdot wt^2 - 1.61 \times 10^{-5} \cdot wt^3 -$$
$$(1.76 + 2.52 \times 10^{-4} \cdot wt^2) \cdot T^{0.5} + \frac{(-805.89 + 253.05 \cdot wt^{0.076})}{T^{0.5}} \qquad (3.20)$$

And:

$$\alpha_{H_2O} = \frac{p_{H_2O}}{p_{H_2O}^o} \qquad (3.21)$$

where: $p_{H_2O}^o$,   saturation water vapour pressure (mbar)
         p_{H_2O},   partial pressure of water (mbar)

At low pH S(IV) is present in solution as $SO_{2(aq.)}$ and to a smaller extent as HSO_3^-. In order to investigate the contribution of S(IV) oxidation by O_3, H_2O_2, HOX, the respective reaction constants ($k_{ox.}$) are corrected to account for sulphuric acid chemical activity (Rattigan et al., 2000), as following illustrated:

$$k_{O_3}^{'} = k_{0(O_3)} \cdot \frac{K_{a1} \cdot \alpha_{H_2O}}{a_H^+} \qquad (3.22)$$

$$k_{H_2O_2}^{'} = k_{H_2O_2} \cdot \frac{K_{a1} \cdot \alpha_{H_2O}}{a_H^+} \qquad (3.23)$$

$$k_{HOX}^{'} = k_{HOX+HSO_3^-} \cdot \frac{K_{a1} \cdot \alpha_{H_2O}}{a_H^+} \qquad (3.24)$$

Where K_{a1} represents the first S(IV) dissociation constant. The new reaction constants are used to estimate single SO_2 uptake coefficients. Values used to evaluate SO_2 reactive uptakes are summarised in Table:3.3. The total SO_2 net uptake on sulphate aerosols is evaluated considering liquid phase reactions as parallel resistances:

$$\frac{1}{\gamma_{tot}} = \frac{1}{\Gamma_d} + \frac{1}{\alpha} + \frac{1}{\Gamma_{(b,tot)}} \qquad (3.25)$$

Where:

$$\frac{1}{\Gamma_{(b,tot)}} = \frac{1}{\sum_i \Gamma_{(b,i)}} = \frac{1}{\Gamma_{(b,H_2O_2)} + \Gamma_{(b,HOX)} + \Gamma_{(b,O_3)} + \Gamma_{(b,O_2)}} \qquad (3.26)$$

Recall that in the resistor model the bulk phase resistance to uptake $\Gamma_{b,i}$ is expressed as a function of the reacto-diffusive length (l, cm) and species Henry's law coefficients:

$$l = \sqrt{\frac{D_{l,i}}{k'_{ox.}}} \tag{3.27}$$

$$\frac{1}{\Gamma_{(b,i)}} = \frac{4H_i RT}{\overline{\nu}_i} \cdot \sqrt{D_{l,i} \cdot k'_{ox.}} \cdot [coth(R_p/l) - (l/R_p)] \tag{3.28}$$

Preliminary estimations in our case show that the major resistance to reactive uptake of SO_2 originates from processes in the bulk phase of sulphate aerosols (see Table:5.2). Therefore, it is possible to approximate the net reactive uptake coefficient to:

$$\gamma_{tot} \approx \sum_i \Gamma_{(b,i)} \tag{3.29}$$

Table 3.2: Major resistances evaluated for single SO_2 reactive uptake channels in the resistor model

Aqueous reaction	$\frac{1}{\Gamma_d}$	$\frac{1}{\alpha_{SO_2}}$	$\frac{1}{\Gamma_{(b,i)}}$
$SO_2 + O_3$	15	10^6	8.4×10^{19}
$SO_2 + H_2O_2$	15	10^6	1.5×10^{16}
$SO_2 + O_2$ /TMI	15	10^6	3.1×10^{20}
$SO_2 + HOX$	15	10^6	5.3×10^{29}

Table 3.3: Henry's law coefficients and physical parameters used during sulphate aerosols (SA) simulations.

Specie	α_i	H (M)	$k_{ox.}$
hydrogen peroxide			K = 13 M^{-1}
H_2O_2	8.0×10^{-4}	see Ref.	$7.5 \cdot 10^7 M^{-2}s^{-1}$
hypobromous acid			
HOBr	0.05	see Ref.	$7.6 \cdot 10^8 M^{-1}s^{-1}$
hypochlorous acid			
HOCl	0.06	see Ref.	$3.2 \cdot 10^8 M^{-1}s^{-1}$
ozone			
O_3	1.47×10^{-6}	see Ref.	$2.4 \cdot 10^4 M^{-1}s^{-1}$
oxygen			
O_2			see Eq.:3.17

The values for Henry's law coefficient and accommodation coefficients for SA simulations are taken from JPL's datasheets (DeMore et al., 1997; Sander et al., 2006).

It follows that the total rate of uptake can be split into single uptake channels γ_j, that represent the respective rates of SO_2 oxidation in the liquid phase:

$$f_j = \frac{\Gamma_{(b,j)}}{\sum_i \Gamma_{(b,i)}} \tag{3.30}$$

$$\gamma_j \approx \gamma_{tot} \cdot f_j \tag{3.31}$$

Finally, single rates of SO_2 uptake can be defined as:

$$-\left(\frac{d[SO_2]}{dt}\right)_j = \gamma_{tot} \cdot f_j \cdot \frac{\overline{\nu}_{SO_2}}{4} \cdot S \cdot [SO_2] \tag{3.32}$$

Where S is the surface area density of the considered condensed phase (the condensed phase surface area per unit volume of air), and $\overline{\nu}_{SO_2}$ represents the average molecular speed of SO_2 in the gas phase. The final single SO_2 uptake rates are used to assess the contribution of different heterogeneous SO_2 oxidation reactions within non-condensing volcanic plumes, hence O-MIF transfer to sulphate during SO_2 heterogeneous oxidation.

2 Halogen chemistry

Halogen chemistry is enhanced in presence of atmospheric particles, which promote mobilization of hydrogen halides from the liquid phase. Halogens mobilisation from liquid phase leads to the production of highly reactive radical species, which induce ozone destruction (Vance et al., 2010; Boichu et al., 2011; von Glasow and Crutzen, 2013).

There is growing evidence that halogen heterogeneous reactions in volcanic plumes follow similar reaction mechanisms as the ones observed during bromine explosion events over sea-salt lakes. Notably, detection of BrO in multiple volcanic plumes suggests that HBr is transformed to reactive bromine via heterogeneous reactions on the surface of sulphate aerosols (Bobrowski and Platt, 2007; Bobrowski et al., 2007; Roberts et al., 2009; von Glasow and Crutzen, 2013; Jourdain et al., 2016).

In this new version of CiTTyCAT the major halogens heterogeneous reactions are included in the chemical scheme (see Chapter 5 for a detailed description of halogens heterogeneous chemistry). Besides, compared to sulphur chemistry less data are available on halogen liquid phase reactions, and therefore it is rather challenging to explicitly model heterogeneous chemistry. There is, indeed, a lack of understanding on liquid phase reaction and reaction mechanisms and therefore, more investigations are still needed. Nonetheless, halogens heterogeneous reactions can be integrated in chemical models via reactive uptake coefficients measured during laboratory experiments. These variables commonly have different values depending on the composition of the liquid phase and on the temperature of the system. Notably, extreme pH of sulphate

aerosols and temperatures below water freezing point have an influence on reactive uptake rates. Therefore, the same reactive uptake values should not be used for sulphate aerosols and water droplets when possible. However, in CiTTyCAT some reactive uptake values for SA have also been used for acidic water droplets, because of the lack of experimental data. This assumption is fairly valid for halogens-rich water phases, where excess of X^- ($X^- = Cl^- + Br^-$) should promote the uptake reactions. Net reactive uptakes for halogen reactions implemented in this new version of CiTTyCAT are summarized in Table:3.4.

Some halogens can partition between water and gas phase, and their Henry's law coefficient are known. Therefore, in the condensing volcanic scenario halogens Henry's equilibria are accounted for some species of interest (i.e. HOBr, HOCl, HCl, HBr, Br_2, Cl_2, BrCl). In this case, partitioning between gas and aqueous phases of halogens species are explicitly modelled via mass-transfer fluxes. On the contrary, in the non-condensing plume scenario, only S(VI) transfer from the gas phase is accounted. It is assumed, therefore, that other heterogeneous chemistry reaction products would be released immediately in the gas phase, due to the extreme acidity within sulphate aerosols.

Within halogens heterogeneous reactions, dihalogens production (i.e. Br_2, BrCl and Cl_2) is fundamental for halogens mobilization from the liquid phase. Notably, Br_2 is less soluble than BrCl and Cl_2, and its release in the gas phase is fundamental to development of "bromine explosion events". In the liquid phase dihalogens undergo multi-step equilibrium reactions, which commonly promote formation of Br_2 over BrCl for $[Br^-]/[Cl^-]$ aqueous ratios above 7.2×10^{-5} (Gerlach, 2004; Roberts et al., 2009; Grellier et al., 2014). The main aqueous reactions regulating halogens production in aqueous phase are:

$$BrCl + Br^- \rightleftharpoons Br_2Cl^-$$
$$Br_2Cl^- \longrightarrow Br_2 + Cl^-$$
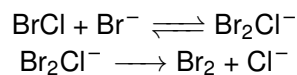
In the water droplet scenario the model takes into account explicitly for the multi-step equilibrium between Br_2, BrCl, Br^-, and Cl^-, since aqueous Br_2 and BrCl are explicitly modelled. However, the multi-step equilibrium between Br_2, BrCl, Br^-, and Cl^-, has to be parametrised differently for the non-condensing plume scenario. BrCl and Br_2 production are estimated via introduction of a branching ratio for HOBr uptake into sulphate aerosols (Roberts et al., 2009; Jourdain et al., 2016). The production terms are computed as follows:

Reaction	γ_i
$HOBr + Cl^-_{(aq.)} + H^+ \longrightarrow BrCl + H_2O$	$0.2 \cdot \dfrac{[BrCl_{aq.}]}{[BrCl_{aq.}] + [Br_{2,aq.}]}$
$HOBr + Br^-_{(aq.)} + H^+ \longrightarrow Br_2 + H_2O$	$0.2 \cdot \dfrac{[Br_{2,aq.}]}{[BrCl_{aq.}] + [Br_{2,aq.}]}$

Table 3.4: Values of γ_i used during water droplets (WD) and sulphate aerosols (SA) simulations (Sander et al., 2006).

Reaction	γ_i (SA)	γ_i (WD)
$HOCl + Br^-_{(aq.)} + H^+ \longrightarrow Cl_{2(aq.)} + H_2O$	0.002	=
$HOBr + Cl^-_{(aq.)} + H^+ \longrightarrow BrCl_{(aq.)} + H_2O$	$0.2 \cdot \dfrac{[BrCl]_{aq.}}{[BrCl]_{aq.} + [Br_2]_{aq.}}$	=
$HOBr + Br^-_{(aq.)} + H^+ \longrightarrow Br_{2(aq.)} + H_2O$	$0.2 \cdot \dfrac{[Br_2]_{aq.}}{[BrCl]_{aq.} + [Br_2]_{aq.}}$	=
$BrONO_2 + H_2O \longrightarrow HOBr_{(aq.)} + HNO_{3(aq.)}$	0.8	$3 \cdot 10^{-2}$
$ClONO_2 + H_2O \longrightarrow HOCl_{(aq.)} + HNO_{3(aq.)}$	-	$2.5 \cdot 10^{-2}$
$N_2O_5 + H_2O \longrightarrow 2\,HNO_{3(aq.)}$	0.03	=

3 Modelling O-MIF transfer to S(VI)

Oxygen MIF in tropospheric S(VI) originates mostly from isotopic anomalies transferred by O_3 and H_2O_2. Based on the number of oxygen atoms which are transferred from reactants to sulphate, a fraction of the initial anomaly is conserved in the final product (Savarino and Thiemens, 1999b,a; Savarino et al., 2000).

In order to predict final values of $\Delta^{17}O(S(VI))$, it is necessary to evaluate single sulphate production rates and the corresponding fraction of isotopic anomaly transferred during the oxidation. The S(IV) chemical continuity equation is coupled to an isotopic mass-balance scheme to create a new continuity equation, which can follow both chemical and isotopic evolution of sulphate. A new variable defined as **anomaly product** (AP) is created by merging S(VI) concentration with the corresponding isotopic anomaly evolving in relation to sulphate production. In order to evaluate the evolution of the anomaly product single isotopic transfer rates are coupled to the respective sulphate production channels.

For the condensing plume scenario the new continuity equation for the anomaly product is expressed as:

$$
\begin{aligned}
\frac{d}{dt}[S(VI)] \cdot \Delta^{17}O(S(VI)) = {} & k_{OH}[SO_2][OH] \cdot \Delta^{17}O(S(VI))_{OH} + \\
& + \sum_i K_{eq,i}^{l-g} \cdot [S(IV)][Ox.]_i^{l-g} \cdot \Delta^{17}O(S(VI))_i - \\
& - Mx \cdot \Delta^{17}O(S(VI)) - D \cdot \Delta^{17}O(S(VI))
\end{aligned}
\tag{3.33}
$$

In the non-condensing plume scenario the rates of sulphate production are evaluated via uptake coefficients, and the final continuity equation for the anomaly product is expressed as:

$$\frac{d}{dt}[\text{S(VI)}] \cdot \Delta^{17}\text{O(S(VI))} = k_{OH}[\text{SO}_2][\text{OH}] \cdot \Delta^{17}\text{O(S(VI))}_{OH}+$$

$$+ \sum_i \gamma_{r(i)} \cdot [\text{SO}_2] \cdot \Delta^{17}\text{O(S(VI))}_i - Mx \cdot \Delta^{17}\text{O(S(VI))}- \qquad (3.34)$$

$$-D \cdot \Delta^{17}\text{O(S(VI))}$$

3.1 Isotopic mass-balance equations for S(IV) oxidation

The value of oxygen isotopic anomaly (O-MIF) in produced sulphate depends on the relative importance of individual SO_2 oxidation pathways, and their respective transfer of O-MIF ($\Delta^{17}\text{O(S(VI))}_j$). In order to use isotopic sulphate ^{17}O-excess to constrain individual SO_2 oxidation pathways, it is first necessary to characterise the specific $\Delta^{17}\text{O}$ transferred to sulphate by each channel of SO_2 oxidation. These estimation are conducted via isotopic mass-balance equations.

In this work, it is assumed that both volcanic SO_2 and water do not carrying initial O-MIF. Nowadays, measurements regarding the isotopic composition of basaltic lavas suggest no significant $\Delta^{17}\text{O}$, $\Delta^{33}\text{S}$ and $\Delta^{36}\text{S}$ for magmatic SO_2, hence possibly for degassing SO_2 (Eiler, 2001; Bindeman et al., 2007). At the same time, atmospheric H_2O and SO_2 do not carry O-MIF (Holt et al., 1981; Uemura et al., 2010). Following water vapour release from the plume and quick reactions in volcanic vents, it is assumed that volcanic SO_2 and H_2O would have the same isotopic composition of their tropospheric counterparts. As a result, it is assumed that O-MIF found in sulphates originates only from the transmission of isotopic anomaly during aforementioned reactions of sulphur oxidation.

Oxidation by ozone

The few isotopic measurements of tropospheric ozone indicate values of $\Delta^{17}\text{O}$ ($\text{O}_{3,bulk}$) ranging from 20 to 40 ‰ with a mean value of about 25 ‰ (Krankowsky et al., 1995; Johnston and Thiemens, 1997; Thiemens, 2006; Vicars and Savarino, 2014). The location of oxygen isotopes within the structure of ozone is not uniform and heavier isotopes are mostly located at the extremities of the molecule (Janssen, 2005; Bhattacharya et al., 2008). Indeed, molecules that have asymmetrical geometrical structures, and bearing heavier oxygen isotopes on terminal sites, are more energetically stable than their symmetric counterparts (Marcus, 2013). This enrichment in heavy oxygen isotopes at terminal locations of ozone is confirmed by laboratory measurements (Bhattacharya et al., 2008). The characteristic structure of molecular ozone is illustrated in **Fig.:3.2**.

Ozone does not always react with other molecules via terminal oxygen atoms, although this reaction mechanism is energetically favourable since it requires the breaking of only one molecular bond. During the oxidation of reactive nitrogen
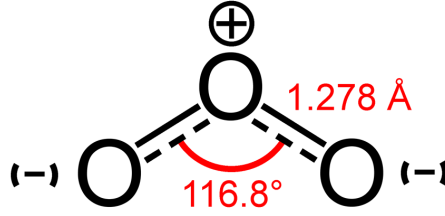
Figure 3.2: Geometrical structure of molecular ozone. Statistical thermodynamics and experimentalp measurements suggest that heavier oxygen isotopes are mostly confined at termial locations.

leading to production of atmospheric nitrate, most of the oxygen atoms involved in the reaction are from terminal sites (Savarino et al., 2008). Multiple studies found a similar selective reactivity indeed, as during photochemical reactions or for reactions of ozone on solid substrates (Sheppard and Walker, 1983; Bhattacharya et al., 2008). Considering the mean bulk O-MIF and terminal isotopic enrichments, a mean reactive ozone O-MIF (Δ^{17}O ($O_3^\star$)) of 36 ‰ has been derived (Bhattacharya et al., 2008; Savarino et al., 2008). This value is used throughout this study, since it is in accordance with parametrizations used in previous successful model simulations (Michalski et al., 2003; Alexander et al., 2002; Morin et al., 2007; Alexander et al., 2009; Morin et al., 2011).

The value of O-MIF in sulphates generated during the aqueous oxidation by ozone is determined by identifying the origins of each oxygen atom in sulphate during the reaction of oxidation. Since ozone transfers only one oxygen atom during the reaction, the equation describing the transfer of O-MIF to sulphate during oxidation by ozone is:

$$\Delta^{17}O(S(VI))_{O_3+SO_2} = \frac{1}{2} \cdot \Delta^{17}O(SO_2) + \frac{1}{4} \cdot \Delta^{17}O(H_2O) + \frac{1}{4} \cdot \Delta^{17}O(O_3{}^*)$$
(3.35)

This equation can be simplified because the O-MIF anomalies in SO_2 and H_2O are negligible:

$$\Delta^{17}O(S(VI))_{O_3+SO_2} = \frac{1}{4} \cdot \Delta^{17}O(O_3{}^*)$$
(3.36)

Therefore, the isotopic anomaly in atmospheric sulphates produced in the model during the oxidation of dissolved SO_2 through O_3 is Δ^{17}O $(S(VI))_{O_3+SO_2}$ = 9 ‰ (Morin et al., 2007, 2011).

Oxidation by hydroxyl radical

Tropospheric OH radicals are not thought to carry O-MIF anomaly because the exchange of oxygen atoms with water vapour is so fast that it erases any

inherited isotopic anomaly in OH. Recall, that tropospheric H_2O does not carry any O-MIF because the tropospheric H_2O cycle is entirely controlled by physical processes (condensation, evaporation) and not by chemical processes involving ozone. As a result, the O-MIF signature in OH radicals is expected to be null ($\Delta^{17}O$ (OH) = 0.0 ‰) (Morin et al., 2011). However, when the humidity and hence H_2O levels are very low (e.g. upper troposphere), the rate of isotopic exchange between OH radicals and H_2O molecules decreases so much that freshly produced OH radicals may have time to react with other molecules before losing their isotopic anomaly by isotopic exchange with H_2O (Morin et al., 2007). Under those conditions, when the OH loss reactions and cycling compete with the isotopic exchange with H_2O, some of the initial O-MIF originating from ozone is still present in reacting OH. It is also possible for OH destruction channels to compete with the oxygen isotopic exchange with H_2O, notably when OH reacting species concentrations is highly enhanced. This may be the case in volcanic plumes, when SO_2 levels are so high that the SO_2 + OH reaction might become the dominant OH chemical reaction rate instead of the isotopic exchange with H_2O.

In order to account for this possibility, instead of assuming a null O-MIF for OH, the O-MIF in the steady-state OH ($\Delta^{17}O$ (OH)) is calculated explicitly using the approach developed by Morin et al. (Morin et al., 2007). $\Delta^{17}O$ (OH) is simply derived from the competing balance between the O-MIF erasing isotopic exchange and the total OH loss, typically the reactions with CO and CH_4 in the troposphere. Since sulphur and halogens rich volcanic plumes and clouds are considered in this study, the reaction between OH and SO_2, and the between OH and HCl are also taken into account.

Considering all the transfers of oxygen atoms, the isotopic mass-balance equation for the OH pathway can be expressed as:

$$\Delta^{17}O(S(VI))_{OH+SO_2} = \frac{1}{2} \cdot \Delta^{17}O(SO_2) + \frac{1}{4} \cdot \Delta^{17}O(OH) + \frac{1}{4} \cdot \Delta^{17}O(H_2O)$$
(3.37)

Since tropospheric H_2O and volcanic SO_2 are not thought to carry any O-MIF, the equation can be simplified:

$$\Delta^{17}O(S(VI))_{OH+SO_2} = \frac{1}{4} \cdot \Delta^{17}O(OH)$$
(3.38)

The O-MIF of OH can be derived using the following equation

$$\Delta^{17}O(OH) = x \cdot \Delta^{17}O(OH^*_{prod.})$$
(3.39)

with

$$\Delta^{17}O(OH^*_{prod.}) = \frac{1}{2} \cdot \Delta^{17}O(O_3^*)$$
(3.40)

and

$$x = \frac{D}{D + k^*_{OH+H_2O} \cdot [H_2O]}$$
(3.41)

67

$$D = k_{\mathrm{OH+CO}} \cdot [\mathrm{CO}] + k_{\mathrm{OH+CH_4}} \cdot [\mathrm{CH_4}] + k_{\mathrm{OH+SO_2}} \cdot [\mathrm{SO_2}] + k_{\mathrm{OH+HCl}} \cdot [\mathrm{HCl}]$$

(3.42)

In this approach x represents the competition between the O-MIF erasing effect of isotopic exchange and the O-MIF retaining effect of OH chemical loss; only important loss reactions for tropospheric OH are considered here. $\Delta^{17}\mathrm{O}(\mathrm{OH}^{\star}_{\mathrm{prod.}})$ is the O-MIF of the OH radical freshly produced, and it is assumed that OH is mostly formed by the photolysis of ozone followed by the reaction of $\mathrm{O}^1(\mathrm{D})$ with $\mathrm{H_2O}$.

The O-MIF in OH ($\Delta^{17}\mathrm{O}(\mathrm{OH})$) is determined by this x factor. If OH chemical loss is much faster than the isotopic exchange, $\Delta^{17}\mathrm{O}(\mathrm{OH}) = 0.5 \cdot \Delta^{17}\mathrm{O}(\mathrm{O}^{\star}_3)$ (i.e. $x = 1$). If chemical loss is much slower than the isotopic exchange, $\Delta^{17}\mathrm{O}(\mathrm{OH}) \approx 0\text{\textperthousand}$ (i.e. $x \ll 1$).

Oxidation by hydrogen peroxide

In the troposphere, $\mathrm{H_2O_2}$ can quickly dissolve into liquid water phases (Seinfeld and Pandis, 2016). In a volcanic plume, these phases can be either water droplets or water condensed on solid particles, typically on ash particles. Once in the aqueous phase, $\mathrm{H_2O_2}$ oxidizes $\mathrm{SO_2}$ by nucleophilic displacement, and its two oxygen atoms are transmitted to the produced sulphate molecule (McArdle and Hoffmann, 1983; Brandt and van Eldik, 1995).

The isotopic balance for the oxidation by $\mathrm{H_2O_2}$ in the liquid phase is:

$$\Delta^{17}\mathrm{O}(\mathrm{S(VI)})_{\mathrm{H_2O_2+SO_2}} = \frac{1}{2} \cdot \Delta^{17}\mathrm{O}(\mathrm{SO_2}) + \frac{1}{2} \cdot \Delta^{17}\mathrm{O}(\mathrm{H_2O_2}) \qquad (3.43)$$

Since volcanic $\mathrm{SO_2}$ is thought to carry no significant O-MIF, the final O-MIF transfer can be simplified:

$$\Delta^{17}\mathrm{O}(\mathrm{S(VI)})_{\mathrm{H_2O_2+SO_2}} = \frac{1}{2} \cdot \Delta^{17}\mathrm{O}(\mathrm{H_2O_2}) \qquad (3.44)$$

Isotopic measurements of $\Delta^{17}\mathrm{O}$ of tropospheric $\mathrm{H_2O_2}$ range between 1.30 and 2.20 ‰ with a mean O-MIF of 1.70 ‰ (Savarino and Thiemens, 1999b,a; Alexander et al., 2012). Using this mean value, sulphate produced by the $\mathrm{H_2O_2}$ oxidation is assumed to carry a $\Delta^{17}\mathrm{O}(\mathrm{S(VI)})_{\mathrm{H_2O_2+SO_2}} = 0.87$ ‰ (Savarino et al., 2000).

Oxidation by $\mathrm{O_2}$ /TMI

Isotopic measurements of atmospheric $\mathrm{O_2}$ indicate that its O-MIF anomaly is rather small (Luz et al., 1999; Barkan and Luz, 2003). Kinetic isotope fractionation associated to the Dole effect (Dole, 1936) and stratospheric influx

of O_2 generates a slightly negative O-MIF in tropospheric O_2. As theoretical investigations suggest, a slight depletion of ^{17}O is indeed found in tropospheric O_2, which is accompanied by a slightly negative O-MIF (Barkan and Luz, 2003). Theoretical calculations predict $\Delta^{17}O$ (O_2) as low as -0.344 ‰ (Pack et al., 2007) or even, more recently, -0.410 ‰ for tropospheric O_2 (Young et al., 2014). Other theoretical calculations suggest a $\Delta^{17}O$ (O_2) between 0.141 and -0.305 ‰ (Young et al., 2002).

In this work is assumed that $\Delta^{17}O$ (O_2) is equal to -0.340 ‰ (Miller, 2002). This value is chosen because it gives a reasonably good agreement between isotopic measurements (Martin, 2018) and models (Miller, 2002; Young et al., 2002; Pack et al., 2007). In addition, it has to be kept in mind that there are large uncertainties associated with the exact reaction mechanism of SO_2 oxidation catalysed by TMI. Consequently, in this study it is assumed that only one oxygen atom is transmitted from O_2 to sulphate during SO_2 oxidation (Brandt and van Eldik, 1995; Herrmann et al., 2000).

With these assumptions, the isotopic mass-balance equation for SO_2 oxidation by $O_{2/}$TMI is given by:

$$\Delta^{17}O(S(VI))_{O_2+SO_2} = \frac{3}{4} \cdot \Delta^{17}O(S(IV)) + \frac{1}{4} \cdot \Delta^{17}O(O_2) \qquad (3.45)$$

Since volcanic SO_2 is thought to carry no significant O-MIF, it is possible to assume that initial S(IV) species do not carry any O-MIF. Consequently, the isotopic signature associated to this oxidation pathway can be simplified:

$$\Delta^{17}O(S(VI))_{O_2+SO_2} = \frac{1}{4} \cdot \Delta^{17}O(O_2) \qquad (3.46)$$

$\Delta^{17}O$ (O_2) being taken as -0.34 ‰ (see above), sulphate produced through this pathway carries a O-MIF ($\Delta^{17}O(S(VI))_{O_2+SO_2}$) almost null, of about -0.09 ‰ (Savarino et al., 2000).

Oxidation by HOX

Atmospheric HOX is formed as a byproduct of multiple reactions involved in halogen heterogeneous chemistry (see Table:3.4, and Chapter 5). The reaction of S(IV) with HOX is initialised by the nucleophilic attack of S(IV) species to the respect of aqueous hypohalous acids (Vogt et al., 1996; Von Glasow et al., 2002b). The reaction is followed by fast hydrolysis of XSO_3^-, hence production of S(VI). No measurements regarding $\Delta^{17}O$(HOX) have been conducted so far, but it has been suggested that the new oxygen atom transferred to S(VI) during the reaction originates from water (Fogelman et al., 1989; Troy and Margerum, 1991; Chen et al., 2016). Consequently, a potential O-MIF carried by HOX would not affect eventually the final signature of produced S(VI). For this channel of

oxidation the balance equation for $\Delta^{17}O(S(VI))_{HOX+S(IV)}$ takes the following form:

$$\Delta^{17}O(S(VI))_{HOX+S(IV)} = \frac{1}{2} \cdot \Delta^{17}O(SO_2) + \frac{1}{2} \cdot \Delta^{17}O(H_2O) \qquad (3.47)$$

Since it is assumed that volcanic SO_2 and H_2O do no carry significant O-MIF, the final isotopic signature of sulphates generated via this channel of oxidation is:

$$\Delta^{17}O(S(VI))_{HOX+S(IV)} = 0 \qquad (3.48)$$

It is then expected that sulphates generated via oxidation of S(IV) by HOX do not carry oxygen isotopic anomaly (Chen et al., 2016).

3.2   Solving the continuity equation

Once the isotopic mass-balance equations have been defined, the O-MIF of produced sulphate and its evolution are monitored via the external integration module of the anomaly product (see Chapter 2). The fraction of isotopic anomaly transferred by single sulphate production channels is equal for sulphate aerosol chemistry and water droplets. It is assumed, indeed, that in both scenarios S(IV) oxidation follows the same oxidation mechanisms. Considering the external integration of the anomaly product via 4th-RKM, $\Delta^{17}O(S(VI))_t$ is evaluated by Eq.:3.49-3.51:

$$\Delta^{17}O(S(VI))_f(t) = \frac{[S(VI)]_{RKM}(t)}{[S(VI)]_{CTC}(t)} \cdot \Delta^{17}O(S(VI))_{RKM}(t) \qquad (3.49)$$

$$[S(VI)]_{CTC}(t) = [S(VI)]_{RKM}(t) \qquad (3.50)$$

$$\Delta^{17}O(S(VI))_f(t) \approx \Delta^{17}O(S(VI))_{RKM}(t) \qquad (3.51)$$

where: $[S(VI)]_{RKM}(t)$,   [S(VI)] evaluated via 4th-RKM at time t

         $[S(VI)]_{CTC}(t)$,   [S(VI)] calculated by CiTTyCAT at time t

         $\Delta^{17}O(S(VI))_{RKM}$ (t),   O-MIF evaluated via 4th-RKM at time t

Note, that the anomaly product integration is implemented separately from the chemical scheme. As a result, the isotopic transfer scheme does not affect the chemical scheme added to CiTTyCAT for halogens and sulphur chemistry.

Photochemical box-modelling of volcanic SO$_2$ oxidation: isotopic constraints

Tommaso Galeazzo[1,2], Slimane Bekki[1], Erwan Martin[2], Joël Savarino[3], and Stephen R. Arnold[4]

[1] LATMOS/IPSL, Sorbonne Université, UVSQ, Université Paris-Saclay, CNRS, Paris, France; [2] ISTeP, Sorbonne Université, CNRS, Paris, France; [3] IGE, Univ. Grenoble Alpes, CNRS, IRD, INP-G, 38000 Grenoble, France; [4] Institute for Climate and Atmospheric Science, School of Earth and Environment, University of Leeds, Leeds, UK

Abstract: The photochemical box-model CiTTyCAT is used to analyse the absence of oxygen mass-independent anomalies (O-MIF) in volcanic sulphates produced in the troposphere. An aqueous sulphur oxidation module is implemented in the model and coupled to an oxygen isotopic scheme describing the transfer of O-MIF during the oxidation of SO$_2$ by OH in the gas-phase, and by H$_2$O$_2$, O$_3$ and O$_2$ catalysed by TMI in the liquid phase. Multiple model simulations are performed in order to explore the relative importance of the various oxidation pathways for a range of plausible conditions in volcanic plumes. Note that the chemical conditions prevailing in dense volcanic plumes are radically different from those prevailing in the surrounding background air.

The first salient finding is that, according to model calculations, OH is expected to carry a very significant O-MIF in sulphur-rich volcanic plumes and, hence, that the volcanic sulphate produced in the gas phase would have a very significant positive isotopic enrichment. The second finding is that, although H$_2$O$_2$ is a major oxidant of SO$_2$ throughout the troposphere, it is very rapidly consumed in sulphur-rich volcanic plumes. As a result, H$_2$O$_2$ is found to be a minor oxidant for volcanic SO$_2$. According to the simulations, oxidation of SO$_2$ by O$_3$ is negligible because volcanic aqueous phases are too acidic. The model predictions of minor or negligible sulphur oxidation by H$_2$O$_2$ and O$_3$, two oxidants carrying large O-MIF, are consistent with the absence of O-MIF seen in most isotopic measurements of volcanic tropospheric sulphate. The third finding is that oxidation by O$_2$/TMI in volcanic plumes could be very substantial and, in some cases, dominant, notably because the rates of SO$_2$ oxidation by OH, H$_2$O$_2$, and O$_3$ are vastly reduced in a volcanic plume compared to the background air. Only cases where sulphur oxidation by O$_2$/TMI is very dominant can explain the isotopic composition of volcanic tropospheric sulphate.

1 Introduction

Volcanic activity is one of the major natural forcers of the Earths climate, as volcanic emissions alter the chemical composition and radiative properties of the atmosphere, at local, regional and even global scales (Stocker et al., 2013; Langmann, 2014). Beyond their environmental impacts, sulphuric acid aerosols have adverse effects on human health since they are linked to cardiovascular and respiratory diseases (Pope III, 2002; World Health Organization, 2009). Moreover, sulphate aerosols can lead to acid rain causing damage to vegetation and to urban infrastructures. Over the last decades, our understanding of volcanic emissions in the atmosphere have greatly improved, thanks to satellite and field measurements, and to more sophisticated physical-chemical models (Robock, 2000; Bobrowski et al., 2003; Mather et al., 2003; Textor et al., 2004; Roberts et al., 2009; von Glasow, 2010; Roberts et al., 2012, 2014). The main gases emitted to the atmosphere by volcanic activity are respectively H_2O, CO_2, SO_2, H_2S, and halogen species, such as HCl, HBr and HF (Textor et al., 2004; Rose et al., 2006; Oppenheimer et al., 2013). In addition, measurements at crater rims of volcanoes suggest also direct emissions of small amounts of sulphate aerosols (Allen et al., 2002; De Moor et al., 2013).

Among all the compounds emitted, volcanic sulphur gases, and in particular SO_2, are considered to be the most effective in affecting climate. Climatic perturbations from volcanic emissions are principally caused by conversion of sulphur gases into sulphate aerosols, which can then interact with solar and terrestrial radiation via scattering and absorption (Stocker et al., 2013). Once injected into the troposphere, volcanic SO_2 is converted in few days typically to H_2SO_4 by a range of gas-phase and liquid-phase reactions taking place in volcanic plumes and clouds (Chin and Jacob, 1996; Stevenson et al., 2003a). In the atmosphere, depending on the oxidation pathway, H_2SO_4 is produced either in the gas phase or liquid phase. When generated in the gas-phase, volcanic H_2SO_4 condenses very rapidly onto pre-existing particles, or it may even form very small sulphate particles by nucleation. In the boundary layer, sulphate aerosols have a residence time much shorter than a week because of the fast wet and dry depositions. However, at higher altitudes, such as in the free troposphere, removal is much slower; consequently, volcanic sulphate aerosols can have a much longer residence time of up to a few weeks (Stevenson et al., 2003b,a; Kristiansen et al., 2016). In addition, the residence time of volcanic aerosols in the stratosphere can reach lifetimes of about a year (Thomason, L. and Peter, 2006).

Nowadays, anthropogenic SO_2 emissions outweigh those from natural sources (Smith et al., 2011). Volcanic quiescent degassing and eruptions is an important natural source of SO_2, notably to the free troposphere (Bates et al., 1992; Graf et al., 1998). Volcanic emissions release about 10-13 $Tg \cdot y^{-1}$ of SO_2 to the atmosphere (Andres and Kasgnoc, 1998) and contribute to up to 10% to total sulphur emissions to the atmosphere (Stevenson et al., 2003a).

Remarkably, volcanic emissions also have a bigger impact on the tropospheric aerosol burden than other sulphur sources (Graf et al., 1998) because volcanoes tend to emit SO_2 at higher altitudes than most other surface sulphur emissions, where the lifetime is longer.

Most of the tropospheric sulphate is generated in the liquid phase (Alexander et al., 2009) via oxidation of aqueous SO_2 by dissolved oxidants of the atmosphere, such as H_2O_2, O_3, O_2 catalysed by transition metal ions (Fe(III) and Mn(II)) and, possibly HOBr and HOCl (Vogt et al., 1996; Von Glasow et al., 2002b; Stevenson et al., 2003a; Berglen et al., 2004; Park et al., 2004; Alexander et al., 2009; von Glasow and Crutzen, 2013; Chen et al., 2016). Note that the importance of the halogen oxidation pathway remains unclear. A significant amount of tropospheric H_2SO_4 is formed in the gas phase via the termolecular reaction between SO_2 and hydroxyl radicals (OH) (Calvert et al., 1978). In presence of liquid water and for typical pH values of atmospheric water droplets (3.0 ¡ pH ¡ 5.6), SO_2 is quickly oxidized by dissolved H_2O_2, and the two species rarely coexist in liquid phases (Gervat et al., 1988; Chandler et al., 1988; Daum et al., 1990; Zuo and Hoigne, 1993; Laj et al., 1997). At acidic pH values, synergism among transition metal ions (TMI) enhances the rate of SO_2 oxidation by dissolved O_2 (Brandt et al., 1994; Brandt and van Eldik, 1995), which can thus compete with the other SO_2 oxidation channels. Particular attention has been paid recently to this heterogeneous oxidation pathway, since its contribution could have been underestimated in previous budget assessments of sulphate production in the troposphere (Alexander et al., 2009; Goto et al., 2011; Harris et al., 2013). During eruptive events, volcanoes emit large quantities of ash and coarse material rich in iron-minerals (mainly glass, and in lesser extents magnetite and hematite), which can easily dissolve in water because of the high acidity reached in volcanic cloud droplets and aerosols (Ayris and Delmelle, 2012a; Hoshyaripour et al., 2015; Maters et al., 2016). As a consequence, the O_2/TMI heterogeneous oxidation reaction may be more significant than previously thought.

Quantifying the importance of the different SO_2 oxidation pathways is challenging. It requires the quantification of, among other things, the rates of the different oxidation processes. Conventional methods rely mostly on models that are evaluated and constrained with atmospheric concentration measurements of oxidants, because there is no direct means of measuring chemical fluxes associated with individual reactions (Morin et al., 2008). Simultaneous measurements of SO_2 oxidants in both the gas- and liquid phases in the atmosphere, let alone specifically in a volcanic plume, would be experimentally challenging. Alternative approaches need to be considered to reduce the uncertainty in the relative contributions from the different oxidation pathways. Isotopic approaches can provide such constraints (Brenninkmeijer et al., 2003; Thiemens, 2006). Isotopic ratios, indeed, provide direct insights into the nature and importance of individual oxidation fluxes (Savarino et al., 2007; Morin et al., 2008; Martin et al., 2014).

Thanks to peculiar distribution of isotopes among its three oxygen atoms, ozone and its chemistry provides a useful tool of investigation for atmospheric processes using isotopic signatures. Ozone bears a very significant non-mass dependent (also called mass-independent) isotopic fractionation, which is due to its formation mechanism (Heidenreich III et al., 1986; Krankowsky et al., 1995; Marcus, 2013). Since oxygen atoms in tropospheric oxygen-bearing species sometimes originate directly or indirectly from ozone via multiple photo-chemical reactions, a variety of atmospheric species carry anomalous isotopic mass-independent fractionations (MIFs) (Thiemens, 2006). For oxygen-bearing species, the anomalous oxygen MIF (Δ^{17}O, O-MIF) is calculated with respect to a reference standard:

$$\Delta^{17}O = \delta^{17}O - 0.52 \times \delta^{18}O \tag{4.1}$$

Where δ^{17}O and δ^{18}O represent deviations to the reference standard isotopic ratios (R_{std}):

$$R_x = \frac{^xO}{^{16}O} \qquad x = 17; 18 \tag{4.2}$$

And:

$$\delta^xO = \frac{R_x}{R_{std}} - 1 \tag{4.3}$$

Ozone is a key chemical reactive species of the troposphere. Its isotopic anomaly is intrinsically generated (through photolysis and recombination reactions) instead of being inherited by isotopes transfer like for most atmospheric species (Marcus, 2013). Other oxygen-bearing species in the atmosphere can gain excess-[17]O by transfer of this ozone anomaly via reactions with ozone itself, reactions with species that have already inherited the ozone anomaly or via anomalous kinetic isotopic effect (Roeckmann, 1998; Lyons, 2001; Michalski et al., 2003). As a consequence, transfer of oxygen MIF among atmospheric species is process-specific and can be used as a signature to trace the chemistry of species as they react with specific oxidants. Once the isotopic anomalies of the oxidants are characterised, the resulting Δ^{17}O of an end-oxidation product is simply a linear combination of the isotopic signatures of all the oxidation channels weighted by their respective contributions, to the total production of the end-oxidation products. During the last decade, there has been an increasing number of studies that have used O-MIF oxygen anomalies in oxidation products to constrain oxidation channels, often coupling isotopic measurements and photochemical isotopic modelling (Michalski et al., 2003; Alexander et al., 2005; Morin et al., 2008; Gromov et al., 2010; Michalski and Xu, 2010).

The isotopic signature in sulphates generated in the troposphere, the so-called secondary sulphate (by opposition to sulphate directly emitted in the atmosphere, the so-called primary sulphate) reflects the competition within different oxidation channels. In the liquid phase, sulphate oxygen MIF is produced during sulphur oxidation by transfer of isotopic anomalies from ozone and H_2O_2,

whereas sulphate with O-MIF very close to 0 ‰ is produced in the liquid phase via O_2/TMI oxidation (i.e. -0.08 ‰). Mass-dependent (MIF anomaly = 0 ‰) sulphate is generally produced via OH oxidation in the gas-phase (Savarino and Thiemens, 1999b,a; Savarino et al., 2000; Martin et al., 2014).

Most present-day tropospheric sulphates have O-MIF anomalies ($\Delta^{17}O$) of the order of 1 ‰ typically (Lee et al., 2001; Lee and Thiemens, 2001). However, there is some variability. For instance, O-MIF of sulphate aerosols generated in marine environments are higher compared to isotopic anomalies found in continental sulphates (Alexander et al., 2005). Very significant $\Delta^{17}O$ have also been found in volcanic sulphates collected from ash deposits dating back to the Miocene and the Oligocene, whose values reach 3.5 - 5.8 ‰. These peculiar isotopic anomalies have been linked to a different oxidative state of the atmosphere at that time (Bao et al., 2000, 2003). Tropospheric volcanic sulphates of the present era distinguish themselves from other tropospheric sulphates by having a $\Delta^{17}O$ often close to 0 (within the measurement error of about 0.1‰). This feature is found all over the world in sulphates collected from volcanic ashes of small and medium-size tropospheric explosive eruptions, independently from location, or geology of ash-deposits (Bao et al., 2003; Bindeman et al., 2007; Martin et al., 2014) (see Table:4.1). Notably, this is often the case for volcanic sulphate extracted from ash-deposits which are found very far from volcanoes, where secondary sulphate is expected to dominate. The only exception is volcanic sulphates in ice cores originating from very large volcanic eruptions. This sulphate had formed and transited through the stratosphere (Savarino et al., 2003a; Baroni et al., 2007).

The question is why tropospheric volcanic sulphate from volcanic ash-deposits does not appear to carry some isotopic O-MIF as for other types of tropospheric sulphates. One might expect that part of sulphate produced by tropospheric oxidation of volcanic SO_2 to carry some MIF isotopic anomaly because the dominant SO_2 oxidants in the troposphere are thought to be species carrying O-MIFs (O_3 and H_2O_2) with some contribution from O_2/TMI (Martin et al., 2014). An important difference between volcanic sulphur and most other sources of sulphur is that it is often emitted within dense volcanic plumes whose chemical compositions are radically different from the background air. The purpose of the present box-modelling study is to explore in detail the oxidation and fate of volcanic sulphur in dense volcanic clouds and the resulting isotopic MIF signature in volcanic sulphate. The objective is to see to what extent the chemical environment of dense volcanic plumes may affect sulphur dynamics and pathways of oxidation and, hence, sulphate isotopic composition.The focus here is on volcanic clouds that are rich in sulphur but poor in halogens, such in the case of intra-plate and rifting plate volcanoes (e.g. Nyarogongo in Congo, Ertaale in Ethiopia, Kīlauea in Hawai'i) (Aiuppa, 2009; Oppenheimer et al., 2013).Volcanic eruptions with remarkable low halogens to sulphur emissions are the Holuhraun (Bárðarbunga) eruption of 2012-2014 in Iceland (Ilyinskaya et al., 2017; Stefánsson et al., 2017), and the Kīlauea eruption of 2008 in Hawaii

Table 4.1: Oxygen isotopic composition of volcanic sulphates from different tropospheric emissions of the present geological era.

Volcano & Date of Eruption	Sample distance (km)	Source	$\Delta^{17}O$ (‰)	Reference
Popocatépetl (Mexico), 2008	25	ash	0.35	(Martin et al., 2014)
Spurr (Alaska, USA), 1992	265	ash	-0.14	(Martin et al., 2014)
Fuego (Guatemala), 1974	57	ash	-0.04	(Martin et al., 2014)
Negro Cerro (Nicaragua), 1947	12	ash	-0.06	(Martin et al., 2014)
Paricutin (Mexico), 1948	5	ash	0.13	(Martin et al., 2014)
Mt. St. Helens (USA), 1980	400	ash	0.02	(Martin et al., 2014)
Gjálp (Iceland), 1998	< 30	ash	-0.07	(Martin et al., 2014)
Pinatubo (Philippines), 1991	< 50	ash	-0.04	(Bindeman et al., 2007)
Pinatubo (Philippines), 1991	< 50	ash	0.19	(Bindeman et al., 2007)
Spurr (USA), 1953	n.a.	ash	0.06	(Bindeman et al., 2007)
Vesuvius (Italy), 1872	n.a.	ash	-0.07	(Bao et al., 2003)
Popocatépetl (Mexico), 1997	n.a.	ash	-0.08	(Bao et al., 2003)
Spurr (USA), 1992	n.a.	ash	0.06	(Bao et al., 2003)
Fuego (Guatemala), 1974	55	ash	-0.03	(Bao et al., 2003)
Pinatubo (Philippines), 1991	n.a.	anhydrite from pumice	-0.01	(Bao et al., 2003)
Santorini (Greece), Minoan age	n.a.	pumice + ash	0.09	(Bao et al., 2003)
Masaya (Nicaragua), 2003	0	aerosols	0.1	(Mather et al., 2006)
Masaya (Nicaragua), 2003	0	aerosols	0.2	(Mather et al., 2006)

* Refer to (Martin, 2018) for a more extensive description regarding oxygen isotopic anomalies measured in tropospheric volcanic sulphate of present and past geological eras.

(Mather et al., 2012). In particular, HCl/SO$_2$ ratios of the order of 10^{-2} have been observed for the Kīlauea eruption of 2008 (i.e. HCl $\approx$ 10-50 ppbv).

The second section of this work describes the photochemical model, including its sulphur heterogeneous chemistry scheme and the associated oxygen isotopic scheme. The mass balance equations used to evaluate the transfer of MIF oxygen anomaly from ozone to volcanic sulphate via different oxidation pathways are also presented. The third section is devoted to the study of individual and combined oxidation pathways and the resulting isotopic signatures in numerical experiments for this work standard volcanic plume conditions. The fourth section covers sensitivity model studies, investigating how different parameters in volcanic plumes affect the final isotopic anomaly in sulphate. Dominant oxidation pathways are identified and the ability of the model to reproduce observed isotopic signatures of volcanic sulphate is assessed.

2 Modelling approach

The photochemical box-model used during simulation is the Cambridge Tropospheric Trajectory model of Chemistry and Transport (CiTTyCAT), a photochemical box-model developed to simulate tropospheric chemistry (Evans et al., 2000; Sander et al., 2006; Real et al., 2007; Pugh et al., 2012). It describes the standard gas-phase photochemistry accounting for: kinetics of tropospheric species (bimolecular, termolecular, and photodissociation reactions), and deposition of gases and particles. Photolysis reaction rates are evaluated using the Fast-J code (Wild et al., 2000). Kinetic data are taken from JPL's datasheets (Sander et al., 2006). CiTTyCAT had already been used with success to constrain seasonal pathways of reactive nitrogen species in the troposphere, through the implementation of its chemical scheme with an isotopic transfer scheme accounting for Δ^{17}O production in nitrates (Morin et al., 2008). We have extended the capabilities of the model by including parameterisations of the transfer of soluble species between liquid and gas phases, of SO$_2$ heterogeneous chemistry, of pH in the liquid phase and of MIF of oxygen atoms in sulphates.

2.1 General continuity equations

The model resolves differential coupled mass balance equations (continuity equations) describing the time evolution of species concentrations in the troposphere. For given initial (e.g. initial concentrations of species) and environmental conditions (e.g. pressure, temperature), mass balance equations are solved for each species, accounting for production and loss as follows:

$$\frac{dC_i}{dt} = P_i - L_i \qquad (4.4)$$

where C$_i$ is the concentration of species i, P$_i$ the sum of physical and chemical

77

production rates for i, and L_i the sum of the physical and chemical loss rates of i.

Production and loss terms are calculated using chemical reaction kinetics, where time evolution of concentrations of chemical species depends on the relevant rate constants (k_i) and on concentrations of reactants. They also include liquid-gas transfer and deposition. In addition, mixing of air between the volcanic sulphur cloud and the outside background air is also accounted for. It is parametrised by a simple linear relaxation scheme resulting in an exponential decay of plume concentrations towards background concentrations (Methven et al., 2006; Arnold et al., 2007).

$$\left(\frac{dC_i}{dt}\right)_{mixing} = K_{mix} \cdot (C_i - C_{i(bck)}) \tag{4.5}$$

where K_{mix} is a first-order mixing rate coefficient representing all the processes mixing volcanic air with the background atmosphere and $C_{(i,bck)}$ is the concentration of species i in the background air. K_{mix} is set to 0.1 day^{-1}, a value typical of low mixing in the free troposphere and corresponding to a characteristic mixing timescale of 10 days (Methven et al., 2006; Arnold et al., 2007).

2.2   Liquid-gas mass transfer

Concentrations of relevant soluble species are calculated taking into account its partition between the gas and liquid phases. The transfer in both directions (evaporation, condensation) is dynamically computed. At each time step, rates of transfer are defined as:

$$\frac{d[C_{(aq)}]}{dt} = J_i \cdot \left(C_{(i)} - C_{(i,s)}\right) \tag{4.6}$$

where $C_{(i)}$ is gaseous concentration of species i far from liquid droplets, $C_{(i,s)}$ is the gaseous concentration of species i at the surface of droplets (which is assumed to be the equilibrium saturation vapour of i over the liquid), and J_i is the coefficient of condensation (from gas phase to liquid droplet) for species i, which is calculated using the Dahneke's expression (Dahneke, 1983) to cover mass-transfer from the continuum to the kinetic regime (see pg. 502 of Seinfeld and Pandis, 2016).

Throughout all the model simulations, droplets are assumed to be very large, with a radius of 5.0 μm. The sensitivity of the results to the assumed amount of liquid phase is explored varying the concentration of water droplets (and hence the liquid water content) instead of varying the size of droplets. It is also possible that emitted water condenses onto ash particles. Our treatment does not discriminate between liquid droplets and liquid phases at the surface of solid particles.

2.3 Gaseous and heterogeneous sulphur chemistry

The model already describes the SO_2 gas-phase chemistry. Since SO_2 is a mildly soluble species undergoing acid-base equilibrium in the liquid phase, we have added the gas-liquid transfer and the chemical reactions and equilibrium associated with its presence in the liquid phase (see Table:4.2). The extent of SO_2 dissolution into water droplets is controlled by the pH. The oxidation of S(IV) species ($HSO_3{}^-$, $SO_3{}^{2-}$, $SO_{2(aq.)}$) by reactions with H_2O_2, O_3 or O_2 in the liquid phase pushes the gas-liquid partition towards dissolution of gaseous SO_2. A diagram of the sulphur chemical model is presented in **Fig.:4.1**. Since the model CiTTyCAT resolves continuity equations for species with gas-phase concentration units, liquid phase concentrations (e.g. M) and rate constants have to be expressed into gas-phase units in the code in order to be treated by the CiTTyCAT chemistry solver (Seinfeld and Pandis, 2016).

The species involved in the acid-base equilibriums of SO_2 and H_2SO_4 are often grouped together according to their oxidation state:

$$S(IV) = SO_{2(g.)} + SO_{2(aq.)} + HSO_3{}^- + SO_3{}^{2-}$$
$$S(VI) = H_2SO_{4(g.)} + HSO_4{}^- + SO_4{}^{2-}$$
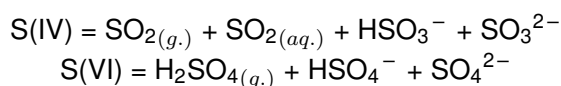
In these equations, dissolved H_2SO_4 is assumed to be totally dissociated. Ultimately, S(VI) in droplets ends up deposited at the Earths surface. In the model, the amount of sulphate deposited is evaluated as a variable.
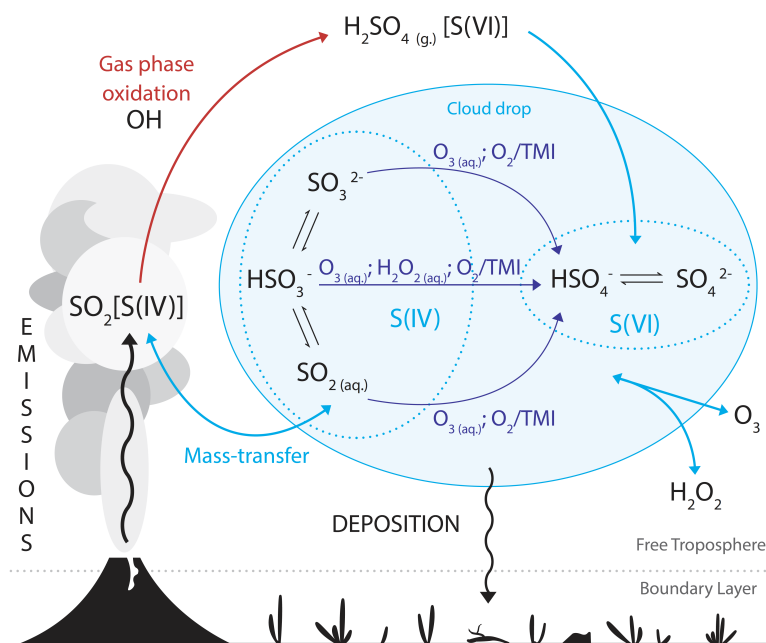
Figure 4.1: Diagram of the sulphur scheme implemented in CiTTyCAT.

The pH of volcanic water droplets is also a prognostic variable because sulphur species reaction rates and partitioning are pH dependent (Seinfeld and Pandis, 2016). It is dynamically calculated considering the most significant species dissolved in droplets:

$$[\text{H}^+] = [\text{HSO}_3{}^-] + 2\cdot [\text{SO}_3{}^{2-}] + [\text{HSO}_4{}^-] + 2\cdot [\text{SO}_4{}^{2-}]$$

The main aqueous equilibrium reactions and S(IV) oxidation reactions added to the chemical scheme are summarized in Table:4.2. The final continuity equation for single SO_2 oxidation channels can be expressed as:

$$-\frac{d[\text{SO}_2]}{dt} = k_{\text{OH}^+\text{SO}_2} \cdot [\text{SO}_2][\text{OH}] + \sum_j (k_j \cdot [\text{S(IV)}]_{aq}[\text{C}_j]_{aq.}) \tag{4.7}$$

where $k_{\text{OH}^+\text{SO}_2}$ is the rate constant of the gas-phase reaction between OH and SO_2 (Sander et al., 2006), k_j the rate constant of the aqueous reaction between SO_2 and species C_j, whose concentration in the aqueous phase is expressed as $[\text{C}_j]_{aq.}$.

Similar continuity equations can easily be derived for all the sulphur species. The continuity equation for atmospheric sulphate S(IV) can be determined by summing all the individual continuity equations of S(IV) species:

$$\frac{d[\text{S(IV)}]}{dt} = -k_{\text{OH}^+\text{SO}_2} \cdot [\text{SO}_2][\text{OH}] - \sum_j (k_j \cdot [\text{S(IV)}]_{aq.}[\text{C}_j]_{aq.}) -$$
$$-k_d \cdot [\text{SO}_{2(\text{aq.})} + \text{HSO}_3{}^- + \text{SO}_3{}^{2-}] - K_{mix} \cdot ([\text{SO}_2] - [\text{SO}_2]_{(bck)}) \tag{4.8}$$

where k_j the rate constant of the aqueous reaction between oxidant C_j and relevant [S(IV)] species (see the list of aqueous oxidation reaction in Table:4.2), and k_d is the deposition coefficient of dissolved sulphur species. Dry deposition as such is not expected to be important in the plume itself compared to wet deposition for our cloudy conditions. Since only wet deposition is considered, only species dissolved in water phases such as aqueous S(IV) ($\text{SO}_{2(\text{aq})} + \text{HSO}_3^-$ + SO_3^{2-}) and S(VI) (HSO_4^- + SO_4^{2-}) species are deposited in the model. The deposition is treated as a first order loss with $k_d = 2\cdot10^{-6}$ s^{-1}, equivalent to a characteristic time scale of 5.7 days (Stevenson et al., 2003b).

The same approach can be used for S(VI) and deposited S(VI):

$$\frac{d[\text{S(VI)}]}{dt} = k_{\text{OH}^+\text{SO}_2} \cdot [\text{SO}_2][\text{OH}] + \sum_j (k_j \cdot [\text{S(IV)}]_{aq}[\text{C}_j]_{aq}) -$$
$$-k_d \cdot [\text{HSO}_4{}^- + \text{SO}_4{}^{2-}] - K_{mix} \cdot ([\text{S(VI)}] - [\text{S(VI)}]_{(bck)}) \tag{4.9}$$

$$\frac{d[\text{S(VI)}_{\text{dep}}]}{dt} = k_d \cdot [\text{HSO}_4{}^- + \text{SO}_4{}^{2-}] \tag{4.10}$$

Table 4.2: Sulphur aqueous equilibria and reactions

Equilibrium	K (M^{-1}),	k$_{298(forward)}$ (M^{-1}s^{-1}),	E$_a$/R (K),	k$_{298(back)}$ (M^{-2}s^{-1}),
SO$_{2(aq.)}$ + H$_2$O $\rightleftharpoons$ HSO$_3^-$ + H$_3$O$^+$	3.13·10^{-4}	6.27·10^4	-1940	2·10^8 [a,c]
HSO$_3^-$ + H$_2$O $\rightleftharpoons$ SO$_3^{2-}$ + H$_3$O$^+$	6.22·10^{-8}	3110	-1960	5·10^{10} [a,c]
H$_2$SO$_4$ + H$_2$O $\rightarrow$ HSO$_4^-$ + H$_3$O$^+$		∞		
HSO$_4^-$ + H$_2$O $\rightleftharpoons$ SO$_4^{2-}$ + H$_3$O$^+$	1.02·10^{-2}	1.02·10^9	-2700	1·10^{11} [b,c]

[a] (Beilke and Gravenhorst, 1978); [b] (Redlich, 1946); [c] (Graedel and Weschler, 1981)

Gaseous reaction	k			units
SO$_2$ + OH + M $\rightarrow$ HOSO$_2$ + M	4.62·10^{-31} · $(T/298.0)^{-3.90}$			cm^{6}molecule^{-2}s^{-1} [d]
HOSO$_2$ + O$_2$ $\rightarrow$ HO$_2$ + SO$_3$	1.30·10^{-12} · $(-330/T)^{-3.90}$			cm^{3}molecule^{-1}s^{-1} [d]
SO$_3$ + H$_2$O $\rightarrow$ H$_2$SO$_4$	9.10·10^{-13}			cm^{3}molecule^{-1}s^{-1} [d]

Aqueous reaction	k(aq)			units; (T)
SO$_{2(aq.)}$ + O$_3$ $\rightarrow$ S(VI) + O$_2$	2.4·10^4			Ms^{-1} [b]
HSO$_3^-$ + O$_3$ $\rightarrow$ S(VI) + O$_2$	3.7·10^5			Ms^{-1} [b]
SO$_3^{2-}$ + O$_3$ $\rightarrow$ S(VI) + O$_2$	1.5·10^9			Ms^{-1} [b]
HSO$_3^-$ + H$_2$O$_2$ $\rightarrow$ S(VI) + H$_2$O	$\dfrac{k_{\text{H}_2\text{O}_2} \cdot [\text{H}^+]}{1 + K_{(eq.)} \cdot [\text{H}^+]}$			Ms^{-1} [e]
	with $K_{(eq.)}$ = 13			M^{-1} [e]
	and $k_{\text{H}_2\text{O}_2}$ = 7.5·10^7			M^{-2}s^{-1} [e]
S(IV) + $\dfrac{1}{2}$ O$_2$ $\xrightarrow{TMI}$ S(VI)	750·[Mn(II)] + 2600·[Fe(III)] + 1.0·10^{10}[Mn(II)][Fe(III)]			s^{-1} [f]

[d] (Atkinson et al., 2004); [e] (Hoffmann, 1986); [f] (Martin and Good, 1991)

where S(VI)$_{\text{dep}}$ is the sulphate deposited at the surface.

$$\frac{d}{dt}[\text{S(VI)}] \cdot \Delta^{17}\text{O(S(VI))} = \sum_j [P_j \cdot \Delta^{17}\text{O(S(VI)}_{\text{prod}})_j] - k_d \cdot \Delta^{17}\text{O(S(VI))}$$

(4.11)

where Δ^{17}O(S(VI)) is the final isotopic anomaly observed on atmospheric sulphate, Δ^{17}O(S(VI)$_{\text{prod.}}$)$_j$ is the O-MIF anomaly transferred to sulphate through the specific oxidation channel j, and P$_j$ is the oxidation rate of channel j. Δ^{17}O(S(VI)$_{\text{prod.}}$)$_j$ is fixed for ozone, H$_2$O$_2$, and TMI oxidation pathways but it is a prognostic variable for OH (see Table:4.3).

As deposited sulphate is a variable in the model (S(VI)$_{dep}$), the transfer of isotopic anomaly during deposition is also monitored following a similar equation,

$$\frac{d}{dt}[\text{S(VI)}_{dep}] \cdot \Delta^{17}\text{O(S(VI))} = k_d \cdot [\text{S(VI)}] \cdot \Delta^{17}\text{O(S(VI))}$$

(4.12)

The value of oxygen isotopic anomaly (O-MIF) in sulphate depends on the relative importance of individual SO$_2$ oxidation pathways (P$_j$) and their respective transfer of O-MIF (Δ^{17}O(S(VI))$_j$). Note that the continuity equations of S(VI) and S(VI)$_{\text{dep}}$ isotopes tracers are integrated with a 4th order Runge-Kutta method algorithm instead of using the CiTTyCAT chemistry solver with the oxidation rates (i.e. P$_j$ in 5.52) kept constant over a time step (Morin et al., 2007, 2008). This approach allows to keep the chemistry module totally independent from the oxygen isotopic module. The external integration tool does not affect significantly the results. Throughout this study, it is assumed that both SO$_2$ and water vapour (H$_2$O) are not carrying any initial O-MIF. The isotopic composition of magmatic SO$_2$, indeed, follows mass-dependent fractionations and no significant Δ^{17}O, Δ^{34}S and Δ^{36}S have been measured so far (Eiler, 2001). Measurements show that tropospheric H$_2$O does not carry any O-MIF (Uemura et al., 2010), and the same is found for atmospheric SO$_2$ (Holt et al., 1981). It is therefore assumed that the O-MIF found in sulphates only originates from the transmission of isotopic anomaly during the aforementioned reactions of sulphur oxidation.

In order to constrain individual SO$_2$ oxidation pathways from isotopic information, it is first necessary to characterise the specific O-MIFs they transfer to sulphate using isotopic transfer equations.

Table 4.3: O-MIF signatures of S(IV) oxidation pathways in the model

Oxidant	O-MIF pathway (‰)
OH	calculated (0 to a maximum of 4.5)
H$_2$O$_2$	0.87
O$_3$	9
O$_2$/TMI	-0.09

Oxidation by ozone

The few isotopic measurements of tropospheric ozone indicate values of $\Delta^{17}O$ ($O_{3,bulk}$) ranging from 20 to 40 ‰ with a mean value of about 25 ‰ (Krankowsky et al., 1995; Johnston and Thiemens, 1997; Thiemens, 2006; Vicars and Savarino, 2014). The location of oxygen isotopes within the structure of ozone is not uniform and heavier isotopes are mostly located at the extremities of the molecule (Janssen, 2005; Bhattacharya et al., 2008). Indeed, molecules that have asymmetrical geometrical structures, and bearing heavier oxygen isotopes on terminal sites, are more energetically stable than their symmetric counterparts (Marcus, 2013). This enrichment in heavy oxygen isotopes at terminal locations of ozone is confirmed by laboratory measurements (Bhattacharya et al., 2008). Ozone does not always react with other molecules via terminal oxygen atoms, although this reaction mechanism is energetically favourable since it requires the breaking of only one molecular bond. During the oxidation of reactive nitrogen leading to production of atmospheric nitrate, most of the oxygen atoms involved in the reaction are from terminal sites (Savarino et al., 2008). Multiple studies found a similar selective reactivity indeed, as during photochemical reactions or for reactions of ozone on solid substrates (Sheppard and Walker, 1983; Bhattacharya et al., 2008). Considering the mean bulk O-MIF and terminal isotopic enrichments, a mean reactive ozone O-MIF ($\Delta^{17}O$ (O_3^*)) of 36 ‰ has been derived (Bhattacharya et al., 2008; Savarino et al., 2008; Morin et al., 2007). This value is used throughout this study, since it is in accordance with parametrizations used in previous successful model simulations (Michalski et al., 2003; Alexander et al., 2002; Morin et al., 2007; Alexander et al., 2009; Morin et al., 2011).

The value of O-MIF in sulphates generated during the aqueous oxidation by ozone is determined by identifying the origins of each oxygen atom in sulphate during the reaction of oxidation. Ozone transfers to sulphate only one oxygen atom during aqueous sulphur oxidation, while another oxygen atom derive from the water molecule forming aqueous S(IV). The equation describing the transfer of O-MIF to sulphate during oxidation by ozone is:

$$\Delta^{17}O(S(VI))_{O_3+SO_2} = \frac{1}{2} \cdot \Delta^{17}O(SO_2) + \frac{1}{4} \cdot \Delta^{17}O(H_2O) + \frac{1}{4} \cdot \Delta^{17}O(O_3{}^*)$$
(4.13)

This equation can be simplified because the O-MIF anomalies in SO_2 and H_2O are negligible:

$$\Delta^{17}O(S(VI))_{O_3+SO_2} = \frac{1}{4} \cdot \Delta^{17}O(O_3{}^*)$$
(4.14)

Therefore, the isotopic anomaly in atmospheric sulphates produced in the model during the oxidation of dissolved SO_2 through O_3 is $\Delta^{17}O$ $(S(VI))_{O_3+SO_2}$ = 9 ‰ (Morin et al., 2007, 2011).

Oxidation by hydroxyl radical

In the atmosphere, OH radicals are formed as a result of ozone photolysis in presence of water vapour. In particular, ozone photodissociation can produce an $O^1(D)$ radical, which react with a water molecule to produce two OH radicals. Tropospheric OH radicals are thought not to carry O-MIF anomaly because the exchange of oxygen atoms with water vapour is so fast that it erases any inherited isotopic anomaly in OH. Recall that tropospheric H_2O does not carry any O-MIF because the tropospheric H_2O cycle is entirely controlled by physical processes (condensation, evaporation) and not by chemical processes involving ozone. As a result, the O-MIF signature in OH radicals is expected be zero ($\Delta^{17}O$ (OH) = 0.0 ‰) (Morin et al., 2011). However, when the humidity and hence H_2O levels are very low (e.g. upper troposphere), the rate of isotopic exchange between OH radicals and H_2O molecules decreases so much that freshly produced OH radicals may have time to react with other molecules before losing their isotopic anomaly by isotopic exchange with H_2O (Morin et al., 2007). Under those conditions, when the OH loss reactions and cycling compete with the isotopic exchange with H_2O, some of the initial O-MIF originating from ozone is still present in reacting OH. It is also possible for OH loss to compete with the H_2O isotopic exchange when the rate of OH loss is highly enhanced instead of having a reduced rate of H_2O isotopic exchange. This may be the case in volcanic plumes, when SO_2 levels are so high that the SO_2 + OH reaction become the dominant chemical loss (Bekki, 1995), accelerating the OH cycling. In order to account for this possibility, instead of assuming a null O-MIF for OH, the O-MIF in the steady-state OH ($\Delta^{17}O$ (OH)) is calculated explicitly using the approach developed by Morin et al. (Morin et al., 2007). $\Delta^{17}O$ (OH) is simply derived from the competing balance between the O-MIF erasing isotopic exchange and the total OH loss, typically the reactions with CO and CH_4 in the troposphere. Since we consider sulphur-rich volcanic plumes and clouds, the reaction between OH and SO_2 is also taken into account.

Considering all the transfers of oxygen atoms, the isotopic mass-balance equation for the OH pathway can be expressed as:

$$\Delta^{17}O(S(VI))_{OH+SO_2} = \frac{1}{2} \cdot \Delta^{17}O(SO_2) + \frac{1}{4} \cdot \Delta^{17}O(OH) + \frac{1}{4} \cdot \Delta^{17}O(H_2O)$$
(4.15)

Since tropospheric H_2O and volcanic SO_2 are not thought to carry any O-MIF, the equation can be simplified:

$$\Delta^{17}O(S(VI))_{OH+SO_2} = \frac{1}{4} \cdot \Delta^{17}O(OH)$$
(4.16)

The O-MIF of OH can be derived using the following equation

$$\Delta^{17}O(OH) = x \cdot \Delta^{17}O(OH^*_{prod.})$$
(4.17)

with

$$\Delta^{17}O(OH^*_{prod.}) = \frac{1}{2} \cdot \Delta^{17}O(O_3^*) \qquad (4.18)$$

and

$$x = \frac{D}{D + k^*_{OH+H_2O} \cdot [H_2O]} \qquad (4.19)$$

$$D = k_{OH+CO} \cdot [CO] + k_{OH+CH_4} \cdot [CH_4] + k_{OH+SO_2} \cdot [SO_2] \qquad (4.20)$$

where $k^*_{OH+H_2O}$ is the rate constant for the oxygen atoms exchange reaction between OH and H_2O, and k_{OH+CH_4} and k_{OH+CO} are the reaction rate constants for the gas phase reaction of OH with CH_4 and CO respectively.

In this approach x represents the competition between the O-MIF erasing effect of isotopic exchange and the O-MIF retaining effect of OH chemical loss; only important loss reactions for tropospheric OH are considered here. $\Delta^{17}O(OH^*_{prod.})$ is the O-MIF of the OH radical freshly produced, and it is assumed that OH is mostly formed by the photolysis of ozone followed by the reaction of $O^1(D)$ with H_2O.

The O-MIF in OH ($\Delta^{17}O(OH)$) is determined by this x factor. If OH chemical loss is much faster than the isotopic exchange, $\Delta^{17}O(OH) = 0.5 \cdot \Delta^{17}O(O_3^*)$ (i.e. $x = 1$). If chemical loss is much slower than the isotopic exchange, $\Delta^{17}O(OH) \approx 0‰$ (i.e. $x \ll 1$).

Oxidation by hydrogen peroxide

In the troposphere, H_2O_2 can quickly dissolve into liquid water phases (Chandler et al., 1988). In a volcanic plume, these phases can be either water droplets or water condensed on solid particles, typically on ash particles. Once in the aqueous phase, H_2O_2 oxidizes SO_2 by nucleophilic displacement, and its two oxygen atoms are transmitted to the produced sulphate molecule (McArdle and Hoffmann, 1983; Brandt and van Eldik, 1995).

The isotopic balance for the oxidation by H_2O_2 in the liquid phase is:

$$\Delta^{17}O(S(VI))_{H_2O_2+SO_2} = \frac{1}{2} \cdot \Delta^{17}O(SO_2) + \frac{1}{2} \cdot \Delta^{17}O(H_2O_2) \qquad (4.21)$$

Since volcanic SO_2 is thought to carry no significant O-MIF, the final O-MIF transfer can be simplified:

$$\Delta^{17}O(S(VI))_{H_2O_2+SO_2} = \frac{1}{2} \cdot \Delta^{17}O(H_2O_2) \qquad (4.22)$$

Isotopic measurements of $\Delta^{17}O$ of tropospheric H_2O_2 range between 1.30 and 2.20 ‰ with a mean O-MIF of 1.70 ‰ (Savarino and Thiemens, 1999b,a). Using this mean value, sulphate produced by the H_2O_2 oxidation is assumed to carry a $\Delta^{17}O(S(VI))_{H_2O_2+SO_2}$ = 0.87 ‰ (Savarino et al., 2000).

Oxidation by O$_2$/TMI

Isotopic measurements of atmospheric O$_2$ indicate that its O-MIF anomaly is rather small (Luz et al., 1999; Barkan and Luz, 2003). Kinetic isotope fractionation associated to the Dole effect (Dole, 1936) and stratospheric influx of O$_2$ generates a slightly negative O-MIF in tropospheric O$_2$. As theoretical investigations suggest, a slight depletion of ^{17}O is indeed found in tropospheric O$_2$, which is accompanied by a slightly negative O-MIF (Barkan and Luz, 2003). Theoretical calculations predict Δ^{17}O (O$_2$) as low as -0.344 ‰ (Pack et al., 2007) or even, more recently, -0.410 ‰ for tropospheric O$_2$ (Young et al., 2014). Other theoretical calculations suggest a Δ^{17}O (O$_2$) between 0.141 and -0.305 ‰ (Young et al., 2002).

We assume a Δ^{17}O (O$_2$) of -0.340 ‰ (Miller, 2002). This value is chosen because it gives a reasonably good agreement between isotopic measurements (Martin et al., 2014) and models (Miller, 2002; Young et al., 2002; Pack et al., 2007). In addition, it has to be kept in mind that there are large uncertainties associated with the exact reaction mechanism of SO$_2$ oxidation catalysed by TMI. We assume that only one oxygen atom of O$_2$ is transmitted to sulphate during the SO$_2$ oxidation (Brandt and van Eldik, 1995; Herrmann et al., 2000).

With these assumptions, the isotopic mass-balance equation for SO$_2$ oxidation by O$_2$/TMI is given by:

$$\Delta^{17}O(S(VI))_{O_2+SO_2} = \frac{3}{4} \cdot \Delta^{17}O(S(IV)) + \frac{1}{4} \cdot \Delta^{17}O(O_2) \qquad (4.23)$$

Since volcanic SO$_2$ is thought to carry no significant O-MIF, we can assume that initial S(IV) species do not carry any O-MIF. Consequently, the isotopic signature associated to this oxidation pathway can be simplified:

$$\Delta^{17}O(S(VI))_{O_2+SO_2} = \frac{1}{4} \cdot \Delta^{17}O(O_2) \qquad (4.24)$$

Δ^{17}O (O$_2$) being taken as -0.34 ‰ (see above), sulphate produced through this pathway carries a O-MIF ($\Delta^{17}O(S(VI))_{O_2+SO_2}$) almost null, of about -0.09 ‰ (Savarino et al., 2000). The O-MIF signatures of all the S(IV) oxidation pathways used in the model are summarized in Table:4.3.

3 Box model set up

3.1 Standard case: initial conditions

All simulations are run for springtime conditions and start at 8.00 a.m. at tropical latitudes (8.3° N). In order to reach stable chemical compositions, notably for medium- and short-lived reactive species, the model is run for 3 days before injecting SO$_2$, then, the evolution of the chemical composition is followed for 7

days. This timescale corresponds approximately to the lifetime of a plume in the free troposphere, in occurrence of low turbulence and low wind shear (Arnold et al., 2007).

Since most of volcanoes are situated in remote areas with their peaks close to the free troposphere, or, at least, with volcanic plumes often ending up in the free troposphere, the environmental conditions are chosen to be representative of the lower free troposphere with temperature set at 283.15 K, and pressure fixed at 640 mbar (about 3 km altitude). Since we consider cloudy conditions, the relative humidity is set to 100%.

Furthermore, concentrations of reactive species are also set to typical levels found in the tropical lower free troposphere: O_3 = 45 ppbv and H_2O_2 = 0.1 ppbv. Finally, initial SO_2 is set to a mean volcanic plume concentration of 1 ppmv, a value typical of volcanic plumes during degassing (Robock, 2000; Herrmann et al., 2000; Wardell et al., 2004; Mather et al., 2006; Roberts et al., 2012; De Moor et al., 2013; Voigt et al., 2014). The initial pH of the aqueous phase is set to 4.5. It has no impact on the overall model results because the pH is almost immediately driven by SO_2 uptake and sulphur oxidation. Preliminary simulations have shown that the initial SO_2 concentration is a critical input.

Due to the large amounts of water that can be injected during explosive eruptions, in our simulations it is assumed that volcanic water vapour is largely in excess compared to relative humidity of the free troposphere. Moreover, due to low temperature and pressure of the lower free troposphere, for our simulations it is assumed that volcanic water vapour would mostly condense to produce cloud droplets or to coat ash particles. Therefore, throughout this study relative humidity (RH) inside volcanic plumes is set at 100%, the water saturation point corresponding to the pressure and temperature of the background atmosphere. The LWC (Liquid Water Content) parametrises the amount of liquid water within plumes. High levels of LWC (Liquid Water Content) can be reached, indeed, within volcanic plumes from explosive eruptions. Modelling simulations suggest that LWC as high as 1.6 $g\,m^{-3}$ could be reached at the core of water-rich volcanic clouds condensing in the troposphere (Aiuppa et al., 2006b). It is possible that, during the first stages of medium-size eruptions, LWC within the plume could be at least comparable to LWC values of growing cumulus clouds. For all the simulations LWC is set to 1.0 $g\,m^{-3}$, a value between experimental measurements (e.g. meteorological clouds) and modelling studies of water-rich volcanic plumes reaching the upper troposphere (Tabazadeh and Turco, 1993; Hoshyaripour et al., 2015). Like SO_2, LWC is found to be a critical model input.

TMI concentrations in the liquid phase are set to [Fe(III)] = 0,5 μM and to [Mn(II)] = 0,05 μM. These values are at the lower end of typical tropospheric measurements with [Fe(III)] concentrations ranging between 0.5 and 2 μM (Martin and Good, 1991; Parazols et al., 2006). Because of uncertainties associated with iron dissolution in volcanic plumes, our TMI concentrations are lower than concentrations found in dust-rich polluted conditions where [Fe(III)] can reach concentrations of around 5 μM (Herrmann et al., 2000; Parazols et al.,

2006). TMI concentrations follow the same relation throughout the whole study and for each simulation [Mn(II)] = 0.1 · [Fe(III)] (Martin and Good, 1991).

3.2 Model experiments

The objective of the first set of numerical experiments is to assess the competition among oxidation pathways in SO_2-rich plumes/clouds for the standard case. Three simulations (S1-S3) are run with oxidation schemes of increasing complexity. They simulate oxidation of SO_2: (S1) by OH in gas phase, (S2) by OH in gas phase, and H_2O_2 and O_3 in aqueous phase, and (S3) by OH in gas phase, and H_2O_2, O_3 and O_2/TMI in aqueous phase.

Since initial SO_2 levels, LWC and TMI concentrations in volcanic plumes are relatively uncertain and are key model inputs, the sensitivity of the results to varying conditions within plausible ranges is also explored in additional simulations. Isotopic anomaly transfers are investigated for atmospheric concentrations stretching from passive degassing/quiescent conditions to sulphur-rich volcanic clouds with varying levels of TMI. The intervals used for the different sensitivity studies are summarised in Table:4.4.

The first set of sensitivity simulations is devoted to the sensitivity of results to initial SO_2 levels in the case of the S1 simulation. It is designed to explore not only the impact of varying SO_2 levels on sulphate O-MIF produced by the OH oxidation pathway, but also on OH isotopic signature itself. Recall that the OH isotopic signature ($\Delta^{17}O$ (OH)) is generally assumed zero in the literature (see section 2.4.2).

It is widely recognized that SO_2 is the compound emitted by volcanic activity which causes the largest climatic impacts through its conversion into sulphate aerosols (Graf et al., 1998; Robock, 2000; Textor et al., 2004; Langmann, 2014). Emissions of volcanic SO_2 have been measured both in proximity of volcanic vents and in aged plumes. It is possible to constrain a range of concentrations, considering age of plumes and distance from points of emissions. During first stages of plume development concentrations of SO_2 in the range of 10-50 ppmv can be reached right in proximity of volcanic vents (Aiuppa et al., 2005b, 2006a; Roberts et al., 2012), while concentrations in the range of 0.1-1 ppmv can be found in aged plumes at longer distances from points of emissions (Delmelle, 2003; Carn et al., 2011). These results are confirmed by modelling simulations which can constrain volcanic emissions by accounting for quick dilution after plume ejection from the vent (Gerlach, 2004; Aiuppa et al., 2006b; Roberts et al., 2009). Consequently, based on atmospheric simulations and on in-situ measurements, the SO_2 concentration is set to 1.0 ppmv in the standard case, and is varied from 0.1 to 10 ppmv in the sensitivity simulations.

LWC plays a crucial role in aqueous oxidation of volcanic SO_2. The range of LWC considered has been chosen based on LWC observed for different cloud typologies such as mean saturated clouds (0.1 $g\,m^{-3}$), water-rich cumulus clouds (0.5-1 $g\,m^{-3}$), and cumulonimbus clouds (1-2 $g\,m^{-3}$) (Laj et al., 1997;

Rosenfeld and Lensky, 1998; Pruppacher et al., 1998; Korolev et al., 2007; Carey et al., 2008). LWC is set to 1 $g\,m^{-3}$ in the standard case and is varied from 0.1 to more extreme values of 2.5 $g\,m^{-3}$ for sensitivity simulations (Tabazadeh and Turco, 1993; Aiuppa et al., 2006b).

Aqueous concentrations of iron ([Fe(tot)] = [Fe(II)] + [Fe(III)]) can peak to 9-10 μM in the troposphere (Desboeufs et al., 1999, 2001) with [Fe(III)] concentrations between 2.0 μM and 5.0 μM in polluted conditions if photochemical cycling between [Fe(II)]-[Fe(III)] is inhibited (Parazols et al., 2006). Volcanic eruptions inject large quantities of solid material into the atmosphere in the form of ash. As a result, volcanic plumes/clouds are characterised by high concentrations of ash and minerals (Mather et al., 2003). Ash particles have sizes as large as few mm and they are mainly composed of silica and crystalline minerals of magmatic origin. Glass, olivine, magnetite, hematite and fayelite are among the most common minerals injected during eruptions (Rose and Durant, 2009; Langmann, 2014; Hoshyaripour et al., 2015). These minerals are composed in different proportions by Fe(II) and Fe(III), which are entrapped in the crystalline structure of rocks in different morphologies and compositions. Since large quantities of water are also injected during eruptions, water can condense on mineral particles, especially as the volcanic column reaches higher altitudes and lower temperatures in the troposphere (Tabazadeh and Turco, 1993; Hoshyaripour et al., 2015). Once mineral particles are coated by water, dissolution of iron from the solid mineral surface to the thin liquid water film may take place depending on the acidity of the aqueous phase (Ayris and Delmelle, 2012a; Langmann, 2014; Maters et al., 2016). Acidic conditions (pH ¡ 2.0) due to H_2SO_4 condensation or formation within the liquid phase favour the solubility of minerals containing iron and dissolution of [Fe(III)] (Solmon et al., 2009; Ayris and Delmelle, 2012a). Up to a third of total Fe at the ash surface can dissolve into the liquid phase coating volcanic particles (Hoshyaripour et al., 2014) depending on rock composition and gases in the volcanic clouds. Laboratory experiments on dissolution in acidic water of iron from volcanic ashes suggest that [Fe(III)] concentrations of up to 2 μM can be reached quickly in the liquid phase when pH reaches $\sim$ 2 (Maters et al., 2016). Concentrations as high as [Fe(III)] = 3 μM could be reached if pH reaches 1 (Maters et al., 2016). Mobilization of iron ions from ashes could be enhanced for plumes reaching the upper troposphere and undergoing ice formation (Jeong et al., 2012; Shi et al., 2012). High concentrations of [Fe(III)] might persist in the liquid phase depending on the lifetime of water droplets, notably driven by evaporation and condensation cycles (Desboeufs et al., 2001; Langmann, 2014).

Cloud properties are affected by evaporation and condensation cycles changing the pH, the size and number of droplets, while formation of insoluble salts at the surface of ash particles entrapped in cloud droplets can affect mobilization of ions (Ayris and Delmelle, 2012a; Langmann, 2014). Therefore, lower acidity combined with the presence of insoluble salts may result in a reduced availability of dissolved TMI in volcanic clouds as the volcanic cloud ages. Over the long

term, these conditions can lead to concentration of Fe(III) in water droplets of volcanic clouds which can be lower than typical concentrations found in tropospheric clouds (Desboeufs et al., 1999, 2001). In this study, [Fe(III)] is set to $0.5\,\mathrm{g\,m^{-3}}$ in the standard case and is varied from 0.1 to 3 μM in the sensitivity simulations to cover the wide range of possible [Fe(III)] concentrations.

The resulting model $\Delta^{17}O(S(VI))$ (i.e. from standard and sensitivity simulations) are compared to sulphate O-MIF found in tropospheric volcanic sulphates extracted from ash-deposits of small and medium-size tropospheric explosive eruptions of the present geological era (Bindeman et al., 2007; Martin et al., 2014; Bao, 2015), or in sulphate aerosols collected at volcanic vents, most certainly primary sulphate (Mather et al., 2006).

Table 4.4: Ranges of SO_2, LWC and TMI explored in the sensitivity studies

SO_2	$0.1 - 10.0$ ppmv
LWC	$0.1 - 2.5\,\mathrm{gm^{-3}}$
TMI	$0.1 - 3.0\,\mu$M

4 Results and discussion

4.1 Isotopic constraints on individual oxidation pathways of volcanic SO_2

Gaseous oxidation by OH

S1 simulates the O-MIF transfer to sulphate in the absence of aqueous oxidation for standard conditions; H_2SO_4 is only produced by the reaction between hydroxyl radicals and SO_2 in the gas phase. As soon as SO_2 is injected, it reacts with OH to produce gaseous H_2SO_4. **Fig.:4.2** shows the decay of SO_2 levels from 1.5 ppmv to 1.26 ppmv after 7 days. As expected, gas-phase concentrations of other SO_2 oxidants (i.e. O_3 and H_2O_2) are not substantially affected by the SO_2 injection. Since H_2SO_4 is very soluble, once produced in the gas phase, it ends up dissolved in the liquid phase where it shifts the pH towards acidic values because of its quasi-complete dissociation.

The concentration of atmospheric sulphate (S(VI)) is driven by the gas-phase production and deposition. Sulphate production follows a diurnal cycle because of the diurnal production of OH. There is no significant production of S(VI) during night-time. **Fig.:4.3** shows the time evolutions of the liquid phase pH, of the atmospheric sulphate O-MIF ($\Delta^{17}O(S(VI))$), and of deposited sulphate O-MIF ($\Delta^{17}O(S(VI))_{dep}$) following the injection of SO_2. The pH exhibits diurnal variations because sulphate is only produced during daytime. After an initial spike around +0.95 ‰, atmospheric sulphate O-MIF ($\Delta^{17}O(S(VI))$) declines very slowly to +0.9 ‰ after 7 days. Since SO_2 is only oxidized by OH, the evolution
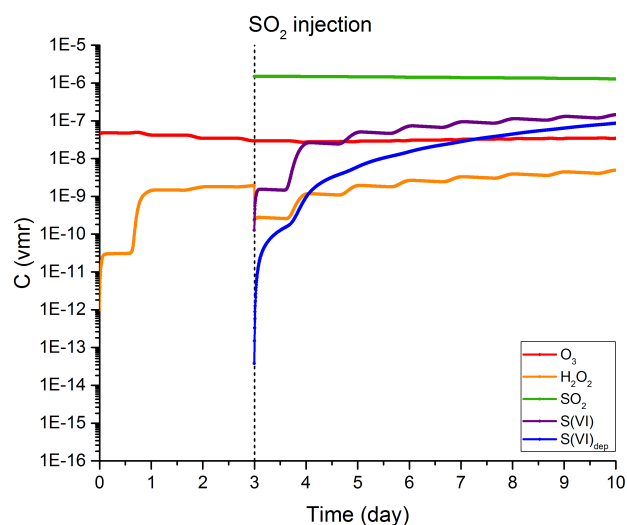
Figure 4.2: Evolution of the gas-phase concentrations of atmospheric species during the S1 simulation (see text). The simulation starts at 8:00 a.m. and SO_2 is injected after 3 days. During S1 simulation the concentration of injected SO_2 drops from 1.5 ppmv to a final value of 1.27 ppmv.
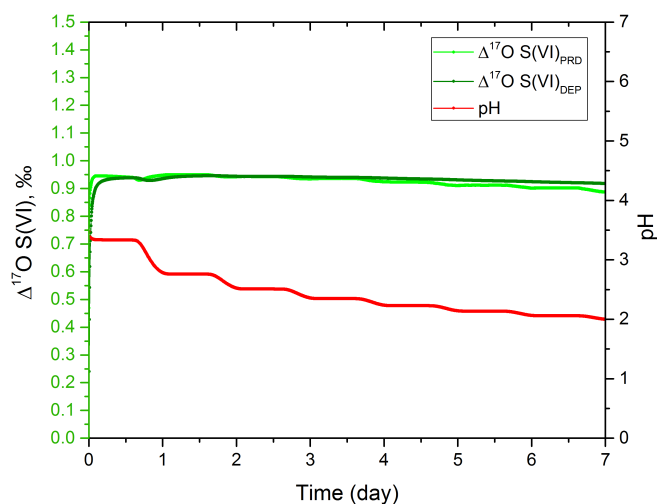
Figure 4.3: Time evolution of $\Delta^{17}O(S(VI))$, and of the pH of the liquid phases in volcanic plumes during simulations S1, following injection of SO_2 in the box. The change of pH in water droplets is also reported as a function of time.

of $\Delta^{17}O(S(VI))$ reflects the evolution of the OH isotopic signature ($\Delta^{17}O$ (OH)). Unexpectedly, it is found to be very different from zero. Usually, the exchange of oxygen atoms with water vapour is so fast in the troposphere that it erases any inherited isotopic anomaly in OH. However, in our standard conditions, SO_2 levels are so high that the SO_2 + OH reaction become the overwhelmingly dominant loss (Bekki, 1995), accelerating greatly the OH cycling. Under those conditions, the OH loss is so enhanced that the reaction competes with the isotopic exchange with H_2O. Therefore OH radicals can react before their isotopic anomaly is entirely erased by the isotopic exchange, and they maintain a significant positive signature. As SO_2 concentration decreases slowly, the rate of OH loss decreases and, as expected, so is $\Delta^{17}O(S(VI))$.

The evolution of deposited sulphate O-MIF somewhat follows the evolution of the atmospheric sulphate O-MIF but with the time lag which is related to the characteristic timescale of the atmospheric sulphate deposition specified in the model (5.7 days). The final O-MIF of deposited sulphate (resulting from the cumulative effect of sulphate deposited since the SO_2 injection) is 0.92 ‰, which is distinctively higher than most measurements from volcanic sulphate sampled in volcanic ash-deposits (see Table:4.1).

Isotopic signature of OH: dependence on initial SO_2

Since $\Delta^{17}O(OH)$ is sensitive to the SO_2 level, additional S1 simulations are carried out with SO_2 concentration differing by 3 orders of magnitude. **Fig.:4.4** shows the time evolution of OH and sulphate O-MIF for two different initial SO_2 concentrations (i.e. 1 ppbv and 1 ppmv). The upper plot shows the time evolution of OH for the two SO_2 cases. As soon as the SO_2 is injected, OH concentration drops sharply in the high SO_2 case, whereas it remains unaffected in the low SO_2 case. At such high SO_2 concentration, the reaction between OH and SO_2 becomes the main OH loss. As a result, OH concentration and lifetime drop and its cycling is much faster. The lower plot of **Fig.:4.4** illustrates the effect on the value of O-MIF transferred to sulphate via OH oxidation.

For 1 ppbv of initial SO_2 instead of 1 ppmv, $\Delta^{17}O(OH)$ is negligible (of the order of 0.01 ‰), thus the sulphate O-MIF is quasi-zero. For 1 ppmv of initial SO_2, shortly after the injection, the sulphate produced has an isotopic signature of 0.7 ‰. It then declines slowly as the SO_2 concentration decays slowly. In Eq.:4.17, the competition between OH loss channels and the isotopic exchange with water is represented by the x ratio. In the simulation with 1 ppmv of initial SO_2, $\Delta^{17}O(OH)$ decreases from 10.8 to 7.6 ‰, whereas the variation is very small in the simulation with 1 ppbv of initial SO_2. These results suggest that OH could have a positive O-MIF in volcanic sulphur-rich plumes and clouds which is subsequently transferred to the produced sulphate. Since most isotopic measurements indicate that O-MIF in volcanic sulphate is very close to zero, at least within the measurement errors of about 0.1 ‰ typically, other oxidation pathways that are mostly mass-dependent (i.e. null O-MIF) have
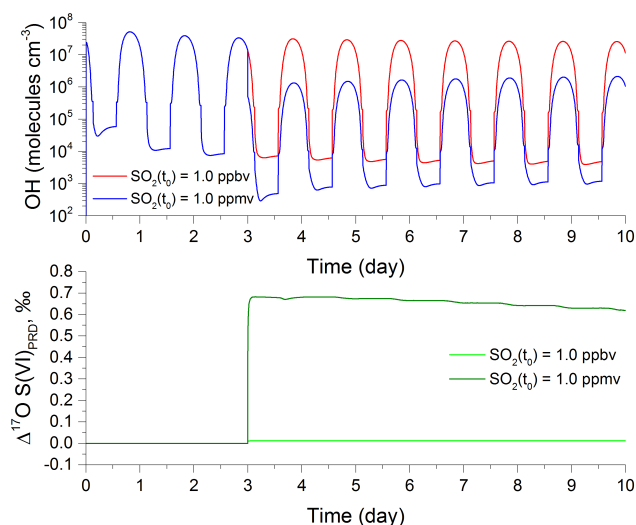
Figure 4.4: Time evolution of the O-MIF transfer from OH to $H_2SO_{4(g)}$ at two different initial concentrations of SO_2. The light green line represents initial concentration of S(IV) = 1 ppbv (e.g. mean troposphere); the dark green line represents an initial concentration of SO_2 = 1 ppmv (e.g. volcanic plumes/clouds). The upper figure shows concentration trends for OH during the two different scenarios.

to contribute very significantly to the formation of volcanic sulphate. The other known oxidation pathways of SO_2 are heterogeneous.

Gaseous and heterogeneous oxidation by O_3 and H_2O_2

The S2 simulation is the same as S1 except that it also includes the aqueous oxidation of SO_2 by H_2O_2 and O_3. **Fig.:4.5** shows evolving concentrations of atmospheric species as oxidation takes place.

Almost as soon as SO_2 is injected, the H_2O_2 concentration drops from about 20 ppbv to less than a pptv. At the same time, as in S1, the pH quickly drops to less than 3 (see Fig:4.6).

Just after the injection, H_2O_2 is initially the overwhelmingly dominant oxidant (Martin et al., 2014). The contribution of oxidation by O_3 is almost negligible under acidic conditions and the oxidation by OH in the gas phase is much slower initially that aqueous oxidation by H_2O_2. However, as the SO_2 concentration vastly exceeds the H_2O_2 concentration (by 3 orders of magnitude), H_2O_2 is very quickly consumed by reaction with SO_2 in the liquid phase; recall for each molecule of SO_2 oxidized by H_2O_2, one molecule of H_2O_2 is consumed. The difference in concentration between SO_2 and H_2O_2 is such that, as soon as a molecule of H_2O_2 enters the liquid phase, it is consumed. The sharp drop in
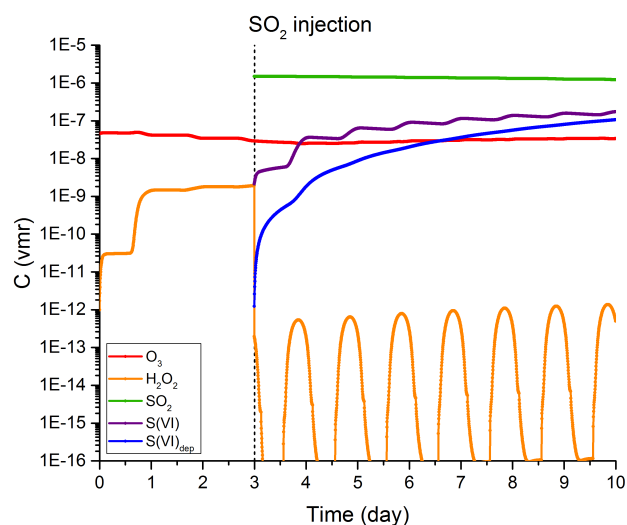
Figure 4.5: Time evolution in the gas-phase concentrations of SO$_2$, its tropospheric oxidants and produced and deposited sulphates during S2. During S2 simulation the concentration of injected SO$_2$ drops from 1.5 ppmv to a final value of 1.2 ppmv.
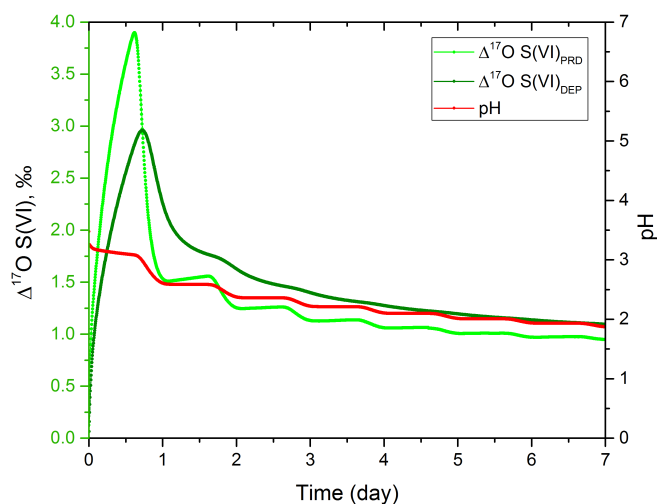
Figure 4.6: Temporal evolution of Δ^{17}O(S(VI)) in produced and deposited sulphates, and of pH during the S2 simulation.

H$_2$O$_2$ concentration is thus limited by H$_2$O$_2$ gas phase diffusion to the surface of the liquid phase, which is followed by its quick reaction with S(IV). After

the initial drop, the H_2O_2 concentration stays very low with very large diurnal variations. The daytime concentration approaches pptv levels because the loss to the liquid phase is balanced by gas-phase photochemical production. After the drop in H_2O_2, most of the SO_2 is oxidised by OH in the gas-phase. As shown in Fig:4.6, the pH in S2 follows a trend similar to the one in S1. The sulphate O-MIF in S2 is higher than in S1. In the first phase, sulphate is produced with a rather high O-MIF signature because the contribution of O_3 to SO_2 oxidation is significant with an initial pH set to 4.5 (i.e. as high as 50% of SO_2 is oxidised by O_3 within the first hours). The O-MIF of produced sulphate ($\Delta^{17}O(S(VI)_{PRD})$) peaks early on at 4 ‰. However, the pH drops very quickly as more S(VI) is produced in the aqueous phase. As a result, the pH-dependent oxidation rate by O_3 decreases quickly and hence so does $\Delta^{17}O(S(VI)_{PRD})$. H_2O_2 is completely consumed within 15 minutes during the first timesteps, and it does not contribute to the SO_2 oxidation thereafter. The oxidation of SO_2 is dominated by OH except during the early phase. The final O-MIF in deposited sulphate is 1.1 ‰, originating mostly from OH oxidation. Recall that, when OH is generated via its main production channel, it carries an isotopic anomaly. Under common (non-volcanic) conditions, the OH anomaly is so rapidly erased by isotopic exchange with H_2O that, when OH reacts, it carries no anomaly. However, when SO_2 levels are very high, OH might react very quickly with SO_2 without having lost its anomaly by isotopic exchange. In this situation, the value of $\Delta^{17}O(OH)$ is determined by the competition between the $SO_2{}^+OH$ reaction and the OH isotopic exchange with H_2O. As SO_2 concentration decays with time, $\Delta^{17}O(OH)$ decreases because the $SO_2{}^+OH$ reaction slows down and becomes less competitive with respect to the isotopic exchange (see Eq.:4.15-4.20). This explains why $\Delta^{17}O(OH)$ decreases from 4 ‰ to roughly 3 ‰ by the end of simulation, resulting in produced sulphates with respectively O-MIF of 1 and 0.75 ‰. The value of O-MIF on deposited sulphates produced in this simulation is still much higher than most O-MIF measurements in tropospheric volcanic sulphates (see Table:4.1). In order to produce mass-dependent sulphates without O-MIF ($\Delta^{17}O= 0.0\pm0.1$‰), another oxidant needs to be dominant and it has to carry a small or null O-MIF anomaly.

Gaseous and heterogeneous oxidation by O_3, H_2O_2 and $O_{2/}$TMI

Simulation S3 includes all the major pathways of oxidation involved during formation of sulphate in SO_2-rich clouds (i.e. without significant halogens concentrations compared to sulphur species). **Fig.:4.7** shows the evolution of the chemical species concentrations. In S3, H_2O_2 is very quickly depleted just after the SO_2 injection as in S2. However, there is much less SO_2 left at the end of the run in S3 than in S2 and S1 and conversely there is more S(VI) produced in S3 than in S2 and S1. With the TMI catalysed oxidation added to the S2 chemical scheme, heterogeneous chemistry becomes competitive with the gas-phase oxidation by OH and lead to faster formation of S(VI). The pH is also lower
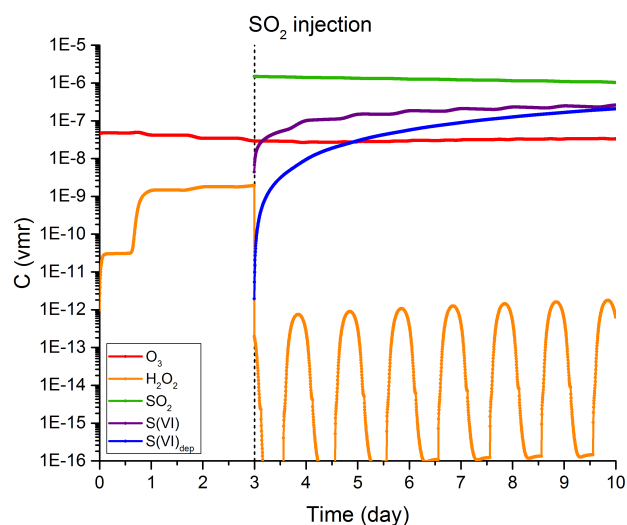
Figure 4.7: Time evolution in the gas-phase concentrations of SO$_2$, its tropospheric oxidants and produced and deposited sulphates during S3. During S3 simulation the concentration of injected SO$_2$ drops from 1.5 ppmv to a final value of 1 ppmv.
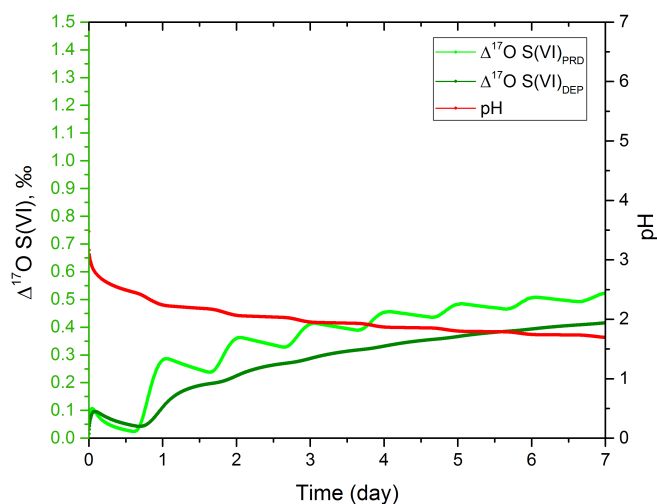
Figure 4.8: Time evolution of $\Delta^{17}O(S(VI))$ in produced and deposited sulphates, and of pH of the liquid phases of volcanic plumes during simulation S3.

(see **Fig.:4.8**), confirming that more sulphates are in aqueous solution. The final O-MIF in deposited sulphates is about 0.3 ‰.

This value is lower than the values calculated in simulations S1 and S2 and closer but still higher than the range of isotopic measurements carried out on volcanic sulphate (see Table:4.1). This result suggests that heterogeneous SO_2 oxidation by $O_{2/}$TMI is the only pathway able to explain sulphate isotopic measurements with the current chemical scheme. Sensitivity studies are however needed to test the responses of the system to varying conditions of heterogeneous oxidation. Consequently, we conduct further simulations to probe the effects of LWC and TMI aqueous concentrations on the final MIF in deposited sulphate and assess the robustness of the overall results.

4.2 Sensitivity studies

Influence of SO_2 on sulphate O-MIF

In the first set of sensitivity simulations (Z1), the response of the system to various concentrations of SO_2 is tested for the standard conditions with all the oxidation channels included in the model. Fig:4.9 shows the time evolution of O-MIF in the produced sulphate for different initial SO_2 concentrations. The initial concentration of volcanic SO_2 is varied from 10 ppbv to 10.0 ppmv. LWC is set to 1.0 $g\,m^{-3}$ and [Fe(III)] = 0.5 μ M. The response of the system and, in particular, of produced sulphate O-MIF to varying SO_2 levels is complex and not at all linear. In Table:4.5 the different contributions of the oxidation pathways are reported for different initial SO_2 concentrations, in function of: O-MIF in OH, O-MIF in deposited sulphate. The isotopic anomalies and the contribution of different pathways of oxidation are reported for one day after sulphur injection, and for the end of the simulations. For an initial SO_2 of 10 ppbv, H_2O_2 is the dominant pathway of sulphur oxidation with the OH oxidation pathway representing about a third of the total; the final O-MIF in the deposited sulphate is 0.50 ‰. When the initial SO_2 concentration is increased (from 10 ppbv to 30 and then 100 ppbv), sulphate O-MIF decreases because the H_2O_2 contribution to SO_2 oxidation drops whereas the OH contribution becomes dominant. The drop in the H_2O_2 contribution is mostly due to the increased acidity of cloud droplets at higher SO_2 concentrations, resulting in much reduced uptake of SO_2 combined to a much smaller fraction of aqueous S(IV) in the form of HSO_3^-, the reactant for the S(IV) oxidation by H_2O_2 (McArdle and Hoffmann, 1983). Above 100 ppbv, instead of decreasing, sulphate O-MIF increases at higher initial SO_2 concentration, with 10 ppmv being the maximum SO_2 concentration considered here. This inversion in the evolution of $\Delta^{17}O(S(VI))$ with increasing SO_2 concentration originates from the change in $\Delta^{17}O(OH)$. Up to 100 ppbv of SO_2, $\Delta^{17}O(OH)$ is more or less negligible and consequently the OH oxidation produces sulphate with insignificant O-MIF. However, at 300 ppbv of initial SO_2, $\Delta^{17}O(OH)$ is equal to 0.8 ‰ at the start of simulation and is still greater than 0.3 ‰ at the end of the run. The higher SO_2 concentration is, the higher $\Delta^{17}O(OH)$ is.
At 10 ppmv of SO_2, $\Delta^{17}O(OH)$ = 11.5 ‰. Recall that the maximum possible

Table 4.5: Contribution to sulphate production from different pathways of sulphur oxidation at varying initial concentration of SO_2

C_0, SO_2 (ppmv)	Time (day)	$\Delta^{17}O(OH)$ (‰)	OH	O_3	H_2O_2	O_2/TMI	$\Delta^{17}O(S(VI), dep.)_f$ (‰)
0.01	1	0	39	0	55	6	0.38
	7	0	35	0	60	5	0.47
0.03	1	0	60	0	30	10	0.18
	7	0	54	0	40	6	0.32
0.1	1	0.3	63	0	22	15	0.15
	7	0.05	66	0	28	6	0.32
0.3	1	0.8	56	0	19	25	0.17
	7	0.3	69	0	22	9	0.29
1	1	2.6	43	0	15	42	0.20
	7	2	62	0	19	19	0.50
3	1	6.2	30	0	10	60	0.23
	7	5.6	51	0	14	35	0.77
10	1	11.5	17	0	5	77	0.19
	7	11.2	33	0	9	58	0.82

98
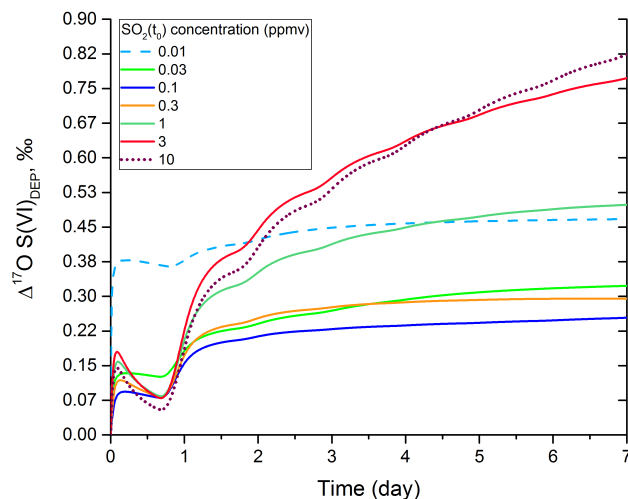
Figure 4.9: Temporal evolution of $\Delta^{17}O(S(VI))_{dep}$ at different initial concentrations of SO_2. The dashed line represents simulation where H_2O_2 is the major SO_2 oxidant, straight lines are simulations for which OH is the major oxidant, and dot lines are simulations for which O_2/TMI is the major pathway of oxidation. The equivalent pathways contributions are summarised in Table:4.5. Other critical parameters are set to: LWC = 1.0 gm^{-3} and [Fe(III)] = 0.5 μM

value of $\Delta^{17}O(OH)$ is 18.0 ‰, corresponding to conditions where the rate of the isotopic exchange is negligible compared to the rate of OH chemical loss. Interestingly, the overall contribution of OH to the sulphur oxidation peaks at 69% for initial SO_2 equal to 300 ppbv. At higher concentrations, the OH contribution decreases reaching 33% for the simulation with 10 ppmv of initial SO_2. At the same time, the contribution of O_2/TMI oxidation (the only channel with a negligible O-MIF signature) increases sharply becoming even dominant (58%) for the simulation with 10 ppmv of initial SO_2. Nonetheless, the very large increase in $\Delta^{17}O(OH)$ is the main driver of $\Delta^{17}O(S(VI))$ for high SO_2 levels, because the OH contribution remains important even for the simulation with 10 ppmv of initial SO_2. Note that the H_2O_2 contribution declines all the way with increasing initial SO_2 (from 10 ppbv to 10 pmmv) which is the inverse of the O_2/TMI contribution evolution.

Overall, the model-calculated contribution of the OH pathway to volcanic sulphur oxidation does not drop below 30% for the standard conditions considered here. As a result, the O-MIF of deposited sulphate O-MIF is expected to depend strongly on the amount of SO_2 injected, via the dependency of OH isotopic signature on SO_2 concentration. Since volcanic SO_2 usually reaches ppmv levels during the first stages of volcanic plume (Roberts et al., 2009,

2012; Oppenheimer et al., 2013; Voigt et al., 2014), our results suggest that volcanic sulphate should carry positive O-MIF anomalies that exceed isotopic measurements uncertainties (≈ 0.1 ‰). This is not supported by atmospheric measurements of volcanic sulphate isotopic composition which mostly lie close to zero within measurements uncertainties. Other environmental conditions or reaction mechanisms have to be considered to explain the lack of O-MIF in volcanic sulphate.

Influence of LWC on sulphate O-MIF

The second set of sensitivity runs (Z2) tests the influence of the LWC amount on model results, notably the final sulphate O-MIF. Fe(III) aqueous concentration is fixed to 0.5 μM, and the initial concentration of SO_2 is set to 1.5 ppmv. Fig:4.10 shows the evolution of $\Delta^{17}O(S(VI), DEP)$ for varying LWC. Unlike the influence of SO_2, sulphate O-MIF is a monotonic function of LWC. The higher the LWC is, the lower the sulphate O-MIF is. Higher values of LWC favours higher dissolution rate of SO_2 in droplets and push the dynamics of oxidation towards liquid phase reactions. Also, at high LWC, H_2O_2 is more quickly depleted from the gas-phase because of faster uptake in the liquid phase. Overall, higher LWC favours the O_2/TMI oxidation pathway since lower acid concentration promotes the dissolution of SO_2 in the aqueous phase.
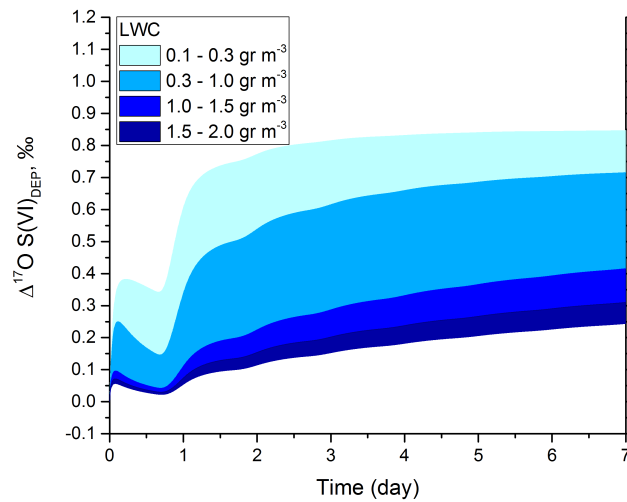
Figure 4.10: Temporal evolution of $\Delta^{17}O(S(VI))_{dep}$ at different values of liquid water content. Other initial critical parameters are set to: [Fe(III)] = 0.5 μM and $[SO_2]_0$ = 1.5 ppmv.

Higher LWC does not directly affect the vapour pressure of the system, because it is assumed that cloud droplets are formed at high water saturation. Therefore, changes in cloud LWC do not affect the the isotopic composition of produced OH. For the range of LWC considered here (from 0.1 to 3 $g\,m^{-3}$), the final O-MIF of deposited sulphate varies from 0.8 to 0.2 ‰.

The results show that, in volcanic clouds and plumes, sulphate O-MIF is affected by the LWC value. However, high LWCs alone do not appear to be sufficient to reproduce most of the isotopic measurements in volcanic sulphate.

Influence of TMI on sulphate O-MIF

The third and last set of sensitivity runs (Z3) tests the influence of TMI concentrations on model results, notably the final sulphate O-MIF. Laboratory experiments on iron mobilization from ash indicate that an average concentrations of [TMI] = 3 μM could be reached within the first hour of ash exposure to very acidic water in the case of silica ashes (Maters et al., 2017). According to the measurements, concentration of dissolved [Fe(III)] generally varies in the range of 0.1 to 2 μM depending on the mineral composition (Hoshyaripour et al., 2015; Maters et al., 2016, 2017). However, there is a lot of uncertainty on the typical concentrations of dissolved iron mobilized in volcanic plumes. In Fig:4.11 the plot shows the evolution of deposited sulphate O-MIF to varying concentrations of dissolved TMI (from 0.1 to 3 μM). At relatively low concentration of dissolved Fe(III) (0.1 -
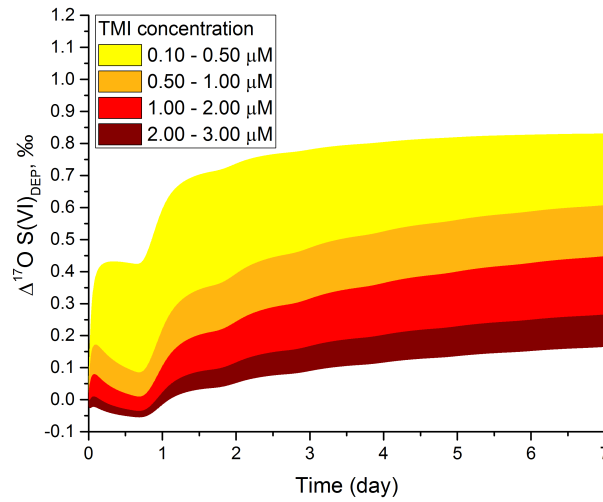
Figure 4.11: Temporal evolution of $\Delta^{17}O(S(VI))_{dep}$ at different concentrations of TMI in aqueous solution. Other initial parameters were set: LWC = 1.0 gm^{-3} and $[SO_2]_0$ = 1.5 ppmv.

1.0 μ M), deposited sulphates are generated with high O-MIFs and a final O-MIF greater than 0.4 ‰. At higher concentrations of [Fe(III)] = 2 or 3 μ M, deposited sulphate O-MIF reaches values as low as 0.25 and 0.15 ‰ respectively. According to the laboratory experiments, these high Fe(III) concentrations require a pH below pH $\leq$ 2, enhancing the mobilization of [Fe(III)]. In the simulations, the pH is close to this threshold value (see **Fig.:4.8**).

In conclusion, the model simulations suggest that deposited sulphate with very low O-MIF values, consistent with most isotopic measurements of volcanic secondary sulphate (less than 0.1 ‰), can only be achieved with highly enhanced Fe(III) mobilization.

5 Conclusions

We use the tropospheric photochemical box-model CiTTyCAT to analyse why most oxygen isotopic measurements of tropospheric volcanic sulphate indicate that volcanic sulphates are essentially mass-dependent (i.e. O-MIF anomalies lying close to zero within measurements uncertainties of $\pm$0.1 ‰ typically). This is also observed for volcanic sulphate collected very far from volcanoes where secondary sulphate (produced by oxidation of volcanic sulphur precursors, mostly SO_2) is expected to vastly dominate. This lack of O-MIF in volcanic sulphate is rather intriguing because secondary sulphates originating from other sources exhibit significant O-MIF. A major difference between volcanic sulphur and other sources is that it is often emitted within very dense volcanic plumes whose chemical compositions are radically different from background air. The chemical environment of the plumes may affect the oxidation pathways and hence sulphate isotopic composition.

A new sulphur isotopic O-MIF scheme is implemented in the model in order to monitor the transfer of O-MIF from oxidants to sulphate during the oxidation of volcanic SO_2. A range of simulations are performed in order to explore in details the different pathways of SO_2 oxidation (gas-phase oxidation by OH and aqueous oxidation by O_3, H_2O_2 and O_2/TMI) and, more importantly for O-MIF, their relative importance for a range of possible volcanic conditions. The first salient finding is that, according to the model calculations, OH should carry a very significant O-MIF in sulphur-rich volcanic plumes. This implies that, when volcanic sulphate is produced in the gas phase via SO_2 oxidation by OH, its O-MIF should have a very significant positive value. Since most isotopic measurements of volcanic sulphate do not indicate the presence of O-MIF, the OH oxidation pathway cannot be the dominant channel for volcanic sulphur. Nonetheless, uncertainties on the rate constant of the isotopic exchange between OH and H_2O (Dubey et al., 1997) and, more generally, on photochemical modelling are substantial (Ridley et al., 2017). It would be useful for this unexpected model predictions of O-MIF in OH, and hence volcanic sulphate produced in gas phase, to be tested in a controlled environment, ideally laboratory experiments of SO_2

oxidation with a well constrained OH chemical budged, notably the loss processes. The second important finding from these simulations is that, although H_2O_2 is a major oxidant of SO_2 throughout the troposphere, it is very rapidly consumed in sulphur-rich volcanic plumes. Since H_2O_2 produced within the plume and the entrainment of H_2O_2 from the atmospheric background represent also relatively weak sources, H_2O_2 is found to be a minor oxidant for volcanic SO_2 whatever the liquid water content. According to the simulations, oxidation of SO_2 by O_3 is negligible because volcanic aqueous phases are too acidic. The model predictions of minor or negligible sulphur oxidation by H_2O_2 and O_3, two oxidants carrying large O-MIF, are consistent with the lack of O-MIF seen in isotopic measurements of volcanic tropospheric sulphate. The third finding is that oxidation by $O_{2/}$TMI in volcanic plumes could be very substantial and, in some cases, dominant, notably because the rates of SO_2 oxidation by OH, H_2O_2, and O_3 are vastly reduced in a volcanic plume compared to the background air. Only cases where sulphur oxidation by $O_{2/}$TMI is very dominant can explain the isotopic measurements of volcanic tropospheric sulphate. We stress that oxidation by $O_{2/}$TMI is poorly constrained in model simulations because of the lack of measurements of TMI aqueous concentrations in volcanic plumes. It is worth pointing out that our model results are only applicable to cloudy volcanic plumes. Nonetheless, water clouds do not always form in volcanic plumes, notably during passive degassing. It would be interesting to also consider cloud-free plumes where the condensed phase is concentrated sulphuric acid within sulphate aerosols. In particular, these particles have a chemical reactivity radically different from water droplets.

A potentially significant limitation of the model simulations is the omission of volcanic halogens. Indeed, volcanic halogens are known to undergo multi-phase chemistry, resulting in ozone depletion and possibly impacting the oxidation of volcanic SO_2 (Bobrowski et al., 2003; Bobrowski and Platt, 2007; Millard et al., 2006; Bobrowski et al., 2007; Roberts et al., 2009; von Glasow, 2010; Roberts et al., 2014; Jourdain et al., 2016). Halogen species such as HOBr may also directly oxidise SO_2 in the aqueous phase (Chen et al., 2017), but this oxidation pathway has not been quantified yet for volcanic plumes. Overall, the present simulations might only be representative of degassing or eruptions with extremely low halogen emissions, typically originating from intraplate and rift volcanic activity. It is certainly worth exploring the potential impact of halogens in the case of halogen-rich eruptions, notably for volcanic plumes where water does not condense and hence only sulphate aerosols are present. Since the heterogeneous conversion of halogen halides into radicals is known to be fast on sulphate aerosols (Bobrowski et al., 2007; Roberts et al., 2009; von Glasow, 2010; von Glasow and Crutzen, 2013), halogens might impact significantly the plume chemistry and the isotopic composition of secondary sulphate for halogens rich conditions.

Halogens role in volcanic sulphur oxidation: photochemical modelling and isotopic constraints

In preparation

Abstract: A photochemical box-model CiTTyCAT is used to simulate sulphur oxidation within the core of volcanic plumes, and the resulting oxygen isotopic composition of volcanic sulphate. The focus is on the role of halogens emitted with sulphur during volcanic eruptions or passive degassing. The model accounts for SO_2 oxidation by OH in the gas phase, and by H_2O_2, O_3, O_2 catalysed by TMI, and HOX (HOX = HOBr + HOCl) in the liquid phase of either water droplets and water on ash, referred here as the case of condensing plum, or sulphate aerosols referred here as non-condensing plume. It also describes transfer of oxygen mass-independent anomalies (O-MIF) from the oxidants to sulphate. For condensing plumes, the first finding from the model results is that ozone depletion events (ODEs) triggered by halogens heterogeneous chemistry may also occur in volcanic plumes in the presence of water droplets. The presence of halogens does not affect the hierarchy of oxidation pathways. The O_2/TMI oxidation of sulphur remains dominant even for relatively low TMI aqueous concentrations, generating volcanic sulphates with low O-MIF, even equal to 0 ‰ in some cases, which are close to most isotopic measurements of sulphates collected on volcanic ash.

For non-condensing (only sulphate aerosols) ODEs occur even at very low halogen loading ($\approx$50 ppbv). The rate of sulphur oxidation is much lower than for condensing plumes, and sulphur oxidation is dominated by H_2O_2 on sulphate aerosols and by OH in the gas phase, instead of O_2/TMI. The relative contributions of H_2O_2 and OH is determined by halogens loading. The higher the halogens concentration is, the higher the H_2O_2 contribution is. The presence of halogens does not impact much the final sulphate O-MIF which varies between 0.8 to 1.4 ‰, in contrast to the lack of O-MIF measured in sulphates on volcanic ash. The condensing and non-condensing results suggest that the sulphate found on volcanic ash-deposits is likely to be formed via oxidation in water-rich phases and not in the gas phase or on sulphate aerosols

during ;passive degassing. Model calculations would certainly be tested with isotopic measurements of volcanic sulphate aerosols in non-condensing plumes. Notably, measurements should be conducted on aged aerosols to maximize the fraction of secondary sulphate with respect to primary sulphate, which have essentially mass-dependent oxygen fractionations.

1 Introduction

Volcanoes release vast amounts of particles and reactive gases into the atmosphere, representing a significant natural source of atmospheric pollutants (Textor et al., 2004; Ayris and Delmelle, 2012a; Mather, 2015). When emitted into the troposphere, the impacts are mostly limited to local and regional scales (Robock, 2000). Volcanoes, however, are often located in remote areas and their peaks frequently overcome the surrounding boundary layer. Consequently, volcanic emissions can have significant influence on the free troposphere. Volcanic emissions into the troposphere can have multiple adverse effects, leading to acid rain events, crop damages, or air traffic perturbations (Delmelle et al., 2001; Delmelle, 2003; Schumann et al., 2011). Exposure to high concentrations of volcanic sulphate particles and sulphur bearing gasses also have detrimental effects on human health (Durand and Grattan, 2001; Longo et al., 2008; Longo, 2013). For instance, volcanic emissions have been linked to the formation of pollution events, notably the production of "vog" (volcanic smog) in urban areas, as observed frequently in Mexico City and on the island of Hawai'i (Raga et al., 1999; de Foy et al., 2009).

The most important volcanic species for the perturbation of the atmosphere and climate is thought to be sulphur. Many observational and modelling results have demonstrated that volcanic sulphur emissions - especially to the stratosphere - have caused major changes in atmospheric composition and climate during present-day and past geological eras (Stocker et al., 2013). Once oxidized to sulphate, sulphur can form aerosol particles that cool the Earth's surface through scattering of incoming solar radiation (LeGrande et al., 2010; Robock, 2013; Stoffel et al., 2015; Zanchettin et al., 2016). When injected in the stratosphere, sulphur is dispersed on an hemispheric or global scale depending on the injection latitude, thus impacting global climate during several years typically, as observed after the eruption of Mount Pinatubo in June 1991 (Minnis et al., 1993b; McCormick et al., 1995; Robock, 2002). In addition, sulphate particles in the present day stratosphere favour the destruction of ozone that screens the Earth from harmful UV radiation (Solomon et al., 2016).

Although most atmospheric and climate studies have focused on sulphur (with the most abundant species being SO_2), volcanic emissions are a rich cocktail composed of a mix of reactive gases, including halogens (i.e. chlorine, bromine, iodine). Halogen species are frequently emitted in very significant amounts, together with sulphur and H_2O (Aiuppa et al., 2009; Hörmann et al.,

2013; Carn et al., 2016). They are released at the magma surface mostly as hydrogen halides (HX = HCl + HBr), which are rather unreactive species. Volcanic halogens have tended to be neglected in atmospheric and climate assessments because it is assumed that hydrogen halides are very efficiently washed out by particles, water droplets, and ash in volcanic plumes. However, there is growing evidence that some hydrogen halides are converted into reactive radicals (BrO, ClO) by high temperature chemistry within the volcanic vent (Gerlach, 2004; Martin et al., 2006; Roberts et al., 2009), and by multi-phase chemistry within young volcanic plumes (Oppenheimer et al., 2006, 2010; von Glasow, 2010), a process called "halogen activation". Numerous detections of bromine radical BrO in volcanic plumes have been reported (Bobrowski et al., 2003, 2007), notably the highest halogen radical concentrations ever recorded in the atmosphere (Bobrowski and Platt, 2007). Halogen radicals are generally less soluble than HX in both aqueous phases and sulphate aerosols (Sander et al., 2006; Sander, 2015). Consequently, HX conversion into radicals makes halogens less likely to be washed out in the atmosphere, thus increasing their atmospheric residence time and the spatial extent of their impacts, including the possibility of transport to the stratosphere (Zuev et al., 2015). Since BrO is very effective at destroying ozone in catalytic cycles, observations of high BrO concentrations in volcanic plumes are frequently associated with ozone depletion events (ODEs) (Millard et al., 2006; Vance et al., 2010; Boichu et al., 2011; Kelly et al., 2013). In particular, tropospheric ODEs are relatively common features observed in halogen-rich environments, notably over sea-salt lakes, in the polar or marine boundary layer and more recently in tropospheric volcanic plumes (Saiz-Lopez, 2004; Stutz, 2002; Hönninger, 2004; Millard et al., 2006; Vance et al., 2010; Kelly et al., 2013). By destroying ozone, halogen radicals also influence the atmospheric oxidizing capacity of volcanic plumes because ozone is a major source of hydroxyl radical OH, the dominant atmospheric oxidant (von Glasow and Crutzen, 2013). Therefore, through their impact on ozone halogens also influence the oxidation rate of volcanic sulphur (Jourdain et al., 2016). Finally, there is also increasing observational evidence that present-day volcanism can inject significant amounts of halogens directly into the stratosphere (Carn et al., 2016; Theys et al., 2009, 2014). The potential of volcanic halogens injection into the stratosphere to cause massive ozone depletion have recently been highlighted (Cadoux et al., 2015; Vidal et al., 2016).

Heterogeneous chemistry is crucial in converting volcanic HX into reactive radicals (i.e. halogens activation). Within a volcanic plume there are two main potential sites for heterogeneous: sulphate particles and water droplets (including water on ash particles). A small fraction of sulphur is directly emitted from the volcanic vent as small sulphate particles (considered here as primary sulphate), which provide immediately heterogeneous chemistry sites within very young volcanic plumes (Allen et al., 2002; Mather et al., 2006). Meanwhile, volcanic sulphur (i.e. mostly SO_2) is slowly oxidised to sulphate (secondary sulphate), thus increasing the sulphate aerosols loading. Many laboratory

studies have been devoted to chemistry occurring on sulphate particles, notably regarding halogens heterogeneous processing (Sander et al., 2006; Ammann et al., 2013). However, there are still large uncertainties on the kinetics of elementary reactions in the bulk phase of sulphate aerosols (sulphuric acid solution) (Hanson et al., 1994; Davidovits et al., 2006). On the top of sulphate particles, when large amounts of water vapour are also emitted and temperatures are sufficiently low, water can condense to cloud droplets, either on the surface of primary sulphate aerosols or ash particles surfaces when solid emissions are also present. In these cases, water-rich phases can also act as sites for heterogeneous chemistry. Aqueous chemical reactions involving sulphur species and, to a smaller extent halogens, have been rather extensively studied in laboratory (Sander et al., 2006). Note that the term cloud droplets is used thereafter in a loose sense, it is meant to cover any water-rich aqueous phases, including those at the surface of volcanic ash.

Halogens heterogeneous chemistry is complex, and not enough bromine radicals can be formed by high-temperature gas-phase chemistry within the hot vent compared to BrO observations (Gerlach, 2004; Roberts et al., 2009). Continuous radical cycling and HX conversion are required to promote sustained BrO production within volcanic plumes. The only large source of reactive bromine in a plume is the mobilization of bromine halides from liquid phases through heterogeneous chemistry (Saiz-Lopez and von Glasow, 2012; von Glasow and Crutzen, 2013; Simpson et al., 2015). Sustained halogens mobilization from condensed phase also requires HOX production (i.e. hypohalous acids, HOX = HOBr + HOCl) in the gas phase, especially during the first minutes after release from the vent (von Glasow, 2010). Besides its role in bromine activation, HOX production may have additional consequences on in-plume chemistry, in particular volcanic sulphur oxidation. When HOX concentrations are highly enhanced compared to the background atmosphere, the oxidation of SO_2 by HOX could greatly contribute to sulphur oxidation, as observed in the marine boundary layer (MBL) where up to 30% of sulphate may be produced via this SO_2 oxidation channel (Vogt et al., 1996; Von Glasow et al., 2002a,b). Recent investigations suggest that even at low HOX concentrations (i.e. HOX below 1 pptv), this SO_2 aqueous oxidation pathway can be significant, influencing the oxygen isotopic composition of sulphate (Chen et al., 2016).

During the last decades, there has been an increasing number of studies that have used isotopic composition measurements to constrain atmospheric oxidation channels (Michalski et al., 2003; Alexander et al., 2005; Morin et al., 2008; Gromov et al., 2010; Michalski and Xu, 2010). The triple oxygen isotope composition ($\Delta^{17}O$, see Eq.:) of end-oxidation products such as nitrate or sulphate, indeed, reflects (as the result of mass-independent isotopic fractionation during the formation of O_3) the number of oxygen atoms derived from O_3 that are involved in the oxidation of nitrogen (Michalski et al., 2003; Morin et al., 2008; Alexander et al., 2009; Tsunogai et al., 2010, 2016; Nelson et al., 2018) or sulphur oxides (Savarino and Thiemens, 1999b,a; Savarino et al., 2000; Bao et al.,

2003; Mather et al., 2006; Martin et al., 2014; Chen et al., 2016). Typically, when atmospheric oxidants are characterised by a specific oxygen isotopic anomaly, they can transfer part of this anomalous oxygen isotopic distribution to their oxidation product. As a result, isotopic composition of oxidation end-products may be used to track back specific dominant oxidants. Note that anomalous oxygen isotopic compositions refer to oxygen atoms distributions that do not follow the canonical ratio between oxygen isotopes. Most processes generate isotopic fractionations that are mass-dependent . Nonetheless, some others, like O_3 formation, generate ans excess of ^{17}O, and therefore a a non-mass dependent fractionation (also referred as mass-independent fractionation, MIF) are mass-dependent, and hence follow standard isotopic distributions. Mass-dependent fractionations induce a change in $^{17}O/^{16}O$ ratios which is commonly half the magnitude of the respective change in $^{18}O/^{16}O$ ratios. The non-mass dependent isotopic anomaly (also named Mass Independent Fractionations (MIFs) anomaly) is defined with respect to a mass-dependent reference line. The oxygen MIF anomaly (O-MIF = $\Delta^{17}O$) for its linear approximation is expressed as:

$$\Delta^{17}O = \delta^{17}O - 0.52 \times \delta^{18}O \tag{5.1}$$

Where $\delta^{17}O$ and $\delta^{18}O$ are the deviations from isotopic ratios of a standard reference (R_{std}):

$$R_x = \frac{^xO}{^{16}O} \qquad x = 17 - 18 \tag{5.2}$$

And:

$$\delta^xO = \frac{R_x}{R_{std}} - 1 \tag{5.3}$$

When a molecule of SO_2 is oxidised via a specific oxidation reaction chain, a given fraction of the oxidant-specific $\Delta^{17}O$ is transmitted to the produced molecule of sulphate. Therefore, the resulting product $\Delta^{17}O$ value is simply a linear combination of the oxidant-specific isotopic signatures weighted by their respective contributions to the total sulphate production. Obviously, the specific $\Delta^{17}O$ signatures transmitted to sulphate by the different oxidants have all to be known if different oxidation pathways are to be constrained simply and even inferred in some cases.

Secondary sulphates are generally produced by oxidation of SO_2 through different pathways, and their oxygen isotopic composition reflects the competition between the different production channels. During sulphur oxidation, the transfer of isotopic anomalies from ozone and H_2O_2 produces sulphates with very significant O-MIF ($\Delta^{17}O \neq 0 \pm 0.1‰$), whereas SO_2 oxidation by OH in the gas phase, and by O_2/TMI and HOX in the liquid phase, are thought to produce sulphate without significant O-MIF anomalies ($\Delta^{17}O = 0 \pm 0.1‰$) (Savarino and Thiemens, 1999b,a; Savarino et al., 2000; Martin et al., 2014; Chen et al., 2016). Note that the uncertainty on the $\Delta^{17}O$ determination on sulphate is 0.1‰ (Bao et al., 2003; Martin and Bindeman, 2009).

This value of 0.1‰ is typical of oxygen isotopic measurement errors. Most sulphates collected in the troposphere have a $\Delta^{17}O$ of about 1 ‰ typically (Lee et al., 2001; Lee and Thiemens, 2001), reflecting the importance of ozone and H_2O_2 as sulphur oxidants. In contrast, most sulphates extracted from volcanic ashes of historical and present eruptions are characterised by negligible O-MIFs ($\Delta^{17}O$ ¡ 0.1‰), independently from distances of volcanic ash-deposits from the volcanic sources (5-400 km) (Bao et al., 2003; Mather et al., 2006; Martin et al., 2014; Martin, 2018). With the exception of volcanic sulphates collected from ice cores (i.e. formed and transported within the stratosphere, and of tropospheric super-eruptions), it is a peculiarity that most volcanic sulphate collected on volcanic ash-deposits, even far from volcanoes, do not carry any O-MIFs, because most of the sulphate is expected to be secondary sulphate produced during oxidation of volcanic SO_2 by common tropospheric oxidants.

The present work is a follow-on of a detailed photochemical modelling study on sulphur oxidation in volcanic plumes and on the implications for oxygen isotopic compositions of volcanic sulphate (Galeazzo et al., 2018). Although a range of conditions and scenarios were explored, the model had great difficulty in reproducing volcanic sulphate isotopic composition measurements (i.e. a negligible O-MIF). Potentially important elements were previously neglected, notably the presence of volcanic halogens and heterogeneous chemistry on sulphate particles. The purpose of the present work is to address these limitations. It aims at gauging the role of halogens in sulphur oxidation within volcanic plumes. Some volcanic plumes contain, indeed, very high levels of halogens, which, in some cases, can be as high as sulphur levels (Aiuppa et al., 2009; Cadoux et al., 2015).

In the background troposphere, a combination of several oxidants is involved in sulphur oxidation: radical OH in the gas phase, H_2O_2, O_3, O_2 catalysed by Transition Metal Ions (TMI), and HOX in the liquid phase (Vogt et al., 1996; Seinfeld and Pandis, 2016). In the atmosphere, SO_2 can be oxidised also by NO_2, especially within fogs and in polluted conditions (Chen et al., 2016). However, volcanic cloud droplets and sulphate aerosols are too acidic and the NO_2 contribution to SO_2 oxidation is negligible. Due to the intensity and composition of volcanic emissions, the chemistry of a dense volcanic plume is certainly very different from the chemistry of the surrounding background atmosphere. Therefore, the nature of sulphate production in terms of the mix of oxidants involved is also expected to be very different. The implications for the isotopic composition of volcanic secondary sulphate are analyses here. Isotopic measurements of volcanic sulphate, indeed, are increasingly considered for inferring oxidant contributions to volcanic sulphur oxidation. This is particularly useful for the distant past when no oxidant measurements are available. However, note that halogen chemistry usually tends to be ignored in this type of inference (Savarino et al., 2000; Alexander et al., 2009; Martin et al., 2014).

The main tool of the present study is a photochemical box-model (CiTTyCat) which already describes standard tropospheric chemistry and sulphur aqueous

chemistry in cloud water droplets (Galeazzo et al., 2018). It also contains a sulphur isotopic scheme tracking O-MIF anomalies during sulphur oxidation. Its chemical scheme is here extended to include sulphur heterogeneous chemistry on sulphate aerosols and halogen heterogeneous chemistry on both sulphate particles and water droplets. Diverse model simulations are carried out for a range of environmental conditions and scenarios. Model results are used to investigate in details the chemistry of volcanic halogen-rich plumes and to elucidate the role of halogens in tropospheric volcanic plumes, notably during sulphur oxidation. Model-calculated sulphate isotopic compositions are compared to volcanic sulphate isotopic measurements, i.e. collected either in proximity of volcanic vents or from volcanic ash deposits from past and current geological eras (Bao et al., 2003; Mather et al., 2006; Martin et al., 2014). Results enable to assess the constraints on sulphur oxidation brought by sulphate isotopic measurements regarding sulphur oxidants in the presence of varying levels of halogens.

This paper is organized as follows. The second section describes halogens gas phase and heterogeneous chemistry operating in volcanic plumes. The third section presents the modelling methodology adopted for the in-plume halogens and sulphur chemistry. This section also covers the extension of the chemistry scheme, and of the isotopic balance equations implemented in CiTTyCAT to cover the SO_2 oxidation by halogens. The fourth section presents and discusses model results for typical (here called standard) conditions, when only specific processes are considered (sulphate particles or cloud droplets, with or without halogens). The focus is on analysing the role of heterogeneous chemistry and of halogens in sulphur oxidation, and the implications for sulphate isotopic compositions. The fifth section is devoted to sensitivity studies where extreme cases are considered. They are conducted to investigate how sensitive the model results, notably the sulphate isotopic composition, are to different in-plume parameters (e.g. liquid water content, HX/SO_2 ratios, initial SO_2 concentrations, and TMI aqueous concentration). Dominant SO_2 oxidation pathways are identified for the two main liquid phase model scenarios (cloud droplets, sulphate aerosols). Finally, the main findings are recalled in the final section. The model ability to reproduce observed isotopic compositions from volcanic sulphate ash-deposits and from volcanic sulphate aerosols is also further discussed.

2 Halogen chemistry and sulphur oxidation in volcanic plumes

2.1 Halogen chemistry

The most abundant volcanic halogen species are chlorine, fluorine and bromine, emitted at the vent respectively as HCl, HF, and HBr (Aiuppa et al., 2009; Oppenheimer et al., 2013). Because of its very low reactivity, fluorine is not

involved in significant tropospheric chemistry, leaving bromine and chlorine as the only relevant volcanic halogen species.

Bromine activation and HOBr production

Because of high temperature, a small fraction of bromine comes out of volcanic vents in the form of BrO (Gerlach, 2004). Atmospheric HBr processing in the plumes can lead to production of bromine radicals, notably BrO, and HOBr. Gas-phase reaction of HBr with OH results into BrO production in a two-step process:

$$HBr + OH \rightarrow Br + H_2O \tag{5.4}$$

$$Br + O_3 \rightarrow BrO + O_2 \tag{5.5}$$

The high levels of SO_2 and/or HCl prevailing in the core of young volcanic plume reduce greatly OH concentrations. Therefore, R5.4 can at best be effective at the edges of the plume. In order to explain the sustained production of BrO observed in volcanic plumes, even far from volcanoes (Boichu et al., 2011), other sources of reactive bromine need to be invoked (von Glasow, 2010). In volcanic plumes, reactive bromine can be produced via mechanisms similar to the bromine explosion, commonly observed over sea-salt lakes and in the polar boundary layer (von Glasow et al., 2004; Simpson et al., 2015). In the plume core, production of reactive bromine could be initiated by gas-phase reactions of BrO originating from the vent with hydrogen and nitrogen radicals, resulting in the production of HOBr (R5.6) and $BrONO_2$ (R5.7) during the first minutes from plume release:

$$BrO + HO_2 \rightarrow HOBr + O_2 \tag{5.6}$$

$$BrO + NO_2 \rightarrow BrONO_2 \tag{5.7}$$
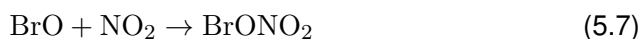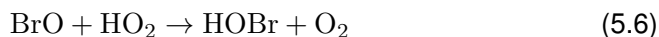
HOBr and $BrONO_2$ can then react heterogeneously with condensed halide anions (i.e. $X^- = Br^- + Cl^-$) (Martin et al., 2012), thus promoting halogens mobilisation from liquid phases and releasing reactive bromine :

$$HOBr + X^-_{(l)} + H^+ \rightarrow BrX_{(l)} + H_2O \tag{5.8}$$

$$BrONO_2 + X^-_{(l)} + H^+ \rightarrow BrX_{(l)} + HONO_2 \tag{5.9}$$
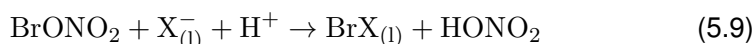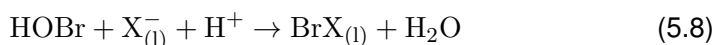
With X^- being either Br^- or Cl^-.

The reactive uptakes of HOBr and $BrONO_2$ are acid catalysed and are promoted by low pH in sulphate aerosols and volcanic cloud droplets (Allen et al., 2002; Mather et al., 2003; Galeazzo et al., 2018). Products of reactions R5.8 and R5.9 are either BrCl or Br_2 (i.e. BrX) with the respective yield depending on the Br^-/Cl^- ratio and on aqueous-phase equilibria (Wang et al., 1994; Roberts et al., 2009; Jourdain et al., 2016). For typical emissions of arc volcanoes (emissions of bromine versus chlorine), Br_2 formation is largely favoured to the detriment of BrCl (Wexler and Clegg, 2002; Gerlach, 2004). It has been observed, indeed,

that BrCl might only be preferentially formed in plumes when HBr/HCl emission ratios are 100 to 1000 times below those of arc-mean composition (i.e. HBr/HCl $\approx 2 \times 10^{-3}$) (Gerlach, 2004; Aiuppa et al., 2009; Roberts et al., 2009).

Both Br_2 and BrCl are rather insoluble in the liquid phase, and therefore easily released in the gas phase, where they are quickly photolyzed.

$$BrX_{(l)} \rightarrow BrX \tag{5.10}$$

$$Br_2 + h\nu \rightarrow 2\,Br \tag{5.11}$$

$$BrCl + h\nu \rightarrow Br + Cl \tag{5.12}$$

Br production is of particular interest because it reacts rapidly with O_3 to form BrO (R5.5), a major ozone-destroying radical. Once HO_x and NO_x are depleted from the gas-phase, BrO self-reaction becomes the limiting step in the ozone-destruction catalytic cycle responsible for ozone depletion events in volcanic plumes. The self-reaction gives either Br_2 or Br:

$$BrO + BrO \rightarrow Br_2 + O_2 \tag{5.13}$$

$$BrO + BrO \rightarrow 2\,Br + O_2 \tag{5.14}$$
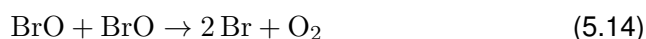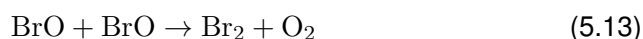
Finally, bromine radicals are typically de-activated via the following termination reactions:

$$Br + HCHO \rightarrow HBr + HCO \tag{5.15}$$

$$Br + HO_2 \rightarrow HBr + O_2 \tag{5.16}$$
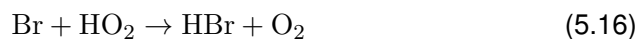
Reactions R5.8-R5.9 are necessary to maintain high BrO levels in the young plume core, where OH radicals cannot be produced in significant amounts due to ozone depletion, being quickly destroyed by reactions with SO_2 and HCl (von Glasow and Crutzen, 2013).

HOBr can also oxidize SO_2 within sulphate aerosols or water droplets in volcanic plumes, contributing to volcanic sulphate production.

Chlorine activation and HOCl production

Very significant levels of OClO and ClO levels have been observed in volcanic plumes, suggesting that efficient chlorine activation might be occurring (Lee et al., 2005; Theys et al., 2014; Donovan et al., 2014). Note that measurements of OClO and ClO in volcanic plumes are quite challenging because their absorption spectra overlap with those of BrO and SO_2 respectively (Lee et al., 2005; Bobrowski and Platt, 2007; Kern et al., 2009). It is difficult to distinguish between OClO and ClO directly emitted from the volcanic vent, from those produced by chemical processing within a very young plume.

There are several possible mechanisms of chlorine activation (conversion of unreactive chlorine species into radicals). Within the volcanic vent, a small but

significant quantity of ClO radicals is expected to be formed by high temperature chemistry and released at the vent (Gerlach, 2004; Roberts et al., 2009). BrCl production via reactions R5.8-R5.9 also leads to chlorine activation, since BrCl is quickly photolyzed to release atomic chlorine Br (see 5.12). Once formed, Cl reacts quickly with O_3 to produce ClO:

$$Cl + O_3 \rightarrow ClO + O_2 \tag{5.17}$$

In the gas phase, ClO reacts with BrO, which is present at relatively high concentrations in most plumes, to give OClO, a by-product and an indicator of chlorine activation:

$$BrO + ClO \rightarrow OClO + Br \tag{5.18}$$

At the same time, ClO can also react with HO_2 to produce HOCl:

$$ClO + HO_2 \rightarrow HOCl + Cl \tag{5.19}$$

Relatively high HOCl concentrations within the young plume might promote an equivalent chlorine radical mechanism similar to the "bromine explosion" (Roberts et al., 2009). Nonetheless, despite an initial injection of chlorine radicals within young plumes, chemistry models are still not able to reproduce the levels of OClO and ClO observed in both young and aged plumes. This could suggest that other reactive chlorine species are produced in the young plume instead of HOCl, and that some chlorine activation mechanism might be missing in models chemical schemes (Bobrowski and Platt, 2007; Roberts et al., 2009; von Glasow, 2010). In contrast to Br, in the troposphere Cl is less reactive towards O_3, because of fast reactions with tropospheric CH_4 and other organics.

Like HOBr, HOCl could also oxidize SO_2 in the liquid phase, contributing to volcanic sulphate production, especially if significant amounts of HOCl are produced via R5.19.

Oxidation of SO_2 by hypohalous acids

Gaseous SO_2 dissolves in liquid phase, where it forms HSO_3^- and SO_3^{2-} depending on pH. At pH<6, S(IV) partitioning is largely shifted towards $SO_{2(aq.)}$ and HSO_3^-, while SO_3^{2-} aqueous concentration is negligible (Seinfeld and Pandis, 2016). HOX is produced during the first stages of young plume development via reactions R5.6 and R5.19. It can produce secondary sulphate via reactions R5.20-R5.21 with SO_3^{2-} and HSO_3^- (Fogelman et al., 1989; Troy and Margerum, 1991; Vogt et al., 1996; Von Glasow et al., 2002a,b):

$$SO_3^{2-} + HOX \rightarrow XSO_3^- + OH^- \tag{5.20}$$

$$HSO_3^- + HOX \rightarrow XSO_3^- + H_2O \tag{5.21}$$

$$XSO_3^- + H_2O \rightarrow SO_4^{2-} + X^- + 2\,H^+ \tag{5.22}$$
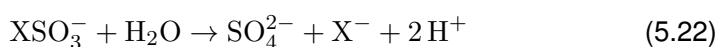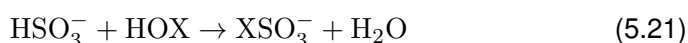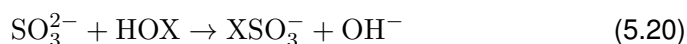
It has been suggested that the first step of reaction could be a nucleophilic attack by S(IV) species on HOX halogen atoms (R5.20) or (R5.21) (Chen et al., 2016). The second step is the quick XSO_3^- hydrolysis (R5.22).

3 Modelling approach

The chosen model to pursue the investigation is the Cambridge Tropospheric Trajectory model of Chemistry and Transport (CiTTyCAT). The box model CiTTy-CAT describes standard tropospheric gas-phase photochemistry (bimolecular, termolecular, and photodissociation reactions), emissions and deposition (Evans et al., 2000; Real et al., 2007; Arnold et al., 2007). The reaction rate constants and photolysis cross-sections are taken from JPL's datasheets (Sander et al., 2006), and photolysis rates are evaluated via the Fast-J code (Wild et al., 2000). The chemistry scheme has been recently extended with aqueous sulphur chemistry, a parametrization of water droplets acidity, and oxygen isotopes transfers occurring during gas and liquid phase sulphate production (Galeazzo et al., 2018).

Here, the scheme is further extended by adding SO_2 oxidation by O_3, H_2O_2, HOX and O_2/TMI on sulphate aerosols, as well as SO_2 oxidation by halogens in both cloud water droplets and sulphate aerosols. Moreover, new reactions have been implemented to account for halogens heterogeneous chemistry in both sulphate aerosols and cloud water droplets. Halogens heterogeneous reactions are generally fast. The elementary aqueous reactions that drive halogens heterogeneous chemistry are not well characterized experimentally. Therefore, it has been chosen to implement halogens heterogeneous chemistry, and all heterogeneous reactions on sulphate aerosols (i.e. also SO_2 oxidation), via reactive uptake coefficients, instead of describing in detail all the elementary reactions occurring within sulphate aerosols or cloud droplets. In contrast, sulphur aqueous reactions occurring within cloud droplets are explicitly modelled. Reaction rates are strongly influenced by chemical activity of water and sulphuric acid, and, indeed, large uncertainties are still pending on chemistry within sulphate aerosols. Throughout this study the "condensing volcanic plume" scenario refers to dense volcanic plumes generated by a more or less large eruption (i.e. ash-rich condensing plume), or by passive degassing in a humid atmosphere. In this case water constitutes the bulk of the liquid phase. On the other hand, the "non-condensing plume" scenario refers to volcanic plumes from passive degassing in a dry atmosphere, and where concentrated sulphuric acid aerosols constitute the bulk of the condensed phase. For the two plume scenarios (i.e. condensing vs non-condensing plume) heterogeneous chemistry is implemented through different modules.

3.1 General continuity equations

CiTTyCAT resolves coupled differential mass balance equations (continuity equations) describing the time evolution of atmospheric species concentrations (Evans et al., 2000; Real et al., 2007; Arnold et al., 2007). For given compounds concentrations and environmental conditions (e.g. pressure, temperature), continuity equations are solved considering chemical production and loss terms, and deposition and mixing with background air:

$$\frac{d[C_i]}{dt} = \sum_k P_k - \sum_j L_j - D_i - M_i \qquad (5.23)$$

where C_i is species i concentration in the plume, P_k the sum of gas phase and heterogeneous chemical production channels for species i, L_j is the sum of gas phase and heterogeneous chemical loss rates for species i, and D_i and M_i represent respectively species i deposition and mixing fluxes. The heterogeneous chemistry terms also include mass-transfer between the gas and condensed phases.

Deposition only applies to liquid phase species dissolved in cloud water droplets or in sulphate aerosols. It is implemented as a first order loss process, where rate coefficients (k_d) are assumed to be proportional to the mean lifetime of cloud droplets and sulphate aerosols in the free troposphere (Stevenson et al., 2003b). Deposition fluxes are defined as:

$$D_i = -k_{dep} \cdot [C]_i \qquad (5.24)$$

Exchange of species between volcanic plumes and background air due to atmospheric mixing is also accounted for. Mixing is parametrised via a simple linear relaxation scheme, inducing an exponential decay of plume concentrations towards background concentrations (Methven et al., 2006; Real et al., 2007; Arnold et al., 2007):

$$M_{(i)} = K_{mix} \cdot \left([C]_i - [C]_{(i,bck)} \right) \qquad (5.25)$$

where K_{mix} is a first-order mixing rate coefficient quantifying volcanic air mixing with the background atmosphere, and $C_{(i,bck)}$ is the concentration of species i in the background air. K_{mix} is set to 0.4 day^{-1}, a value rather more representative of mixing in the lower atmosphere and equivalent to a 2.5 days dilution timescale.

Mass-transfer fluxes between gas phase and condensed phase are modelled considering trace gases non-reactive and reactive uptake into respectively water droplets and sulphate aerosols. The general uptake rate is defined by the following kinetic regime expression (Hanson et al., 1994):

$$-\frac{d[C_i]}{dt} = \gamma_i \cdot \frac{\overline{\nu}_i}{4} \cdot SA \cdot [C_i] \qquad (5.26)$$

where γ_i is species i uptake coefficient onto a specific condensed phase, $\overline{\nu}_i$ represents the average molecular speed of i in the gas phase, and SA is the surface area density of the considered condensed phase (the condensed phase surface area per unit volume of air). Molecular uptake coefficient is not constant for most atmospheric gases, and it varies with time depending on the chemical composition of condensed phase and air. The uptake into a liquid particle, indeed, encompasses into a single variable multiple physical and chemical processes, respectively: molecular diffusion in the gas phase, transfer through the gas-liquid interface, diffusion in the liquid bulk phase, liquid chemical reactions and all the saturation effects (Davidovits et al., 2006; Ammann et al., 2013).

3.2 Heterogeneous chemistry of cloud droplets

Non-reactive uptake

Mass-transfer between gas phase and cloud droplets is treated separately from aqueous chemistry. Therefore, the uptake is treated as a non-reactive uptake. Thermodynamic equilibrium is quickly reached between gas phase near the surface and the liquid sublayer below water droplets surface. The maximum kinetic flux to the liquid phase is therefore proportional to an adsorption probability expressed by the accommodation coefficient (α_i), and to Henry's law coefficients (H).

The mass flux for a species i from gas phase to a single droplet of radius R_p is given by the following kinetic regime expression (Davidovits et al., 2006):

$$J_{K(i)} = \alpha_i \pi R_p^2 \overline{\nu}_i \cdot ([C_i] - [C_i]_s) \tag{5.27}$$

where $[C_i]$ is the concentration of i far from the droplets, $[C_i]_s$ is the concentration of species i at the surface of the droplets. The latter is expressed as $[C_i]_s = C_{i(aq.)}/H_i$, where $C_{i(aq.)}$ is the aqueous concentration of i and H_i is the Henrys law coefficient of i.

A correction factor is implemented into this flux expression in order to cover from kinetic to continuum transport regimes (Seinfeld and Pandis, 2016). In this case, the transition regime correction factor is taken from the Dahneke expression (Dahneke, 1983), and the final flux to a single droplet is defined as:

$$J_{(i)} = 4\pi R_p D_{air} \cdot \frac{1 + K_n}{1 + 2K_n(1 + K_n)/\alpha} \cdot ([C_i] - [C_i]_s) \tag{5.28}$$

where:

$$K_n = \frac{\lambda_i}{R_p} = \frac{2 \cdot D_{air}}{\overline{\nu}_i \cdot R_p} \tag{5.29}$$

$$\lambda_i = \frac{2 \cdot D_{air}}{\overline{\nu}_i} \tag{5.30}$$

where K_n is he Knudsen's number, a variable expressed in function of the gas phase diffusion coefficient of i in air (D_{air}), and λ_i, the molecular mean free-path of i.

Sulphur aqueous chemistry

Sulphur dioxide concentration into water droplets is regulated by the chemical environment of the aqueous phase, and by sulphur aqueous chemical equilibria. Notably, SO$_2$ undergoes multiple dissociations in the aqueous phase, giving HSO_3^- and SO_3^{2-}. Note that to simplify sulphur chemistry description, the whole set of sulphur species in the fourth oxidation state is grouped together to form the S(IV) family:

$$[S(IV)] = [SO_2] + [SO_{2(aq.)}] + [HSO_3^-] + [SO_3^{2-}] \tag{5.31}$$

SO$_2$ is mildly soluble in water and its uptake is regulated by an effective Henry's law coefficient (H_i^*), influenced by S(IV) partitioning and water pH. Water acidity regulates also S(IV) oxidation rates, since different sulphur oxidation channels are more or less effective depending on pH. Also sulphate dissociates in aqueous solution to generate HSO_4^- and SO_4^{2-}. The first dissociation is considered to be virtually complete and instantaneous in cloud droplets, and similarly to S(IV), sulphate species in the sixth oxidation state are grouped together to form the S(VI) family:

$$[S(VI)] = [H_2SO_4] + [HSO_4^-] + [SO_4^{2-}] \tag{5.32}$$

The pH of water droplets that controls sulphate aqueous chemistry, is a prognostic variable of the model. It is calculated dynamically by accounting for the most significant species that can dissolve and dissociate in volcanic water droplets:

$$[H^+] = [HSO_3^-] + 2 \cdot [SO_3^{2-}] + [HSO_4^-] + 2 \cdot [SO_4^{2-}] + [Br^-] + [Cl^-] + [NO_3^-] \tag{5.33}$$

Aqueous S(IV) oxidation is expressed by:

$$-\left(\frac{d[S(IV)]}{dt}\right)_j = K_j^{l-g} \cdot [S(IV)]^{l-g}[C_j]^{l-g} \tag{5.34}$$

where K_j^{l-g} is the gas phase equivalent (meaning conversion into gas-phase units) of the aqueous rate constant of reaction j, $[S(IV)]^{l-g}$ is the gas-phase equivalent of the S(IV) aqueous species concentration, and $[C_j]^{l-g}$ is the gas phase equivalent of the oxidant j aqueous concentration. Together with S(IV) aqueous phase partitioning and oxidation, the model also accounts explicitly for dissolution of O$_3$, H$_2$O$_2$, and HOX, and their aqueous reactions with S(IV). The total sulphur oxidation reactions implemented in the model are summarised in Table:5.1.

Table 5.1: Aqueous reactions during sulphur oxidation in condensing plumes water droplets (X = Br, Cl).

Aqueous reaction	$k_{(aq.)}$	units
$SO_2 + O_3 \rightarrow S(VI) + O_2$	$2.4 \cdot 10^4$	Ms^{-1} [b]
$HSO_3^- + O_3 \rightarrow S(VI) + O_2$	$3.7 \cdot 10^5$	Ms^{-1} [b]
$SO_3^{2-} + O_3 \rightarrow S(VI) + O_2$	$1.5 \cdot 10^9$	Ms^{-1} [b]
$HSO_3^- + H_2O_2 \rightarrow S(VI) + H_2O$	$\dfrac{k_{H_2O_2} \cdot [H^+]}{1 + K_{(eq.)} \cdot [H^+]}$	Ms^{-1} [b]
	with $K_{(eq.)} = 13$	M^{-1} [b]
	and $k_{H_2O_2} = 7.5 \cdot 10^7$	$M^{-2}s^{-1}$ [b]
$S(IV) + \frac{1}{2} O_2 \xrightarrow{TMI} S(VI)$	$750 \cdot [Mn(II)] + 2600 \cdot [Fe(III)] + 1.0 \cdot 10^{10}[Mn(II)][Fe(III)]$	s^{-1} [c]
$HSO_3^- + HOX \rightarrow S(VI) + H^+ + X^-$	$k_{(HSO_3^-,Br)} = 3.2 \cdot 10^9$	Ms^{-1} [d]
	$k_{(HSO_3^-,Cl)} = 7.6 \cdot 10^8$	Ms^{-1} [e]
$SO_3^{2-} + HOX \rightarrow S(VI) + H^+ + X^-$	$k_{(SO_3^{2-},Br)} = 5.0 \cdot 10^9$	Ms^{-1} [f]
	$k_{(SO_3^{2-},Cl)} = 7.6 \cdot 10^8$	Ms^{-1} [e]

[a] (Atkinson et al., 2004); [b] (Hoffmann, 1986); [c] (Martin and Good, 1991); [d] (Liu and Margerum, 2001); [e] (Troy and Margerum, 1991); [f] (Fogelman et al., 1989)

Halogen aqueous chemistry

Gas-liquid equilibria of soluble halogens species between the gas phase and the cloud droplets are also accounted for. In particular, halogens gas-liquid partitioning driven by Henry's law coefficients (i.e. HOBr, HOCl, HCl, HBr, Br_2, Cl_2, BrCl) and halogens aqueous equilibria are included. The model also takes into account the multi-step equilibrium between Br_2, BrCl, Br^-, and Cl^- (Roberts et al., 2009; Jourdain et al., 2016):

$$BrCl + Br^- \rightleftharpoons Br_2Cl^- \tag{5.35}$$

$$Br_2Cl^- \rightleftharpoons Br_2 + Cl^- \tag{5.36}$$

These halogens aqueous exchange reactions (5.35-5.36) are rather relevant since they affect the overall halogens heterogeneous chemistry, hence halogens species uptake and mobilization from the liquid phase. In the aqueous phase, Br_2Cl^- quickly dissociates via reaction 5.36 to form Br_2 and Cl^- (Wang et al., 1994). This equilibrium promotes Br_2 over BrCl formation for $[Br^-]/[Cl^-]$ ratios above 7.2×10^{-5} (Roberts et al., 2009; Grellier et al., 2014). Notably, Br_2 is less soluble in water than BrCl, hence its aqueous production followed by rapid release in the gas phase favours the halogens activation chain.

3.3 Heterogeneous chemistry of sulphate aerosols

This new heterogeneous scheme implemented in CiTTyCAT deals with halogens reactions and SO_2 reactions on or within extremely acidic solutions of sulphate aerosols (non-condensing plumes). A schematic representation of all reactions implemented in the model are summarised in **Fig.: 5.1**. Chemistry within concentrated sulphuric acid solutions is not well constrained in kinetic databases. Consequently, unlike sulphur chemistry in cloud droplets, it has been chosen to not treat separately the physical uptake and chemical equilibria in sulphate particles. Under these conditions, the uptake coefficient in Eq.:5.26 encompasses in a single variable uptake and reactions into sulphate aerosols, hence the coefficient becomes effectively a reactive uptake coefficient (γ_r). Its formulation is based on a resistor model, where the different processes driving the heterogeneous reaction are expressed as separate resistances in series (Hanson et al., 1994; Davidovits et al., 2006). Notably, resistances from three main physico-chemical processes are combined into a single impedance: the diffusion of a species in the gas phase (Γ_d), its adsorption when it strikes the particle (α, surface accommodation coefficient), and diffusion, saturation and reaction within the liquid bulk phase (Γ_b). The final expression of γ_r becomes:

$$\frac{1}{\gamma_r} = \frac{1}{\Gamma_d} + \frac{1}{\alpha} + \frac{1}{\Gamma_b} \tag{5.37}$$

Where, $1/\Gamma_d$ is the resistance for the gas phase diffusion, $1/\alpha$ is the resistance to surface accommodation, and $1/\Gamma_b$ is the resistance to bulk phase processes.

The gas phase diffusion resistance is derived according to (Davidovits et al., 2006):

$$\frac{1}{\Gamma_d} = \frac{0.75 + 0.238 \cdot K_n}{K_n \cdot (1 + K_n)} \tag{5.38}$$

α is derived from the large body of laboratory experiments covering heterogeneous reactions on the surface of sulphuric acid solutions (Sander et al., 2006).

The resistance to chemical retention in the bulk phase depends on diffusion in the liquid phase, on saturation effects and on liquid phase reactivity. The general formula for Γ_b is given by (Hanson et al., 1994; Davidovits et al., 2006; Ammann et al., 2013):

$$\frac{1}{\Gamma_{(b,i)}} = \frac{\overline{\nu}_i}{4H_iRT} \cdot \sqrt{\frac{1}{D_{(l,i)}k'_{(b,i)}}} \tag{5.39}$$

where $D_{(l,i)}$ is the liquid phase diffusion coefficient of i, and $k'_{(b,i)}$ is the pseudo-first order constant of liquid reaction.

Note that, when liquid reactions are second order, the bimolecular constant of reaction is combined with the concentration of liquid species (Y) in excess in solution to provide the equivalent pseudo-first order constant: $k'_{(b,i)} = k''_{(b,i)} \cdot [Y]$. If liquid phase reactions are fast with respect to diffusion, solutes react within
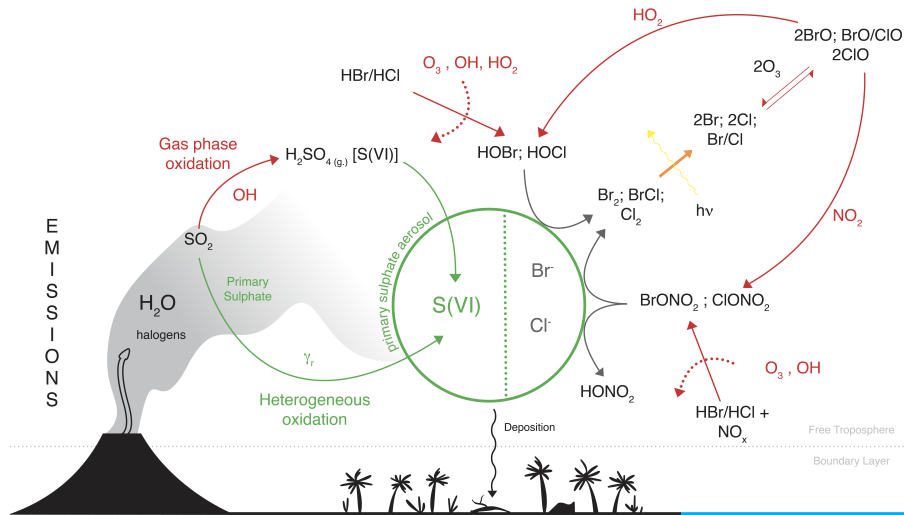
Figure 5.1: A diagram representing the new heterogeneous chemistry scheme implemented in CiTTyCAT, including: SO$_2$ oxidation, and halogens heterogeneous reactions within sulphate aerosols.

the first layers of the particle, hence being proportional to particle surface area. However, if particles are small, molecules can quickly diffuse within the liquid phase, and hence they cover particles diameter before reacting, thus being dependent on the particle volume. The characteristic depth covered by a diffusing an reacting molecule i is given by the reacto-diffusive length (l_i) (Davidovits et al., 2006; Ammann et al., 2013):

$$l_i = \sqrt{\frac{D_{(l,i)}}{k'_{(b,i)}}} \tag{5.40}$$

To account for volumetric effects on molecular uptake, a factor is added to Eq.:5.39:

$$\frac{1}{\Gamma_{(b,i)}} = \frac{\overline{\nu}_i}{4H_i RT} \cdot \sqrt{\frac{1}{D_{(l,i)} k'_{(b,i)}}} \cdot \frac{1}{[coth(R_p/l_i)] - (l_i/R_p)} \tag{5.41}$$

Where R_p is the radius of the sulphate particle.

When a species is involved in multiple reactions in the liquid phase, all the reactions contribute to the uptake coefficient. The total bulk phase resistance is expressed by a combination of multiple parallel resistances, each representing single chemical reactions within the liquid phase. The final expression of $\gamma_{r,tot}$ when multiple liquid reactions occur becomes:

$$\frac{1}{\gamma_{r,tot}} = \frac{1}{\Gamma_d} + \frac{1}{\alpha} + \frac{1}{\sum_i \Gamma_{(b,i)}} \tag{5.42}$$

Where $\sum_i \Gamma_{(b,i)}$ is the sum of reaction coefficients affecting species i uptake.

Within sulphate aerosols, liquid reactions between SO_2 and O_3, H_2O_2, O_2/TMI, or HOX can occur in principle, since all species can still partition between gas and sulphuric acid solution. Henry's law coefficients and liquid phase oxidation reaction rates depend on aerosol sulphate composition, notably reaction constants depend highly on sulphuric acid activity in solution. The values are extrapolated via empirical laboratory observations (DeMore et al., 1997; Rattigan et al., 2000).

When Eq.:5.42 is applied to SO_2 reactive uptake on sulphate aerosols, estimations show that the major resistance originates from the processes occurring in the bulk phase of sulphate aerosols (see Table:5.2), because of the extremely low pH of solution. Therefore, the reactive uptake coefficient in Eq.:5.42 can be approximated by:

$$\gamma_{r,(SO_2,tot)} \approx \sum_{i,j} \Gamma_{(b,j)} \tag{5.43}$$

As a result, the reactive uptake coefficient can be decomposed into several uptake coefficients γ_j, each one representing single contributions to liquid oxidation of SO_2 by O_3, H_2O_2, O_2/TMI, and HOX:

$$\gamma_j \approx \gamma_{r,tot} \cdot f_j \tag{5.44}$$

with,

$$f_j = \frac{\Gamma_{(b,j)}}{\sum_{i,j} \Gamma_{(b,j)}} \tag{5.45}$$

Finally, the rate of SO_2 uptake for each oxidation pathway j can be defined as:

$$-\left(\frac{d[SO_2]}{dt}\right)_j = \gamma_{r,tot} \cdot f_j \cdot \frac{\overline{\nu}_{SO_2}}{4} SA \cdot [SO_2] \tag{5.46}$$

Table 5.2: Major variables within the resistor model for the reactive uptake of SO_2 on primary sulphate aerosols of non-condensing plumes.

Aqueous reaction	$\frac{1}{\Gamma_d}$	$\frac{1}{\alpha_{SO_2}}$	$\frac{1}{\Gamma_{(b,i)}}$
$SO_2 + O_3$	15	10^6	8.4×10^{19}
$SO_2 + H_2O_2$	15	10^6	1.5×10^{16}
$SO_2 + O_{2/}TMI$	15	10^6	3.1×10^{20}
$SO_2 + HOX$	15	10^6	5.3×10^{29}

Halogens heterogeneous reactions implemented in the model, and the relative uptake coefficients are summarized in Table:5.3.

Table 5.3: Values of γ_r used for halogens heterogeneous reactions in condensing plumes (WD) and non-condensing plumes (SA) (Sander et al., 2006).

Reaction	γ_i (SA)	γ_i (WD)
$HOCl + Br^-_{(aq.)} + H^+ \longrightarrow Cl_{2(aq.)} + H_2O$	0.002	=
$HOBr + Cl^-_{(aq.)} + H^+ \longrightarrow BrCl_{(aq.)} + H_2O$	$0.2 \cdot \frac{[BrCl]_{aq.}}{[BrCl]_{aq.} + [Br_2]_{aq.}}$	=
$HOBr + Br^-_{(aq.)} + H^+ \longrightarrow Br_{2(aq.)} + H_2O$	$0.2 \cdot \frac{[Br_2]_{aq.}}{[BrCl]_{aq.} + [Br_2]_{aq.}}$	=
$BrONO_2 + H_2O \longrightarrow HOBr_{(aq.)} + HNO_{3(aq.)}$	0.8	$3 \cdot 10^{-2}$
$ClONO_2 + H_2O \longrightarrow HOCl_{(aq.)} + HNO_{3(aq.)}$	-	$2.5 \cdot 10^{-2}$
$N_2O_5 + H_2O \longrightarrow 2\,HNO_{3(aq.)}$	0.03	=

3.4 Final continuity equations

Based on the physico-chemical framework described above for water droplets and sulphate aerosols heterogeneous chemistry, the mass-balance equation (also defined as continuity equation) for volcanic SO_2 oxidation is expressed differently for condensing and non-condensing plume scenarios. In addition,

deposition of S(IV) species (S(IV) = $SO_{2(g)} + SO_{2(aq)} + HSO_3^- + SO_3^{2-}$) is ignored in non-condensing plumes, because very little S(IV) species are dissolved in sulphate particles due to the extreme pH of solution. Therefore, S(IV) oxidation in sulphate aerosols is assumed to depend almost only on $SO_{2(g)}$, the most important S(IV) species during sulphate production in non-condensing plumes. In conclusion, for this scenario it is assumed that the mass-balance equation for S(IV) oxidation is the same as the one for SO_2, expressed as:

$$\frac{d[\text{S(IV)}]}{dt} = \frac{d[\text{SO}_2]}{dt} = -k_{\text{OH}^+\text{SO}_2} \cdot [\text{SO}_2][\text{OH}] -$$
$$- \left(\sum_j \gamma_j \cdot \frac{\overline{\nu}_{\text{SO}_2}}{4} \cdot SA \cdot [\text{SO}_2] \right) - K_{mix} \cdot \left([\text{SO}_2] - [\text{SO}_2]_{(bck)}\right) \tag{5.47}$$

where $[\text{SO}_2]$ and $[\text{SO}_2]_{(bck)}$ are respectively SO_2 concentration of volcanic plumes and background atmosphere.

The S(IV) continuity equation for condensing volcanic plumes is more complex, and it is expressed as:

$$\frac{d[\text{S(IV)}]}{dt} = -k_{\text{OH}^+\text{SO}_2} \cdot [\text{SO}_2][\text{OH}] - \left(\sum_j K_j^{l-g} \cdot [\text{S(IV)}]_{aq.}^{l-g} [\text{C}_j]_{aq.}^{l-g} \right) -$$
$$- k_{dep} \cdot [\text{S(IV)}] - K_{mix} \cdot \left([\text{S(IV)}] - [\text{S(IV)}]_{(bck)}\right) \tag{5.48}$$

where $[\text{S(IV)}]$ and $[\text{S(IV)}]_{(bck)}$ are respectively S(IV) concentrations in volcanic plumes and in the background atmosphere.

The same approach is used to define sulphate production continuity equations, hence S(VI) production rates either in presence of sulphate aerosols (R5.49), or in presence of water droplets (R5.50):

$$\frac{d[\text{S(VI)}]}{dt} = k_{\text{OH}^+\text{SO}_2} \cdot [\text{SO}_2][\text{OH}] + \left(\sum_j \gamma_j \cdot \frac{\overline{\nu}_{\text{SO}_2}}{4} \cdot SA \cdot [\text{SO}_2] \right) -$$
$$- k_{dep} \cdot [\text{S(VI)}] - K_{mix} \cdot \left([\text{S(VI)}] - [\text{S(VI)}]_{(bck)}\right) \tag{5.49}$$

$$\frac{d[\text{S(VI)}]}{dt} = k_{\text{OH}^+\text{SO}_2} \cdot [\text{SO}_2][\text{OH}] + \left(\sum_j K_j^{l-g} \cdot [\text{S(IV)}]_{aq.}^{l-g} [\text{C}_j]_{aq.}^{l-g} \right) -$$
$$- k_{dep} \cdot [\text{S(VI)}] - K_{mix} \cdot \left([\text{S(VI)}] - [\text{S(VI)}]_{(bck)}\right) \tag{5.50}$$

where $[\text{S(VI)}]$ and $[\text{S(VI)}]_{(bck)}$ are respectively S(VI) concentrations of volcanic plumes and of background atmosphere.

124

In both model scenarios deposited S(VI) (S(VI)$_{dep}$) is a prognostic variable of the system, and it is parametrised as:

$$\frac{d}{dt}[\text{S(VI)}]_{dep} = k_{dep} \cdot [\text{S(VI)}] \tag{5.51}$$

For both plume conditions, the value of k_{dep} is a first-order loss constant derived from the average lifetime of sulphate in the free troposphere (Stevenson et al., 2003a).

3.5 Tracking S(VI) oxygen isotopic signatures

Isotopic chemistry equations

Sulphate mass balance equations are limited to mass tracking of atoms, not isotopes. As a result, they cannot monitor S(VI) and S(VI)$_{dep}$ evolving concentrations. In order to track sulphate Δ^{17}O the continuity equations describing sulphate production are combined to isotopic transfer equations, and a new variable called anomaly product ([S(VI)]·Δ^{17}O(S(VI))) is introduced in the model. Its continuity equation is given by (Morin et al., 2008, 2011; Galeazzo et al., 2018):

$$\frac{d}{dt}\left([\text{S(VI)}] \cdot \Delta^{17}\text{O(S(VI))}\right) = \sum_j [P_j \cdot \Delta^{17}\text{O(S(VI)}_{\text{prd}})_j] - k_{dep} \cdot \Delta^{17}\text{O(S(VI))}$$

$$\tag{5.52}$$

where Δ^{17}O(S(VI)) is the O-MIF of S(VI), P$_j$ is the S(VI) production via oxidation pathway j, and Δ^{17}O(S(VI)$_{\text{prd}})_j$ is the specific transfer of O-MIF to S(VI) during the oxidation of S(IV) via reaction j.

As S(VI)$_{dep}$ is also a variable in the model, the [S(VI)$_{\text{dep}}$]·Δ^{17}O(S(VI)) anomaly product is also a prognostic variable, whose continuity equation is given by:

$$\frac{d}{dt}\left([\text{S(VI)}_{dep}] \cdot \Delta^{17}\text{O(S(VI))}\right) = k_{dep} \cdot [\text{S(VI)}] \cdot \Delta^{17}\text{O(S(VI))} \tag{5.53}$$

The isotopic balance equations define the isotopic anomaly acquired by S(VI) molecules during their production. Each reaction pathway generates, indeed, a specific O-MIF in its produced sulphate. Peculiar signatures for each oxidation pathway are determined by the isotopic anomalies of reactants and the number of oxygen atoms (directly or indirectly originated by ozone) transferred to sulphate during S(IV) oxidation. As a result, the overall sulphate isotopic composition reflects the relative contribution of different sulphate production pathways (P$_j$) weighted by their specific transferred isotopic anomaly Δ^{17}O(S(VI))$_j$).

On top of the oxygen isotopes scheme recently implemented in CiTTyCAT for S(IV) oxidation in cloud droplets (Galeazzo et al., 2018), the isotopic continuity equations for S(IV) and S(VI) are modified to account for halogens chemistry,

including SO_2 oxidation by HOX on sulphate particles and cloud droplets. An HOX isotopic balance equation is derived and the isotopic balance equation for OH is also modified. Isotopic balance equations determine sulphate products O-MIF considering the origins of oxygen atoms inherited by S(VI) during S(IV) oxidation. As a result, O-MIFs of reactants involved in S(VI) production have to be constrained precisely.

It is worth stressing that in the model the continuity equations of S(VI) and S(VI)$_{dep}$ anomaly products are integrated with a 4th order Runge-Kutta method algorithm, instead of using the CiTTyCAT chemistry solver (Morin et al., 2008). Preliminary simulations have shown that model results are not very significantly affected by this splitting method, with the advantage that while using this approach the chemistry module is totally independent from the oxygen isotopic scheme.

Oxidation by O_3, H_2O_2, O_2/TMI, and HOX

In the first place, it is assumed that volcanic SO_2 and H_2O do not carry any significant O-MIF. The oxygen isotopic composition of magmatic SO_2, indeed, is mass-dependent and no $\Delta^{17}O$ (SO_2) has been observed so far in volcanic SO_2 (Eiler, 2001; Martin, 2018). To our knowledge no study covering the isotopic composition of volcanic water emissions has been conducted. It is, therefore, assumed that volcanic water has the same isotopic composition as atmospheric water, and $\Delta^{17}O(H_2O)$ of about $0‰$ (Uemura et al., 2010).

Ozone is a key atmospheric reactant, notably characterised by an intrinsic high O-MIF generated during its formation in the atmosphere (Marcus, 2013). Tropospheric ozone has a large $\Delta^{17}O(O_3, bulk)$ of about 25‰ (Vicars and Savarino, 2014), but its isotopes distribution within the molecular structure is not stochastic. It is suggested, indeed, that heavier oxygen isotopes are located at its molecular extremities (Bhattacharya et al., 2008; Marcus, 2013). Assuming that terminal atoms are generally more likely to be involved in chemical reactions, because only one chemical bond needs to be broken, a mean reactive ozone MIF ($\Delta^{17}O$ ($O_3^\star$)) can be defined by encompassing isotopic enrichments of terminal sites and their enhanced reactivity. In relation to typical tropospheric ozone O-MIF, a $\Delta^{17}O$ ($O_3^\star$) of about 40‰ is derived (Morin et al., 2007, 2008; Bhattacharya et al., 2008; Savarino et al., 2008; Vicars and Savarino, 2014). In this work it has been chosen to use a value of $\Delta^{17}O$ ($O_3^\star$) equal to 36‰, because modelling simulations assuming using this value have shown good agreement with experimental observations (Morin et al., 2008). Part of reactive ozone isotopic anomaly can be transmitted to reaction products, including oxidants, when molecules react with O_3. For SO_2 oxidation by O_3 out of four S(IV) oxygen atoms one is inherited from ozone during SO_2 oxidation. Therefore, the produced sulphate have a $\Delta^{17}O$ (S(VI))$_{O_3+S(IV)}$ = 9 ‰.

Other atmospheric oxidants inherit O-MIF directly or indirectly from atmospheric ozone via photochemical reactions (Thiemens, 2006). Notably, among

SO$_2$ atmospheric oxidants, H$_2$O$_2$ carries a significant O-MIF (Δ^{17}O (H$_2$O$_2$) equals to 1.75‰) (Savarino and Thiemens, 1999a). While reacting with S(IV), H$_2$O$_2$ transfers two oxygen atoms to S(IV) via a nucleophilic substitution, resulting in a produced sulphate with Δ^{17}O (S(VI))$_{\mathrm{H_2O_2+S(IV)}}$ equal to 0.87‰. Atmospheric O$_2$ is another SO$_2$ oxidant characterised by a peculiar O-MIF equal to -0.34 ‰ (Young et al., 2002; Barkan and Luz, 2003). The oxidation of S(IV) by O$_2$ is catalysed by TMI via a chain of radical reactions. There are, however, large uncertainties regarding the mechanism of S(IV) oxidation. Therefore, it is assumed here that only one oxygen atom is transferred from O$_2$ to S(IV), resulting in produced sulphate with a Δ^{17}O (S(VI))$_{\mathrm{O_2/TMI+S(IV)}} \approx -0.09$‰. This value is within errors interval of experimental isotopic measurements; thus this produced sulphate would be classified as mass-dependent in experimental measurements.

No investigation regarding Δ^{17}O(HOX) has been conducted so far. Nonetheless, any potential O-MIF carried by HOX would not affect the final isotopic signature of S(VI), since the new oxygen atom transferred to HSO$_3^-$ and SO$_3^{2-}$ originates from water and not from hypohalous acids (Fogelman et al., 1989; Troy and Margerum, 1991; Chen et al., 2016). Therefore, the isotopic mass-balance equation for HOX oxidation takes the following form:

$$\Delta^{17}\mathrm{O(S(VI))}_{\mathrm{HOX+S(IV)}} = \frac{1}{2} \cdot \Delta^{17}\mathrm{O(SO_2)} + \frac{1}{2} \cdot \Delta^{17}\mathrm{O(H_2O)} \qquad (5.54)$$

Assuming that no isotopic anomaly is carried by volcanic H$_2$O and SO$_2$, the final isotopic balance equation is simplified to:

$$\Delta^{17}\mathrm{O(S(VI))}_{\mathrm{HOX+S(IV)}} = 0 \qquad (5.55)$$

In conclusion, it is expected that sulphates generated via S(IV) oxidation by HOX would not carry an O-MIF, instead being equal to 0 ‰ (Chen et al., 2016). A summary of the isotopic signatures of different oxidation channels is reported in Table:5.4.

Table 5.4: O-MIF signatures of S(IV) oxidation pathways in the model

Oxidant	O-MIF pathway (‰)
OH	calculated (0 to a maximum of 4.5)
H$_2$O$_2$	0.87
O$_3$	9
O$_2$/TMI	-0.09
HOX	0

Oxidation by OH

Atmospheric OH is a major tropospheric oxidant, generated mostly by ozone photochemistry, specifically by the reaction between O^1(D) and H$_2$O. OH is

initially formed with a relatively high O-MIF because it has a 50% chance of inheriting an oxygen atom from O_3. It is generally thought that at average tropospheric conditions the inherited isotopic anomaly is rapidly lost by the quick O-isotopic exchange between OH and H_2O, happening before the hydroxyl radical could have reacted with other species. OH MIF is the result of the competition between OH rates of destruction (i.e. reaction with CH_4 and CO) and the isotopic exchange with H_2O. However, this competition depends on environmental and atmospheric conditions (Dubey et al., 1997; Lyons, 2001). In the core of volcanic plumes, large amounts of volcanic SO_2 and HCl can react with OH, thus significantly enhancing the OH destruction rate. Consequently, in contrast to background atmospheric conditions, OH formed in volcanic plume may conserve some of its initial O-MIF, which then would be further transmitted to other products of its reaction. $\Delta^{17}O(OH)$ is considered a prognostic variable in the model, and it is evaluated by the following equation (Morin et al., 2011; Galeazzo et al., 2018):

$$\Delta^{17}O(OH) = x \cdot \Delta^{17}O(OH^*_{prod.}) \tag{5.56}$$

with

$$\Delta^{17}O(OH^*_{prod.}) = \frac{1}{2} \cdot \Delta^{17}O(O_3^*) \tag{5.57}$$

and

$$x = \frac{D}{D + k^*_{OH+H_2O} \cdot [H_2O]} \tag{5.58}$$

$$D = k_{OH+CO} \cdot [CO] + k_{OH+CH_4} \cdot [CH_4] + k_{OH+SO_2} \cdot [SO_2] + k_{OH+HCl} \cdot [HCl] \tag{5.59}$$

The isotopic signature transmitted to sulphate via this channel of oxidation is therefore given by (Savarino et al., 2000):

$$\Delta^{17}O(S(VI))_{OH+SO_2} = \frac{1}{2} \cdot \Delta^{17}O(SO_2) + \frac{1}{4} \cdot \Delta^{17}O(OH) + \frac{1}{4} \cdot \Delta^{17}O(H_2O) \tag{5.60}$$

Since $\Delta^{17}O(H_2O)$ and $\Delta^{17}O(SO_2)$ are thought to be negligible the equation is finally simplified to:

$$\Delta^{17}O(S(VI))_{OH+SO_2} = \frac{1}{4} \cdot \Delta^{17}O(OH) \tag{5.61}$$

As a result, the OH O-MIF ($\Delta^{17}O(OH)$) can vary between 0 ‰ and 18 ‰ in volcanic plumes and hence sulphate formed by OH oxidation can have an O-MIF between 0 ‰ and 4.5 ‰, depending on HCl, SO_2 and water vapour levels within the plume.

In order to illustrate how $\Delta^{17}O(OH)$ can vary with the SO_2 and HCl loadings, OH O-MIF is plotted for standard conditions in function of the SO_2 or HCl concentration in **Fig.:5.2**. $\Delta^{17}O(OH)$ is calculated for 3 different conditions. The first two cases are rather hypothetical because one concerns a volcanic

plume with varying sulphur levels but no halogens, and the other case concerns a volcanic plume with varying halogen levels but no sulphur. Nonetheless, the results give some idea about the levels of SO_2 and HCl required to affect significantly the OH O-MIF. The third case is more realistic, it is about a plume with varying halogen levels and one ppmv of SO_2.

The first two cases show that it is only when SO_2 or HCl concentration is greater than tens of ppbv that OH carries an O-MIF sufficiently high (O-MIF > 0.4 ‰) to generate sulphate with an O-MIF greater than 0.1 ‰, the typical error for isotopic measurement. This implies that OH loss by reaction with SO_2 or HCl starts competing with the isotopic exchange with H_2O around these concentrations. The last case shows that, in the presence of a ppmv of SO_2, HCl needs to be above 50 ppbv to influence significantly OH O-MIF. Halogens reaction with OH has to compete, indeed, with the combined OH losses due to the isotopic exchange with H_2O, and the reaction with SO_2.
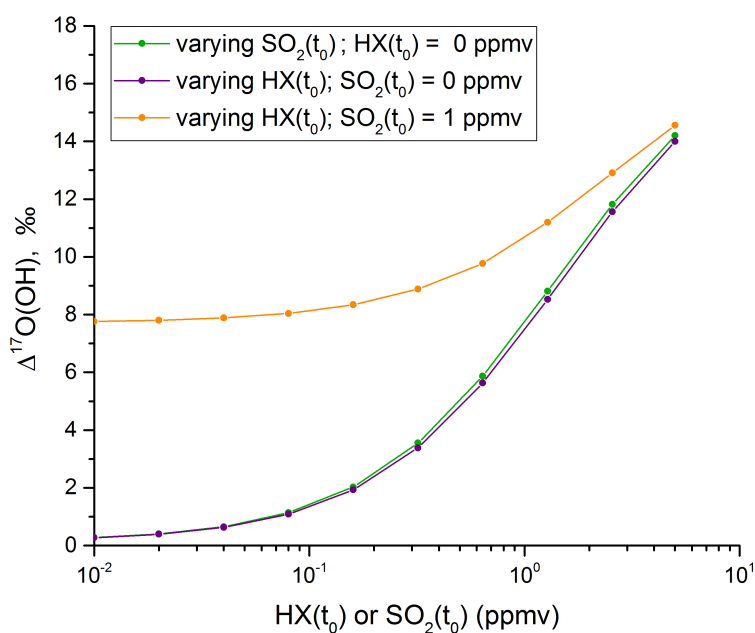
Figure 5.2: Variation of $\Delta^{17}O(OH)$ in relation to initial halogens and SO_2 loading within a non-condensing plume.

4 Box model set up

4.1 Standard initial conditions

All simulations are run for springtime conditions and start at midday at the tropics (i.e. 115.5° E 8.3° S, Mt. Agung, Indonesia). In order to reach stable chemical compositions, notably for medium- and short-lived reactive species, the model is run for 3 days before injection of halogens and/or SO_2 (i.e. plume injection). The evolution of the chemical composition is then followed for 7 days, in order to cover the evolution from highly concentrated to highly diluted plumes in the troposphere.

Since most of large volcanoes are situated in remote areas with their peaks often close to the free troposphere, volcanic plumes tend to end up in the free troposphere, at relatively high altitudes. For this reason, the base model is set at 3 km of altitude, with pressure set at 640 mbar and T set at 283.15 K. Background concentrations of reactive species are set to typical atmospheric levels observed in the tropical free troposphere (Wang et al., 2001; Pan et al., 2015). In the standard conditions, initial concentrations are set to: O_3 = 35 ppbv and H_2O_2 = 0.1 ppbv (Herrmann et al., 2000). Within water droplets and sulphate aerosols, it is assumed that TMI concentrations are correlated with each other, i.e. that [Mn(II)] = 0.1 · [Fe(III)], as observed in tropospheric aerosols and atmospheric hydrometeors (Seinfeld and Pandis, 2016).

Typical halogens emissions within volcanic plumes are not well characterised, because they vary from one volcanic system to another, and even between different phases of the same erupting event. Modelling and field observations suggest typical HCl/SO_2 ratios of about 0.5, and mean HBr/HCl ratios of about 2×10^{-3} (Gerlach, 2004; Aiuppa et al., 2005a; Aiuppa, 2009). These initial ratios (HCl/SO_2, HBr/HCl) are used in almost all simulations when halogens are injected, except when sensitivity to SO_2 or halogens loading is explored. To account for the extreme variability in halogens levels, sensibility simulations are finally performed.

In both condensing (water droplets) and non-condensing (sulphate aerosols) plume standard simulations SO_2 concentration is set to 1.5 ppmv, a value commonly observed at the proximity of volcanic vents during passive degassing (Robock, 2000; Rose et al., 2006; Mather et al., 2006; Roberts et al., 2012; De Moor et al., 2013; Voigt et al., 2014).

Specific input parameters: condensing volcanic plumes

In all condensing plume simulations, volcanic water is assumed to condense either forming water droplets, or coating ash particles. It constitutes the bulk of the liquid phase, quantified by the liquid water content (LWC). At standard conditions the LWC is set to $0.3 \, \mathrm{g \, m^{-3}}$, a value commonly observed for tropospheric clouds (Korolev et al., 2007; Carey et al., 2008). It is assumed that water

droplets have a fixed radius of 5 μm. The droplets concentration is then derived from the specific LWC. The initial pH of the aqueous phase is set to 4.5, but it has no impact on the overall model results, since water droplets pH is almost immediately driven by SO_2, HBr and HCl uptake, and by S(IV) oxidation.

Large uncertainties are pertaining to iron release from volcanic ashes in aqueous phase (Hoshyaripour et al., 2015; Maters et al., 2016). Standard TMI concentrations are set to values corresponding to the lower range of tropospheric conditions (Herrmann et al., 2000; Parazols et al., 2006), but to the mean range of model calculations regarding iron release within volcanic plumes (Hoshyaripour et al., 2015). At standard conditions, TMI concentrations in water droplets are set to: [Fe(III)] = 0,5 μM, and hence [Mn(II)] = 0,05 μM.

Specific input parameters: non-condensing volcanic plumes

The radius of primary volcanic sulphate aerosols is fixed at 0.5 μm in the accumulation mode, while aerosols concentration is fixed at 1000 particles per cm^3 of air. Both values are chosen in relation to atmospheric observations of primary sulphate emissions at volcanic vents (Mather et al., 2003).

In non-condensing volcanic plumes, the liquid phase is composed of sulphuric acid, since water vapour pressure does not reach saturation. The relative humidity (RH) is specified and the sulphate aerosol composition (i.e. sulphuric acid weight percentage, wt) is calculated from RH, temperature, and pressure (DeMore et al., 1997). The aerosol composition is a critical factor for gas-liquid partitioning of species and also for the chemistry operating within the liquid. During non-condensing plume simulations, RH is set to 45%, a rather average value observed during volcanic plumes degassing (Mather et al., 2006; Kroll et al., 2015).

Because of the absence of ash in non-condensing plumes from passive degassing, it is assumed that iron is not released in significant amounts from magma bubbles burst (Mather et al., 2003). As a result, aerosols TMI concentration is set to 0.001 μM, the lowest iron mobilization value suggested by volcanic plumes model simulations (Hoshyaripour et al., 2015).

4.2   Model experiments

Standard simulations

The objective of the first set of numerical experiments is to assess the competition among SO_2 oxidants in presence or absence of halogens. Six simulations (C1-C3, and N1-N3) are run with oxidation schemes of increasing complexity for both condensing (C_n) and non-condensing volcanic plumes (N_n). The different cases of SO_2 oxidation considered in the simulations are oxidation by: only OH in gas phase (C1; N1), OH in gas phase, and H_2O_2, O_3 and O_2/TMI in liquid phase (C2; N2), and by OH in gas phase, and H_2O_2, O_3, O_2/TMI and HOX

in liquid phase (C3; N3). C1, N1, C2 and N2 do not have halogens, whereas C3 and N3 correspond to halogens injection. The standard simulations are designed to explore the effect of different processes for standard conditions.

Sensitivity simulations

Initial SO_2 levels, LWC, TMI and halogen concentrations are key model inputs, but they are subjected to large uncertainties and variability. The sensitivity of the results to input conditions varying within plausible ranges is explored in additional simulations. O-MIF transfers are investigated for an array of initial concentrations ranging from highly diluted to dense volcanic plumes. In the case of condensing plumes, the sensitivity to varying levels of TMI is also explored. On the other hand, preliminary simulations have shown that, within the range of plausible TMI concentrations, TMI catalysed oxidation is negligible in non-condensing plumes. Simulations S1, S2 and S3 explore model responses for condensing plumes, while Z1 and Z2 simulations investigate the sensitivity of non-condensing plumes.

The first set of sensitivity simulations (S1-Z1) is devoted to the sensitivity to initial SO_2 concentration, which is varied from 0.05 to 5 ppmv. The idea is to consider a range of values representative of a variety of observed volcanic plumes (Aiuppa et al., 2005b, 2006b; Carn et al., 2011; Roberts et al., 2012). Initial halogens concentrations are fixed during the S1 set, they do not vary with the SO_2 initial concentrations.

The second set of sensitivity simulations (S3) investigates the sensitivity of condensing plumes to LWC. Large amounts of water, indeed, can be injected by volcanoes, hence various kinds of plume can develop. The chosen values are selected to represent different cloud typologies: from light mean saturated clouds (0.1-0.5 $g\,m^{-3}$), to water-rich cumulonimbus clouds (1-2 $g\,m^{-3}$) (Laj et al., 1997; Rosenfeld and Lensky, 1998; Pruppacher et al., 1998; Korolev et al., 2007; Carey et al., 2008).

The third of sensitivity studies (S4) explores the sensitivity to TMI concentrations within condensing volcanic plumes. It is supposed to cover the possible range of TMI aqueous concentrations resulting from mineral dissolution. Volcanic eruptions can inject large quantities of mineral solid material in the form of ash, commonly composed of minerals with different proportions of Fe(II) and Fe(III) within their crystalline structure (Rose and Durant, 2009; Langmann, 2014). Depending on ash content and plume chemical composition, TMI concentrations vary within volcanic aqueous phases (Hoshyaripour et al., 2015). Fe(III) mobilization depends on ash composition and water acidity, since low pH promotes dissolution of iron minerals (Maters et al., 2016). However, the extent to which halogen halides and sulphate can promote iron dissolution is rather uncertain. During S4, [Fe(III)] varies from 0.1 to 2 μM, based on model simulations and laboratory experiments on iron release from volcanic ash (Hoshyaripour et al., 2015; Maters et al., 2016).

The last set of sensitivity studies (Z2) concerns the sensitivity of non-condensing plumes chemistry to the initial halogens loading. The amounts of halogens emitted vary greatly from one volcanic system to another, and major differences are observed between rift and arc volcanoes (Aiuppa et al., 2009). Intraplate systems (e.g. rift and hotspot volcanic systems) are characterised, indeed, by HBr/SO_2 emission ratios of the order of 10^{-5}, while arc volcanic systems exhibit HBr/SO_2 ratios as high as 10^{-2} (Aiuppa, 2009; Aiuppa et al., 2009; Mather et al., 2012). At the same time, HCl/SO_2 ratios up to 1 have been observed in halogen-rich plumes of arc volcanoes (Aiuppa et al., 2005a; Witt et al., 2008). Consequently, for the Z2 set, the HX/SO_2 ratio varies from 0.01 to 0.8, while keeping initial SO_2 at 1 ppmv.

A summary of all simulations, and relative specific conditions, is reported in Table:5.5.

5 Results and discussion

5.1 Isotopic constraints on S(IV) oxidation: condensing volcanic plumes (water droplets)

Standard simulations

The first simulation (C1, only OH oxidation) investigates O-MIF transfer to sulphate for standard conditions in the absence of heterogeneous chemistry (S(VI) produced only by SO_2 reaction with hydroxyl radicals). **Fig.:5.3** shows the evolution of SO_2, O_3, H_2O_2, and S(VI) concentrations during the run. SO_2 concentration drops from 1.5 ppmv to 0.06 ppmv 7 days after injection. At the end of the run, total atmospheric S(VI) is around 0.09 ppmv, and deposited sulphate is 0.05 ppmv. Most of the SO_2 in the plume is lost through mixing with the background atmosphere. Keep in mind that the mixing description is crude, and that the main focus here is sulphur oxidation within the volcanic plume and the resulting isotopic composition on sulphate.

Since SO_2 is only oxidised by OH, the S(VI) production follows a diurnal cycle. In **Fig.:5.6-5.7** the O-MIF of atmospheric ($\Delta^{17}O(S(VI)_{prd})$) and deposited sulphates in C1 are compared to the isotopic signatures modelled during the following simulations C2 and C3. Within the first minutes from plume injection sulphate with very positive O-MIF is formed, the maximum isotopic anomaly reached by S(IV) during the first day is of about 1.4 ‰. As the plume dilutes through mixing with the background atmosphere, the initial isotopic signature of OH decreases because SO_2 concentration drops due to mixing and gas-phase oxidation. Consequently, over the long run, $\Delta^{17}O(S(VI)_{prd})$ decreases.

Simulation C2 has the same initial conditions of C1, except that now the chemical scheme also includes the aqueous oxidation of S(IV) by H_2O_2, O_3 and O_2/TMI. **Fig.:5.4** shows the evolution of the chemical species concentrations as S(IV) oxidation occurs in both gas and aqueous phases. Within 7 days from

Table 5.5: Summary of model investigations, and related oxidation pathways or range of investigations.

STD	water droplets	sulphate aerosols	OH	O_3	H_2O_2	$O_{2/}$TMI	HOX
C1	x		x				
C2	x		x	x	x	x	
C3	x		x	x	x	x	x
N1		x	x				
N2		x	x	x	x	x	
N3		x	x	x	x	x	x*

Sensitivity set*	water droplets	sulphate aerosols	LWC (g m^{-3})	TMI (μM)	[SO_2]$_0$ (ppmv)	[HX]$_0$/[SO_2]$_0$	range
S1	x				x		0.05 - 5
S2	x		x				0.2 - 2
S3	x			x			0.1 - 2
Z1		x			x		0.05 - 5
Z2		x				x	0.05 - 0.8

During sensitivity simulations all sulphur oxidation channels are active in both condensing and non-condensing plumes.
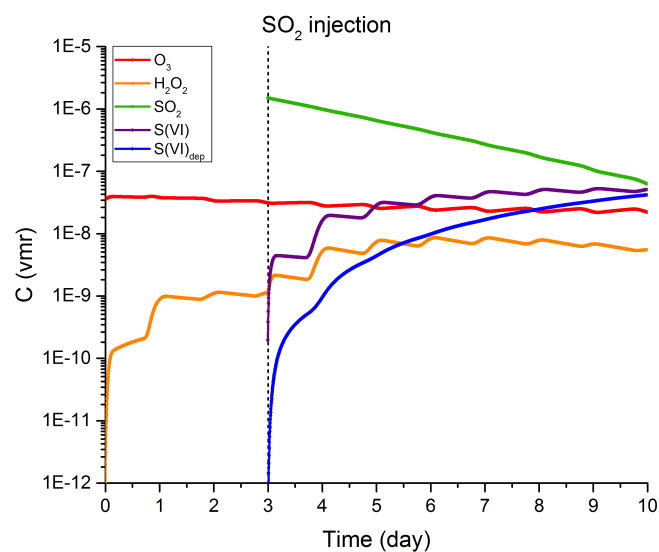
Figure 5.3: Gas-phase concentrations of atmospheric species during the C1 simulation (condensing plume, see text). The simulation starts at 0:00 p.m., and SO_2 is injected after 3 days.
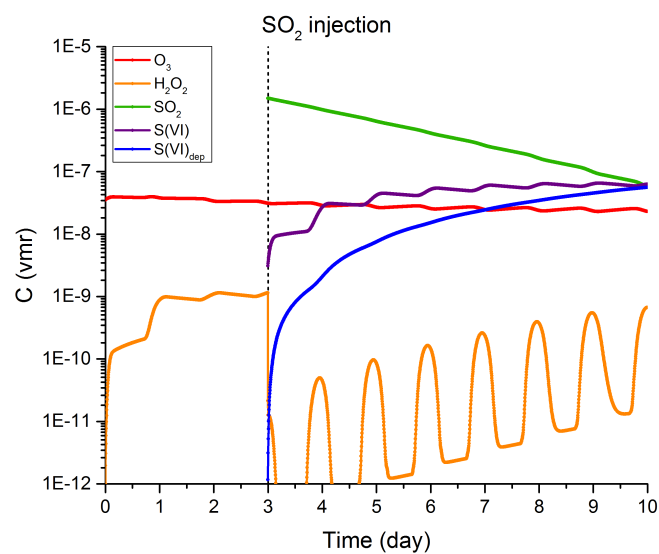
Figure 5.4: Gas-phase concentrations time evolution for SO_2, its tropospheric oxidants and produced and deposited sulphates during C2 (see text); no halogens are released within the plume.
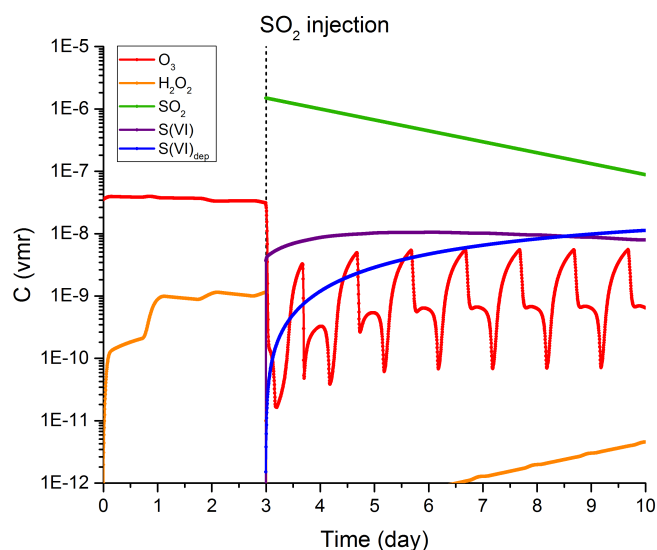
Figure 5.5: Gas-phase concentrations time evolution for SO_2, its tropospheric oxidants and produced and deposited sulphates during simulation C3, and in presence of halogens emissions.

injection, SO_2 concentration drops from 1.5 ppmv to 0.05 ppmv, while total produced S(VI) is around 0.12 ppmv and deposited sulphate reaches 0.06 ppmv. Following SO_2 injection, H_2O_2 is immediately depleted from the plume, reaching concentrations below pptv levels. Significant amounts of H_2O_2 are reformed again after 4 days during day time. Sulphate production follows a diurnal cycle, indicating that OH and H_2O_2 still contribute largely to S(IV) oxidation. Once again, mixing with background air and S(IV) deposition are the main SO_2 losses within the plume. In **Fig.:5.6-5.7** the isotopic composition of atmospheric and deposited sulphates from C2 are compared to C1 and C3. Initially, sulphate with high O-MIF around 0.75 ‰ is produced in the plume. Within the first night, $\Delta^{17}O(S(VI)_{prd})$ decreases to 0.6 ‰, increasing progressively to 0.8 ‰ by the second day. Eventually, sulphate isotopic anomaly decreases steadily throughout the simulation, reaching a final value of 0.55 ‰ by the end of the run; the final O-MIF of deposited sulphate is around 0.7 ‰. Decrease in O-MIF observed during the first night is due to major O_2/TMI contribution to S(IV) oxidation. As the pH of the water phase decreases due to S(VI) production, less S(VI) dissolves into the liquid phase, and S(IV) oxidation is significantly driven by reaction with OH from the third day. By the time OH becomes a main pathway of in-plume oxidation $\Delta^{17}O(OH)$ is significantly lowered due to SO_2 mixing, S(IV) deposition and in-plume reactions. Overall, in presence of 0.5 μM of TMI and in absence of halogens, H_2O_2 and OH contribute the most to S(VI)
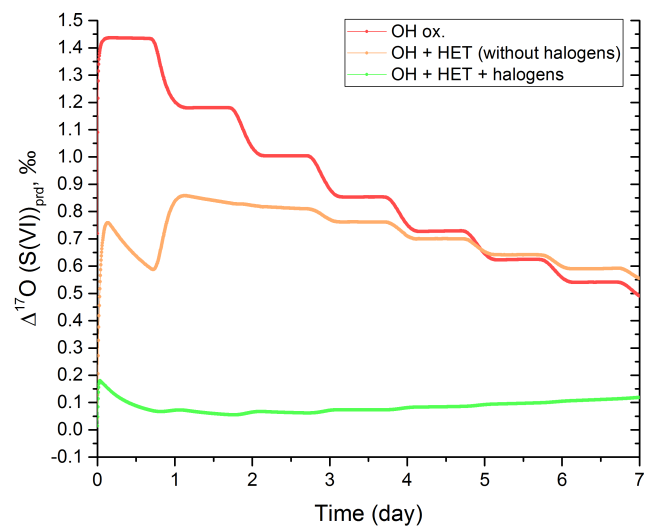
Figure 5.6: Time evolution of $\Delta^{17}O(S(VI))$ in produced sulphates during condensing volcanic plumes simulations C1 (only OH ox.), C2 (OH + HET, without halogens) and C3 (OH + HET + halogens).
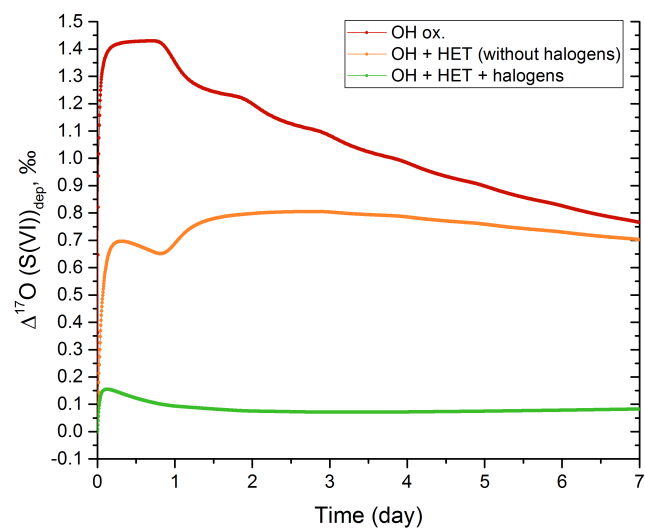
Figure 5.7: Time evolution of $\Delta^{17}O(S(VI))$ in deposited sulphates during condensing volcanic plumes simulations C1 (only OH ox.), C2 (OH + HET, without halogens) and C3 (OH + HET + halogens).

production, thus resulting in a $\Delta^{17}O(S(VI)_{dep})$ of about 0.7 ‰.

Simulation C3 is the same of C2 but it includes all the major pathways of oxidation, including S(IV) aqueous reactions with HOX. Fig:.5.5 shows main species concentrations as halogens are also added to the chemical scheme. By the end of the simulation SO_2 concentration drops from 1.5 ppmv to 0.09 ppmv, while atmospheric S(VI) is around 0.02 ppmv and deposited sulphate is about 0.01 ppmv. Once again most of initial SO_2 is lost due to washing out and mixing with background atmosphere. However, remarkably less S(VI) is produced compared to C1 and C2 simulations. Furthermore, now S(VI) production does not follow a diurnal cycle, indicating that OH and H_2O_2 are not major sulphur oxidants in the C3 simulation. After halogens injection, the O_3 concentration drops dramatically due to injection of radical bromine and activation of HBr. A first ODE (ozone depletion event) is observed within half an hour from plume release during daytime. O_3 reaches less than ppbv levels when the plume is very concentrated in the first day. Following the first ODE, the production of hydrogen radicals results in massive drops in OH and H_2O_2 levels. OH is reformed in significant amounts only after 5 days from plume injection, and H_2O_2 concentration recovers to pptv levels only after 3.5 days. HO_2 depletion from the gas-phase does not allow accumulation of HOX over the long run, and it remains below pptv levels throughout the C3 simulation. As a result, HOX (HOX = HOCl + HOBr) is found in extremely low concentrations in both aqueous and gas phases. Following halogens injection, BrO/SO_2 ratio keeps increasing during the first minutes of plume development, reaching a maximum value of about 2.0×10^{-4} after 30 minutes. Throughout the C3 simulation, BrO/SO_2 ratio fluctuates significantly following a diurnal cycle. The ratio remains within the range of observations (Bobrowski et al., 2003; Oppenheimer et al., 2006; Bobrowski and Platt, 2007; Bobrowski et al., 2007).

In **Fig.:5.6-5.7** the isotopic composition of atmospheric and deposited sulphates of simulation C3 are compared to those of C1-C2. Atmospheric sulphate carries an O-MIF of about 0.2‰ during the first minutes of simulation. Within the first 24 hours from plume injection, the isotopic anomaly drops to about 0.05‰. By the end of the simulation $\Delta^{17}O(S(VI)_{dep})$ is equal to about 0.08‰. The low $\Delta^{17}O(S(VI)_{prd})$ value indicates that sulphate production is predominantly driven by aqueous phase oxidation pathways that produce sulphate with $\Delta^{17}O \approx 0$‰. Within 30 minutes from plume injection very small HOX concentrations are formed in the plume, since HO_x species are massively depleted. The only S(IV) oxidation channel which does not exhibit diurnal variation and independent of the levels of HO_x species and HOX concentrations is the O_2/TMI pathway. It is responsible for most of the sulphate production in the C3 simulation.

Since the results might be sensitive to a number of assumed model inputs several sensitivity studies are carried to assess the robustness of the results and conclusions. The most critical model inputs are the amounts of halogens injected, the assumed TMI concentrations and LWC.

138

Influence of SO$_2$ initial concentration

The first set of sensitivity studies (S1) is devoted to the sensitivity to the three different assumed SO$_2$ initial concentrations (SO$_{2(0)}$). Initial SO$_2$ varies within 0.05 - 5 ppmv. In set S1 set of simulations the initial HX concentration is fixed at 0.75 ppmv, the standard halogens concentration during C3.

In **Fig.:5.8**, the evolution of Δ^{17}O(S(VI)$_{dep}$) is reported for three SO$_2$ concentration scenarios.

For SO$_{2(0)}$ equal to 0.05 ppmv, deposited S(VI) carries an O-MIF of about 0.5 - 0.6 ‰ for most of the simulation, with a final Δ^{17}O(S(VI)$_{dep}$) value of 0.65 ‰. In contrast to C3, the ODE is very small in S1 and ozone does not fall below 1 ppbv, remaining mainly around 10-20 ppbv during most of the run. In simulation S1 SO$_2$ levels are 20 times lower than the ones in simulation C3, and as a result, the concentration of hydrogen species (HO$_2$, OH and H$_2$O$_2$) does not decline much. Substantial levels of HO$_2$ prevents the build-up of BrO concentration. Any BrO available reacts quickly with HO$_2$ to produce HOBr, which is responsible for 16% of S(IV) oxidation within the first 30 minutes. The relatively high levels of HO$_2$ favours the production of HOBr instead of BrONO$_2$. Since, per molecule HOBr is less effective than BrONO$_2$ at cycling bromine in the aqueous phase (see Table:5.3), little BrO production, hence ozone destruction, occur. Overall, S(IV) oxidation by H$_2$O$_2$ is the dominant S(IV) oxidation pathway, followed by the O$_2$/TMI oxidation channel.
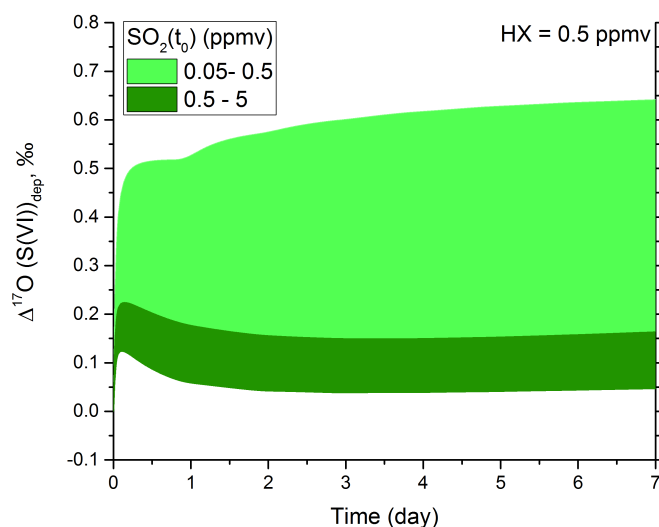
Figure 5.8: Temporal evolution of Δ^{17}O(S(VI)$_{dep}$) at different values of [SO$_2$]$_0$ in condensing plumes. Other initial critical parameters are set to: [Fe(III)] = 0.5 μM, LWC = 0.3 g m^{-3}, [HX]$_0$ = 0.5 ppmv.

For $SO_{2(0)}$ equal to 0.5 ppmv, an ODE appears within the first half an hour from plume injection. Deposited sulphate carries an O-MIF of about 0.16 ‰ throughout the simulation. Following plume injection, H_2O_2 is quickly depleted from the aqueous phase because of reaction with S(IV). H_2O_2 is not reformed because of hydrogen species depletion related to the ODE. During the first couple of hours following halogens and sulphur release, some of S(IV) is oxidised by H_2O_2, explaining the high $\Delta^{17}O(S(VI)_{prd})$ observed initially. Overall, like in previous simulations S(IV) oxidation by OH does not significantly contribute to S(VI) production, and by the time the first ODE occurs, O_2/TMI has become the main S(IV) oxidation channel.

For the last simulation ($SO_{2(0)}$ = 5 ppmv), an ODE is also formed within half an hour. Deposited sulphate carries an O-MIF of about 0.12 ‰ the first day, 0.05‰ by the third day, and it ends at 0.04 ‰. After plume injection, OH is very quickly depleted from the gas phase because of high SO_2 and HCl concentrations. H_2O_2 levels drop also very quickly because it is consumed by S(IV) oxidation, and its production is suppressed by the extremely low levels of HO_2 triggered by the ODE. Consequently, S(IV) oxidation by O_2/TMI becomes and remains the overwhelming S(IV) oxidation pathway, responsible for the very low O-MIF in sulphate.

The results from this set of sensitivity studies suggest that the only way to produce S(VI) with large O-MIF in condensing volcanic plumes is to start with low SO_2 levels compared to the halogens levels. SO_2 level is a key parameter because it controls HO_x and HOBr concentrations, hence halogens mobilization from the liquid phase. For low SO_2 concentrations, HO_2 react with BrO to generate HOBr, which reacts with S(IV) in the liquid phase, preventing the build-up of significant levels of BrO and hence ozone destruction. In contrast, when high SO_2 concentrations are within the plume, HO_x levels are depleted due to the consumption of H_2O_2 in the aqueous phase. In this case, halogens mobilization form the liquid phase is promoted via reaction 5.9, resulting in massive ODEs. In this scenario, O_2/TMI becomes the main S(IV) oxidation pathway, and the isotopic composition falls within the range of observed tropospheric volcanic sulphate O-MIF. Halogens to sulphur ratios seems critical for sulphur oxidation pathways and sulphate O-MIF.

Influence of LWC concentration

The second set of sensitivity studies (S2) is devoted to response of the system to changing LWC in condensing volcanic clouds. **Fig.:5.9** shows the evolution of $\Delta^{17}O(S(VI)_{dep})$ for three different LWC value (0.2 -0.5-1-2 $g\,m^{-3}$). Recall that for these simulations $SO_{2(0)}$ equals 1.5 ppmv, and HX initial concentration is fixed at 0.75 ppmv. In all four simulations an ODE is observed within half an hour from plume injection.

When LWC is set to 0.2 $g\,m^{-3}$, initially $\Delta^{17}O(S(VI)_{dep})$ reaches an O-MIF of about 0.25 ‰. Within a day from injection, O-MIF of deposited sulphate
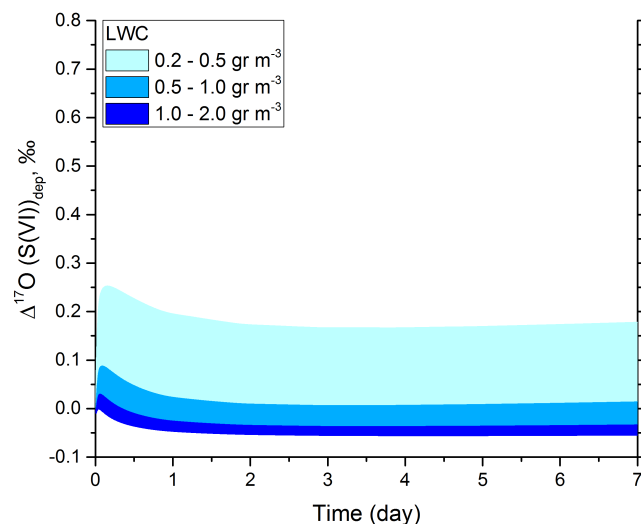
Figure 5.9: Temporal evolution of $\Delta^{17}O(S(VI)_{dep})$ at different values of liquid water content in condensing plumes. Other initial critical parameters are set to: [Fe(III)] = 0.5 μM, [SO$_2$]$_0$ = 1.5 ppmv, [HX]$_0$ = 0.75 ppmv.

declines to roughly 0.15‰, which is also the final $\Delta^{17}O(S(VI)_{dep})$ value. The initial positive O-MIF is linked to the major contribution of OH oxidation to S(VI) production during the first phase of the plume evolution. Smaller concentration and volume density of water droplets leads to lower pH in the aqueous phase. As a result, less SO$_2$ can dissolve in water droplets because of the pH dependency of the SO$_2$ effective Henry's law coefficient. The contribution of OH oxidation increases at the expense of aqueous oxidation. As the first ODE occurs, S(VI) production is driven by O$_2$/TMI, and to a smaller extent by OH as ozone and HO$_x$ levels recover slightly during daytime after few days.

When LWC is set to 0.5 g m^{-3}, $\Delta^{17}O(S(VI)_{dep})$ remains positive although below 0.1 ‰ throughout all the simulation. Within a day from injection, the deposited sulphate O-MIF is close to 0 ‰, and the final $\Delta^{17}O(S(VI)_{dep})$ is about 0.01 ‰. During this simulation, at least 90% of the sulphate is produced by the S(IV) oxidation by O$_2$/TMI. Because of its reaction with S(IV), H$_2$O$_2$ is immediately depleted, and the contribution of HOX oxidation is not significant, except during the first minutes after plume release.

At LWC equal to 1 g m^{-3}, $\Delta^{17}O(S(VI)_{dep})$ stabilizes quickly around 0 ‰ throughout the run. Overall, S(IV) reaction with O$_2$/TMI highly dominates S(VI) production and more sulphate is produced within the plume because of the higher rate of SO$_2$ dissolution. At LWC equal to 2 g m^{-3}, the final $\Delta^{17}O(S(VI)_{dep})$ is around -0.05 ‰. Under these conditions, S(IV) oxidation by O$_2$/TMI accounts

for 98% of total S(VI) production. H_2O_2 and OH contribute at significantly lower extents to sulphate production. Overall, HOX does not contribute to S(IV) oxidation in the aqueous phase.

Results from this set of sensitivity simulations suggest that LWC does not particularly affect S(IV) oxidation dynamics within the aqueous phase, where the O_2/TMI oxidation pathway dominates S(VI) production. Plume LWC has a small impact on initial competition between aqueous and gas phase pathways of oxidation during the first day. The LWC controls, indeed, the pH, hence the SO_2 dissolution rate and the associated H_2O_2 consumption via S(IV) oxidation. In all these simulations, sulphates have O-MIFs below 0.3 ‰ initially, and mostly within the 0.0±0.1 ‰ range by the end. These results suggest that as long as the LWC is greater than 0.3 $g\,m^{-3}$, the sulphate O-MIF falls within the range of observed tropospheric volcanic sulphate measurements. They confirm also that negative O-MIF signatures can only point out towards an overwhelmingly dominant O_2/TMI oxidation pathway.

Influence of TMI concentration

The last set of sensitivity studies (S3) covers the responses to TMI aqueous concentrations. Note that, throughout these simulations initial SO_2 and HX concentrations, and LWC are fixed to standard case values (simulation C3). In all these simulations, an ODE occurs after 30 minutes from plume release. **Fig.:5.10** presents the evolution of $\Delta^{17}O(S(VI)_{dep})$ for different TMI concentrations (0.1-0.5-1-2 μM).

For TMI equal to 0.1 μM, deposited sulphate reaches an O-MIF of about 0.32 ‰ within the first hours from injection. After a day it stabilizes around 0.28 ‰, then it rises slightly to 0.31 ‰ by the end of the run. Interestingly, during the first 12 hours of simulation, HOX contribution to S(IV) oxidation is significant; HOX oxidises more S(IV) than H_2O_2, which is quickly depleted due to its rapid reaction with S(IV). Overall, O_2/TMI contribution to sulphate production is high throughout the simulation, and by the end of the run 50% of S(VI) has been produced via this reaction pathway. The remaining S(VI) is mostly generated via H_2O_2 oxidation during daytime, and to a lower extent by HOX and OH.

For 0.5 μM of TMI, the O-MIF in deposited sulphate initially decreases towards 0.15 ‰. The O-MIF stabilizes, however, around 0.07 ‰ within a day from plume injection; the final $\Delta^{17}O(S(VI)_{dep})$ is 0.08 ‰. There is a small initial HOX contribution to S(VI) production, but from the second day the O_2/TMI reaction is largely the main S(VI) oxidant. Overall, the O_2/TMI represents 83% of the S(IV) oxidation by the end of the simulation.

For 1 μM of TMI, the O-MIF in deposited sulphates remains within 0.06 and 0.02 ‰ throughout the run. By the end of the simulation 90% of S(VI) has been produced by O_2/TMI, and the remaining 10% by even contributions of H_2O_2 and OH.

For 2 μM of TMI, the O-MIF in deposited sulphates remains within 0 and

-0.03 ‰ throughout the simulation. The final $\Delta^{17}O(S(VI)_{dep})$ is at -0.02 ‰. S(IV) oxidation is almost completely driven by O_2/TMI. OH, H_2O_2 and HOX oxidants contribute to only 6% of sulphate production.

In summary, results from these simulations indicate that when TMI concentration is higher than than 0.5 μM, O_2/TMI oxidation vastly dominates sulphur oxidation, resulting in deposited sulphate with an O-MIF mostly within 0 and 0.1 ‰, which is agreement with observed measurements. However, when TMI concentration drops below 0.5 μM, sulphate can have a significant positive anomaly well above $\pm$ 0.1 ‰. For instance, for 0.1 μM of TMI only half of the sulphate is produced via the O_2/TMI pathway. Within the range of TMI considered here, the concentration of TMI does not have any effect on the level of ozone destruction by halogens. Moreover, sulphur oxidation by HOX is very minor if not negligible. The results suggest that the negative O-MIF measured in volcanic sulphate from volcanic ash-deposits in some cases might be indicative of the dominance of the O_2/TMI oxidation pathway, and implicitly of significant iron dissolution in the aqueous phase. Nonetheless, more investigations are needed to assess in more details the role of iron dissolution from volcanic ash. Physico-chemical processing of suspended ash particles can vary, indeed, depending on multiple factors, such as ash mineral composition and aqueous phase evaporation and condensation cycles. In particular, transport to the upper troposphere, hence low temperatures, can promote major iron dissolution (Jeong et al., 2012; Langmann,
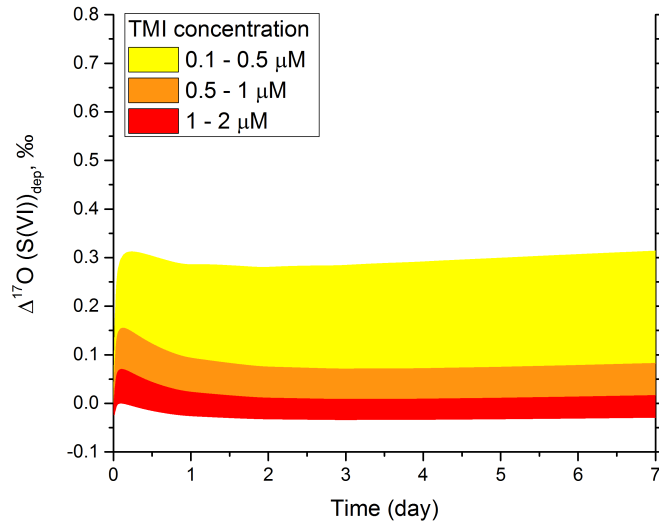
Figure 5.10: Temporal evolution of $\Delta^{17}O(S(VI)_{dep})$ at different values of TMI in the aqueous phase of condensing plumes. Other initial critical parameters are set to: LWC = 0.3 g m^{-3}, [SO$_2$]$_0$ = 1.5 ppmv, [HX]$_0$ = 0.75 ppmv.

2014). Eventually, sulphate isotopic composition found on ashes collected far from points of emission may also reflect particles processing within the upper troposphere.

5.2 Non-condensing volcanic plumes (sulphate aerosols)

Standard simulations

Simulations N1-N3 have the same chemical schemes and model inputs (e.g. initial concentrations) as those of simulations C1-C3, except that this time sulphuric acid aerosols the bulk of the liquid phase. Remember that for N1, N2 and N3 simulations, volcanic particles are composed by sulphate aerosols, and note that SO_2 heterogeneous reactions are now modelled via reactive uptake coefficients. The only difference between C1 and N1 is that the transfer of species between the gas phase and the liquid phase, and the aqueous equilibria are simulated in C1 (but without aqueous oxidation), whereas only gas-phase chemistry is accounted for in N1.

    Fig.:5.11 and **Fig.:5.12** show the time evolution of SO_2, O_3, H_2O_2, and S(VI) concentrations for N1, and N2 respectively. In simulation N1 no heterogeneous chemistry is accounted for and halogens are absent from the plume. Simulation N2 does include heterogeneous chemistry (see Table:5.5) but halogens are absent. In both simulations, SO_2 is depleted from 1.5 ppmv to 0.06 ppmv, deposited S(VI) and atmospheric S(VI) both reach roughly 0.06 ppmv, with S(VI) production exhibiting a diurnal cycle. By the end of the simulations, only 1 ppbv more of S(VI) is produced in N2 compared to N1, out of a total of about 120 and 130 ppbv of sulphate respectively. The heterogeneous SO_2 oxidation by O_3, H_2O_2, and O_2/TMI on sulphuric acid aerosols has a totally negligible contribution to sulphur oxidation in N2. The only noticeable effect is the small H_2O_2 depletion during the first 2 days of simulation N2 compared to N1. This result contrasts significantly with the difference between C1 and C2, where H_2O_2 drops to less than pptv in C2 because of its fast consumption during reaction with S(IV) in the aqueous phase. **Fig.:5.14** and **5.15** show the temporal evolution of the O-MIFs of atmospheric and deposited S(VI) for N1 and N2. As expected, there are no significant differences in $\Delta^{17}O(S(VI)_{prd})$ and $\Delta^{17}O(S(VI)_{dep})$ between N1 and N2. In both runs the sulphate produced initial carries a large O-MIF (peaking at $\approx 2.35‰$), which then declines to about 1.2 ‰ at the end of N1 and N2. However, as SO_2 concentration decays, $\Delta^{17}O(OH)$ decreases following the relationship in Eq.:5.60. Since in both the runs the main oxidant of SO_2 is OH, sulphates O-MIF decrease accordingly.

    In simulation N3, halogens are also injected together with the plume. The evolution of SO_2, O_3, H_2O_2, and S(VI) in N3 are shown in **Fig.:5.13**; SO_2 decreases from 1.5 to 0.09 ppmv during the N3 simulation. The most remarkable difference between N3 and the other standard simulations (C1, C2, C3, N1 and N2) is that very little sulphate is produced in N3 . Only 1.9 ppbv of sulphate
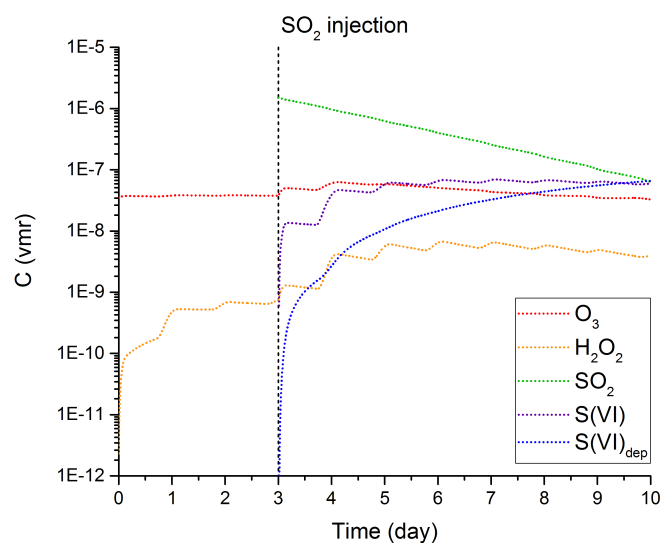
Figure 5.11: Temporal evolution of gas-phase concentrations of atmospheric species in presence of primary sulphate aerosols during the N1 simulation (non-condensing plume, see text). The simulation starts at 0:00 p.m., and SO_2 is injected after 3 days.
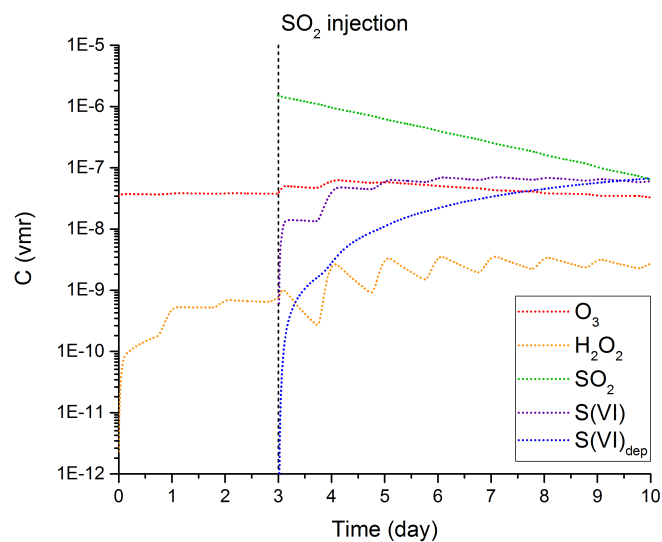
Figure 5.12: Gas-phase concentrations of atmospheric species in presence of primary sulphate aerosols during the N2 simulation (non-condensing plume, see text); no halogens are released within the plume after 3 days.
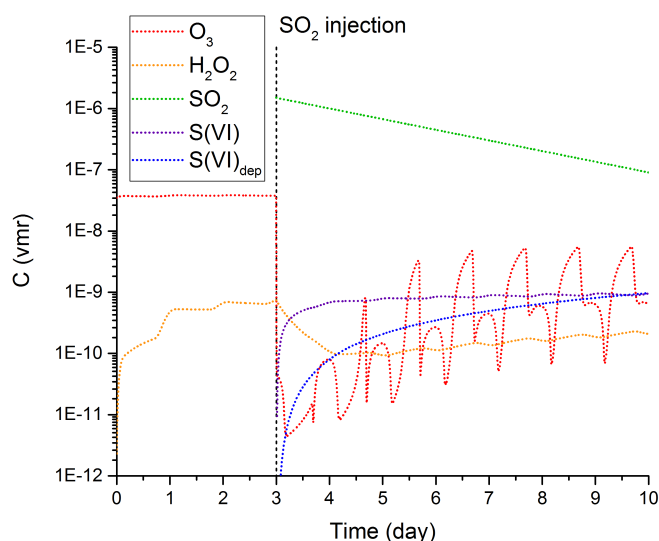
Figure 5.13: Gas-phase concentrations of atmospheric species in presence of primary sulphate aerosols during the N3 simulation (non-condensing plume, see text). Halogens are released within the plume, after 3 days from the start of the run.

(composed by 0.95 ppbv of both deposited and atmospheric sulphate) are produced compared to at least 120 ppbv of other standard simulations. Also, in contrast to other runs, in N3 about half of the sulphate is produced within the first hour. In the N_n standard simulations, the oxidation of SO_2 by heterogeneous pathways is very slow. Initially, the only significant oxidation pathway is the oxidation by OH in the gas phase. The first ODE develops after ≈ 15 min. in N3. It is triggered by the efficient bromine cycling on sulphuric aerosols and the associated ozone destruction. Ozone levels drop to roughly 0.01 ppbv after half an hour, shutting down the production of HO_x, notably OH, and hence sulphur oxidation by OH in N3. Before the O_3 levels drop too much, some SO_2 oxidation by OH occurs, ant it is responsible for half of the sulphate produced in N3. O_3 level recovers a bit after 2 days, reaching $\approx$ 4-5 ppbv during daytime. After a couple of days, O_3 has recovered sufficiently to generate significant OH and restart sulphur oxidation by OH. During the first day, H_2O_2 decreases slowly to 0.1 ppbv, and it is not reformed at appreciable concentrations throughout the N3 run. As a result of O_3 destruction, the photochemical production of H_2O_2 becomes negligible. The only source of H_2O_2 is mixing with the background air. This mixing flux is sufficient to maintain reasonable levels of H_2O_2 (≈ 0.2 ppbv), that are much higher than the ones in C2 and C3 simulations, where the very fast SO_2 oxidation in water droplets consume immediately H_2O_2. This very slow oxidation of SO_2 by H_2O_2 on sulphuric acid aerosols is responsible

146

of about half of the very small amounts of sulphate produced during N3. The low HO_2 concentration inhibits HOX production in the gas phase, resulting in very low HOX concentration throughout N3. BrO/SO_2 ratios reach values of about 6×10^{-4} within 5-10 minutes from plume release, in good agreement with BrO/SO_2 observations in volcanic plumes from passive degassing (Bobrowski et al., 2003; Oppenheimer et al., 2006; Bobrowski and Platt, 2007; Bobrowski et al., 2007).

Fig.:5.14 and **5.15** show the evolution of O-MIF in atmospheric and deposited sulphate in N3 along with those of simulations N1 and N2. Atmospheric sulphate produced initially in N3 carries an O-MIF of about 1.5 ‰. The initial O-MIF is slightly lower in N3 than in N1 and N2 drops because of the very reduced OH level in N3 and a much higher fraction of S(IV) oxidised by H_2O_2.

The isotopic O-MIF transferred to sulphate by H_2O_2 is, indeed, lower than the one by OH in volcanic sulphur rich plumes (Galeazzo et al., 2018); $\Delta^{17}O(OH)$ varies from 11.2 ‰ at the start of the run to 1.7‰ at the end of N3. After a couple of days, the light ozone recovery is sufficient for OH to be again the dominant oxidation pathway in N3. However, by that time, SO_2 level has declined, and hence, the $\Delta^{17}O(OH)$ decreases, producing sulphate with a lower O-MIF than in the first hours. By the end of the simulation, atmospheric sulphate carries an O-MIF of 0.97‰. The final O-MIF on deposited sulphate is ≈ 1.1‰. at the end of the simulation, 59% of S(VI) is produced via SO_2 oxidation by H_2O_2 on aerosols, and the remaining 41% is generated via oxidation by OH in the gas phase.

Results from these simulations indicate that H_2O_2 and OH are major SO_2 oxidants in non-condensing volcanic plumes. Contrary to water droplets simulations, the oxidation of SO_2 on sulphuric acid is very slow. Consequently, unlike for water droplets, H_2O_2 is not quickly consumed by heterogeneous chemistry, because of the low H_2O_2 and SO_2 solubilities in highly concentrated sulphuric acid solutions. During daytime, halogens cause ODEs because of fast bromine activation on sulphate aerosols. However, because of HO_x suppression from ODE and consumption by fast halogens heterogeneous reactions, HOX cannot accumulate in appreciable concentrations in the gas phase, and it does not contribute significantly to S(VI) production. Overall O-MIF of atmospheric sulphate is relatively high and close to 1‰, suggesting that sulphates formed in volcanic plumes during passive degassing should have an O-MIF very close to values measured for anthropogenic sulphates (Lee et al., 2001; Lee and Thiemens, 2001). In the same way as for condensing plumes, sensitivity studies are conducted in order to assess the variability of results to key input parameters and explore the ability of the model to reproduce measured O-MIF in sulphate.

Influence of initial SO$_2$ concentration

The first set of sensitivity studies (Z1) is about the sensitivity to initial SO_2 concentrations $[SO_2]_0$, and in particular, the effect on $\Delta^{17}O(OH)$ and sulphate
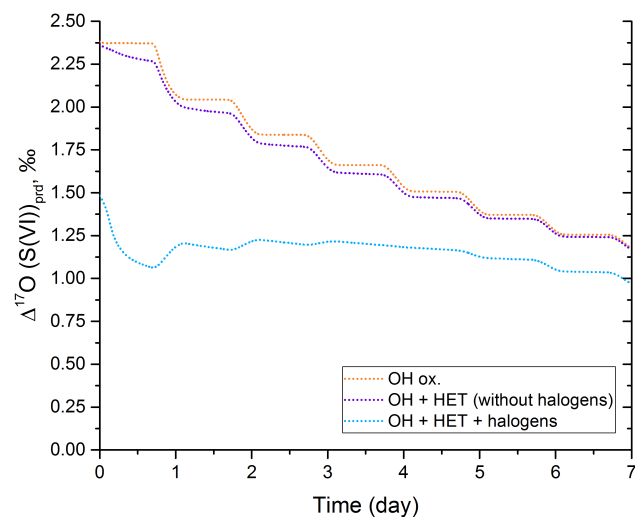
Figure 5.14: Time evolution of $\Delta^{17}O(S(VI))$ in produced sulphates during non-condensing volcanic plumes simulations N1 (only OH ox.), N2 (OH + HET, without halogens) and N3 (OH + HET + halogens).
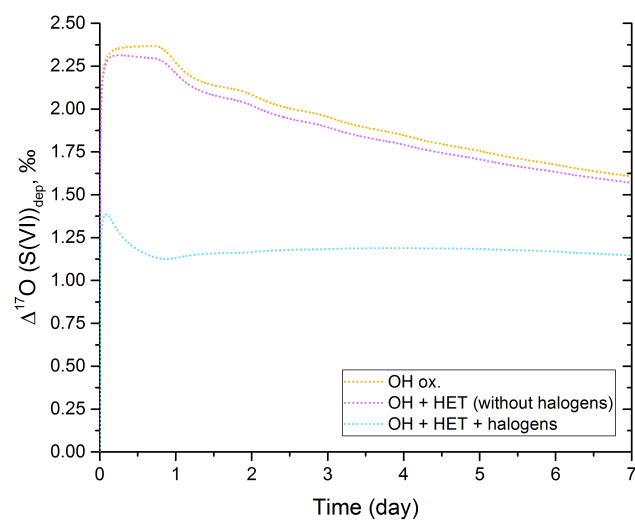
Figure 5.15: Time evolution of $\Delta^{17}O(S(VI))$ in deposited sulphates during NON-condensing volcanic plumes simulations N1 (only OH ox.), N2 (OH + HET, without halogens) and N3 (OH + HET + halogens).

O-MIF. The initial halogen concentration ($[HX]_0$) is fixed at 0.5 ppmv, the standard simulation value (N3), only $[SO_2]_0$ is changed.

First of all, whatever the initial SO_2 concentration (0.05, 0.5, 5 ppmv), the ODE forms within an hour from plume injection. Therefore, the initial SO_2 loading does not appear to influence significantly the formation of ODE, obviously as long as sufficient primary sulphate aerosols are present in the volcanic plume for bromine activation. **Fig.:5.16** shows the evolution of $\Delta^{17}O(S(VI)_{dep})$ for the three different initial SO_2 concentrations.

For the low SO_2 loading case ($[SO_2]_0 = 0.05$ ppmv), deposited sulphate initially carries an O-MIF of about 1.1 ‰. During this initial phase (the first half an hour when the ODE starts forming), OH is not yet completely depleted by the ODE and both OH and H_2O_2 contributes to SO_2 oxidation. The initial sulphate O-MIF reflects both contributions with an O-MIF of 0.87 ‰ for sulphate generated by H_2O_2 oxidation and an O-MIF of about 2 ‰ for sulphate generated by OH oxidation. After this initial phase, sulphate O-MIF decreases from its 1.1 ‰ peak to about 1 ‰ during the first day. The ODE is fully developed after an hour and causes the OH concentration to drop drastically since O_3 is the source of OH. As a result, H_2O_2 becomes the dominant oxidant after an hour. H_2O_2 generates sulphate with an O-MIF which is much lower than the O-MIF generated by OH oxidation. With the addition of the low O-MIF sulphate generated by H_2O_2 oxidation, the deposited sulphate O-MIF decreases during the first day. However, at the same time, the H_2O_2 concentration also decrease
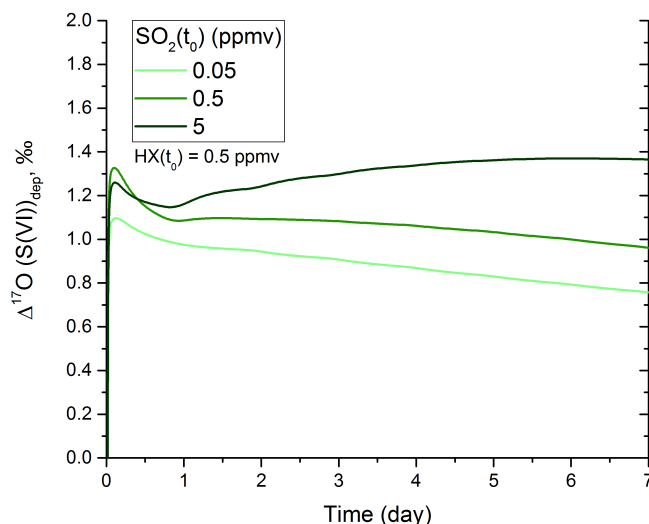
Figure 5.16: Temporal evolution of $\Delta^{17}O(S(VI)_{dep})$ at different values of $[SO_2]_0$ in non-condensing plumes.

gradually because H_2O_2 is slowly consumed when it oxidizes SO_2 on sulphate aerosols. The H_2O_2 concentration declines to 0.3 ppbv by the third day. This decrease in H_2O_2 concentration is much weaker than in the corresponding standard simulation (N3) where H_2O_2 drops quickly to pptv level; since the initial SO_2 loading in N3 is 20 times higher than in this first Z1 simulation, the consumption of H_2O_2 by its heterogeneous reaction with SO_2 is much faster in N3 than in the first Z1 simulation. After the first day, the ODE weakens with the decrease in the halogen concentration from the plume dilution mixing and the influx of O_3 from the surrounding background atmosphere. As O_3 starts to recover, the OH concentration starts also to recover, resulting in increasing amounts of SO_2 being oxidised by OH. After the first day, OH becomes the dominant oxidant. The deposited sulphate O-MIF carries on decreasing during the rest of the simulation, to a final value of 0.75 ‰. This value is well below the characteristic O-MIF (0.87 ‰) for sulphate generated by H_2O_2 oxidation. This is consistent with the dominance of the OH oxidation and the fact that its isotopic signature is lower the isotopic signature of H_2O_2 oxidation when the SO_2 concentration is very low. During that period, the O-MIF ($\Delta^{17}O(OH)$) decreases during the entire simulation from an initial peak value, exceeding 5 ‰, to about 2 ‰ after a day, producing a sulphate with an O-MIF of 0.5 ‰ ($\Delta^{17}O(S(VI))_{OH+SO_2} = 1/4 \cdot \Delta^{17}O(OH)$, see Eq.:5.61). This decline in $\Delta^{17}O(OH)$ is related to the decrease in SO_2 and HX concentrations from the plume dilution. Note that the initial SO_2 concentration is already very low (0.05 ppmv) in this first Z1 simulation. The lower the SO_2 and HX concentrations are, the lower the $\Delta^{17}O(OH)$ is (see Eq.:5.56-5.58). After the first day, the sulphate added to the pre-existing deposited sulphate carries a decreasing O-MIF and consequently $\Delta^{17}O(S(VI)_{dep})$ decreases steadily. Overall, by the end of the simulation, 31% of S(VI) is formed via H_2O_2 oxidation and the remaining 69% is formed via OH oxidation.

For $[SO_2]_0$ = 0.5 ppmv, the initial sulphate carries a peak O-MIF of about 1.3‰. As in the previous Z1 simulation ($[SO_2]_0$ = 0.5 ppmv), OH is the main SO_2 oxidant during the first hour and hence determines the sulphate O-MIF. The initial $\Delta^{17}O(S(VI)_{dep})$ is higher than the initial value in the previous simulation because the SO_2 concentration is an order of magnitude larger and therefore $\Delta^{17}O(OH)$ is higher. After this initial phase, sulphate O-MIF decreases sharply to 1.1 ‰ during the first day. The H_2O_2 concentration is low during this period because of the ODE and the relatively high SO_2 concentration. H_2O_2 oxidation becomes dominant during the first day and adds sulphate with a low O-MIF (0.87 ‰) to the deposited sulphate, causing the sharp decrease in $\Delta^{17}O(S(VI)_{dep})$. After this drop, sulphate O-MIF carries on declining but much more slowly, towards a final value of 0.95 ‰. This corresponds to a phase where OH oxidation dominates again. Again, the pendulum swings away from H_2O_2 oxidation and towards OH oxidation because the H_2O_2 concentration decreases strongly due its consumption by reaction with SO_2, and OH concentration increases due to ozone recovering slowly after the first ODE. The sulphate generated has a

higher O-MIF than in the first Z1 simulation because the SO_2 concentration is much higher and hence so is $\Delta^{17}O(OH)$. By the end of the run 49% of S(VI) is formed by H_2O_2 and the remaining 51% is formed by SO_2 reaction with OH.

For $[SO_2]_0$ = 5 ppmv, deposited sulphate carries an initial O-MIF of 1.25 ‰ which is lower than the initial value for the $[SO_2]_0$ = 0.5 ppmv case. Although the initial OH O-MIF is the highest in this case ($\Delta^{17}O(OH)$=XX), the SO_2 concentration is so high that the reaction between OH and SO_2 becomes the main OH loss, depleting very severely OH (Bekki, 1995). Under those conditions, in contrast to the previous Z1 simulations, H_2O_2 contributes very substantially to SO_2 oxidation even during the initial phase, generating some sulphate with low O-MIF compared to sulphate generated by OH oxidation. This explains the lower peak in sulphate O-MIF compared to the case of $[SO_2]_0$ = 0.5 ppmv. After this initial peak, the isotopic anomaly in deposited sulphate decreases to about 1.15 ‰ during the first day reflecting the increasing contribution of H_2O_2 to SO_2 oxidation. Indeed, after 1 hour, the OH concentration drops dramatically under the combined effect of the ODE and the high SO_2 concentration. associated with the ODE. After the first day, contrary to the first two Z1 simulations, $\Delta^{17}O(S(VI)_{dep})$ increases steadily till the end of the simulation, reaching a final value of about 1.4 ‰ after 7 days. This increase has several origins. First, H_2O_2 concentration decreases much more than in the previous Z1 simulations, to about 0.05 ppbv by the second day, enhancing mechanically the OH contribution to SO_2 oxidation. Second, as in the previous simulations, ozone recovers gently after a day, enhancing the OH concentration and its contribution to SO_2 oxidation. Third, and more importantly, the $\Delta^{17}O(OH)$ is much higher than in the first Z1 simulations because of the extremely high SO_2 concentration. For instance, the initial OH O-MIF is 14.5 ‰ for $[SO_2]_0$ = 5 ppmv whereas it is 7.6 and 5.1 ‰ for $[SO_2]_0$ = 0.5 and 0.05 ppmv respectively. Therefore, the sulphate generated by OH oxidation carries a much higher O-MIF, resulting in a steady increase in $\Delta^{17}O(S(VI)_{dep})$ during the simulation instead of a decrease in the first two Z1 simulations. By the end of the run 56% of S(VI) is formed via H_2O_2 oxidation and the remaining 44% is formed via OH oxidation.

The results from this set of sensitivity studies suggest that the volcanic sulphate O-MIF is affected by the value of the initial SO_2 loading in the volcanic plume. When the sulphur loading increases, the relative contribution of H_2O_2 to sulphur oxidation declines at the expense of OH oxidation contribution. At the same time, the O-MIF of the sulphate generated by OH oxidation increases strongly with increasing sulphur loading. As a result, the final O-MIF of deposited sulphate increases with increasing sulphur loading. Overall, the SO_2 loading does not have a major impact on the sulphate O-MIF since the final deposited sulphate O-MIF varies between about 0.8 and 1.4 ‰ for a 2 orders of magnitude change in the initial SO_2 loading. This range of sulphate O-MIF values is not at all consistent with most O-MIF measurements in sulphate collected on volcanic ash.

Influence of initial halogens concentration

The second set of sensitivity studies (Z2) is about the sensitivity to the initial halogen loading. The purpose is to investigate the effect of varying the initial halogens concentration ($[HX]_0$) on $\Delta^{17}O(OH)$ and sulphate O-MIF, in particular in relation to the formation of ODE which is catalysed by halogen radicals. In all the Z2 simulations, $[SO_2]_0$ is fixed at 1 ppmv, the value corresponding to the standard simulation (N3). $[HX]_0$ is changed progressively from 0 to 0.8 ppmv, giving an initial halogen-to-sulphur $[HX]_0/[SO_2]_0$ varying from 0 to 0.8.

Fig.:5.17 shows the evolution of $\Delta^{17}O(S(VI)_{dep})$ for 6 different initial $[HX]_0$ (0, 0.05, 0.1, 0.2, 0.4, 0.8 ppmv). The simulation with no halogens ($[HX]_0=0$) corresponds to the Z2 simulation. Deposited sulphate O-MIF peaks initially at about 1.9 ‰ and then declines continuously to 1.24 ‰ at the end of the run. As expected, in the absence of halogens, there is no ODE. Without ozone depletion, OH is the dominant oxidant and the sulphate O-MIF produced at a given time reflects the OH O-MIF, modulo a factor 4 (see Eq.:5.61). Since the SO_2 concentration decays with time, the OH O-MIF decreases. Therefore, sulphate with decreasing O-MIF is continuously added to the deposited sulphate, resulting in a decline in deposited sulphate O-MIF.

For $[HX]_0$ = 0.05 ppmv, an ODE develops within 2-3 hours from halogens injection. Even a halogen loading as low as 50 pbbv is sufficient to generate an ODE initially. Nonetheless, the rate of the ODE formation, the extent of the ozone depletion and its persistence are stronger at higher halogen loadings.
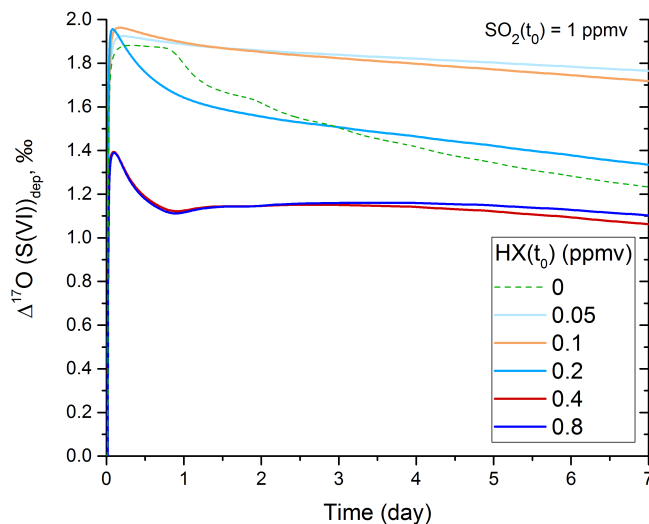
Figure 5.17: Temporal evolution of $\Delta^{17}O(S(VI)_{dep})$ at different values of $[HX]_0$ in non-condensing plumes.

Deposited sulphate initially carries an O-MIF of about 1.95 ‰, which is close to the initial value found in the no-halogen simulation (1.9 ‰). Since OH is the dominant oxidant during the initial phase, this indicates that a 50 ppbv halogen loading is not sufficient to affect significantly the OH O-MIF in the presence of a high SO_2 concentration (see **Fig.:5.2**). By the time the ODE is fully developed (after the initial phase of 3 hours), the OH concentration drops and H_2O_2 oxidation becomes dominant during the first day. This oxidation pathway generates sulphate with an O-MIF (0.87‰) which is lower than the O-MIF in sulphate generated by OH oxidation initially. However, the amount of sulphate produced by H_2O_2 oxidation is very low compared to the sulphate produced during the initial phase (i.e. before the formation of the first full ODE). As a result, the addition of this sulphate carrying a lower O-MIF during this period affects weakly the O-MIF of the deposited sulphate which was produced during the initial phase. Deposited sulphate O-MIF decreases only very slightly during the first day. By the beginning of the second day, O_3 and hence OH concentrations start to recover strongly, making the OH oxidation dominant again. By that time, however, $\Delta^{17}O(OH)$ has decreased from its early peak value, generating sulphate with an O-MIF of about 0.6 ‰ (see Eq.:5.56-5.58). This decline in $\Delta^{17}O(OH)$ is related to decreasing SO_2 and HX concentrations (i.e. 0.2 and 0.01 ppmv respectively), mostly driven by the plume dilution. The effect of declining $\Delta^{17}O(OH)$ on deposited sulphate O-MIF is moderate. Indeed, the rate of sulphate production drops continuously because the SO_2 concentration keeps decreasing. As a result, the amount of sulphate produced with a low O-MIF during the second half of the simulation is much smaller than the amount of sulphate produced with a high O-MIF during the first half. In fine, the large O-MIF of the sulphate produced and deposited during the first few days is not strongly diluted by the sulphate produced afterwards as shown by the slow decline in $\Delta^{17}O(S(VI)_{dep})$. The final O-MIF is about 1.75 ‰. By the end of the run, 13% of the sulphate is produced by H_2O_2 oxidation and the remaining 87% by OH.

The evolution of $\Delta^{17}O(S(VI)_{dep})$ in the $[HX]_0 = 0.1$ ppmv simulation is similar to the one in the first Z2 simulation ($[HX]_0 = 0.05$ ppmv). The first ODE occurs a bit more quickly, within about an hour from plume injection. This causes a drop in the OH concentration and H_2O_2 becoming the main oxidant. While H_2O_2 oxidizes SO_2, it is consumed and its concentration decreases. After 2 days OH becomes again the main oxidant. As in the first Z2 simulation, a large amount of sulphate is produced by OH oxidation before the formation of the first ODE. However, the ODE develops faster than in the first simulation, resulting in a lower amount of sulphate produced during the initial phase (dominated by OH oxidation). Therefore, the sulphate produced with lower O-MIF after the initial phase impacts a bit more the deposited sulphate O-MIF. As a result, the decline in deposited sulphate O-MIF is a bit steeper with a final value of 1.72 ‰ instead of almost 1.77 ‰ in the first simulation. Overall, 19% of S(VI) is formed by SO_2 oxidation via H_2O_2, and the remaining 81% by SO_2 oxidation via OH.

For $[HX]_0 = 0.2$ ppmv, deposited sulphate initially carries a high O-MIF of

about 1.95 ‰, similar to the previous Z2 simulations. The first ODE occurs faster, within half an hour from plume injection. After half an hour, following the drop in O_3 and OH concentrations, H_2O_2 becomes the main oxidant for about 2 days. This period of dominance of the H_2O_2 oxidation is longer than in the first Z2 simulations because the ozone depletion lasts longer at higher halogen loading. The decline in deposited sulphate O-MIF following the formation of the first ODE is much steeper than in the previous Z2 simulations because less sulphate with high O-MIF is produced via OH oxidation during the initial phase lasting only half an hour. Therefore, the sulphate produced with lower O-MIF after this initial phase impacts more strongly the deposited sulphate O-MIF as indicated by the steeper decline in deposited sulphate O-MIF during the first 2 days. Thereafter, with a weakening of the ODE and the decrease in H_2O_2 concentration from its consumption by its SO_2 oxidation, OH is produced again in significant amounts and becomes the main oxidant. During the last phase, the OH O-MIF is low (i.e. $\Delta^{17}O(OH) \approx 0.7‰$) because of the dilution-driven decline in SO_2 and HCl concentrations. However, less sulphate is produced in this phase than the first 2 days of the simulation. Therefore, the decrease in deposited sulphate O-MIF is relatively limited with final O-MIF of about 1.33 ‰. Overall, 42% of S(VI) is formed by SO_2 oxidation via H_2O_2 and the remaining 58% is formed by SO_2 oxidation via OH.

The evolutions of $\Delta^{17}O(S(VI)_{dep})$ in the $[HX]_0 = 0.4$ ppmv and $[HX]_0 = 0.8$ ppmv simulations are very similar. The initial peak in deposited sulphate O-MIF ($\Delta^{17}O(S(VI)_{dep}) = 1.4$ ‰) is distinctly lower than in the low halogen Z2 simulations. The first ODE forms within the first 20 minutes for the $[HX]_0 = 0.4$ ppmv simulation and within the first 15 minutes for the $[HX]_0 = 0.8$ ppmv simulation. Although the initial OH O-MIF is a bit higher than in the low halogen Z2 simulations, the ozone destruction is so fast that the H_2O_2 oxidation is still very significant compared to OH oxidation during the initial phase in the high halogen Z2 simulations, resulting in a lower peak value in sulphate O-MIF. The OH O-MIF in the $[HX]_0 = 0.8$ ppmv simulation is slightly higher than in the $[HX]_0 = 0.4$ ppmv simulation. However, with respect to the impact on deposited sulphate O-MIF, it is compensated by a faster and stronger ozone destruction in the $[HX]_0 = 0.8$ ppmv simulation and hence a lower contribution of OH to sulphate production in the $[HX]_0 = 0.8$ ppmv simulation. When they are compared to the low halogen Z2 simulations, the amounts of sulphate produced during the initial phase are small, making $\Delta^{17}O(S(VI)_{dep})$ more sensitive to the subsequent decline in the O-MIF of produced sulphate. In both simulations, H_2O_2 becomes quickly the overwhelmingly dominant oxidant and $\Delta^{17}O(S(VI)_{dep})$ decreases quite sharply to 1.1‰ after a day. By that time, in the $[HX]_0 = 0.4$ ppmv simulation, a bit less than half of deposited sulphate has been produced by H_2O_2 oxidation, while the remaining amount has been produced by OH oxidation. In the $[HX]_0 = 0.8$ ppmv simulation, slightly more than half of the sulphate has been produced by H_2O_2 oxidation. After 2-3 days, the ODE weakens and, as the OH concentrations increases, the OHoxidation dominates again. However, the

sulphate then produced carries a low O-MIF, because OH O-MIF has dropped with the dilution-driven decreases in SO_2 and HCl concentrations. As a result, the O-MIF on deposited sulphate is not significantly affected by the newly sulphate after a couple of days, resulting in a final O-MIF value of about 1.1‰. Overall, in the $[HX]_0 = 0.4$ ppmv simulation, 51% of S(VI) is formed by H_2O_2 oxidation and the remaining 49% by OH oxidation. In the case of the $[HX]_0 = 0.8$ ppmv simulation, 56% of S(VI) is formed by H_2O_2 oxidation and the remaining 44% is formed by OH oxidation.

The results from this set of sensitivity simulations for non-condensing volcanic plumes suggest that even relatively small halogen loadings induce ODEs. Obviously, the speed of formation, amplitude and duration of the OH drop depend on the initial halogen loading. The ODE is fully developed within 2-3 hr after the injection for the lowest halogen loading considered here (0.05 ppmv) and within 15-20 mn for the highest halogen loading (0.4-0.8 ppmv). The ODE generates a drastic drop in the OH concentration. As a result, the contribution of OH oxidation also drops and the H_2O_2 contribution becomes dominant. After 1 to 3 days after the volcanic injection, the OH oxidation becomes again dominant because the ODE has weakened and H_2O_2 concentration has dropped. The net effect of increasing the halogen loading is to increase the relative contribution of H_2O_2 to sulphur oxidation because the extent and duration of the drop in OH oxidation depends the magnitude and duration of the ODE. The higher the halogen loading is, the stronger is the ODE. The sulphate O-MIF is also affected by the initial halogen loading. The O-MIF of the sulphate generated by OH oxidation increases with increasing halogen loading via the effect of HCl concentration on OH O-MIF. However, the net effect of the halogen loading on sulphate O-MIF is dominated by its influence on the relative contributions of OH and H_2O_2 to sulphur oxidation. When the halogen loading increases, the relative contribution of H_2O_2 to sulphur oxidation increases. As for the Z1 sensitivity simulations (varying the initial sulphur loading), the halogen loading does not have a major impact on the sulphate O-MIF since the final deposited sulphate O-MIF varies between about 1.0 and 1.4 ‰ for a change in halogen loading going from no halogen to a halogen-to-sulphur ratio close to 1. This range of sulphate O-MIF values is not at all consistent with most O-MIF measurements in tropospheric volcanic sulphate extracted from volcanic ash.

6   Summary and concluding remarks

We use the tropospheric photochemical box-model CiTTyCAT to simulate the oxidation of sulphur within the core of tropospheric volcanic plumes in the presence of halogens and the resulting oxygen isotopic compositions in the produced and deposited sulphate. So far, most isotopic measurements indicate that tropospheric sulphates collected from volcanic ash-deposits do not carry significant O-MIFs (i.e. oxygen mass-independent sulphate) (Bao et al., 2003;

Martin et al., 2014). Volcanic plumes are peculiar chemical environments, radically different from background air. It is mostly a mix of volcanic water, sulphur and halogens species. Almost the entire sulphur is emitted in the form of SO_2 with a very small fraction of it, typically less than 1%, in the form of primary sulphate particles. This work is a follow-on of a modelling study on sulphur oxidation in a volcanic plume and the resulting secondary sulphate isotopic composition (Galeazzo et al., 2018). Halogens and heterogeneous chemistry on primary sulphate aerosols had been neglected. The present study aims to extend the previous investigation on volcanic SO_2 oxidation and to cover the missing processes (Galeazzo et al., 2018). The focus is on the role of halogens in plume chemistry and the implications for the isotopic composition of volcanic secondary sulphate. A heterogeneous chemistry scheme for halogens has been implemented in the model. In addition, a new heterogeneous chemistry scheme has been added to account also for SO_2 oxidation on sulphate aerosols. We consider two typical situations: a condensing plume (i.e. water droplets) and non-condensing plume (i.e. sulphate aerosols). Interestingly, very different results and conclusions are drawn for these two situations.

With regard to condensing plumes, the first finding is that ozone depletion events (ODE) catalysed by halogens might occur in presence of water droplets. The ODE is initiated by emitted bromine and chlorine radicals, and then developed through heterogeneous chemistry mobilizing halogens from water droplets. The second salient finding is that, in presence of halogens, SO_2 oxidation by both H_2O_2 in water droplets and OH in the gas-phase are negligible. Within a condensing plume, H_2O_2 is immediately consumed by its oxidation of sulphur (reaction between SO_2 and S(IV) in the aqueous phase), while the gas-phase OH concentration is severely depressed by the ozone destruction. At the same time, O_3 is also a negligible oxidant, because the ozone concentration is very low and, more importantly, the aqueous phase is much too acidic. In addition, HOCl and HOBr do not contribute significantly to the sulphur oxidation because their concentrations are very low under the effect of the fast heterogeneous halogens reactions converting them into radicals. Consequently, according to the model calculations, in volcanic plumes with water liquid phases SO_2 oxidation is dominated by S(IV) aqueous reaction with O_2/TMI, even for relatively low TMI aqueous concentrations. As the plume mixes with the background air and becomes more diluted halogens radical cycling weakens and, the O_3, OH and H_2O_2 concentrations increase substantially. Nonetheless, the O_2/TMI oxidation remains the dominant oxidation pathway. Even without halogens, this sulphate production pathway can be dominant for TMI concentrations typical of atmospheric cloud droplets (Galeazzo et al., 2018). As a result of the domination of O_2/TMI oxidation, volcanic sulphate carries a low mass-independent isotopic anomaly in oxygen (O-MIF). In some cases, the sulphate O-MIF is equal to 0 ‰ (mass-dependent sulphate). It is consistent with most isotopic measurements on sulphate collected on volcanic ash, which indicate mass-dependent sulphate within the typical measurement error (0.1 ‰). The model calculates

sulphate O-MIF below 0.1 ‰ only if the concentration of TMI is significant. Model calculations would be much better constrained, if more measurements of TMI concentrations in volcanic water phases to be performed.

With regard to non-condensing plumes (i.e. only sulphate aerosols), even for relatively low halogen loadings (about 50 ppbv), an ODE occurs. Obviously, the speed of formation, amplitude and duration of the ODE depend on the initial halogen loading. The ozone depletion leads to a drastic drop in the OH concentration. The first finding is that the rate of SO_2 oxidation and hence of the amount of sulphate produced is much lower in non-condensing plume simulations than in condensing plumes simulations. Overall, the sulphate production is found to be inversely correlated to halogen emissions via the dependence of the ODE magnitude and duration on the amount of halogen emitted. Both the O_2/TMI and HOX oxidation on sulphate aerosols are totally negligible. The sulphur oxidation is dominated by H_2O_2 oxidation on sulphate aerosols and OH oxidation in the gas-phase. The H_2O_2 oxidation is very significant because, contrary to a condensing plume simulation, the H_2O_2 concentration does not drop instantaneously in a non-condensing plume simulation. H_2O_2 is consumed very slowly by its reaction with SO_2 on sulphate aerosols because of the low solubility of H_2O_2 in concentrated sulphuric acid solutions. At the same time, gas-phase SO_2 oxidation is severely reduced after the formation of the ODE (within 15 min. to 2-3 hr. depending on the halogen loading) because of the drop in OH concentration generated by the ozone depletion. The relative contributions of OH and H_2O_2 to the total sulphur oxidation vary with the initial sulphur and halogen loadings. When the sulphur loading is decreased or when the halogen loading is increased, the relative contribution of H_2O_2 to sulphur oxidation increases at the expense of the OH oxidation contribution. Typically, at low halogen loadings, the contribution of OH oxidation is higher than the H_2O_2 contribution and, at high loadings, it is the reverse.

The O-MIF carried by the generated sulphate depends on the respective contributions of OH and H_2O_2 to sulphur oxidation. Sulphur oxidation by H_2O_2 generate sulphate with a positive Δ^{17} O (0.87 ‰). The Δ^{17} O in sulphate generated by OH oxidation is a quarter of the O-MIF in OH. OH MIF is found to vary strongly with the sulphur and halogen loadings in the volcanic plume. It was already shown that OH Δ^{17} O was expected to be large in the presence of high SO_2 concentrations (Galeazzo et al., 2018). The present model calculations indicate that OH MIF is further enhanced when the HCl concentration increases. Therefore, sulphur oxidation by OH generates sulphate with a higher O-MIF when the halogen loading is high. However, the net effect of the halogen loading on sulphate Δ^{17} O is dominated by its influence on the relative contributions of OH and H_2O_2 to sulphur oxidation. When the sulphur loading increases, the relative contribution of H_2O_2 to sulphur oxidation increases and hence the overall sulphate Δ^{17} O decreases. Overall, in the non-condensing plumes simulations (including the sensitivity), the final deposited sulphate O-MIF is high, varying between about 0.8 and 1.4 ‰. It is at all not consistent with

157

most isotopic measurement on sulphate collected on volcanic ash. Recall that the heterogeneous oxidation of SO_2 by H_2O_2 on sulphate particles is highly uncertain. Without this pathway of sulphur oxidation model calculated O-MIF would be considerably higher. Even for extremely high reactive uptake coefficients, model calculated O-MIF tends towards 0.87‰. Therefore, the uncertainties on the SO_2 oxidation by H_2O_2 on sulphate aerosols does not affect the main conclusion regarding the inability of the model to reproduce, or even approach, the isotopic measurements of sulphates collected on volcanic ash-deposits. In conclusion, these results suggest that sulphate collected in volcanic ash-deposits is not produced in non-condensing plumes, and it is possibly generated in condensing plumes or in water phase at the surface of ash.

There are several ways of testing these model predictions. First of all, the prediction of a high $\Delta^{17}O$ in volcanic sulphate produced by OH oxidation should be first tested. In principle, laboratory chamber experiments should be able to do it, notably in a controlled setting (i.e. humidity, ozone, SO_2 or halogen loadings) where OH chemical sources and losses are well constrained; obviously, only the isotopic composition of sulphate aerosols created in the heart of the chamber and not on the walls should have to be analysed. It could also be interesting to collect sulphate aerosols in the atmosphere during field campaigns, preferably far from volcanic vents (where the secondary sulphate dominates the composition of sulphate), and analyse their isotopic composition. The field campaign should take place in a location where the contribution of background non-volcanic sulphur aerosols (e.g. anthropogenic or sea-salt sulphates) to the total sulphate budget can be subtracted. This can be done easily for sea-salt sulphate; therefore, a campaign around a strong halogen and sulphur-rich degassing volcano in the middle of an ocean (such as on Ambrym, Vanuatu) would be the ideal location.

Conclusions and further perspectives

The primary goal of this work is to investigate in-plume reaction dynamics leading to volcanic sulphate production in the troposphere. Whereas chemical models are usually limited to the description of sulphur aqueous chemistry, SO_2 oxidation on tropospheric sulphate aerosols is also accounted, though quite uncertain. The role of volcanic halogens chemistry during in-plume oxidation of volcanic SO_2 is also explored for different kinds of volcanic emissions and eruptions.

The photochemical box-model CiTTyCAT has been used to purse the investigation. It has been implemented with sulphur and halogens heterogeneous chemistry. In order to evaluate model results with sulphate isotopic composition measurements, the model has been enriched by an isotopic transfer scheme describing the evolution of oxygen mass-independent fractionation signatures (O-MIFs, quantified via $\Delta^{17}O$) in produced sulphates (secondary sulphate). Sulphates O-MIF signatures, indeed, provide precious informations on SO_2 processing in the atmosphere, since they are inherited directly and indirectly from ozone and other atmospheric oxidants.

The major SO_2 oxidation pathways here considered are gas phase oxidation by OH, and liquid phase oxidation by O_3, H_2O_2, O_2/TMI, and HOX (HOX = HOCl + HOBr) in water rich phases (condensing plumes) or on primary sulphate aerosols emitted from the vent (non-condensing plumes). Liquid phase oxidation of SO_2 by NO_2 is not accounted in the model. So far, only little amounts of NO_x have been observed in volcanic plumes, and large uncertainties are still pertaining to in-plume nitrogen chemistry (Roberts et al., 2009; von Glasow, 2010). Notably, nitrogen compounds are involved mostly in halogens heterogeneous chemistry, which is very fast at acidic conditions. Consequently, it is hereby assumed that NO_x chemistry should not have an impact on volcanic

SO_2 oxidation.

In-plume chemistry is investigated via chemical schemes of increasing complexity, considering the influences of high SO_2 concentrations and of halogens chemistry on in-plume reaction dynamics. Sensitivity studies are also conducted to investigate volcanic SO_2 oxidation for different passive degassing conditions, spanning from condensing plumes enriched in ash, to non-condensing plumes with small ash-content. Finally, modelled $\Delta^{17}O$ are compared to O-MIFs measured in volcanic sulphates collected from tropospheric volcanic ash-deposits.

1   Major Findings

Halogens-poor condensing plumes

In a first place the new version of CiTTyCAT is used to investigate volcanic sulphate formation and relative isotopic signatures in halogens-poor condensing volcanic plumes. This is the case of hotspot and rift volcanoes, whose sulphur emissions are more abundant than halogenic ones. It is assumed that halogens would be washed out by plume liquid water droplets and ash.

This first part of the study is conducted for ash-rich condensing plumes from degassing, where iron mobilization to the aqueous phase could be promoted. The purpose is to identify the major pathways of aqueous and gas phase SO_2 oxidation in a volcanic plume, a chemical environment so radically different from background air and rich in water vapour.

According to model calculations:

- **OH should carry a significant and positive O-MIF**
  This first finding suggests that in a dense volcanic plume OH carries a positive O-MIF. Because of high SO_2 concentrations, indeed, the rate of oxygen isotopes exchange between OH and H_2O is inhibited, and the rate of OH destruction is enhanced. During simulations OH maintains mostly a positive mass-independent fractionation, which can be transmitted to gas-phase secondary sulphate. As a result, sulphate produced in the gas phase via SO_2 oxidation by OH should have a significant positive O-MIF. This result indicates that OH should not be the dominant in-plume SO_2 oxidant, since most O-isotopic ratios measurements of volcanic sulphate from tropospheric volcanic ash-deposits show a $\Delta^{17}O \approx 0‰$.

- **H_2O_2 cannot be a major SO_2 oxidant**
  The second salient finding is that, overall, H_2O_2 should be a minor SO_2 oxidant in ash-rich condensing volcanic plumes. Notably, H_2O_2 is very rapidly consumed in the aqueous phase, where at acidic pH it reacts rapidly with excess S(IV). Mixing with background air is a weak source of H_2O_2.

- **O_2/TMI could be the major pathway of sulphate production**
  The third major finding is that the O_2/TMI pathway could be very substantial and, in some cases, the dominant in-plume SO_2 oxidation pathway. The rates of SO_2 oxidation by OH, H_2O_2, and O_3 are, indeed, vastly reduced in a condensing volcanic plume compared to the background air. According to model simulations, at TMI concentrations above 1 μM, the aqueous reaction with O_2/TMI is the major SO_2 oxidation pathway in water droplets of condensing plumes. Independently from plume LWC, this sulphate production channel is dominant. Remarkably, only cases when O_2/TMI channel is truly prevailing, modelled sulphate O-MIFs are similar to the isotopic measurements of tropospheric volcanic sulphates from volcanic ash-deposits, where $\Delta^{17}O \approx 0.0 \pm 0.1‰$.

Halogens-rich plumes: condensing and non-condensing plumes

In a second place a new version of CiTTyCAT has been used to investigate volcanic sulphate formation and relative oxygen isotopic signatures in halogens-rich volcanic plumes.

The heterogeneous chemical scheme has been extended with halogens and sulphur heterogeneous chemistry within liquid water droplets (condensing plumes) and on primary sulphate aerosols (non-condensing plumes). The new model is used to investigate the relation between halogens reactivity and volcanic SO_2 oxidation within a plume. Notably, this time HOX (HOX = HOCl + HOBr) is also included among the possible SO_2 oxidants within the liquid phase. Sensitivity simulations cover a broad range of volcanic plume scenarios, with different halogens and sulphur loadings.

Some results are shared for both plume models, since they are independent from liquid phase composition. According to model calculations, indeed:

- **OH could carry a very significant and positive O-MIF**
  The first salient finding is that OH should carry a very positive isotopic anomaly in halogens-rich volcanic plumes. Volcanic SO_2 and HCl react rapidly with atmospheric OH, competing with the rate of OH isotopic exchange with water molecules. As a result, depending on halogens and SO_2 loadings, sulphate produced in the gas phase could initially carry an O-MIF as high as 4.5‰.

- **HOX should not directly participate to SO_2 oxidation**
  The second relevant finding is that, halogens directly influence O_3 and oxidants concentrations, but they do not directly contribute to SO_2 oxidation. Ozone destruction by halogen radicals inhibits OH and HO_2 formation, hence H_2O_2 production and HOX accumulation within the plume. Notably, HOX is quickly consumed via halogens heterogeneous reactions. Therefore, with the current chemical scheme, according to model calculations halogens do not react significantly with SO_2 in the aqueous phase.

Besides, liquid phase composition and chemical activity influence differently the chemical rates of heterogeneous reactions and liquid phase equilibria. Consequently, other major results are peculiar strictly to condensing or non-condensing volcanic plume scenarios. According to model simulations, with regard to:

1. **Condensing plumes (water droplets)**

    - **ODEs occur, remarkably, also in presence of water droplets**
      The first relevant finding is that ODEs catalysed by halogens might also occur in presence of water droplets. The ODE is initiated by emitted halogens radicals, and then developed through heterogeneous chemistry mobilizing halogens from water droplets. Remarkably, ODEs formation during daytime inhibits OH and HO_2 formation, hence H_2O_2 accumulation in condensing plumes over the long run. Besides, less pervasive and strong ODEs are developed over the long run, because plume dilution in the troposphere weakens halogens reactivity.

    - **H_2O_2 should not be a major SO_2 oxidant in the aqueous phase**
      The second salient finding is that, overall, H_2O_2 should not be a major SO_2 oxidant in halogens-rich condensing volcanic plumes. It is quickly consumed by S(IV) aqueous reactions, and it is not reformed in the plume due to the suppression of HO_x species production due to halogens reactivity. Moreover, the influx of background air is a weak source of H_2O_2 within the plume. Consequently, this pathway of SO_2 oxidation do not significantly contribute to sulphate production over the long run.

    - **O_2/TMI should be the major pathway of sulphate production**
      The third important finding is that in presence of water droplets SO_2 oxidation is dominated by S(IV) aqueous reaction with O_2/TMI, even for relatively low TMI aqueous concentrations ([TMI]<0.5μM). SO_2 oxidation by O_2/TMI is the only channel that can promote sustained and substantial sulphate production. Consequently, for this scenario volcanic sulphate carries a low oxygen mass-independent isotopic anomaly (O-MIF) because of dominant SO_2 oxidation via O_2/TMI aqueous reaction. In some cases, the sulphate O-MIF is equal to 0 ‰ (mass-dependent sulphate), in agreement with isotopic measurements on volcanic sulphates from tropospheric volcanic ash-deposits.

2. **Non-condensing plumes (sulphate aerosols)**

    - **ODEs can occur at very low halogens loading**
      The first salient finding is that ODEs can occur in non-condensing

162

volcanic plumes even for very low halogens loadings ($\approx$50 ppbv). The amplitude and formation speed depend, however, on the initial halogens concentration.

The current chemical scheme can reproduce accurately ODEs formation within non-condensing volcanic plumes. Notably, the model can reproduce BrO/SO_2 ratios measured within the plumes of different volcanoes around the planet.

- **The rate of SO_2 oxidation is extremely low**
  The second important finding is that the rate of SO_2 oxidation, thus sulphate production, is significantly lowered compared to condensing plumes simulations. Halogens reactions inhibit OH, HO_2 and H_2O_2 formation in the gas-phase, and within extremely acidic sulphate aerosols solutions, heterogeneous SO_2 oxidation is negligible. Interestingly, sulphate production is found to be inversely correlated to halogen emissions within the plume.

- **Sulphur oxidation is dominated by OH and H_2O_2 pathways**
  The third relevant finding is that sulphur oxidation is dominated by H_2O_2 oxidation on sulphate aerosols and by OH oxidation in the gas-phase. Remarkably, in contrast to condensing plumes simulations, the H_2O_2 oxidation pathway can be very substantial. In presence of sulphate aerosols the H_2O_2 concentration does not drop instantaneously, because of low solubility in sulphuric acid solutions.

  Finally, it has been found that at low halogen loadings the contribution of OH to SO_2 oxidation is higher. The reverse is valid for H_2O_2 contribution to SO_2 oxidation for high halogen loadings.

- **Secondary sulphate should carry positive O-MIF**
  The fourth noticeable finding is that secondary volcanic sulphate produced during passive degassing could carry initially very positive O-MIF, and its magnitude depends on the respective contributions of OH and H_2O_2 to sulphur oxidation. Within the plume OH bears a non negligible positive O-MIF due to SO_2 and HCl presence, and which varies strongly with the sulphur and halogen. WhileOH O-MIF is a prognostic variable of the model, H_2O_2 produces sulphates with an O-MIF of about 0.87‰.

  According to the non-condensing plumes model simulations conducted in this work, the final deposited sulphate O-MIF is high, varying between 0.8 and 1.4 ‰ depending on in-plume input conditions.

The major findings of this study are briefly summarised in **Fig.:6.1**. Notably, the main SO_2 oxidation pathways for each plume scenario are highlighted with respects to plume environment and halogens content.

163

Oxidants	Condensing plumes		Non-condensing plumes	
	Halogens rich	Halogens poor	Halogens rich	Halogens poor
OH	X	✓	✓	✓
O_3	X	X	X	X
H_2O_2	X	X	✓	✓
O_2/TMI	✓	✓	X	X
HOX	X	X	X	X
$\Delta^{17}O$(sulphate) ‰	~ 0	0 - 0.5	~1	~1.5
SO_2 conversion (%)	~1.5	~15	~0.2	~10

Figure 6.1: Representation of major findings form this study: major SO_2 oxidation pathways for different plume conditions, and in absence or presence of halogens. Most dominant SO_2 oxidation channels are highlighted in shades of green, with dominant pathways in dark shades and competing oxidation pathways in light-green shades.

2   Uncertainties on model results

The version of CiTTyCAT developed throughout this study combines a new chemical module treating sulphur liquid phase chemistry, with an oxygen isotopic anomaly transfer scheme from sulphur oxidants to sulphate products. CiTTyCAT is a well-known Lagrangian photochemical and mixing model, which is suitable for studying chemistry and transport throughout the troposphere. Since its early application it has been applied to multiple investigations, spanning from production and loss of ozone in air masses (Evans et al., 2000), aerosol formation from condensable compounds (Emmerson et al., 2004, 2007), to lifetime of acetone in the upper troposphere (Arnold et al., 2004), and detailed isoprene and monoterpene degradation schemes within the troposphere (Pugh et al., 2012) (see Pugh et al., 2012 for a complete review of the model).

All previous investigations have been validated against numerous field experiments, notably via comparison of model results with concentrations measurements. In contrast to previous model applications, results form this study are validated via the aid of isotopic measurements. This is a totally new approach with regards to conventional methods of model validation, but it provides direct insights into the nature of chemical transformations and reaction fluxes

undergoing in environments that are difficult to probe, such as volcanic plumes.

There are a number of uncertainties associated with the present modelling work, notably input parameters.

2.1 Input parameters: kinetic data

A major source of uncertainty is a strict dependence of results on model inputs, such as kinetic data. Different sources of uncertainties are associated with sulphur atmospheric chemistry, notably with regards to liquid phase reactions. While the recommended kinetic data for gas-phase chemistry is relatively reliable, the uncertainties are much larger for heterogeneous chemistry.

The first weak point for modelling simulations is that the value of the reaction rate constant for oxygen isotopes exchange between OH and H_2O is quite outdated (Dubey et al., 1997). This limitation regards specifically the modelled OH O-MIF signature, and overall the positive signatures modelled for secondary volcanic sulphates.

Other sources of uncertainties are related to SO_2 liquid phase oxidation by O_2 catalysed by transition metal ions. This mechanism of SO_2 oxidation is a complex ensemble of radical reactions, with multiple branch reactions finally resulting in aqueous sulphate production (Brandt et al., 1994; Brandt and van Eldik, 1995). A major limit is imposed by the number of oxygen atoms transferred to final sulphate product via the reaction, which can influence the O-MIF of sulphate produced via SO_2 oxidation by O_2/TMI. Another potential limit is due to the pH dependence of the reaction, which might also alter the reaction rates for acidic pH of volcanic particles and aerosols.

Another uncertainty is introduced with halogens chemistry, notably for reactive uptakes in liquid water droplets. Most measurements on halogens reactive uptakes are limited to reactions within sulphate aerosols, notably for temperatures below 273.15 K (Sander et al., 2006; Ammann et al., 2013). During this study, however, it has been assumed that the high Br and Cl concentrations within volcanic plumes and the low pH of liquid phases would result in very similar halogens reactive uptakes for both water droplets and sulphate aerosols. This assumption is a quite crude approximation, which, however, cannot be treated differently in model simulations due to the lack of experimental data on the subject.

In conclusions, the results from these model simulations are subjected to uncertainties associated with reactions kinetic data. Moreover, it is also possible that some of the key reactions have not been identified yet. It is difficult to assess the implications of all these uncertainties on model results, because sometimes the error bars on some reactions are unknown. It would also be very demanding computing-wise to carry out a Monte Carlo simulation to test the sensitivity of model results to all the kinetic uncertainties. Ideally, the results from this study would gain in robustness in presence of a qualitative and significant revision of

current kinetic data, notably with regards to halogens chemistry and sulphur oxidation in liquid phase.

2.2 Input parameters: isotopic signatures

The combination of stable isotopes approaches and modelling is a rather new field within atmospheric sciences. Isotopic investigations rely heavily on isotopic signatures of atmospheric species, in this case oxygen isotopes signature of atmospheric oxidants. Most laboratory experiments agree on the extent of isotopic anomaly observed in major atmospheric oxidants, but few uncertainties are still pertaining to the extent of isotopic anomaly transferable from ozone to its reaction products.

In this study, it is assumed that ozone has a transferable isotopic signature of about 36 ‰, as observed during NO_x production in polar regions (Morin et al., 2007, 2008). This value results in sulphate produced via SO_2 oxidation by ozone bearing an isotopic anomaly of 9 ‰, and in hydroxil radicals produced in the gas-phase with an initial O-MIF of about 4.5 ‰. The chosen ozone O-MIF is at the upper end of ozone oxygen isotopic anomaly, whose average value is around 26 ‰ (Vicars and Savarino, 2014), and which results in sulphates with an isotopic anomaly of 6.5 ‰, and hydroxil radicals produced in the gas-phase with initial O-MIF of about 3.25 ‰. While in volcanic plumes SO_2 does not react with ozone because of the low pH of volcanic liquid phases, OH can still contribute significantly to volcanic SO_2 oxidation. Therefore, the chosen value for O_3 O-MIF introduces some uncertainty regarding the OH radicals O-MIF. Finally, gas-phase sulphates O-MIF and the overall results might be slightly overestimated. It is, however, difficult to assess the extent of O-MIF uncertainty, mostly because of the lack of in-depth investigations on OH O-MIF. The only way to address this issue would be a thorough investigation (ideally laboratory experiments) on the SO_2 + OH mechanism of reaction, and on the resulting sulphate O-MIF. In conclusions, results from these simulations would greatly benefit in robustness from laboratory experiments investigating formation and transfer of OH O-MIF to sulphate in the atmosphere.

2.3 Box modelling (0-D models)

The box modelling (0-D) approach used here is not entirely appropriate. It is assumed implicitly that the variable species concentrations within volcanic plumes can be approximated to average plume concentrations. Clearly, it is a simplification or even an oversimplification. A 1-D plume chemical model would be more appropriate, with the 1-D dimension being the variations of species concentrations perpendicular to the plume axis. This way, the core and the edges of the volcanic plume could be distinguished in terms of composition and photochemistry. Ideally, a 3-D high-resolution chemistry-transport model should be used. However, the drawback with complex models is that they are very

expensive in terms of computing power and storage. Therefore, they have to be run with relatively simplified chemical schemes. This approximation would result in an oversimplification of specific chemical processes at the core of isotopic signatures production within atmospheric species.

3   Further perspectives

This study suggests that the composition and nature of volcanic emissions and plume particles can highly influence volcanic SO_2 oxidation in the troposphere. In particular, according to model simulations it has been found that sulphates produced in non-condensing plumes from passive degassing should carry a positive $\Delta^{17}O$. This result is clearly in contrast with oxygen isotopic ratios from sulphates from tropospheric volcanic ash-deposits (Martin, 2018). Therefore, this investigation suggests that the only cases when sulphate with very small isotopic signatures is generated, as in most isotopic measurements from tropospheric volcanic sulphates (Martin, 2018), is when the SO_2 oxidation by O_2/TMI dominates. It suggests also that sulphates with mass-dependent O-MIF should be produced only in the aqueous phases of condensing plumes. Following some uncertainties related to the model simulations, additional investigations are suggested to better consolidate these unexpected results.

On a general level, as previously stated uncertainties on photochemical modelling and simulations can be per se quite substantial (Ridley et al., 2017). One option to consolidate the results from this study, would be to test sulphate formation via OH in a controlled environment, ideally via laboratory experiments at high SO_2 loadings and with a well constrained OH chemical budget, notably loss processes and relative humidity. Another suggestion would be also to re-examine via ab-initio calculations the value of the reaction constant for the isotopic exchange reaction between OH and H_2O. In particular, high level computational chemistry theories (such as the Coupled Cluster Theory) and RRKM estimations should provide relatively accurate results. In addition, such theoretical investigations should not be computationally too expensive, for reactions involving molecules with relatively low degrees of freedom (such as OH and H_2O). Ideally, chamber experiments and theoretical ab-initio calculations should be performed in a parallel study.

Another option would be to conduct a measurement campaign with the purpose of collecting and measuring the isotopic composition of secondary sulphates formed during passive degassing. In particular, it would be useful to collect volcanic sulphates far from volcanic vents, within a radius of distance where secondary sulphate dominates the total composition of volcanic sulphate. Moreover, the most ideal location would be a volcano where the contribution of background non-volcanic sulphur aerosols (e.g. anthropogenic or sea-salt sulphates) to the total sulphate budget could be negligible or easily subtracted. Sulphates differentiation and separation could be done easily for sulphates from

sea-salt aerosols, and, therefore, a campaign around a strong halogens and sulphur-rich degassing volcano in the middle of an ocean (such as on Ambrym, Vanuatu) would be the ideal location.

Further studies are also needed to constrain iron mobilization from ash to the aqueous phase of volcanic water droplets. There is high uncertainty on the extent of TMI dissolution from volcanic ash water phases, especially with regards to plumes from passive degassing. Ideally, it would be very useful to conduct more thorough investigations on iron mobilization in plume from passive degassing, and a measurement campaign could provide some constraints to the extent of iron concentrations within both sulphate aerosols from non-condensing plumes, and water droplets of condensing plumes.

Finally, during degassing within the free troposphere volcanic water might be converted to ice because of the low temperatures of the upper troposphere, as observed in plumes from explosive eruptions where volcanic water can cool to form ice particles (Tabazadeh and Turco, 1993; Herzog et al., 1998; Durant, 2007; Pitari et al., 2016). Recent investigations suggest that larger dissolution of iron oxides can be obtained when water coating dust particles drops below freezing point (Jeong et al., 2012). As a result, larger TMI concentrations could be reached also on within volcanic particles reaching the upper troposphere. The ice-particle scenario is rather interesting, because halogens heterogeneous reactions and cycling are faster at lower temperatures and on the surface of ice droplets (Huff and Abbatt, 2000; Sander et al., 2006; Rose et al., 2006; Ammann et al., 2013). The combined effects of enhanced iron mobilization and halogens reactivity suggest that volcanic SO_2 oxidation on the surface of ice particles might follow specific pathways of oxidation. Consequently, volcanic sulphates produced in the upper troposphere might have peculiar O-MIFs, depending on halogens loading, altitude and notably ice or liquid water speciation. The new version of CiTTyCAT implemented during this work could be further extended to include SO_2 processing and halogens heterogeneous reactions on the surface of ice particles. Ideally, results from this model extension could provide some constraints regarding the contribution of volcanic sulphate and BrO within the respective chemical budgets to upper free troposphere (Schmidt et al., 2016), and on the production of sulphates in cold environments.

Bibliography

Aiuppa, A. (2009). Degassing of halogens from basaltic volcanism: Insights from volcanic gas observations. *Chem. Geol.*, 263(1-4):99–109.

Aiuppa, A., Baker, D. R., and Webster, J. D. (2009). Halogens in volcanic systems. *Chem. Geol.*, 263(1-4):1–18.

Aiuppa, A., Federico, C., Franco, A., Giudice, G., Gurrieri, S., Inguaggiato, S., Liuzzo, M., McGonigle, A. J., and Valenza, M. (2005a). Emission of bromine and iodine from Mount Etna volcano. *Geochemistry, Geophys. Geosystems*, 6(8):1–8.

Aiuppa, A., Federico, C., Giudice, G., Gurrieri, S., Liuzzo, M., Shinohara, H., Favarra, R., and Valenza, M. (2006a). Rates of carbon dioxide plume degassing from Mount Etna volcano. *J. Geophys. Res. Solid Earth*, 111(9):1–8.

Aiuppa, A., Franco, A., von Glasow, R., Allen, a. G., D'Alessandro, W., Mather, T. a., Pyle, D. M., and Valenza, M. (2006b). The tropospheric processing of acidic gases and hydrogen sulphide in volcanic gas plumes as inferred from field and model investigations. *Atmos. Chem. Phys. Discuss.*, 6(6):11653–11680.

Aiuppa, A., Inguaggiato, S., McGonigle, A. J., O'Dwyer, M., Oppenheimer, C., Padgett, M. J., Rouwet, D., and Valenza, M. (2005b). H_2S fluxes from Mt. Etna, Stromboli, and Vulcano (Italy) and implications for the sulfur budget at volcanoes. *Geochim. Cosmochim. Acta*, 69(7):1861–1871.

Alexander, B., Allman, D. J., Amos, H. M., Fairlie, T. D., Dachs, J., Hegg, D. A., and Sletten, R. S. (2012). Isotopic constraints on the formation pathways of sulfate aerosol in the marine boundary layer of the subtropical northeast Atlantic Ocean. *J. Geophys. Res. Atmos.*, 117(6):1–17.

Alexander, B., Park, R. J., Jacob, D. J., and Gong, S. (2009). Transition metal-catalyzed oxidation of atmospheric sulfur: Global implications for the sulfur budget. *J. Geophys. Res. Atmos.*, 114(2):1–13.

Alexander, B., Park, R. J., Jacob, D. J., Li, Q. B., Yantosca, R. M., Savarino, J., Lee, C. C. W., and Thiemens, M. H. (2005). Sulfate formation in sea-salt aerosols: Constraints from oxygen isotopes. *J. Geophys. Res. D Atmos.*, 110(10):1–12.

Alexander, B., Savarino, J., Barkov, N. I., Delmas, R. J., and Thiemens, M. H. (2002). Climate driven changes in the oxidation pathways of atmospheric sulfur. *Geophys. Res. Lett.*, 29(14):30–1–30–4.

Allen, A. G., Oppenheimer, C., Ferm, M., Baxter, P. J., Horrocks, L. A., Galle, B., McGonigle, A. J. S., and Duffell, H. J. (2002). Primary sulfate aerosol and associated emissions from Masaya Volcano, Nicaragua. *J. Geophys. Res. Atmos.*, 107(D23).

Alt, J. C., Shanks, W. C., and Jackson, M. C. (1993). Cycling of sulfur in subduction zones: The geochemistry of sulfur in the Mariana Island Arc and back-arc trough. *Earth Planet. Sci. Lett.*, 119(4):477–494.

Ammann, M., Cox, R. A., Crowley, J. N., Jenkin, M. E., Mellouki, A., Rossi, M. J., Troe, J., and Wallington, T. J. (2013). Evaluated kinetic and photochemical data for atmospheric chemistry: Volume VI heterogeneous reactions with liquid substrates. *Atmos. Chem. Phys.*, 13(16):8045–8228.

Andres, R. J. and Kasgnoc, a. D. (1998). A time-averaged inventory of subaerial volcanic sulfur emissions. *J. Geophys. Res.*, 103(D19):25251.

Arnold, S. R., Chipperfield, M. P., Blitz, M. A., Heard, D. E., and Pilling, M. J. (2004). Photodissociation of acetone: Atmospheric implications of temperature-dependent quantum yields. *Geophys. Res. Lett.*, 31(7):4–7.

Arnold, S. R., Methven, J., Evans, M. J., Chipperfield, M. P., Lewis, A. C., Hopkins, J. R., McQuaid, J. B., Watson, N., Purvis, R. M., Lee, J. D., Atlas, E. L., Blake, D. R., and Rappenglück, B. (2007). Statistical inference of OH concentrations and air mass dilution rates from successive observations of nonmethane hydrocarbons in single air masses. *J. Geophys. Res. Atmos.*, 112(10):1–15.

Atkinson, R., Baulch, D. L., Cox, R. A., Crowley, J. N., Hampson, R. F., Hynes, R. G., Jenkin, M. E., Rossi, M. J., and Troe, J. (2004). Evaluated kinetic and photochemical data for atmospheric chemistry: Volume I - gas phase reactions of O_x, HO_x, NO_x and SO_x species. *Atmos. Chem. Phys.*, 4(6):1461–1738.

Ayris, P. and Delmelle, P. (2012a). Volcanic and atmospheric controls on ash iron solubility: A review. *Phys. Chem. Earth*, 45-46(August 2008):103–112.

170

Ayris, P. M. and Delmelle, P. (2012b). The immediate environmental effects of tephra emission. *Bull. Volcanol.*, 74(9):1905–1936.

Bao, H. (2015). Sulfate : A time capsule for Earth's O_2, O_3, and H_2O. *Chem. Geol.*, 395:108–118.

Bao, H., Thiemens, M. H., Farquhar, J., Campbell, D. A., Lee, C. C.-W., Heine, K., and Loope, D. B. (2000). Anomalous [17]O compositions in massive sulphate deposits on the Earth. *Nature*, 406(6792):176–178.

Bao, H., Thiemens, M. H., Loope, D. B., and Yuan, X. L. (2003). Sulfate oxygen-17 anomaly in an Oligocene ash bed in mid-North America: Was it the dry fogs? *Geophys. Res. Lett.*, 30(16).

Barkan, E. and Luz, B. (2003). High-precision measurements of [17]O/^{16}O and ^{18}O/^{16}O of O_2 and O_2/Ar ratio in air. *Rapid Commun. Mass Spectrom.*, 17(24):2809–2814.

Baroni, M., Savarino, J., Cole-Dai, J., Rai, V. K., and Thiemens, M. H. (2008). Anomalous sulfur isotope compositions of volcanic sulfate over the last millennium in Antarctic ice cores. *J. Geophys. Res.*, 113(D20):D20112.

Baroni, M., Thiemens, M. H., Delmas, R. J., and Savarino, J. (2007). Mass-Independent Sulfur Isotopic Compositions in Stratospheric Volcanic Eruptions. *Science (80-.).*, 315(5808):84–87.

Bates, T. S., Lamb, B. K., Guenther, A., Dignon, J., and Stoiber, R. E. (1992). Sulfur emissions to the atmosphere from natural sources. *J. Atmos. Chem.*, 14(1-4):315–337.

Beilke, S. and Gravenhorst, G. (1978). Heterogeneous SO_2-oxidation in the droplet phase. *Atmos. Environ.*, 12(1-3):231–239.

Bekki, S. (1995). Oxidation of volcanic SO_2: A sink for stratospheric OH and H_2O. *Geophys. Res. Lett.*, 22(8):913–916.

Berglen, T. F., Berntsen, T. K., Isaksen, I. S. A., and Sundet, J. K. (2004). A global model of the coupled sulfur/oxidant chemistry in the troposphere: The sulfur cycle. *J. Geophys. Res. Atmos.*, 109(D19):n/a—-n/a.

Bhattacharya, S. K., Pandey, A., and Savarino, J. (2008). Determination of intramolecular isotope distribution of ozone by oxidation reaction with silver metal. *J. Geophys. Res.*, 113(D3):D03303.

Bindeman, I. N., Eiler, J. M., Wing, B. A., and Farquhar, J. (2007). Rare sulfur and triple oxygen isotope geochemistry of volcanogenic sulfate aerosols. *Geochim. Cosmochim. Acta*, 71(9):2326–2343.

Bobrowski, N., Hönninger, G., Galle, B., and Platt, U. (2003). Detection of bromine monoxide in a volcanic plume. *Nature*, 423(6937):273–276.

Bobrowski, N. and Platt, U. (2007). SO_2/BrO ratios studied in five volcanic plumes. *J. Volcanol. Geotherm. Res.*, 166(3-4):147–160.

Bobrowski, N., von Glasow, R., Aiuppa, A., Inguaggiato, S., Louban, I., Ibrahim, O. W., and Platt, U. (2007). Reactive halogen chemistry in volcanic plumes. *J. Geophys. Res. Atmos.*, 112(6):1–17.

Boichu, M., Oppenheimer, C., Roberts, T. J., Tsanev, V., and Kyle, P. R. (2011). On bromine, nitrogen oxides and ozone depletion in the tropospheric plume of Erebus volcano (Antarctica). *Atmos. Environ.*, 45(23):3856–3866.

Brandt, C., Fábián, I., and van Eldik, R. (1994). Kinetics and Mechanism of the Iron(III)-catalyzed Autoxidation of Sulfur(IV) Oxides in Aqueous Solution. Evidence for the Redox Cycling of Iron in the Presence of Oxygen and Modeling of the Overall Reaction Mechanism. *Inorg. Chem.*, 33(4):687–701.

Brandt, C. and van Eldik, R. (1995). Transition Metal-Catalyzed Oxidation of Sulfur(IV) Oxides. Atmospheric-Relevant Processes and Mechanisms. *Chem. Rev.*, 95(1):119–190.

Brenninkmeijer, C. A. M., Janssen, C., Kaiser, J., Röckmann, T., Rhee, T. S., and Assonov, S. S. (2003). Isotope effects in the chemistry of atmospheric trace compounds. *Chem. Rev.*, 103(12):5125–62.

Cadoux, A., Scaillet, B., Bekki, S., Oppenheimer, C., and Druitt, T. H. (2015). Stratospheric Ozone destruction by the Bronze-Age Minoan eruption (Santorini Volcano, Greece). *Sci. Rep.*, 5(November 2014):1–12.

Calvert, J. G., Su, F., Bottenheim, J. W., and Strausz, O. P. (1978). Mechanism of the homogeneous oxidation of sulfur dioxide in the troposphere. *Atmos. Environ.*, 12(1-3):197–226.

Carey, L. D., Niu, J., Yang, P., Kankiewicz, J. A., Larson, V. E., and Vonder Haar, T. H. (2008). The vertical profile of liquid and ice water content in midlatitude mixed-phase altocumulus clouds. *J. Appl. Meteorol. Climatol.*, 47(9):2487–2495.

Carn, S. A., Clarisse, L., and Prata, A. J. (2016). Multi-decadal satellite measurements of global volcanic degassing. *J. Volcanol. Geotherm. Res.*, 311:99–134.

Carn, S. A., Froyd, K. D., Anderson, B. E., Wennberg, P., Crounse, J., Spencer, K., Dibb, J. E., Krotkov, N. A., Browell, E. V., Hair, J. W., Diskin, G., Sachse, G., and Vay, S. A. (2011). In situ measurements of tropospheric volcanic plumes in Ecuador and Colombia during TC[4]. *J. Geophys. Res. Atmos.*, 116(9):1–24.

Carslaw, K. S., Boucher, O., Spracklen, D. V., Mann, G. W., Rae, J. G. L., Woodward, S., and Kulmala, M. (2009). Atmospheric aerosols in the earth system: a review of interactions and feedbacks. *Atmos. Chem. Phys. Discuss.*, 9(3):11087–11183.

Chandler, A. S., Choularton, T. W., Dollard, G. J., Eggleton, A. E. J., Gay, M. J., Hill, T. A., Jones, B. M. R., Tyler, B. J., Bandy, B. J., and Penkett, S. A. (1988). Measurements of H_2O_2 and SO_2 in clouds and estimates of their reaction rate. *Nature*, 336(6199):562–565.

Chen, Q., Geng, L., Schmidt, J. A., Xie, Z., Kang, H., Dachs, J., Cole-Dai, J., Schauer, A. J., Camp, M. G., and Alexander, B. (2016). Isotopic constraints on the role of hypohalous acids in sulfate aerosol formation in the remote marine boundary layer. *Atmos. Chem. Phys.*, 16(17):11433–11450.

Chen, Q., Schmidt, J. A., Shah, V., Jaeglé, L., Sherwen, T., and Alexander, B. (2017). Sulfate production by reactive bromine: Implications for the global sulfur and reactive bromine budgets. *Geophys. Res. Lett.*, 44(13):7069–7078.

Chin, M. and Jacob, D. J. (1996). Anthropogenic and natural contributions to tropospheric sulfate: A global model analysis. *J. Geophys. Res. Atmos.*, 101(D13):18691–18699.

Chin, M., Jacob, D. J., Gardner, G. M., Foreman-Fowler, M. S., Spiro, P. A., and Savoie, D. L. (1996). A global three-dimensional model of tropospheric sulfate. *J. Geophys. Res. Atmos.*, 101(D13):18667–18690.

Chin, M., Rood, R. B., Lin, S.-J., Müller, J.-F., and Thompson, A. M. (2000). Atmospheric sulfur cycle simulated in the global model GOCART: Model description and global properties. *J. Geophys. Res. Atmos.*, 105(D20):24671–24687.

Claire, M. W., Kasting, J. F., Domagal-Goldman, S. D., Stüeken, E. E., Buick, R., and Meadows, V. S. (2014). Modeling the signature of sulfur mass-independent fractionation produced in the Archean atmosphere. *Geochim. Cosmochim. Acta*, 141:365–380.

Coplen, T. B. (1994). Reporting of stable hydrogen, carbon, and oxygen isotopic abundances (Technical Report). *Pure Appl. Chem.*, 66(2):31–34.

Coplen, T. B. (2011). Guidelines and recommended terms for expression of stable-isotope-ratio and gas-ratio measurement results. *Rapid Commun. Mass Spectrom.*, 25(17):2538–2560.

Cwiertny, D. M., Young, M. A., and Grassian, V. H. (2008). Chemistry and Photochemistry of Mineral Dust Aerosol. *Annu. Rev. Phys. Chem.*, 59(1):27–51.

Dahneke, B. (1983). Simple Kinetic Theory of Brownian Diffusion in Vapors and Aerosols. In R.E.Meyer, editor, *Theory Dispersed Multiph. Flow*, pages 97–133. Elsevier, New York.

Daum, P. H., Kleinman, L. I., Hills, A. J., Lazrus, A. L., Leslie, A. C. D., Busness, K., and Boatman, J. (1990). Measurement and Interpretation of Concentrations of H_2O_2 and Related Species in the Upper Midwest During Summer. 95(90):9857–9871.

Davidovits, P., Kolb, C. E., Williams, L. R., Jayne, J. T., and Worsnop, D. R. (2006). Mass accommodation and chemical reactions at gas-liquid interfaces. *Chem. Rev.*, 106(4):1323–1354.

de Foy, B., Krotkov, N. A., Bei, N., Herndon, S. C., Huey, L. G., Martínez, A.-P., Ruiz-Suárez, L. G., Wood, E. C., Zavala, M., and Molina, L. T. (2009). Hit from both sides: tracking industrial and volcanic plumes in Mexico City with surface measurements and OMI SO_2 retrievals during the MILAGRO field campaign. *Atmos. Chem. Phys.*, 9(24):9599–9617.

De Moor, J. M., Fischer, T. P., Sharp, Z. D., Hauri, E. H., Hilton, D. R., and Atudorei, V. (2010). Sulfur isotope fractionation during the May 2003 eruption of Anatahan volcano, Mariana Islands: Implications for sulfur sources and plume processes. *Geochim. Cosmochim. Acta*, 74(18):5382–5397.

De Moor, J. M., Fischer, T. P., Sharp, Z. D., King, P. L., Wilke, M., Botcharnikov, R. E., Cottrell, E., Zelenski, M., Marty, B., Klimm, K., Rivard, C., Ayalew, D., Ramirez, C., and Kelley, K. A. (2013). Sulfur degassing at Erta Ale (Ethiopia) and Masaya (Nicaragua) volcanoes: Implications for degassing processes and oxygen fugacities of basaltic systems. *Geochemistry, Geophys. Geosystems*, 14(10):4076–4108.

Delmelle, P. (2003). Environmental impacts of tropospheric volcanic gas plumes. *Geol. Soc. London, Spec. Publ.*, 213(1):381–399.

Delmelle, P., Stix, J., Bourque, C. P. A., Baxter, P. J., Garcia-Alvarea, J., and Barqueror, J. (2001). Dry deposition and heavy acid loading in the vicinity of Masaya Volcano, a major sulfur and chlorine source in Nicaragua. *Environ. Sci. Technol.*, 35(7):1289–1293.

DeMore, W. B., Sander, S. P., Golden, D. M., Hampson, R. F., Kurylo, M. J., Howard, C. J., Ravishankara, A. R., Kolb, C. E., and Molina, M. J. (1997). Chemical Kinetics and Photochemical Data for Use in Stratospheric Modeling Supplement to Evaluation 12: Update of Key Reactions. Evaluation Number 13. *JPL Publ.*, 00-3(13):74.

Desboeufs, K. V., Losno, R., and Colin, J. L. (2001). Factors influencing aerosol solubility during cloud processes. *Atmos. Environ.*, 35(20):3529–3537.

Desboeufs, K. V., Losno, R., Vimeux, F., and Cholbi, S. (1999). The pH-dependent dissolution of wind-transported Saharan dust. *J. Geophys. Res. Atmos.*, 104(D17):21287–21299.

Ding, T., Valkiers, S., Kipphardt, H., De Bièvre, P., Taylor, P., Gonfiantini, R., and Krouse, R. (2001). Calibrated sulfur isotope abundance ratios of three IAEA sulfur isotope reference materials and V-CDT with a reassessment of the atomic weight of sulfur. *Geochim. Cosmochim. Acta*, 65(15):2433–2437.

Dole, M. (1936). The Relative Atomic Weight of Oxygen in Water and in Air A Discussion of the Atmospheric Distribution of the Oxygen Isotopes and of the Chemical Standard of Atomic Weights. *J. Chem. Phys.*, 4(4):268.

Donovan, A., Tsanev, V., Oppenheimer, C., and Edmonds, M. (2014). Reactive halogens (BrO and OClO) detected in the plume of Soufrière Hills Volcano during an eruption hiatus. *Geochemistry, Geophys. Geosystems*, 15(8):3346–3363.

Dubey, M. K., Mohrschladt, R., Donahue, N. M., and Anderson, J. G. (1997). Isotope Specific Kinetics of Hydroxyl Radical (OH) with Water (H_2O): Testing Models of Reactivity and Atmospheric Fractionation. *J. Phys. Chem. A*, 101(8):1494–1500.

Duggen, S., Olgun, N., Croot, P., Hoffmann, L., Dietze, H., and Teschner, C. (2009). The role of airborne volcanic ash for the surface ocean biogeochemical iron-cycle: a review. *Biogeosciences Discuss.*, 6(4):6441–6489.

Durand, M. and Grattan, J. (2001). Effects of volcanic air pollution on health. *Lancet*, 357(9251):164.

Durant, A. J. (2007). On water in volcanic clouds. *ProQuest Diss. Theses*, 3278728:242.

Eatough, D. J., Caka, F. M., and Farber, R. J. (1994). The conversion of SO_2 to sulfate in the atmosphere. *Isr. J. Chem.*, 34(3-4):301–314.

Eiler, J. M. (2001). Oxygen Isotope Variations of Basaltic Lavas and Upper Mantle Rocks. *Rev. Mineral. Geochemistry*, 43:319–364.

Emmerson, K. M., Carslaw, N., Carslaw, D. C., Lee, J. D., McFiggans, G., Bloss, W. J., Gravestock, T., Heard, D. E., Hopkins, J., Ingham, T., Pilling, M. J., Smith, S. C., Jacob, M., and Monks, P. S. (2007). Free radical modelling studies during the UK TORCH Campaign in Summer 2003. *Atmos. Chem. Phys.*, 7(1):167–181.

Emmerson, K. M., Mackenzie, A. R., Owen, S. M., and Evans, M. J. (2004). A Lagrangian model with simple primary and secondary aerosol scheme 1 : comparison with UK PM 10 data. pages 3127–3157.

175

Evans, M., Shallcross, D., Law, K., Wild, J., Simmonds, P., Spain, T., Berrisford, P., Methven, J., Lewis, A., McQuaid, J., Pilling, M., Bandy, B., Penkett, S., and Pyle, J. (2000). Evaluation of a Lagrangian box model using field measurements from EASE (Eastern Atlantic Summer Experiment) 1996. *Atmos. Environ.*, 34(23):3843–3863.

Faloona, I. (2009). Sulfur processing in the marine atmospheric boundary layer: A review and critical assessment of modeling uncertainties. *Atmos. Environ.*, 43(18):2841–2854.

Farquhar, J. (2000). Atmospheric Influence of Earth's Earliest Sulfur Cycle. *Science (80-.).*, 289(5480):756–758.

Farquhar, J. and Wing, B. A. (2003). Multiple sulfur isotopes and the evolution of the atmosphere. *Earth Planet. Sci. Lett.*, 213(1-2):1–13.

Fogelman, K. D., Walker, D. M., and Margerum, D. W. (1989). Nonmetal redox kinetics: hypochlorite and hypochlorous acid reactions with sulfite. *Inorg. Chem.*, 28(6):986–993.

Gaillard, F., Scaillet, B., and Arndt, N. T. (2011). Atmospheric oxygenation caused by a change in volcanic degassing pressure. *Nature*, 478(7368):229–232.

Galeazzo, T., Bekki, S., Martin, E., Savarino, J., and Arnold, S. R. (2018). Photochemical box-modelling of volcanic SO_2 oxidation: isotopic constraints. *Atmos. Chem. Phys. Discuss.*, (April):1–38.

Gao, C., Robock, A., and Ammann, C. (2008). Volcanic forcing of climate over the past 1500 years: An improved ice core-based index for climate models. *J. Geophys. Res. Atmos.*, 113(23):1–15.

Gerlach, T. M. (2004). Volcanic sources of tropospheric ozone-depleting trace gases. *Geochemistry, Geophys. Geosystems*, 5(9).

Gervat, G. P., Clark, P. A., Marsh, A. R. W., Teasdale, I., Chandler, A. S., Choularton, T. W., Gay, M. J., Hill, M. K., and Hill, T. A. (1988). Field evidence for the oxidation of SO_2 by H_2O_2 in cap clouds. *Nature*, 333(6170):241–243.

Goto, D., Nakajima, T., Takemura, T., and Sudo, K. (2011). A study of uncertainties in the sulfate distribution and its radiative forcing associated with sulfur chemistry in a global aerosol model. *Atmos. Chem. Phys.*, 11(21):10889–10910.

Graedel, T. E. and Weschler, C. J. (1981). *Chemistry within aqueous atmospheric aerosols and raindrops*, volume 19.

Graf, H.-F., Feichter, J., and Langmann, B. (1997). Volcanic sulfur emissions: Estimates of source strength and its contribution to the global sulfate distribution. *J. Geophys. Res. Atmos.*, 102(D9):10727–10738.

Graf, H. F., Langmann, B., and Feichter, J. (1998). The contribution of Earth degassing to the atmospheric sulfur budget. *Chem. Geol.*, 147(1-2):131–145.

Grellier, L., Marécal, V., Josse, B., Hamer, P. D., Roberts, T. J., Aiuppa, A., and Pirre, M. (2014). Towards a representation of halogen chemistry within volcanic plumes in a chemistry transport model. *Geosci. Model Dev. Discuss.*, 7(2):2581–2650.

Gromov, S., Joeckel, P., Sander, R., and Brenninkmeijer, C. A. M. (2010). A kinetic chemistry tagging technique and its application to modelling the stable isotopic composition of atmospheric trace gases. *Geosci. Model Dev.*, 3(2):337–364.

Han, X., Guo, Q., Liu, C., Fu, P., Strauss, H., Yang, J., Hu, J., Wei, L., Ren, H., Peters, M., Wei, R., and Tian, L. (2016). Using stable isotopes to trace sources and formation processes of sulfate aerosols from Beijing, China. *Sci. Rep.*, 6(February):29958.

Hanson, D. R., Ravishankara, a. R., and Solomon, S. (1994). Heterogeneous reactions in sulfuric acid aerosols: A framework for model calculations. *J. Geophys. Res.*, 99(D2):3615.

Harris, E. (2013). Enhanced Role of Transition Metal Ion Catalysis During In-Cloud Oxidation of SO_2. *Science (80-.).*, 340(6133):727–730.

Harris, E., Sinha, B., Foley, S., Crowley, J. N., Borrmann, S., and Hoppe, P. (2012a). Sulfur isotope fractionation during heterogeneous oxidation of SO_2 on mineral dust. *Atmos. Chem. Phys.*, 12(11):4867–4884.

Harris, E., Sinha, B., Hoppe, P., Crowley, J. N., Ono, S., and Foley, S. (2012b). Sulfur isotope fractionation during oxidation of sulfur dioxide: Gas-phase oxidation by OH radicals and aqueous oxidation by H_2O_2, O_3 and iron catalysis. *Atmos. Chem. Phys.*, 12(1):407–424.

Harris, E., Sinha, B., Hoppe, P., Foley, S., and Borrmann, S. (2012c). Fractionation of sulfur isotopes during heterogeneous oxidation of SO_2 on sea salt aerosol: A new tool to investigate non-sea salt sulfate production in the marine boundary layer. *Atmos. Chem. Phys.*, 12(10):4619–4631.

Harris, E., Sinha, B., Hoppe, P., and Ono, S. (2013). High-precision measurements of ^{33}S and ^{34}S fractionation during SO_2 oxidation reveal causes of seasonality in SO_2 and sulfate isotopic composition. *Environ. Sci. Technol.*, 47(21):12174–83.

Harris, E., Sinha, B., Van Pinxteren, D., Schneider, J., Poulain, L., Collett, J., D'Anna, B., Fahlbusch, B., Foley, S., Fomba, K. W., George, C., Gnauk, T., Henning, S., Lee, T., Mertes, S., Roth, A., Stratmann, F., Borrmann, S., Hoppe, P., and Herrmann, H. (2014). In-cloud sulfate addition to single particles resolved with sulfur isotope analysis during HCCT-2010. *Atmos. Chem. Phys.*, 14(8):4219–4235.

Haywood, J. and Boucher, O. (2000). Estimates of the direct and indirect radiative forcing due to tropospheric aerosols: A review. *Rev. Geophys.*, 38(4):513–543.

He, H., Wang, Y., Ma, Q., Ma, J., Chu, B., Ji, D., Tang, G., Liu, C., Zhang, H., and Hao, J. (2014). Mineral dust and NOx promote the conversion of SO_2 to sulfate in heavy pollution days. *Sci. Rep.*, 4(2):1–6.

Heidenreich III, J. E., Thiemens, M. H., Heidenreich, J. E., and Thiemens, M. H. (1986). A non-mass-dependent oxygen isotope effect in the production of ozone from molecular oxygen: The role of molecular symmetry in isotope chemistry. *J. Chem. Phys.*, 84(4):2129–2136.

Herrmann, H., Ervens, B., Jacobi, H. W., Wolke, R., Nowacki, P., and Zellner, R. (2000). CAPRAM2.3: A chemical aqueous phase radical mechanism for tropospheric chemistry. *J. Atmos. Chem.*, 36(3):231–284.

Herzog, M., Graf, H.-F., Textor, C., and Oberhuber, J. M. (1998). The effect of phase changes of water on the development of volcanic plumes. *J. Volcanol. Geotherm. Res.*, 87(1-4):55–74.

Hoffmann, M. R. (1986). On the kinetics and mechanism of oxidation of aquated sulfur dioxide by ozone. *Atmos. Environ.*, 20(6):1145–1154.

Holt, B. D., Kumar, R., and Cunningham, P. T. (1981). Oxygen-18 study of the aqueous-phase oxidation of sulfur dioxide. *Atmos. Environ.*, 15(4):557–566.

Hönninger, G. (2004). Reactive bromine and sulfur emissions at Salar de Uyuni, Bolivia. *Geophys. Res. Lett.*, 31(4):L04101.

Hörmann, C., Sihler, H., Bobrowski, N., Beirle, S., De Vries, M. P., Platt, U., and Wagner, T. (2013). Systematic investigation of bromine monoxide in volcanic plumes from space by using the GOME-2 instrument. *Atmos. Chem. Phys.*, 13(9):4749–4781.

Hoshyaripour, G., Hort, M., Langmann, B., and Delmelle, P. (2014). Volcanic controls on ash iron solubility: New insights from high-temperature gas-ash interaction modeling. *J. Volcanol. Geotherm. Res.*, 286:67–77.

Hoshyaripour, G. A., Hort, M., and Langmann, B. (2015). Ash iron mobilization through physicochemical processing in volcanic eruption plumes: a numerical modeling approach. *Atmos. Chem. Phys.*, 15(16):9361–9379.

Huebert, B., Vitousek, P., Sutton, J., Elias, T., Heath, J., Coeppicus, S., Howell, S., and Blomquist, B. (1999). Volcano fixes nitrogen into plant-available forms. *Biogeochemistry*, 47(1):111–118.

Huff, A. K. and Abbatt, J. P. D. (2000). Gas-phase Br_2 production in heterogeneous reactions of Cl_2, HOCl, and BrCl with halide-ice surfaces. *J. Phys. Chem. A*, 104(31):7284–7293.

Ilyinskaya, E., Schmidt, A., Mather, T. A., Pope, F. D., Witham, C., Baxter, P., Jóhannsson, T., Pfeffer, M., Barsotti, S., Singh, A., Sanderson, P., Bergsson, B., McCormick Kilbride, B., Donovan, A., Peters, N., Oppenheimer, C., and Edmonds, M. (2017). Understanding the environmental impacts of large fissure eruptions: Aerosol and gas emissions from the 20142015 Holuhraun eruption (Iceland). *Earth Planet. Sci. Lett.*, 472:309–322.

Janssen, C. (2005). Intramolecular isotope distribution in heavy ozone ($^{16}O^{18}O^{16}O$ and $^{16}O^{16}O^{18}O$). *J. Geophys. Res. Atmos.*, 110(D8):n/a—-n/a.

Janssen, C. and Tuzson, B. (2006). A diode laser spectrometer for symmetry selective detection of ozone isotopomers. *Appl. Phys. B Lasers Opt.*, 82(3):487–494.

Jeong, D., Kim, K., and Choi, W. (2012). Accelerated dissolution of iron oxides in ice. *Atmos. Chem. Phys.*, 12(22):11125–11133.

Johnston, J. C. and Thiemens, M. H. (1997). The isotopic composition of tropospheric ozone in three environments. *J. Geophys. Res. Atmos.*, 102(D21):25395–25404.

Jourdain, L., Roberts, T. J., Pirre, M., and Josse, B. (2016). Modeling the reactive halogen plume from Ambrym and its impact on the troposphere with the CCATT-BRAMS mesoscale model. *Atmos. Chem. Phys.*, 16(18):12099–12125.

Kasting, J. F., Catling, D. C., and Zahnle, K. (2012). Atmospheric oxygenation and volcanism. *Nature*, 487(7408):E1–E1.

Kelley, D. S., Baross, J. A., and Delaney, J. R. (2002). Volcanoes, Fluids, and Life at Mid-Ocean Ridge Spreading Centers. *Annu. Rev. Earth Planet. Sci.*, 30(1):385–491.

Kelly, P. J., Kern, C., Roberts, T. J., Lopez, T., Werner, C., and Aiuppa, A. (2013). Rapid chemical evolution of tropospheric volcanic emissions from Redoubt Volcano, Alaska, based on observations of ozone and halogen-containing gases. *J. Volcanol. Geotherm. Res.*, 259:317–333.

Kern, C., Sihler, H., Vogel, L., Rivera, C., Herrera, M., and Platt, U. (2009). Halogen oxide measurements at Masaya Volcano, Nicaragua using active long

path differential optical absorption spectroscopy. *Bull. Volcanol.*, 71(6):659–670.

Koike, M., Jones, N. B., Matthews, W. A., Johnston, P. V., McKenzie, R. L., Kinnison, D., and Rodriguez, J. (1994). Impact of Pinatubo aerosols on the partitioning between NO_2 and HNO_3. *Geophys. Res. Lett.*, 21(7):597–600.

Korolev, A. V., Isaac, G. A., Strapp, J. W., Cober, S. G., and Barker, H. W. (2007). In situ measurements of liquid water content profiles in midlatitude stratiform clouds. *Q. J. R. Meteorol. Soc.*, 133(628):1693–1699.

Krankowsky, D., Bartecki, F., Klees, G. G., Mauersberger, K., Schellenbach, K., and Stehr, J. (1995). Measurement of heavy isotope enrichment in tropospheric ozone. *Geophys. Res. Lett.*, 22(13):1713–1716.

Kristiansen, N. I., Stohl, A., Olivié, D. J., Croft, B., Søvde, O. A., Klein, H., Christoudias, T., Kunkel, D., Leadbetter, S. J., Lee, Y. H., Zhang, K., Tsigaridis, K., Bergman, T., Evangeliou, N., Wang, H., Ma, P. L., Easter, R. C., Rasch, P. J., Liu, X., Pitari, G., Di Genova, G., Zhao, S. Y., Balkanski, Y., Bauer, S. E., Faluvegi, G. S., Kokkola, H., Martin, R. V., Pierce, J. R., Schulz, M., Shindell, D., Tost, H., and Zhang, H. (2016). *Evaluation of observed and modelled aerosol lifetimes using radioactive tracers of opportunity and an ensemble of 19 global models*, volume 16.

Kroll, J. H., Cross, E. S., Hunter, J. F., Pai, S., Wallace, L. M., Croteau, P. L., Jayne, J. T., Worsnop, D. R., Heald, C. L., Murphy, J. G., and Frankel, S. L. (2015). Atmospheric evolution of sulfur emissions from Kilauea: Real-time measurements of oxidation, dilution, and neutralization within a volcanic plume. *Environ. Sci. Technol.*, 49(7):4129–4137.

Krouse, H. and Grinenko, V. (1991). *Stable isotopes: Natural and anthropogenic sulphur in the environment*. John Wiley and Sons, United Kingdom.

Laj, P., Fuzzi, S., Facchini, M. C., Lind, J. A., Orsi, G., Preiss, M., Maser, R., Jaeschke, W., Seyffer, E., Helas, G., Acker, K., Wieprecht, W., Moller, D., Arends, B. G., Mols, J. J., Colvile, R. N., Gallagher, M. W., Beswick, K. M., and Hargreaves, K. J. (1997). Cloud processing of soluble gases. *Atmos. Environ.*, 31(16):2589–2598.

Langmann, B. (2014). On the role of climate forcing by volcanic sulphate and volcanic ash. *Adv. Meteorol.*, 2014.

Lee, C., Kim, Y. J., Tanimoto, H., Bobrowski, N., Platt, U., Mori, T., Yamamoto, K., and Hong, C. S. (2005). High ClO and ozone depletion observed in the plume of Sakurajima volcano, Japan. *Geophys. Res. Lett.*, 32(21):1–4.

Lee, C. C. W., Savarino, J., and Thiemens, M. H. (2001). Mass independent oxygen isotopic composition of atmospheric sulfate: Origin and implications for the present and past atmosphere of Earth and Mars. *Geophys. Res. Lett.*, 28(9):1783–1786.

Lee, C. C.-W. and Thiemens, M. H. (2001). The δ^{17}O and δ^{18}O measurements of atmospheric sulfate from a coastal and high alpine region: A mass-independent isotopic anomaly. *J. Geophys. Res. Atmos.*, 106(D15):17359–17373.

LeGrande, A. N., Anchuikaitis, K., von Gunten, L., and Goodwin, L. (2010). Volcanoes and climate. Technical Report 6.

Liu, Q. and Margerum, D. W. (2001). Equilibrium and kinetics of bromine chloride hydrolysis. *Environ. Sci. Technol.*, 35(6):1127–1133.

Longo, B. M. (2013). Adverse Health Effects Associated with Increased Activity at Kilauea Volcano: A Repeated Population-Based Survey. *ISRN Public Health*, 2013(April 2008):1–10.

Longo, B. M., Rossignol, A., and Green, J. B. (2008). Cardiorespiratory health effects associated with sulphurous volcanic air pollution. *Public Health*, 122(8):809–820.

Luterbacher, J. and Pfister, C. (2015). The year without a summer. *Nat. Geosci.*, 8(4):246–248.

Luz, B., Barkan, E., and Bender, M. L. (1999). Triple-isotope composition of atmospheric oxygen as a tracer of biosphere productivity. *Nature*, 400(6744):547–550.

Lyons, J. R. (2001). Transfer of mass-independent fractionation in ozone to other oxygen-containing radicals in the atmosphere. *Geophys. Res. Lett.*, 28(17):3231–3234.

Lyons, J. R. (2007). Mass-independent fractionation of sulfur isotopes by isotope-selective photodissociation of SO_2. *Geophys. Res. Lett.*, 34(22):1–5.

Mandeville, C. W., Webster, J. D., Tappen, C., Taylor, B. E., Timbal, A., Sasaki, A., Hauri, E., and Bacon, C. R. (2009). Stable isotope and petrologic evidence for open-system degassing during the climactic and pre-climactic eruptions of Mt. Mazama, Crater Lake, Oregon. *Geochim. Cosmochim. Acta*, 73(10):2978–3012.

Marcus, R. A. (2013). Theory of mass-independent fractionation of isotopes, phase space accessibility, and a role of isotopic symmetry. *Proc. Natl. Acad. Sci.*, 110(44):17703–17707.

Martin, E. (2018). Volcanic Plume Impact on the Atmosphere and Climate : O- and S-Isotope Insight into Sulfate Aerosol Formation. 1991:1–23.

Martin, E., Bekki, S., Ninin, C., and Bindeman, I. (2014). Volcanic sulfate aerosol formation in the troposphere. *J. Geophys. Res. Atmos.*, 119(22):12,660–12,673.

Martin, E. and Bindeman, I. (2009). Mass-independent isotopic signatures of volcanic sulfate from three supereruption ash deposits in Lake Tecopa, California. *Earth Planet. Sci. Lett.*, 282(1-4):102–114.

Martin, L. and Good, T. W. (1991). Catalyzed oxidation of sulfur dioxide in solution: The iron-manganese synergism. *Atmos. Environ. Part A. Gen. Top.*, 25(10):2395–2399.

Martin, R. S., Mather, T. A., and Pyle, D. M. (2006). High-temperature mixtures of magmatic and atmospheric gases. *Geochemistry, Geophys. Geosystems*, 7(4).

Martin, R. S., Wheeler, J. C., Ilyinskaya, E., Braban, C. F., and Oppenheimer, C. (2012). The uptake of halogen (HF, HCl, HBr and HI) and nitric (HNO_3) acids into acidic sulphate particles in quiescent volcanic plumes. *Chem. Geol.*, 296-297:19–25.

Maters, E. C., Delmelle, P., and Bonneville, S. (2016). Atmospheric Processing of Volcanic Glass: Effects on Iron Solubility and Redox Speciation. *Environ. Sci. Technol.*, 50(10):5033–5040.

Maters, E. C., Delmelle, P., and Gunnlaugsson, H. P. (2017). Controls on iron mobilisation from volcanic ash at low pH: Insights from dissolution experiments and Mössbauer spectroscopy. *Chem. Geol.*, 449:73–81.

Mather, T., Pyle, D. M., and Oppenheimer, C. (2003). Tropospheric volcanic aerosol. *Volcanism Earth's Atmos.*, pages 189–212.

Mather, T. A. (2008). Volcanism and the atmosphere: the potential role of the atmosphere in unlocking the reactivity of volcanic emissions. *Philos. Trans. R. Soc. A Math. Phys. Eng. Sci.*, 366(1885):4581–4595.

Mather, T. A. (2015). Volcanoes and the environment: Lessons for understanding Earth's past and future from studies of present-day volcanic emissions. *J. Volcanol. Geotherm. Res.*, 304:160–179.

Mather, T. A., McCabe, J. R., Rai, V. K., Thiemens, M. H., Pyle, D. M., Heaton, T. H. E., Sloane, H. J., and Fern, G. R. (2006). Oxygen and sulfur isotopic composition of volcanic sulfate aerosol at the point of emission. *J. Geophys. Res. Atmos.*, 111(18):1–9.

Mather, T. A., Oppenheimer, C., Allen, A. G., and McGonigle, A. (2004a). Aerosol chemistry of emissions from three contrasting volcanoes in Italy. *Atmos. Environ.*, 38(33):5637–5649.

Mather, T. A., Tsanev, V. I., Pyle, D. M., McGonigle, A. J., Oppenheimer, C., and Allen, A. G. (2004b). Characterization and evolution of tropospheric plumes from Lascar and Villarrica volcanoes, Chile. *J. Geophys. Res. D Atmos.*, 109(21).

Mather, T. A., Witt, M. L., Pyle, D. M., Quayle, B. M., Aiuppa, A., Bagnato, E., Martin, R. S., Sims, K. W., Edmonds, M., Sutton, A. J., and Ilyinskaya, E. (2012). Halogens and trace metal emissions from the ongoing 2008 summit eruption of Klauea volcano, Hawaìi. *Geochim. Cosmochim. Acta*, 83:292–323.

Mazzocchi, M., Hansstein, F., and Ragona, M. (2010). The 2010 Volcanic Ash Cloud and Its Financial Impact on the European Airline Industry. *CESifo Forum*, 11(2):92–100.

McArdle, J. V. and Hoffmann, M. R. (1983). Kinetics and mechanism of the oxidation of aquated sulfur dioxide by hydrogen peroxide at low pH. *J. Phys. Chem.*, 87(26):5425–5429.

McCormick, M. P., Thomason, L. W., and Trepte, R. C. (1995). Atmospheric effects of the Mt Pinatubo eruption. *Nature*, 373(February 1995):399–404.

Methven, J., Arnold, S. R., Stohl, A., Evans, M. J., Avery, M., Law, K., Lewis, A. C., Monks, P. S., Parrish, D. D., Reeves, C. E., Schlager, H., Atlas, E. L., Blake, D. R., Coe, H., Crosier, J., Flocke, F. M., Holloway, J. S., Hopkins, J. R., McQuaid, J., Purvis, R., Rappenglück, B., Singh, H. B., Watson, N. M., Whalley, L. K., and Williams, P. I. (2006). Establishing Lagrangian connections between observations within air masses crossing the Atlantic during the International Consortium for Atmospheric Research on Transport and Transformation experiment. *J. Geophys. Res. Atmos.*, 111(23):1–21.

Michalski, G., Scott, Z., Kabiling, M., and Thiemens, M. H. (2003). First measurements and modeling of $\Delta^{17}O$ in atmospheric nitrate. *Geophys. Res. Lett.*, 30(16):1870.

Michalski, G. and Xu, F. (2010). Isotope modeling of nitric acid formation in the atmosphere using ISO-RACM: testing the importance of NO oxidation, heterogeneous reactions, and trace gas chemistry. *Atmos. Chem. Phys. Discuss.*, 10(3):6829–6869.

Millard, G. A., Mather, T. A., Pyle, D. M., Rose, W. I., and Thornton, B. (2006). Halogen emissions from a small volcanic eruption: Modeling the peak concentrations, dispersion, and volcanically induced ozone loss in the stratosphere. *Geophys. Res. Lett.*, 33(19):6–11.

Miller, M. F. (2002). Isotopic fractionation and the quantification of ^{17}O anomalies in the oxygen three-isotope system: An appraisal and geochemical significance. *Geochim. Cosmochim. Acta*, 66(11):1881–1889.

Minnis, P., Harrison, E. F., Stowe, L. L., Gibson, G. G., Denn, F. M., Doelling, D. R., and Smith, W. L. (1993a). Radiative climate forcing by the mount Pinatubo eruption. *Science*, 259(5100):1411–5.

Minnis, P., Harrison, E. F., Stowe, L. L., Gibson, G. G., Denn, F. M., Doelling, D. R., and Smith, W. L. (1993b). Radiative climate forcing by the mount Pinatubo eruption. *Science*, 259(5100):1411–5.

Morin, S., Sander, R., and Savarino, J. (2011). Simulation of the diurnal variations of the oxygen isotope anomaly (Δ^{17}O) of reactive atmospheric species. *Atmos. Chem. Phys.*, 11(8):3653–3671.

Morin, S., Savarino, J., Bekki, S., Gong, S., and Bottenheim, J. W. (2007). Signature of Arctic surface ozone depletion events in the isotope anomaly (Δ^{17}O) of atmospheric nitrate. *Atmos. Chem. Phys.*, 7(5):1451–1469.

Morin, S., Savarino, J., Frey, M. M., Yan, N., Bekki, S., Bottenheim, J. W., and Martins, J. M. F. (2008). Tracing the origin and fate of NO$_x$ in the Arctic atmosphere using stable isotopes in nitrate. *Science*, 322(5902):730–2.

Nelson, D. M., Tsunogai, U., Ding, D., Ohyama, T., Komatsu, D. D., Nakagawa, F., Noguchi, I., and Yamaguchi, T. (2018). Triple oxygen isotopes indicate urbanization affects sources of nitrate in wet and dry atmospheric deposition. *Atmos. Chem. Phys.*, 18(9):6381–6392.

Newhall, C. G. and Self, S. (1982). The volcanic explosivity index (VEI) an estimate of explosive magnitude for historical volcanism. *J. Geophys. Res.*, 87(C2):1231.

Nielsen, H., Pilot, J., Grinenko, L., Grinenko, V., Lein, A., Smith, J., and Pankina, R. (1991). *Stable Isotopes: Natural and Anthropogenic Sulphur in the Environment - chapter 4*. John Wiley and Sons, United Kingdom.

Ono, S. (2017). Photochemistry of Sulfur Dioxide and the Origin of Mass-Independent Isotope Fractionation in Earth's Atmosphere. *Annu. Rev. Earth Planet. Sci.*, 45(1):301–329.

Ono, S., Whitehill, A. R., and Lyons, J. R. (2013). Contribution of isotopologue self-shielding to sulfur mass-independent fractionation during sulfur dioxide photolysis. *J. Geophys. Res. Atmos.*, 118(5):2444–2454.

Oppenheimer, C., Fischer, T. P., and Scaillet, B. (2013). *Volcanic Degassing: Process and Impact*, volume 4.

Oppenheimer, C., Kyle, P., Eisele, F., Crawford, J., Huey, G., Tanner, D., Kim, S., Mauldin, L., Blake, D., Beyersdorf, A., Buhr, M., and Davis, D. (2010). Atmospheric chemistry of an Antarctic volcanic plume. *J. Geophys. Res. Atmos.*, 115(4):1–15.

Oppenheimer, C., Tsanev, V. I., Braban, C. F., Cox, R. A., Adams, J. W., Aiuppa, A., Bobrowski, N., Delmelle, P., Barclay, J., and McGonigle, A. J. S. (2006). BrO formation in volcanic plumes. *Geochim. Cosmochim. Acta*, 70(12):2935–2941.

Oxford Economics (2010). The economic impacts of air travel restrictions due to volcanic ash. page 15.

Pack, A., Toulouse, C., and Przybilla, R. (2007). Determination of oxygen triple isotope ratios of silicates without cryogenic separation of NF_3 technique with application to analyses of technical O_2 gas and meteorite classification. *Rapid Commun. Mass Spectrom.*, 21(22):3721–3728.

Pan, L. L., Honomichl, S. B., Randel, W. J., Apel, E. C., Atlas, E. L., Beaton, S. P., Bresch, J. F., Hornbrook, R., Kinnison, D. E., Lamarque, J. F., Saiz-Lopez, A., Salawitch, R. J., and Weinheimer, A. J. (2015). Bimodal distribution of free tropospheric ozone over the tropical western Pacific revealed by airborne observations. *Geophys. Res. Lett.*, 42(18):7844–7851.

Parazols, M., Marinoni, A., Amato, P., Abida, O., Laj, P., and Mailhot, G. (2006). Speciation and role of iron in cloud droplets at the puy de Dôme station. *J. Atmos. Chem.*, 54(3):267–281.

Park, R. J., Jacob, D. J., Field, B. D., Yantosca, R. M., and Chin, M. (2004). Natural and transboundary pollution influences on sulfate-nitrate-ammonium aerosols in the United States: Implications for policy. *J. Geophys. Res. D Atmos.*, 109(15).

Parrella, J. P., Jacob, D. J., Liang, Q., Zhang, Y., Mickley, L. J., Miller, B., Evans, M. J., Yang, X., Pyle, J. A., Theys, N., and Van Roozendael, M. (2012). Tropospheric bromine chemistry: Implications for present and pre-industrial ozone and mercury. *Atmos. Chem. Phys.*, 12(15):6723–6740.

Patris, N., Cliff, S. S., Quinn, P. K., Kasem, M., and Thiemens, M. H. (2007). Isotopic analysis of aerosol sulfate and nitrate during ITCT-2k2: Determination of different formation pathways as a function of particle size. *J. Geophys. Res.*, 112(D23):D23301.

Pavlov, A. A. and Kasting, J. F. (2002). Mass-Independent Fractionation of Sulfur Isotopes in Archean Sediments: Strong Evidence for an Anoxic Archean Atmosphere. *Astrobiology*, 2(1):27–41.

Pavlov, A. A., Mills, M. J., and Toon, O. B. (2005). Mystery of the volcanic mass-independent sulfur isotope fractionation signature in the Antarctic ice core. *Geophys. Res. Lett.*, 32(12):1–4.

Peterson, D. W. (1988). Volcanic hazards and public response. *J. Geophys. Res.*, v. 93(no. B5):paper no. 7B7068, p. 4161–4170.

Pitari, G., Visioni, D., Mancini, E., Cionni, I., Di Genova, G., and Gandolfi, I. (2016). Sulfate aerosols from non-explosive volcanoes: Chemical-radiative effects in the troposphere and lower stratosphere. *Atmosphere (Basel).*, 7(7):1–24.

Pope III, C. A. (2002). Lung Cancer, Cardiopulmonary Mortality, and Long-term Exposure to Fine Particulate Air Pollution. *Jama*, 287(9):1132.

Pruppacher, H. R., Klett, J. D., and Wang, P. K. (1998). Microphysics of Clouds and Precipitation. *Aerosol Sci. Technol.*, 28(May):381–382.

Pugh, T. A., Cain, M., Methven, J., Wild, O., Arnold, S. R., Real, E., Law, K. S., Emmerson, K. M., Owen, S. M., Pyle, J. A., Hewitt, C. N., and MacKenzie, A. R. (2012). A Lagrangian model of air-mass photochemistry and mixing using a trajectory ensemble: The Cambridge Tropospheric Trajectory model of Chemistry And Transport (CiTTyCAT) version 4.2. *Geosci. Model Dev.*, 5(1):193–221.

Pyle, D. M. and Mather, T. A. (2009). Halogens in igneous processes and their fluxes to the atmosphere and oceans from volcanic activity: A review. *Chem. Geol.*, 263(1-4):110–121.

Raga, G. B., Kok, G. L., Baumgardner, D., Báez, A., and Rosas, I. (1999). Evidence for volcanic influence on Mexico City aerosols. *Geophys. Res. Lett.*, 26(8):1149–1152.

Rattigan, O. V., Boniface, J., Swartz, E., Davidovits, P., Jayne, J. T., Kolb, C. E., and Worsnop, D. R. (2000). Uptake of gas-phase SO 2 in aqueous sulfuric acid: Oxidation by H_2O_2, O_3, and HONO. *J. Geophys. Res. Atmos.*, 105(D23):29065–29078.

Real, E., Law, K. S., Weinzierl, B., Fiebig, M., Petzold, A., Wild, O., Methven, J., Arnold, S., Stohl, A., Huntrieser, H., Roiger, A., Schlager, H., Stewart, D., Avery, M., Sachse, G., Browell, E., Ferrare, R., and Blake, D. (2007). Processes influencing ozone levels in Alaskan forest fire plumes during long-range transport over the North Atlantic. *J. Geophys. Res. Atmos.*, 112(D10):n/a—-n/a.

Redlich, O. (1946). The Dissociation of Strong Electrolytes. *Chem. Rev.*, 39(2):333–356.

Rees, C. and Holt, B. (1991). *Stable Isotopes: Natural and Anthropogenic Sulphur in the Environment - chapter 3*. John Wiley and Sons, United Kingdom.

Ridley, D. A., Cain, M., Methven, J., and Arnold, S. R. (2017). Sensitivity of tropospheric ozone to chemical kinetic uncertainties in air masses influenced by anthropogenic and biomass burning emissions. *Geophys. Res. Lett.*, 44(14):7472–7481.

Roberts, T. J., Braban, C. F., Martin, R. S., Oppenheimer, C., Adams, J. W., Cox, R. A., Jones, R. L., and Griffiths, P. T. (2009). Modelling reactive halogen formation and ozone depletion in volcanic plumes. *Chem. Geol.*, 263(1-4):151–163.

Roberts, T. J., Braban, C. F., Oppenheimer, C., Martin, R. S., Freshwater, R. A., Dawson, D. H., Griffiths, P. T., Cox, R. A., Saffell, J. R., and Jones, R. L. (2012). Electrochemical sensing of volcanic gases. *Chem. Geol.*, 332-333:74–91.

Roberts, T. J., Martin, R. S., and Jourdain, L. (2014). Reactive bromine chemistry in Mount Etna's volcanic plume: The influence of total Br, high-temperature processing, aerosol loading and plume-air mixing. *Atmos. Chem. Phys.*, 14(20):11201–11219.

Robock, A. (2000). Volcanic eruptions and climate. *Rev. Geophys.*, 38(2):191–219.

Robock, A. (2002). Pinatubo eruption: The Climatic Aftermath. *Science (80-.).*, 295(5558):1242–1244.

Robock, A. (2013). Introduction: Mount Pinatubo as a Test of Climate Feedback Mechanisms. *Volcanism Earth's Atmos.*, pages 1–8.

Roeckmann, T. (1998). Mass-Independent Oxygen Isotope Fractionation in Atmospheric CO as a Result of the Reaction CO+OH. *Science (80-.).*, 281(5376):544–546.

Rose, W. I. and Durant, A. J. (2009). Fine ash content of explosive eruptions. *J. Volcanol. Geotherm. Res.*, 186(1-2):32–39.

Rose, W. I., Millard, G. A., Mather, T. A., Hunton, D. E., Anderson, B., Oppenheimer, C., Thornton, B. F., Gerlach, T. M., Viggiano, A. A., Kondo, Y., Miller, T. M., and Ballenthin, J. O. (2006). Atmospheric chemistry of a 33-34 hour old volcanic cloud from Hekla Volcano (Iceland): Insights from direct sampling and the application of chemical box modeling. *J. Geophys. Res. Atmos.*, 111(20):1–17.

Rosenfeld, D. and Lensky, I. M. (1998). Satellite-Based Insights into Precipitation Formation Processes in Continental and Maritime Convective Clouds. *Bull. Am. Meteorol. Soc.*, 79(11):2457–2476.

Saiz-Lopez, A. (2004). Bromine oxide in the mid-latitude marine boundary layer. *Geophys. Res. Lett.*, 31(3):L03111.

Saiz-Lopez, A. and von Glasow, R. (2012). Reactive halogen chemistry in the troposphere. *Chem. Soc. Rev.*, 41(19):6448.

Sander, R. (2015). Compilation of Henry law constants (version 4.0) for water as solvent. *Atmos. Chem. Phys.*, 15(8):4399–4981.

Sander, S. P., Friedl, R. R., Golden, D. M., Kurylo, M. J., Moortgat, G. K., Wine, P. H., Ravishankara, a. R., Kolb, C. E., Molina, M. J., Diego, S., Jolla, L., Huie, R. E., and Orkin, V. L. (2006). Chemical Kinetics and Photochemical Data for Use in Atmospheric Studies Evaluation Number 15. *Cross Sect.*, California(15):1–153.

Savarino, J., Bekki, S., Cole-Dai, J., and Thiemens, M. H. (2003a). Evidence from sulfate mass independent oxygen isotopic compositions of dramatic changes in atmospheric oxidation following massive volcanic eruptions. *J. Geophys. Res. Atmos.*, 108(D21):1–6.

Savarino, J., Bhattacharya, S. K., Morin, S., Baroni, M., and Doussin, J.-F. (2008). The NO+O_3 reaction: a triple oxygen isotope perspective on the reaction dynamics and atmospheric implications for the transfer of the ozone isotope anomaly. *J. Chem. Phys.*, 128(19):194303.

Savarino, J., Kaiser, J., Morin, S., Sigman, D. M., and Thiemens, M. H. (2007). Nitrogen and oxygen isotopic constraints on the origin of atmospheric nitrate in coastal Antarctica. *Atmos. Chem. Phys.*, 7(8):1925–1945.

Savarino, J., Lee, C. C. W., and Thiemens, M. H. (2000). Laboratory oxygen isotopic study of sulfur (IV) oxidation: Origin of the mass-independent oxygen isotopic anomaly in atmospheric sulfates and sulfate mineral deposits on Earth. *J. Geophys. Res. Atmos.*, 105(D23):29079–29088.

Savarino, J., Romero, A., Cole-Dai, J., Bekki, S., and Thiemens, M. H. (2003b). UV induced mass-independent sulfur isotope fractionation in stratospheric volcanic sulfate. *Geophys. Res. Lett.*, 30(21):2131.

Savarino, J. and Thiemens, M. H. (1999a). Analytical procedure to determine both $\delta^{18}O$ and $\delta^{17}O$ of H_2O_2 in natural water and first measurements. *Atmos. Environ.*, 33(22):3683–3690.

Savarino, J. and Thiemens, M. H. (1999b). Mass-independent oxygen isotope (^{16}O, ^{17}O, ^{18}O) fractionation found in H_x, O_x reactions. *J. Phys. Chem. A*, 103(46):9221–9229.

Schmidt, J. A., Jacob, D. J., Horowitz, H. M., Hu, L., Sherwen, T., Evans, M. J., Liang, Q., Suleiman, R. M., Oram, D. E., Breton, M. L., Percival, C. J., Wang,

S., Dix, B., and Volkamer, R. (2016). Modeling the observed tropospheric BrO background : Importance of multiphase chemistry and implications for ozone, OH, and mercury. pages 819–835.

Schumann, U., Weinzierl, B., Reitebuch, O., Schlager, H., Minikin, A., Forster, C., Baumann, R., Sailer, T., Graf, K., Mannstein, H., Voigt, C., Rahm, S., Simmet, R., Scheibe, M., Lichtenstern, M., Stock, P., Rüba, H., Schäuble, D., Tafferner, A., Rautenhaus, M., Gerz, T., Ziereis, H., Krautstrunk, M., Mallaun, C., Gayet, J. F., Lieke, K., Kandler, K., Ebert, M., Weinbruch, S., Stohl, A., Gasteiger, J., Gross, S., Freudenthaler, V., Wiegner, M., Ansmann, A., Tesche, M., Olafsson, H., and Sturm, K. (2011). Airborne observations of the Eyjafjalla volcano ash cloud over Europe during air space closure in April and May 2010. *Atmos. Chem. Phys.*, 11(5):2245–2279.

Seinfeld, J. H. and Pandis, S. N. (2016). *Atmospheric chemistry and physics: from air pollution to climate change*. John wiley edition.

Sheppard, M. G. and Walker, R. B. (1983). Wigner method studies of ozone photodissociation. *J. Chem. Phys.*, 78(12):7191–7199.

Shi, Z., Krom, M. D., Jickells, T. D., Bonneville, S., Carslaw, K. S., Mihalopoulos, N., Baker, A. R., and Benning, L. G. (2012). Impacts on iron solubility in the mineral dust by processes in the source region and the atmosphere: A review. *Aeolian Res.*, 5:21–42.

Simpson, W. R., Brown, S. S., Saiz-Lopez, A., Thornton, J. A., and Von Glasow, R. (2015). Tropospheric Halogen Chemistry: Sources, Cycling, and Impacts. *Chem. Rev.*, 115(10):4035–4062.

Small, C. and Naumann, T. (2001). The global distribution of human population and recent volcanism. *Glob. Environ. Chang. Part B Environ. Hazards*, 3(3-4):93–109.

Smith, S. J., van Aardenne, J., Klimont, Z., Andres, R. J., Volke, A., and Delgado Arias, S. (2011). Anthropogenic sulfur dioxide emissions: 1850-2005. *Atmos. Chem. Phys.*, 11(3):1101–1116.

Solmon, F., Chuang, P. Y., Meskhidze, N., and Chen, Y. (2009). Acidic processing of mineral dust iron by anthropogenic compounds over the north Pacific Ocean. *J. Geophys. Res. Atmos.*, 114(2):1–20.

Solomon, S., Ivy, D. J., Kinnison, D., Mills, M. J., Neely, R. R., and Schmidt, A. (2016). Emergence of healing in the Antarctic ozone layer. *Science (80-.)*., 353(6296):269–274.

Stefánsson, A., Stefánsdóttir, G., Keller, N. S., Barsotti, S., Sigurdsson, Á., Thorláksdóttir, S. B., Pfeffer, M. A., Eiríksdóttir, E. S., Jónasdóttir, E. B., von

Löwis, S., and Gíslason, S. R. (2017). Major impact of volcanic gases on the chemical composition of precipitation in Iceland during the 2014-2015 Holuhraun eruption. *J. Geophys. Res. Atmos.*, 122(3):1971–1982.

Stenchikov, L., Kirchner, I., Robock, A., Grainger, R. G., Lambert, A., and Thomason, L. (1998). Radiative forcing from the 1991 Mount Pinatubo volcanic eruption. *J. Geophys. Res. Atmos.*, 103.

Stevenson, D. S., Johnson, C. E., Collins, W. J., and Derwent, R. G. (2003a). The tropospheric sulphur cycle and the role of volcanic SO_2. *Geol. Soc. London, Spec. Publ.*, 213(1):295–305.

Stevenson, D. S., Johnson, C. E., Highwood, E. J., Gauci, V., Collins, W. J., and Derwent, R. G. (2003b). Atmospheric impact of the 1783-1784 Laki eruption: Part I Chemistry modelling. *Atmos. Chem. Phys. Discuss*, 3:551–596.

Stocker, T., Qin, D., Plattner, G.-K., Tignor, M., Allen, S., Boschung, J., Nauels, A., Xia, Y., Bex, V., Midgley, P., and (eds.) (2013). *Climate Change 2013: The Physical Science Basis. Contribution of Working Group I to the Fifth Assessment Report of the Intergovernmental Panel on Climate Change*. Number 5th. Cambridge University Press, Cambridge, United Kingdom and New York, NY, USA.

Stoffel, M., Khodri, M., Corona, C., Guillet, S., Poulain, V., Bekki, S., Guiot, J., Luckman, B. H., Oppenheimer, C., Lebas, N., Beniston, M., and Masson-Delmotte, V. (2015). Estimates of volcanic-induced cooling in the Northern Hemisphere over the past 1,500 years. *Nat. Geosci.*, 8(10):784–788.

Straub, S. M. and Layne, G. D. (2003). The systematics of chlorine, fluorine, and water in Izu arc front volcanic rocks: Implications for volatile recycling in subduction zones. *Geochim. Cosmochim. Acta*, 67(21):4179–4203.

Stutz, J. (2002). Atmospheric reactive chlorine and bromine at the Great Salt Lake, Utah. *Geophys. Res. Lett.*, 29(10):18–21.

Tabazadeh, A. and Turco, R. P. (1993). Stratospheric Chlorine Injection by Volcanic Eruptions: HCl Scavenging and Implications for Ozone. *Science (80-.).*, 260(5111):1082–1086.

Tanaka, N., Rye, D. M., Xiao, Y., and Lasaga, A. C. (1994). Use of stable sulfur isotope systematics for evaluating oxidation reaction pathways and in-cloud-scavenging of sulfur dioxide in the atmosphere. *Geophys. Res. Lett.*, 21(14):1519–1522.

Textor, C., Graf, H.-F., Timmreck, C., and Robock, A. (2004). Emissions from volcanoes. In *Emiss. Atmos. trace Compd.*, pages 269–303.

Theys, N., De Smedt, I., Van Roozendael, M., Froidevaux, L., Clarisse, L., and Hendrick, F. (2014). First satellite detection of volcanic OClO after the eruption of Puyehue-Cordõn Caulle. *Geophys. Res. Lett.*, 41(2):667–672.

Theys, N., Van Roozendael, M., Dils, B., Hendrick, F., Hao, N., and De Mazière, M. (2009). First satellite detection of volcanic bromine monoxide emission after the Kasatochi eruption. *Geophys. Res. Lett.*, 36(3):1–5.

Thiemens, M. H. (2006). History and applications of mass-independent isotope effects. *Annu. Rev. Earth Planet. Sci.*, 34(1):217–262.

Thomason, L. and Peter, T., editor (2006). *SPARC Assessment of Stratospheric Aerosol Properties (ASAP)*. SPARC Office, no. 4 edition.

Troy, R. C. and Margerum, D. W. (1991). Non-Metal Redox Kinetics: Hypobromite and Hypobromous Acid Reactions with Iodide and with Sulfite and the Hydrolysis of Bromosulfate. *Inorg. Chem.*, 30(18):3538–3543.

Tsunogai, U., Komatsu, D. D., Daita, S., Abbas Kazemi, G., Nakagawa, F., Noguchi, I., and Zhang, J. (2010). Tracing the fate of atmospheric nitrate deposited onto a forest ecosystem in eastern Asia using Δ^{17}O. *Atmos. Chem. Phys. Discuss.*, 9(6):23073–23101.

Tsunogai, U., Miyauchi, T., Ohyama, T., Komatsu, D. D., Nakagawa, F., Obata, Y., Sato, K., and Ohizumi, T. (2016). Accurate and precise quantification of atmospheric nitrate in streams draining land of various uses by using triple oxygen isotopes as tracers. *Biogeosciences*, 13(11):3441–3459.

Uemura, R., Barkan, E., Abe, O., and Luz, B. (2010). Triple isotope composition of oxygen in atmospheric water vapor. *Geophys. Res. Lett.*, 37(4).

Vance, A., McGonigle, A. J., Aiuppa, A., Stith, J. L., Turnbull, K., and Von Glasow, R. (2010). Ozone depletion in tropospheric volcanic plumes. *Geophys. Res. Lett.*, 37(22).

Veale, L. and Endfield, G. H. (2016). Situating 1816, the year without summer', in the UK. *Geogr. J.*, 182(4):318–330.

Vicars, W. C. and Savarino, J. (2014). Quantitative constraints on the ^{17}O-excess (Δ^{17}O) signature of surface ozone: Ambient measurements from 50N to 50S using the nitrite-coated filter technique. *Geochim. Cosmochim. Acta*, 135:270–287.

Vidal, C. M., Métrich, N., Komorowski, J. C., Pratomo, I., Michel, A., Kartadinata, N., Robert, V., and Lavigne, F. (2016). The 1257 Samalas eruption (Lombok, Indonesia): The single greatest stratospheric gas release of the Common Era. *Sci. Rep.*, 6(September):1–13.

Vogt, R., Crutzen, P. J., and Sander, R. (1996). A mechanism for halogen release from sea-salt aerosol in the remote marine boundary layer.

Voigt, C., Jessberger, P., Jurkat, T., Kaufmann, S., Baumann, R., Schlager, H., Bobrowski, N., Giuffrida, G., and Salerno, G. (2014). Evolution of CO_2, SO_2, HCl, and HNO_3 in the volcanic plumes from Etna. *Geophys. Res. Lett.*, 41(6):2196–2203.

von Glasow, R. (2010). Atmospheric chemistry in volcanic plumes. *Proc. Natl. Acad. Sci.*, 107(15):6594–6599.

von Glasow, R. and Crutzen, P. J. (2013). Tropospheric Halogen Chemistry. *Treatise Geochemistry Second Ed.*, 5:19–69.

Von Glasow, R., Sander, R., Bott, A., and Crutzen, P. J. (2002a). Modeling halogen chemistry in the marine boundary layer 1. Cloud-free MBL. *J. Geophys. Res. Atmos.*, 107(17).

Von Glasow, R., Sander, R., Bott, A., and Crutzen, P. J. (2002b). Modeling halogen chemistry in the marine boundary layer 2. Interactions with sulfur and the cloud-covered MBL. *J. Geophys. Res. Atmos.*, 107(17):1–13.

von Glasow, R., von Kuhlmann, R., Lawrence, M. G., Platt, U., and Crutzen, P. J. (2004). Impact of reactive bromine chemistry in the troposphere. *Atmos. Chem. Phys.*, 4(11/12):2481–2497.

Wallace, P. J. (2001). Volcanic SO_2 emissions and the abundance and distribution of exsolved gas in magma bodies. *J. Volcanol. Geotherm. Res.*, 108(1-4):85–106.

Wang, T. X., Kelley, M. D., Cooper, J. N., Beckwith, R. C., and Margerum, D. W. (1994). Equilibrium, Kinetic, and UV-Spectral Characteristics of Aqueous Bromine Chloride, Bromine, and Chlorine Species. *Inorg. Chem.*, 33(25):5872–5878.

Wang, Y., Liu, S. C., Wine, P. H., Davis, D. D., Sandholm, S. T., Atlas, E. L., Avery, M. A., Blake, D. R., Blake, N. J., Brune, W. H., Heikes, B. G., Sachse, G. W., Shetter, R. E., Singh, H. B., Talbot, R. W., and Tan, D. (2001). Factors controlling tropospheric O_3, OH, NO_x and SO_2 over the tropical Pacific during PEM-Tropics B. *J. Geophys. Res. Atmos.*, 106(D23):32733–32747.

Wardell, L. J., Kyle, P. R., and Chaffin, C. (2004). Carbon dioxide and carbon monoxide emission rates from an alkaline intra-plate volcano: Mt. Erebus, Antarctica. *J. Volcanol. Geotherm. Res.*, 131(1-2):109–121.

Wexler, A. S. and Clegg, S. L. (2002). Atmospheric aerosol models for systems including the ions H^+, NH_4^+, Na^+, SO_4^{2-}, NO_3^-, Cl^-, Br^-, and H_2O. *J. Geophys. Res.*, 107(D14):4207.

Whitehill, A. R., Jiang, B., Guo, H., and Ono, S. (2015). SO_2 photolysis as a source for sulfur mass-independent isotope signatures in stratospehric aerosols. *Atmos. Chem. Phys.*, 15(4):1843–1864.

Whitehill, A. R. and Ono, S. (2012). Excitation band dependence of sulfur isotope mass-independent fractionation during photochemistry of sulfur dioxide using broadband light sources. *Geochim. Cosmochim. Acta*, 94:238–253.

Whitehill, A. R., Xie, C., Hu, X., Xie, D., Guo, H., and Ono, S. (2013). Vibronic origin of sulfur mass-independent isotope effect in photoexcitation of SO_2 and the implications to the early earth's atmosphere. *Proc. Natl. Acad. Sci. U. S. A.*, 110(44):17697–702.

Wild, O., Zhu, X., and Prather, M. J. (2000). Fast-J: Accurate simulation of in- and below-cloud photolysis in tropospheric chemical models. *J. Atmos. Chem.*, 37(3):245–282.

Witt, M. L., Mather, T. A., Pyle, D. M., Aiuppa, A., Bagnato, E., and Tsanev, V. I. (2008). Mercury and halogen emissions from Masaya and telica volcanoes, Nicaragua. *J. Geophys. Res. Solid Earth*, 113(6):1–15.

World Health Organization (2009). The European Health Report 2009 - Health and health systems. pages 1–191.

Young, E. D., Galy, A., and Nagahara, H. (2002). Kinetic and equilibrium mass-dependant isotope fractionation laws in nature and their geochemical and cosmochemical significance. *Geochim. Cosmochim. Acta*, 66(6):1095–1104.

Young, E. D., Yeung, L. Y., and Kohl, I. E. (2014). On the $\delta^{17}O$ budget of atmospheric O_2. *Geochim. Cosmochim. Acta*, 135(June):102–125.

Zanchettin, D., Khodri, M., Timmreck, C., Toohey, M., Schmidt, A., Gerber, E. P., Hegerl, G., Robock, A., Pausata, F. S., Ball, W. T., Bauer, S. E., Bekki, S., Dhomse, S. S., Le Grande, A. N., Mann, G. W., Marshall, L., Mills, M., Marchand, M., Niemeier, U., Poulain, V., Rozanov, E., Rubino, A., Stenke, A., Tsigaridis, K., and Tummon, F. (2016). The Model Intercomparison Project on the climatic response to Volcanic forcing (VolMIP): Experimental design and forcing input data for CMIP6. *Geosci. Model Dev.*, 9(8):2701–2719.

Zuev, V. V., Zueva, N. E., Savelieva, E. S., and Gerasimov, V. V. (2015). The Antarctic ozone depletion caused by Erebus volcano gas emissions. *Atmos. Environ.*, 122:393–399.

Zuo, Y. and Hoigne, J. (1993). Evidence for Photochemical Formation of H_2O_2 and Oxidation of SO_2 in Authentic Fog Water. *Science (80-.)*., 260(5104):71–73.